Laboratory for Radiopharmacy
Faculty of Pharmaceutical Sciences
Gent University

SYNTHESIS, IN VITRO/IN VIVO EVALUATION OF 2-IODO-L-PHENYLALANINE AND ITS D-ISOMER AS TUMOUR TRACERS IN ONCOLOGY.

Veerle Kersemans

Proefschrift voorgelegd tot het verkrijgen van de graad van Doctor in de Farmaceutische Wetenschappen.

Juni 2005

Promotor: Prof. Dr. Sc. Apr. G. Slegers
Co-promotor: Prof. Dr. J. Mertens

Het denken mag zich nooit onderwerpen
noch aan een dogma
noch aan een partij
noch aan een hartstocht
noch aan een belang
noch aan een vooroordeel
noch aan om het even wat
maar uitsluitend aan de feiten zelf
want zich onderwerpen betekent
het einde van alle denken.

Henri Poincaré.

Promotor:

Prof. Dr. Sc. Guido Slegers,
Ghent University
Faculty of Pharmaceutical Sciences
Department of Radiopharmacy
Harelbekestraat 72
B-9000, Gent
Belgium

Co-Promotor:

Prof. Dr. John Mertens
Free University of Brussels
Laboratory for Medical Imaging and Physics
Laarbeeklaan 103
B-1090, Jette
Belgium

Preface

At the beginning of my academic career, performing a PhD has always been a dream. This desire of exploration was even stimulated during the fine years at the Vrije Universiteit Brussel where our critical sense was encouraged. After 4 years, I graduated as a Biomedical Scientist: ready to dive into research to still my scientific hunger.

After the search for the "holy grail", an interesting research project to expand my knowledge, I entered the fascinating world of radiopharmacy and nuclear medicine at the Gent University. These years have passed with tremendous speed and now, as a result of 4 years of intense work, I can finally finish this interesting chapter of my life. Although the life of a PhD student is characterized by numerous obstacles, I am happy that I have walked this path.

Now, the time has come to express my gratitude to many people who have supported me the last years.

In this respect, I would first like to thank my promoter Prof. Guido Slegers who offered me the opportunity to perform a PhD on the intriguing topic of tumour detection using radiolabelled amino acid analogues. Prof. Slegers provided me with multiple research opportunities in a multidisciplinary environment and he was always there to advise me and to fill in the gaps in my research work. Thanks to Prof. Slegers, many symbioses were accomplished with other research institutions.

During my research I have had the privilege to cooperate with many scientists. In particular, I wish to express my gratitude to my co-promotor Prof. John Mertens. Many in-depth discussions, his value suggestions and his meticulous proofreading of the manuscripts, have guided me through these difficult years of research. In addition, I am most gratefull to Conny Joos, who was always there to reach me a helping hand, and to Matthias Bauwens for the endless discussions.

A very special word of thanks goes to Dr. Bart De Spiegeleer. I wish to express my respect and gratitude to Bart for being a superb scientific coach and mentor. He guided me through the difficult period of writing my PhD in spite of his own heavy workload. His analytical way of thinking advised me through the interpretation of my results.

As a result of the multidisciplinary aspects of my work, I would also like to express a word of thanks to Prof. Rudi Dierckx (Nuclear Medicine Department, Gent University Hospital) for proofreading my manuscripts and for offering me the opportunity to discover the world of nuclear medicine. The following persons affiliated to the division deserve a special word of thanks. Filip De Vos for milking the "^{99m}Tc-cow", for his contribution to a fruitful scientific collaboration and for the animated discussions. Erik Nolf, Johan Keppens and Filip Jacobs for their guidance during scanning.

At the division of Radiotherapy (Ghent University Hospital), I would like to thank Prof. Dr. De Neve who introduced us into the fascinating world of radiotherapy. Especially I would like to express my gratitude to Indira who helped me performing the in vivo radiotherapy experiment.

Amongst the other "allies" associated with our department, I would like to thank Kathelijne Peremans who gave us the opportunity to diagnose cancer lesions in dogs, Prof. H. Thierens for his advice and expertise in the in vitro radiation therapy evaluation and Prof. E. Achten who gave me the opportunity to use the MRI facilities.

At the Institute for Nuclear Sciences, I would like to thank Johan Sambre for his readiness for donating ^{18}F-FDG, Virginie de Gelder for her assistance in the in vitro radiation therapy and Klaus Bacher for the dosimetry calculations.

On a personal level, I am very grateful for the good moments I shared with my colleagues at our department. Not only my fellow-researchers but also the routine personnel contributed to the most amusable coffee breaks and the (scientific and other) discussions.

Therefore, I would like to thank Christophe, Ingrid, Peter, Elke Wattijn, Rien, Liesbet, Katia, Ruth, Ludo, Elke Michiels, Philippe, Filip, Marleen, Valerie, Nico, Patricia, Dirk, Frank, Magali, Leonie, Sylvie, Davy en Mario. They were always present to make my days at the lab unforgettable. Joeri, Kristof and Sylvie: thanks for your significant contribution to this work.

In addition, there are a number of people from outside the lab who unintentionally supported me during the last 4 years. At first I would like to thank my sensei François van Onckelen, 7th Dan Judo, who accompanied me to succeed for my 3rd Dan test. Moreover, I would like to thank my sparring partners, especially the ladies team, and our coach who led us to the third position in the ranking of the "Dames Interclub, 2de afdeling".
Besides the "judoka's", I would like to thank my friends Koen, Lieve, Jan, Greet and Hans. Although we didn't always get the chance to meet each other as often as one would like, I truly enjoyed our meetings which were an excellent source of distraction during the intense work of writing my PhD dissertation.

Frans, Leona and Tinne: thank you for all your support and distraction during the weekends. Although some of you sneaked off to conquer the Alpes by bike or to run quickly to Brussels, we have had some enjoyable times together.

Guy: thank you to lighten up my weekends. Moreover, I will never forget the great trips to Paris.

I am grateful to my grandparents who always believed in me. However, especially in such situations, I remember "vava" who would have been proud that I have reached this goal in my life.

To Ken: thanks for being such a great brother. I am proud that we could work together for a few years: you are a great scientist. Don't ever doubt about that! Above all, I would never like to miss those wonderful moments we have spent together, from childhood to today. I know we didn't always agree but during the "hard" times we always formed a strong team.

I would also like to thank Carine: I know my brother is in good hands with you. Moreover, thank you Carine for those fine moments during the weekends.

I would like to address a special word of thanks to my parents Vic and Lena. They raised me to the person who I am today. They have always supported me during my studies and scientific work and… not less important, they have showed me the other aspects of life: to explore the world, to respect other people, to discover other cultures and so on (I can go on eternally). Moreover, they were always there to support me in difficult situations: "you can always count on us", as they would say. I truly wander what I would do without you.

Finally, and most importantly, I would like to thank Bart. He was always there to reach me a helping hand during my scientific work and writing. As others say: "we are the

perfect team". Moreover, I always could rely on him during difficult moments, even the past year when he moved to Toronto to continue his research. Finally, after months of intense writing my PhD, I am lucky that I can join him and that we can together explore the fascinating world of radiopharmacy.

And last but not least, the two brothers Casper and Chaplin van de Brabostad, since one year part of the family. Using their "cocker-qualities", they guaranteed the ultimate moments of distraction.

Veerle Kersemans
Gent, June 2005.

Table of Contents

CHAPTER 5: Applications of [^{123}I]-2-iodo-L-phenylalanine

List of abbreviations and symbols.

A: Na^+ dependent amino acid transporter system

A2058: human melanoma cell line

A549: human non-small cellular lung carcinoma cell line

$A(A)_{eq}$: amino acid uptake at equilibrium

AA_t: amino acid uptake at a various time point

Ag: silver

ANOVA: analysis of Variance

ASC: Na^+ dependent amino acid transporter system

ATCC: American Type Cell culture collection

Aza-Tyr: Iodo-Aza-tyrosine

$B^{0,+}$: Na^+ dependent amino acid transporter system

BCH: 2-Amino-2-norbornane-carboxylic acid

Bq: Becquerel

BSA: Bovine Serum Albumine

C32: human amelanotic melanoma cell line

C6: rat glioma cell line

Capan2: human pancreatic carcinoma cell line

CD: cluster of differentiation = Groups of monoclonal antibodies that identify the same surface molecule.

cDNA: complementary DNA

-COOH: carboxyl group of amino acid

CT: Computed Tomography

DAR: differential absorption ratio

DMEM: Dulbecco's Modified Eagle's Medium

DNA: deoxyribonucleic acid

DOTA:1,4,7,10-tetraazacyclododecane-N,N',N'',N'''-tetraacetic acid

DPI: Dynamic Planar Imaging

DTPA: Diethylenetriamine pentaacetic acid
DUR: Differential Uptake Ratio

EDTA: ethylenediaminetetraacetic acid
EF43fgf4: mouse breast carcinoma cell line

Fab: antibody fragment with antigen binding site
FBAU: 2'-deoxy-2'-fluoro-5-bromo-1-β-D-arabinofuranosyluracil
FBS: Fetal Bovine Serum
FCH: [^{18}F]-fluorocholine
^{18}F-FDG: [^{18}F]-fluorodeoxyglucose
FEC: 2-[^{18}F]-fluoro-ethylcholine
FET: O-(2-[^{18}F]fluoroethyl)-Tyrosine
FLT: 3'-fluorothymidine
FMAU: 2'-fluoro-5-methyl-1-β-D-arabinofuranosyluracil
FMT: L-3-[^{18}F]fluoro-α-methyl tyrosine
FOV: field of view
F-TYR: 2-[^{18}F]fluoro-L-tyrosine

GABA: Gamma-aminobutyric-acid
GLUT: glucose transporter

Hepes: N-2-hydroxyethylpiperazine-N'-2-ethanesulfonic acid
HPLC: high Pressure Liquid Chromatography
HSA: human serum albumine
HT29: human colon adenocarcinoma cell line
HYNIC: Hydrazino-nicotinamide

2-I-L-Phe: 2-iodo-L-phenylalanine
[$^{123/125}$I]-2-I-L-Phe: [$^{123/125}$I]-2-iodo-L-phenylalanine
IA: injected activity
IAPA: 4-amino-3-iodo-phenylalanine
ID: injected dose
Iodogen: 1, 3, 4, 6-tetrachloro-3α, 6α-diphenylglycouracil

IMT: L-3-Iodo-α-methyltyrosine
IP: intraperitoneal
4IPHE: 4-Iodo-L-phenylalanine
2IT: 2-Iodo-L-tyrosine
3IT: 3-Iodo-L-tyrosine
ITIC: L-Iodo-1,2,3,4-tetrahydro-7-hydroxyisoquinoline-3-carboxylic acid
IV: intraveneously

$k_{1,0}$: elimination velocity derived from 2-compartment modelling
$k_{1,2}$: distribution velocity from the central to the peripheral compartment; derived from 2-compartment modelling
$k_{2,1}$: distribution velocity from the peripheral to the central compartment; derived from 2-compartment modelling
k': capacity factor
keV: kilo electron Volt
K_i: inhibition constant derived from Lineweaver-Burk
K_m: Michaelis-Menten constant and measures enzyme/substrate affinity
$K_{m,apparent}$: combination of the K_m constants related to the transporter system(s) involved.

LAT: L amino acid transporter type L
LC-MS: Liquid Chromatography – Mass Spectroscopy
LWB: Lineweaver-Burk-plot

MAbs: monoclonal antibodies
MeAIB: α-(methylamino) isobutyric acid
MEM: Minimal Essential Medium
MET: [^{11}C]-Methionine
MIBG: meta-iodobenzylguanidine
MIP: maximum intensity projection
MRI: Magnetic Resonance Imaging
mRNA: messenger RNA
mSv: milli Sievert

-NH2: amino group of amino acid

NIH: National Institute of Health
NMDA: N-methyl-D-aspartate
NMR: Nuclear Magnetic Resonance
NMRI: mouse strain; Naval Medical Research Institute
NS: not specified

P: Pixel
PBS: Phosphate Buffered Saline
PET: Positron Emission Tomography
pO_2: partial pressure of oxygen (normal pO_2 of arterial blood is approximately 100 mmHg).

R^2: correlation coefficient
R-group: variable group of amino acid
R1M: rabdomyosarcoma cell line
RNA: ribonucleic acid
ROI: region of interest
RP-HPLC: reversed phase High Pressure Liquid Chromatography
RTB: ratio tumour to contralateral background
RIB: ratio inflammation to contralateral background
RT-PCR: reverse transcriptase poly chain reaction

SA: specific activity
SC: subcutaneously
SCC: synovial cell carcinoma
SEC: Size exclusion chromatography
SPECT: Single Photon Emission Tomography
SWISS~*nu/nu*: athymic mouse strain

$t_{1/2}$: halfwaarde tijd
tRNA: transporter RNA
TLC: thin layer chromatography
TUNEL: terminal uridine deoxynucleotidyl end-labelling

US: Ultrasound

USA: United States of America

UV: ultra violet

V_0 : initial velocity

V_1 : distribution volume; derived from 2-compartment modelling

V_{max}: Maximum rate when applying Michaelis-Menten kinetics; $V_{max} = V / (S/(S + K_m))$ where [S] is the substrate concentration.

y^+: cationic amino acid transporter

CHAPTER 1:

Introduction

Introduction

1.1 BASIC ASPECTS

At present, there is no single test that can accurately diagnose cancer. The complete evaluation of a patient usually requires a detailed history and physical examination along with diagnostic testing. Many tests are needed to determine whether a person has cancer, or if another condition (such as an infection) is mimicking the symptoms of cancer. Effective diagnostic testing is crucial to confirm or eliminate the presence of disease, monitor the disease process, and to plan and/or evaluate the effectiveness of treatment.
Medical imaging has become vital in the early detection and diagnosis of cancer, and can allow treatment of cancer before it spreads to other parts of the body. In many cases, if cancer is detected soon enough, early treatment can lead to complete cure. Early detection of cancer helps to minimize the need for massive therapeutic treatment and reduces pain and suffering (1,2).

Medical imaging is the process of producing valuable pictures of body structures and organs. It is used to detect tumours and other abnormalities, to determine the extent of disease, and to evaluate the effectiveness of treatment. Over the last decades, medical imaging has gained much more success due to its non invasive character and due to its generation of results. There are three types of imaging used for diagnosing cancer:

- transmission imaging : X-rays, computed tomography scans (CT scans), and fluoroscopy
- reflection imaging: ultrasound, and
- emission imaging: Magnetic resonance imaging (MRI), nuclear imaging.

Each technique uses a different process and figure 1.1 gives an overview of the medical imaging techniques and their application field (1).

FIGURE 1.1: Medical imaging techniques and their application field.

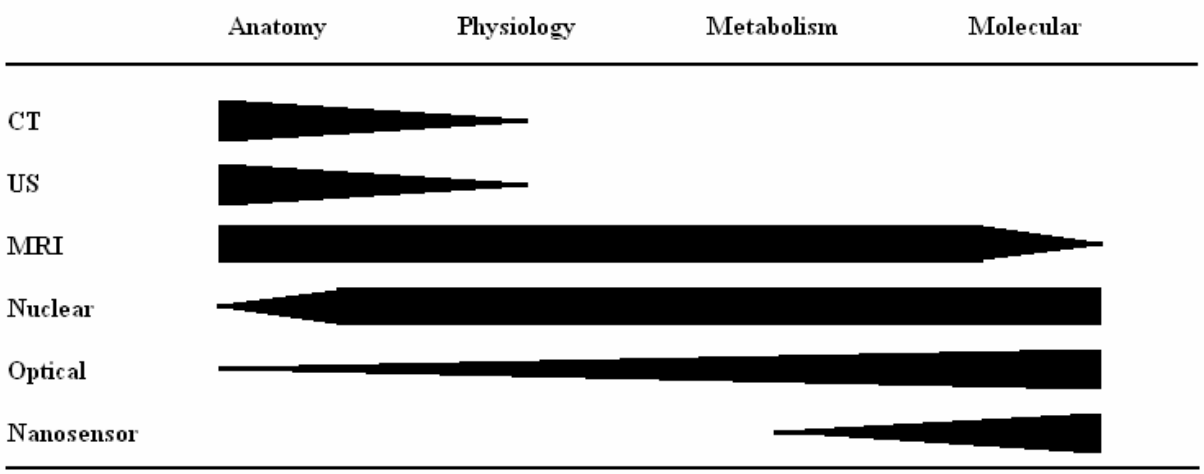

Imaging is fundamental to the practice of oncology from screening through diagnosis, staging, response assessment and tumour survival during follow up.

The first objective evidence of malignancy is often an abnormality on plain X-ray, CT-scan or ultrasound (US), as performed on indication of a clinical sign or symptom. Ultimately diagnosis can only be made on histological assessment although imaging has an important role to guide the biopsy to avoid the need of more invasive surgery. Imaging could provide accurate information of the location, the extent and nature of the tumour.
It is in the scope of this thesis that only nuclear imaging shall be discussed.

1.2 MOLECULAR IMAGING

Molecular imaging can be broadly defined as the in vivo characterisation and measurement of biological processes at the cellular and molecular level. In contradiction to the "classical imaging", molecular imaging focuses on the molecular abnormalities that are the basis of the disease rather than to image the final morphological effects of these alterations. This means that not only more selective pharmaceuticals could be developed but that also the specificity and sensitivity of diagnostic tools could be improved. Consequently, imaging of the underlying molecular changes of malignancies will result in directly detection of the disease in a "pre-disease stage" and in directly determining the effectiveness of treatment shortly after therapy has been initiated. In contradiction to the classical methods, no months will be wasted to determine whether pharmacologic or biologic intervention has been beneficial.

The last decade, molecular imaging has gained much more interest. On the one hand efforts have been directed towards understanding the cellular and molecular mechanisms of the disease but on the other side, efforts have been directed toward the development of non invasive, high resolution, in vivo imaging technology.

Although cranial CT and MRI are unsurpassed diagnostic modalities for the detection of cerebral space-occupying lesions, the differentiation of tumour tissue from oedematous, necrotic and fibrotic tissue with these methods is not optimal.

One of the applications of molecular imaging is nuclear medicine imaging which includes a variety of techniques that use radiopharmaceuticals. These consist of either gamma (for Single Photon Emission Computed Tomography; SPECT) or positron (for Positron Emission Tomography; PET) emitting radionuclides bound to ligands which accumulate differentially in malignant tissue as compared to normal tissue. Differences in tumour biology such as blood flow, metabolism, hypoxia, concentration of specific receptors or differences in antigen expression, are exploited in order to target the radionuclides to the tumour tissue.

Two major instruments of nuclear imaging used for cancer imaging are PET and SPECT. The characteristics of both imaging devices are compared in table 1.1 and presents the advantages and disadvantages of each technique (3-5).

TABLE 1.1: Characteristics of PET and SPECT imaging.

	PET	**SPECT**
Availability in Hospitals	Poor (few)	Very good
Infrastructure	Complex	More simple
Costs	Expensive	Much cheaper
Isotopes	^{15}O, ^{13}N, ^{11}C, ^{18}F	^{99m}TC, $^{123/131}I$, ^{111}In, ^{201}Tl, ^{67}Ga
Half life of Isotopes	2 min – 2 hours	6 hours – 8 days
Radioactivity	From on-site cyclotron	Purchased or from generator
Type of radiation	511 keV	70 – 511 keV
Tracer synthesis	On-site lab or from external after rapid transport	On site kit-preparation or from external
Scanning possible after tracer injection	0 – 2 hours	<24 hours – 10 days
Camera axial Field-of-View	11 – 16 cm	40 cm
Image Resolution	High (<5mm)	Lower (7-12mm)

1.2.1 Positron Emission Tomography (PET)

This imaging device uses radiopharmaceuticals labelled with a positron emitter such as ^{11}C, ^{13}N, ^{15}O or ^{18}F. During the decay process, the radionuclide emits a positron which, after travelling a short distance (3-5 mm), annihilates with an electron from the surrounding environment. As a result, two gamma rays of 511 keV each are sent in opposite directions.
The image acquisition is based on the external detection in coincidence of the emitted γ-rays, and a valid annihilation event requires a coincidence within 12 nanoseconds between two detectors on opposite sides of the scanner. For accepted coincidences, lines of response connecting the coincidence detectors are drawn through the object and used in the image reconstruction (5-7).

1.2.2 Single Photon Emission Tomography (SPECT)

Similar to PET, single photon emission computed tomography (SPECT) uses radioactive tracers which are labelled with isotopes producing a single γ-ray such as ^{99m}Tc, $^{123/131}I$, ^{111}In, ^{201}Tl or ^{67}Ga.

The image acquisition is based on the external detection of the emitted γ-rays. Before these γ-rays reach the camera they pass first through a collimator. The latter is a device made of a highly absorbing material such as lead which will serve to suppress scatter but also to select a γ-ray orientation. The simplest collimators contain parallel holes, but various other arrangements are in use. The basic principle of SPECT acquisition is presented in figure 1.2 (6-7).

FIGURE 1.2: Basis principle of SPECT imaging.

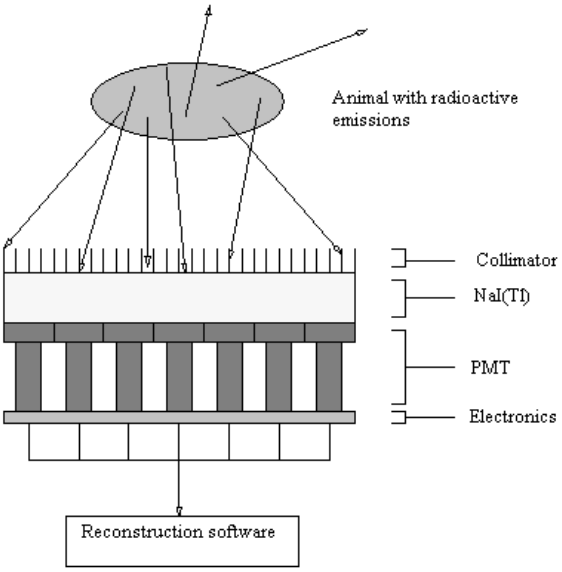

1.3 NUCLEAR ONCOLOGY: A FAST GROWING FIELD OF NUCLEAR MEDICINE

Nuclear medicine in oncology has been for a long time synonymous with bone scintigraphy and with the treatment of thyroid cancer with iodine-131. During the past decade, there has been a fast improvement in understanding the molecular basis of cancer. Along with this development in the molecular and cellular biology, remarkable advances in imaging technology and methodology have been made. The development of specific probes and ligands has allowed in vivo investigation of metabolic pathways and specific cellular functions. As a consequence, benign lesions can be distinguished from malignant lesions on the basis of differences in metabolic activity and viable tumour areas could be identified from necrotic tissue.

To date, several imaging strategies are developed to image cancerous lesions which will be briefly summarized in this chapter. In the scope of this thesis it is not the intention to present a complete overview about the possible imaging modalities but rather to give an idea of what is possible today.

1.3.1 Hypoxia imaging

Hypoxia plays a role in the resistance of tumours for radiotherapy. It has been shown that reduced haemoglobin levels and low tumour pO_2 values are associated with higher treatment failure rates (8-9). Consequently, identification and quantification of tumour hypoxia will help to identify those patients who might benefit from radiotherapy and valuable time will be saved.

Several hypoxia imaging tracers has been developed, either for SPECT or PET. The first class of radiopharmaceuticals contain a 2-nitro-imidazole group which acts as a bioreductive molecule, accepting a single electron and producing a free radical anion. After

further reduction, the latter will be incorporated into cell constituents under hypoxic conditions. Examples are ^{18}F-misoimidazole, ^{123}I-arabinoside and ^{99m}Tc-BRU-59-21. The second class does not contain an imidazole function and are believed to bioreduce themselves. Examples are ^{99m}Tc-4,9-diaza-3,3,10,10-tetramethyldodecan-2,11-dione dioxime and ^{62}Cu-diacetyl-bis(*N*-4-methylthiosemicarbazone) (10).

However, a lot of research has to be performed concerning these hypoxia tracers and a confirmation with a golden standard is urging. Generally, low tumour to background ratios has been reported and the cut-off values to distinguish normoxic from hypoxic are to low leading to significant overlap. These characteristics limit the use in clinical practice (11).

1.3.2. Cell death imaging

Apoptosis or programmed cell death is a natural, orderly, energy-dependent process that causes cells to die without inducing inflammation and auto-immunity reactions. Phosphatidyl serine, a cell membrane phospholipid, is a key molecule in imaging apoptosis. Normally, this molecule is restricted to the intracellular part of the plasma membrane. As cells undergo apoptosis, this phosphatidyl serine will be exposed at the extracellular part of the membrane due to the activity of floppase. One of the most studied apoptosis agents is Annexin-V which selectively binds to the extracellular exposed phosphatidyl serine. Thus, when radiolabelled, Annexine-V will provide accurate information about the extent of apoptosis without the need for invasive biopsy. To date Annexin-V and Annexine-V mutants could be radiolabelled in many different ways: from all forms of halogenation over ^{99m}Tc-labelling using different chelators, direct ^{99m}Tc-labelling, ^{111}In-DTPA labelling to ^{64}Cu-, ^{67}Ga- and ^{68}Ga-DOTA-labelling.

Due to dehalogenation of radioiodinated Annexine-V, ^{99m}Tc-HYNIC (hydrazinonicotinamide) labelled Annexine-V was developed. In vivo studies have already shown that quantitative ^{99m}Tc-HYNIC Annexine-V correlates with the levels of ongoing apoptosis as confirmed by terminal uridine deoxynucleotidyl end-labelling (TUNEL) assays. Studies are still ongoing to determine whether this tracer could monitor response to treatment and whether necrosis has an impact on the imaging results (12).

1.3.3 Membrane lipid metabolism imaging: choline analogues

The cell malignant transformation is linked with the enhanced activity of the choline kinase, which is itself related to tumour proliferation and the need for cytoplasmic membrane components, in particular phosphorylcholine and phosphatidylcholine (13-14). Choline synthesis in tumour cells is slow so that the increased uptake of radiolabelled choline reflects the cell duplication rate (15).

Several tumours have been studied with ^{11}C-choline but due to the short half life of ^{11}C, several fluorinated choline analogues have been developed such as 2-[^{18}F]-fluoro-ethylcholine (FEC) and [^{18}F]-fluorocholine (FCH). Preliminary studies of the latter compounds were in prostate cancer. FCH detected more primary lesions and metastases in comparison to 18F-FDG and FEC showed similar uptake results as compared to ^{11}C-choline. However, little is known about the specificity of the tracers and infection animal models reported high accumulation of the choline analogues (16). Nevertheless, given the high prevalence of prostate carcinoma and the absence of any satisfying PET tracer, fluorinated choline are widely used prostate imaging tracer.

1.3.4. Intracellular receptor imaging: estrogen, progesterone and androgen analogues

This group of radiopharmaceuticals is developed to image alterations concerning the estrogen receptor, progesteron receptor or the androgen receptor.
Several halogenated estradiol derivatives have been synthesized, a number of which have reached the clinical stage. Examples are 16α-^{77}Br-bromoestradiol, 16α-^{123}I-iodoestradiol-17β, 16α-^{18}F-fluoroestradiol, cis-methoxy-^{123}I-iodoestradiol, vinylestradiol, hexestrol and radiolabelled tamoxifen derivatives. The latter shows specific interaction with the estrogen receptor and provides useful information in predicting therapy response to the chemotherapeuticum tamoxifen in patients with metastatic and recurrent breast cancers (17). Moreover, tamoxifen derivatives not only allowed clinicians to monitor tamoxifen treatment in 1 episode (in stead of 2 episodes for estradiol derivatives) but also helped in understanding the working mechanisms of the drug. However, the tumour's need for estradiol is highly variable amongst tumours and can vary over time, depending on local conditions.

Since the progesteron receptor is an estrogen response element which is transcribed after effective binding of estrogen to its receptor, several progestines have been developed to predict therapy response to antiestrogen treatment. However, their potential has to be assessed.

The last targeted intracellular receptor is the androgen receptor. Although androgen receptor concentrations are not reliable to predict therapy response of prostate cancer to hormonal therapy, several researchers thought that an androgen receptor based tracer might be useful to stage and evaluate therapy response through sequential imaging of prostate cancer. Several fluorine-18 labelled androgens have been developed, including testosterone derivatives, dihydrotestosterone and miboreline, which bind the androgen receptor with high affinity in several animal models. However, no human studies with these agents have been reported so far (18).

1.3.5. Cell surface receptor imaging

Cell surface receptors could be divided into three families: (1) G-protein coupled receptors, (2) tyrosine kinase receptors and (3) the non-tyrosine kinase receptors. In cancer, many of these receptor systems are altered by mutations, most commonly resulting in deactivation, deletion or constitutive activation. The first two receptor families will be discussed briefly.

1.3.5.1 G-protein coupled receptors

The first class of cell surface receptors has been the primer topic of investigation. The radiopharmaceuticals involved target somatostatine receptors, the gastrin releasing peptide receptors, cholecystokinin-B receptors, vasoactive intestinal peptide receptors, the sigma receptors, the neurotensin receptors, the melanocortin-1 receptors and the calcitonine receptors. Amongst these receptor families, the somatostatine receptor is one of the most intensively studied receptors. To date, a large number of radiopharmaceuticals have been developed such as the depreotide (19), vapreotide (20) and octreotide (21). The latter can be radiolabelled with indium-111, ^{99m}Tc-HYNIC and the ^{90}Yt and ^{177}Lu (via macrocyclic chelators). ^{111}In-labelled octreotide was proven to be an effective imaging agent in the management of patients with neuroendocrine tumours, not only for tumour detection but also for predicting therapy response. Today, only ^{99m}Tc-depreotide has become commercially available and introduced into clinical practice. However, despite to the successful use of the

somatostatine analogues, only a restricted group of tumour types express the somatostatine receptor family.

In the search for a "more universal " peptide, able to bind to the majority of tumour types, vasoactive intestinal peptide is one of the most promising peptides due to its widely expressed receptor system (22). However, during the development several limitations rised: it is difficult to prepare a routine radiolabelling kit, it is very unstable in the blood and it is pharmacologically very potent which results in toxic effects in the sub-microgram range.

The other mentioned receptor systems are studied in a much less extent and a lot of clinical studies are ongoing. Thus, a wide spectrum of peptides has been proposed to target cell types and tumour groups. However, the clinical role for these imaging agents remains unclear but it is very likely that most of them will serve the purpose of selecting patients for therapy.

1.3.5.2 Tyrosine Kinase receptor family

This receptor family guarantees the signal transduction when growth factors bind to their receptors which posses an intrinsic tyrosine kinase activity. These receptors are frequently overexpressed in tumours or are constitutively activated and they are in general associated with a high metastatic rate and increased tumour proliferation (23).Consequently, an inverse relationship between the receptor expression and the survival of the patient has been reported for a variety of tumours (24). Four receptors are intensively studied: the epidermal growth factor receptor, the orphan Her-neu receptor, the insuline-like growth factor receptor and the vasular endothelial growth factor receptor (18). Several receptor ligands, such as the epidermal growth factor, insuline-like growth factor, fibroblast growth factor and the vascular endothelial growth factor, have been successfully labelled with iodine-123, Technetium-99m and/or Indium-111. Again, the clinical role for these imaging agents still needs to be defined. Radiolabelled vascular endothelial growth factor might serve as an imaging agent to monitor the angiogenetic treatment. However, the detailed angiogenetic pattern of most tumours still needs to be established.

1.3.6 Tumour specific antigen imaging

Antibody molecules are Y-shaped structures and consist of two identical light and heavy chains. The variable regions of those light and heavy chains form a unique antigen-binding site that engages an antigenic determinant. Antibodies are generated by a complex process in which gene segments are rearranged randomly into functional genes. As a consequence, billions of different antibodies with different specificities could be generated (25).

Because antibodies have high specificity towards their antigens, tumour-antigen specific antibodies are considered to be attractive molecules for targeted delivery of imaging agents for the diagnosis of both primary and metastatic malignancies. Currently there are 12 therapeutic monoclonal antibodies (MAbs) available on the market for human use and only 5 target cancerous lesions: rituximab, trastuzumab (or Herceptin), gemtuzumab, alemtuzumab and ibrituzomab (or Zevalin) (26). However, the use of intact antibodies is troubled by their large molecular size leading to prolonged clearance kinetics, high systemic background and slow tumour uptake. To date many studies are ongoing to solve these problems. The simplest approach is to shorten the MAbs molecules by enzymatic digestion or genetic engineering resulting in smaller-molecular-weight fragments (so called $F(ab)_2$ and Fab' fragments) without altering the specificity but with improved pharmacokinetics (27).

Although only 5 anti-cancer therapeutic antibodies are approved, the number and diversity of the different developed antibodies is immense. Although much research has to be performed, it is likely to believe that these therapeutics will dominate the market in the future.

1.3.7 Metabolic imaging

Differences in metabolic activity could be used to differentiate between benign and malignant lesions. The process of malignant transformation needs that cells acquire and use nutrients efficiently for energy, protein synthesis, and cell division. Consequently, cancer cells demonstrate an increased glucose, amino acid and nucleotide uptake and metabolism which are the basis principle for the use of fluorine-18 labelled fluorodeoxyglucose (^{18}F-FDG), radiolabelled amino acids and nucleotides in oncologic imaging. In this part, I will only discuss ^{18}F-FDG and the use of radiolabelled nucleotides. The application of radiolabelled amino acids will be discussed in paragraph 1.6.

1.3.7.1 Imaging the increased energy metabolism using 18F-FDG

^{18}F-FDG is a glucose analogue where a hydroxyl group had been substituted by a ^{18}F-atom. Its synthesis was published in 1975 and the first human images were obtained in 1976 (28). This compound is recognized by the human cells and especially by tumoural cells as a glucose molecule. FDG-PET in oncology relies on research performed by Warburg decades ago that showed increased glucose metabolism and lactate production and a decrease in oxidative pathways: ^{18}F-FDG exploits the increased glycolysis rate, seen in tumour cells, as a result of both increased glucose uptake and increased activity of the glycolitic enzymes (29). ^{18}F-FDG is taken up by the glucose transporter proteins (mainly by the GLUT-1 transporter) and once in the cell, it is phosphorylated in the same way as glucose by hexokinase. In contrast to glucose, ^{18}F-FDG-6-phosphate cannot be further metabolized and it remains trapped in the cell. As a consequence, the intracellular concentration of ^{18}F-FDG is proportional to the glucose utilisation of the tissues. Because tumours present an enhanced rate of glucose metabolism as compared to healthy tissues, a tumoural area is detected by the abnormal high ^{18}F-FDG concentration. The clinical applications of ^{18}F-FDG are numerous. For example: staging of tumours at initial diagnosis, diagnosis of recurrent lesions, therapy evaluation, therapy response, diagnosis of residual disease. Moreover, in therapy the method could help in defining the radiation borders: which area should be included and what should be spared. The average ^{18}F-FDG PET sensitivity and specificity across all oncology applications are estimated at 84% and 88%, respectively (30-32).

However, there are several well known limitations for the use of ^{18}F-FDG in oncology. First, the glucose metabolism is not significantly increased in some tumour types, such as prostate carcinoma. Second, several recent studies have demonstrated diagnostic limitations of ^{18}F-FDG PET for brain tumour imaging: even for high grade tumours, contrast between tumour tissue and normal brain is often low due to the high glucose utilization of normal grey matter. ^{18}F-FDG uptake of low grade tumours is generally similar to that of normal white matter. The most important drawback of ^{18}F-FDG for oncologic imaging results from its absence of tumour specificity: infection, inflammation, granulomatous diseases (e.g. tuberculosis) and other pathological conditions can all show high ^{18}F-FDG uptake (33-35).

1.3.7.2 Imaging cellular proliferation using radiolabelled nucleotides

The level of proliferation is obviously a key parameter when it comes to characterisation of neoplastic lesions. DNA synthesis is required for cell growth and it is the process that is most reliably associated with proliferation. Nucleotides of the four bases (cytosine, guanine, adenine and thymidine) are essential for DNA synthesis and measurements of the incorporation rate into DNA yield the DNA synthetic rate. Of the four nucleosides, thymidine is the only one which is incorporated into DNA (and not RNA) and thus provides a measurement of DNA synthesis independent from RNA synthesis. Together with the fact thymidine, exogenous to the cell, could be incorporated into DNA, has led to the development of ^{11}C-radiolabelled thymidine and radiofluorinated thymidine analogues. The latter are synthesized in order to overcome the short half life of [^{11}C] and to avoid the formation of radiolabelled metabolites by thymidine phosphorylase. The most intensively studied thymidine analogue is 3'-fluorothymidine (FLT) and a number of clinical studies are ongoing (36). Nucleotide tracers share some features with 18F-FDG: both components are taken up, phosphorylated and trapped into the cell without incorporation and further metabolisation. Despite the possibility to visualize malignant tumours, ^{18}F-fluorinated FLT remains inferior to ^{18}F-FDG: ^{18}F-FLT uptake is lower in nearly all the cases resulting in a lower sensitivity. The specificity is another aspect that needs further validation since a false positive result has been reported (37). Moreover, the relative contributions of the salvage pathway and the de novo synthesis seem to influence ^{18}F-FLT uptake. Furthermore, the physiological uptake of the latter tracer in the liver and the bone marrow hinders the detection of liver and bone metastases.

Other radiolabelled nucleosides include 2'-fluoro-5-methyl-1-β-D-arabinofuranosyluracil (FMAU), 2'-deoxy-2'-fluoro-5-bromo-1-β-D-arabinofuranosyluracil (FBAU), 5'-bromo-2'-fluoro-2'-deoxyuridine and 5-iodo-2'deoxyuridine. The latter two tracers could provide a longer half life but they are still substrates for thymidine phophorylase metabolism. Although FMAU and FBAU have the advantage over ^{18}F-FLT that they are incorporated into DNA, the beneficial characteristics need to be explored to determine their use in clinical practice.

1.3.8 Other strategies to image tumours

Some of the old nuclear imaging techniques remain still in clinical use. Bone scan with technetium-99m labelled diphosphonates is one of them. This tracer targets the perimetastatic bone reaction, observed in all bone metastases except those are purely osteolytic. Bone scan remains the method of choice to detect skeletal metastases in osteophilic tumours such as breast, prostate and lung cancers. A second "old" nuclear imaging agent is iodine-131 in the management of thyroid cancer as the only efficient therapeutic modality beyond surgery (38).

One of the more recently developed techniques, which do not quite fit in the former categories is MIBG (meta-iodobenzylguanidine), a norepinephrine analog which concentrates inside neurosecretory granules in tumours derived from the neuronal crest (such as neuroblastoma in childhood). The latter tumour represents the most common extracranial solid malignant tumour. This tracer permits to characterize and to stage the tumour. Moreover, it can be used as radiotherapeutic agent and as per-operative detection to help the surgeon to detect the tumour (39).

Another modality is sentinel node detection using ^{99m}Tc-labelled colloids, especially in breast cancer and melanoma. The concept of sentinel node detection can be summed up as follows: when a tumour spreads by lymphatic channels, the first node to drain the lesion

(sentinel node) is predictive of the metastatic status of the regional lymph node group. Indeed, if this node is not affected by metastases, it is unlikely that those situated more distally are affected. For example in breast cancer, this technique allows the surgeon to remove only those nodes that are affected resulting in a decrease of unnecessary lymph node dissections and the lymphoedema (39).

Technetium-99m radiolabelled sestamibi is taken up by tumours including lung and breast carcinomas, lymphomas and sarcomas and is able to detect chemotherapeutic resistant tumours. ^{99m}Tc-sestamibi is transported by P-glycoprotein and a correlation has been demonstrated between its efflux and P-glycoprotein expression in untreated breast carcinomas and between rapid tumour clearance and lack of tumour response to neo-adjuvant chemotherapy for breast cancer. These factors indicate that this imaging tool could identify patients who are unlikely to respond to chemotherapy. However, there are some limitations about the use of ^{99m}Tc-sestamibi: it is not taken up by all tumours and due to clearance of the tracer by the liver and biliary route, tumours of the abdomen are difficult to detect (40).

1.4 AMINO ACIDS: BASIC ASPECTS

Amino acids are the monomeric building blocks of proteins and serve many other essential functions in the cells: amino acids are precursors for other biomolecules such as histamine, thyroxine, adrenaline, melanine and serotonine. In addition, amino acids can be crucial in the metabolic cycles: methionine is a methyl group donor in many biosynthetic pathways.

All 20 amino acids demonstrate the same structure: the asymmetric α carbon atom is bound to 4 different chemical groups: an amino ($-NH_2$) group, a carboxyl (-COOH) group, a hydrogen atom and one variable group. Of the 2 stereoisomeric forms, almost all amino acids in proteins possess the L-configuration and all are dipolar molecules or zwitterions.

The amino acids are classified into a few categories based on the characteristics of their side chains. This classification is primarily based on their solubility in water which leads to 4 classes of amino acids: (1) non-polar or hydrophobic R-groups, (2) neutral uncharged, polar R-group, (3) positively charged R-group and (4) negatively charged R group (figure 1.3). Another classification is based on the ability of cells to synthesize amino acids from metabolic pathways. Ten amino acids are referred to as essential and must be obtained from the diet: arginine, histidine, isoleucine, leucine, lysine, methionine, phenylalanine, threonine, tryptophan and valine.

Once transported into the cell, the protein synthesis starts with the esterification of an L-amino acid to amino-acyl-tRNA by the enzyme amino-acyl RNA synthetase. Once the amino-acyl-tRNA has been formed, it will bind to the ribosome and subsequently to the corresponding codon at the mRNA and the polypeptide chain will be formed. Besides these conversions, amino acids may serve as substrate for other metabolic pathways as mentioned above.

Amino acid degradation is a dynamic process. In degradation, the α-amino groups are removed and usually transformed into urea. The resulting molecule is converted into metabolic intermediates which will be transformed in fatty acids, ketones or glucose. In this way, amino acids could serve as metabolic fuel because they cannot be stored in the cell.
In order to better understand the tumour accumulation of amino acids, it is important to learn more about the different uptake mechanisms (41,42).

FIGURE 1.3: Classification of amino acids based on the polarity of their R-groups.

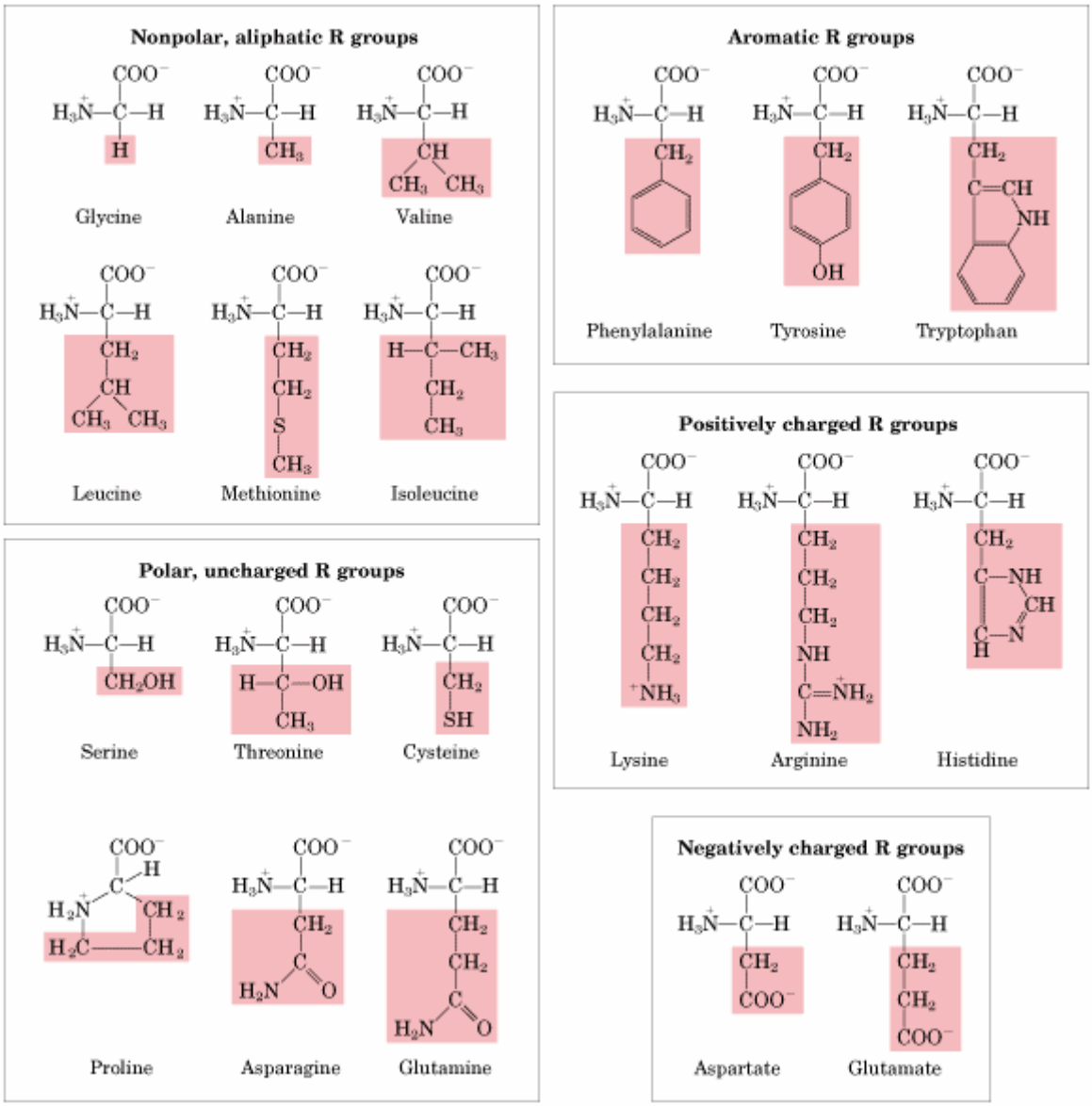

1.5 AMINO ACID TRANSPORT ACROSS THE CELL MEMBRANE

Although amino acids can diffuse into cells, the main movement of amino acids is energy dependent and occurs through carrier-mediated processes. Several transporters can be defined and each family facilitates the transport of a certain group of amino acids across the membrane.

Two groups of carriers can be designated: (1) transport which is Na^+-dependent for its maximal activity and (2) Na^+-independent transporters. The driving force for the first group is the sodium chemical gradient and the membrane electric potential, which is maintained by Na^+ or K^+ pumps. In general, the movement of the second group depends on the intra- and extracellular concentration of the corresponding amino acids and is often associated with

countertransport of a second amino acid whose gradient has been established by a Na^+ dependent carrier.

At present, more than 20 transporter systems have been identified. While less frequent amino acid transport systems are present in various tissues (e.g. $B^{0,+}$ and y^+), the main transporter systems are on the one hand system A and ASC which are Na^+-dependent and on the other side the Na+-independent system L. The latter transporter system, in comparison to the other transporters, shall be discussed in more detail because of its relevance for the experimental work performed in this thesis (43-46).

1.5.1 Amino acid transporter system A

System A is Na+ dependent and transports preferentially short chain neutral amino acids such as alanine, serine and glutamine. This system is often inhibited by intracellular substrates of this system: the intracellular presence of former amino acids shall inhibit the additional uptake (trans-inhibition). Additionally, system A is highly regulated by a wide variety of factors including hormones (e.g. insulin, glucagon, catecholamines and glucocorticoids), growth factors, mitogens, amino acid availability, pH, hyperosmolarity and cellular growth state. System A can be distinguished from other known transport systems for neutral amino acids by its ability to transport N-methylated amino acids such as α-(methylamino) isobutyric acid (MeAIB). Consequently, Na+-dependent transport of MeAIB can be used directly as a measure of system A activity (47-49).

1.5.2 Amino acid transporter system ASC

System ASC mainly acts as a carrier for short chain neutral amino acids such as serine, alanine and cysteine. In contradiction to system A, system ASC is trans-stimulated by the presence of intracellular amino acids and functions predominantly as a mediator of neutral amino acid exchange rather than of net uptake. The high extracellular/intracellular sodium differential is the driving force of this Na+ dependent system (50,51) .

1.5.3. Amino acid transporter system L

System L is the most important and universally found Na+-independent amino acid transporter. This system is responsible for the uptake of neutral branched chain and aromatic amino acids and can be differentiated from other transport systems by its ability to transport 2-Amino-2-norbornane-carboxylic acid (BCH). The system functions as an obligatory amino acid exchanger. Thus, just like system ASC, System L mediates amino acid exchange rather than net uptake.

At the moment, 3 members of the system L family have been discovered: LAT1, LAT2 and LAT3. The proteins encoded by LAT1 and LAT2 cDNAs are composed of 507 and 535 amino acids, respectively and their sequences show a homology of 52%. In contrast to LAT1 and LAT2, the existence of the LAT3 subtype has only recently (2003) been revealed. As a consequence, little is known about LAT3.

Both LAT1 and LAT2 require an additional protein for their functional expression: CD98/glycoprotein 4F2 heavy chain (4F2hc) which forms a heterodimeric complex with the LAT1 or 2 protein. 4F2 brings the LAT proteins to the plasma membrane. In absence of this

glycoprotein, the LAT proteins are found in the intracellular compartment whereas 4F2 can reach the plasma membrane independently.

Although the family members possess similarity in function and substrates, they differ in substrate affinity and specificity and in tissue distribution. LAT1 shows a high affinity and broad substrate selectivity: cysteine, valine, isoleucine, leucine, methionine, histidine, tryptophan, tyrosine, phenylalanine and BCH are transported into the cells with a high affinity (micromolar range). LAT2, on the contrary, exhibits a low substrate affinity (millimolar range) and narrower substrate selectivity: isoleucine, leucine, phenylalanine and BCH are taken up by this subtype. Whereas LAT1 mRNA is widely expressed in non-epithelial cells, LAT2 mRNA expression is restricted to tissues rich in absorbing epithelia.

The obligatory exchange function of LAT1 implies that uptake of an extracellular substrate needs to be coupled to extrusion of an intracellular substrate. The net influx of aromatic amino acids therefore depends on the availability of intracellular exchange substrates. Such intracellular substrates might enter the cell by parallel, unidirectional transporters with overlapping substrate selectivity. Methionine has been suggested to be such a recycling substrate, since it is a poor uptake substrate but a relatively good efflux substrate for LAT1. Once extruded, it is taken up again in the cell by the unidirectional system A, for which it has a high affinity.

LAT3 appears to be distinct from the first two subtypes: LAT3 does not require a glycoprotein for its functional expression and allows both influx and efflux of substrates through facilitated diffusion without the obligatory exchange property (52-57).

1.5.4. Overview

FIGURE 1.4: Overview of the contribution of the 3 main amino acid transporter systems to the transport of several amino acids. A = system A; ASC = system ASC; L = system L and NS = other transporter systems.

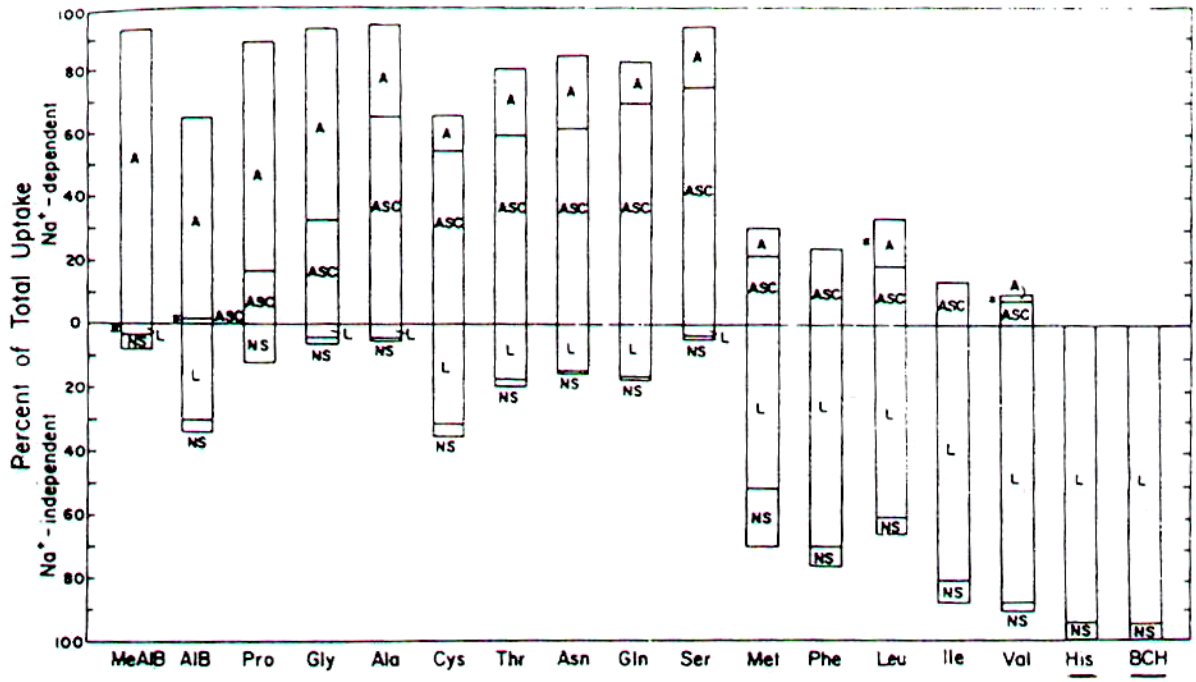

1.6 AMINO ACID TRANSPORT IN MALIGNANCIES

Increased transport and/or protein synthesis in tumour cells was demonstrated more than 40 years ago (45). Like all other cells, tumour cells require nutrients for their growth. Most tumour cells share the ability to concentrate amino acids more efficiently than normal cells. Consequently, amino acid transport is in general increased in malignant transformation. Moreover, this increased transport may be associated with changes of the cell surface. For example: system A, one of the few identified transport systems that is overexpressed in tumour cells, serves as a target for proto-oncogene and oncogene action.

However, the process of malignant transformation necessitates that cells acquire and use nutrients for energy (e.g. glucose and its nuclear medicine application 18F-FDG), protein synthesis (amino acids) and DNA multiplication (e.g. nucleic acids like 18F- 3'-deoxy-3'-fluorothymidine). For this reason, increased transport of amino acids is also an aspecific net result of the increased demand for nutrients.

Of the two major processes in protein metabolism, amino acid uptake and protein synthesis, the former may be more upregulated. To be precise, amino acid transport contributes to several other processes rather than protein synthesis, namely: transamination and transmethylation, the specific role of methionine in the initiation of protein synthesis, the use of amino acids as glutamine for energy and as precursors for other biomolecules. All these nonprotein-synthesis processes contribute to increased transport rather than to increased protein synthesis. On the contrary, the fraction of amino acids entering the protein synthesis might also correlate with proliferation (and thus malignancy) but the protein synthesis for cellular maintenance will disturb this correlation.

Further studies with the unnatural amino acid [^{123}I]-L-3-iodo-α-methyltyrosine (discussed in paragraph 1.7), which cannot be incorporated into cell proteins, show significant correlation between tracer uptake and thus amino acid transport and proliferation. For these reasons, amino acid transport tracers are valuable tracers to reflect the malignancy of tumours.

Over the past decade, many research groups have reported the overexpression of both amino acid transporter systems A and LAT1. This thesis focuses the latter transporter system. The role of this transporter system is to provide cells with essential amino acids for cell growth and tissue development which is reflected in its high upregulation in fetal tissues and tumours. On the contrary, non-proliferating tissues show a low LAT1 expression and the major route for essential amino acid uptake in these tissues is attended by LAT2.
System A shows, besides an upregulation in tumour cells also an ubiquitous tissue expression which could be a disturbing property for oncologic imaging (58-63).

1.7 PRECLINICAL ONCOLOGIC IMAGING USING RADIOLABELLED AMINO ACID ANALOGUES

In recent years, several amino acids have been labelled with either gamma radiation-emitting isotopes or positron-emitting isotopes. Although PET resolution is better, this thesis will focus on the development of radiolabelled amino acids for oncologic SPECT imaging. This because of the three main advantages as mentioned in paragraph 1.2 and the more difficult (radio)chemistry for introducing the positron emitting radionuclides. As a consequence, this paragraph will present a short overview of the most widely used PET tracers and will discuss in more detail the already existing radiolabelled amino acids for

SPECT. A complete overview of the already existing PET amino acid tracers would lead us to far since those tracers are more widely and intensively studied in comparison to the SPECT tracers.

1.7.1 Radiolabelled amino acid analogues for PET

1.7.1.1. ^{11}C-Methionine (MET)

MET is the most frequently used amino acid tracer, due to its simple and fast radiosynthesis with high labelling yields without the need for complex purification procedures. MET uptake is specific and carrier mediated. However, the importance of blood flow demonstrated that a part of MET uptake results from passive diffusion which may occur in areas where the blood brain barrier is damaged (64-65). Autoradiography studies demonstrated the tumour specificity of MET since the tracer was predominantly taken up in viable cells and only in low amounts in macrophages and other cells.

MET was mostly used to perform brain tumour studies. In contrast to 18F-FDG, background activities of MET were low in normal brain tissue, providing good tumour contrast. Moreover, MET was more suitable for tumour grading, it delineates better the tumour margins and the tracer could be used to follow up treatment (66). High sensitivities are reported for patients with high grade brain tumours (97%) but in low grade tumours the sensitivity was dropped to 61% (67). Fewer studies are performed with MET for extracranial tumour detection and evaluation. Sensitivities of 78 – 93 % were reported for tumours outside the brain but due to the limited data, the true therapeutic value and the final values in terms of patient management remains to be established.

1.7.1.2. O-(2-[^{18}F]fluoroethyl)-tyrosine (FET)

The former amino acid analogue MET has been used in many studies but due to the short physical half life of ^{11}C-label, this tracer remains restricted to a few PET centra with an on-site cyclotron. In order to overcome this problem, [^{18}F]-fluorinated amino acids such as FET have been developed. The latter tracer can be easily synthesized with an overall radiochemical yield, after HPLC purification, of 40 % with radiochemical purity between 97 and 99 % (68). FET is not incorporated into proteins and the uptake by tumour cells is stereospecific and mediated by amino acid transport system L (69). Initial clinical studies in human brain tumours have shown similar results to MET (70). Moreover, low uptake in non-neoplastic inflammatory cells and in inflammatory lymph nodes was observed. The first clinical studies with FET in patients with brain tumours showed similar results in comparison to MET. However, preliminary results with FET suggest that this tracer is inferior to 18F-FDG concerning the visualisation of peripheral tumours. Further investigations are needed to determine the tumour imaging capabilities of FET.

1.7.1.3. Other amino acid analogues

Among the other most studied PET amino acid analogues for tumour imaging, [^{18}F]-2-fluoro-L-tyrosine (F-TYR) and [^{18}F]-L-3-fluoro-α-methyl tyrosine (FMT) are investigated with particular scrutiny.

F-TYR is synthesised with low radiochemical yield (5 %). This amino acid analogue is transported by the L-transport system. Although it is incorporated into the cell proteins, the primary mechanism for the accumulation of F-TYR in the tumour cells is the elevated

transport (71). However, recent clinical studies reported somewhat disappointing results in terms of sensitivity of the tracer for the detection of various tumours (72).

The radiosynthesis yields of FMT are very low, as well as its specific activity. However, FMT accumulates more rapidly and intensively in animal tumour lesions in comparison to 18F-FDG.Patient studies revealed that FMT was better in distinguishing benign lesions from malignant tumours but 18F-FDG was found more accurate in grading the tumour lesions (73).

1.7.2 Radiolabelled amino acid analogues for SPECT

1.7.2.1. [^{123}I]-L-3-iodo-α-methyltyrosine (IMT)

The structure of the artificial amino acid [^{123}I]-L-3-iodo-α-methyltyrosine (IMT) is shown is figure 1.5.

FIGURE 1.5: Structure of [^{123}I]-L-3-iodo-α-methyltyrosine. The modifications in comparison with the native L-tyrosine are printed in red.

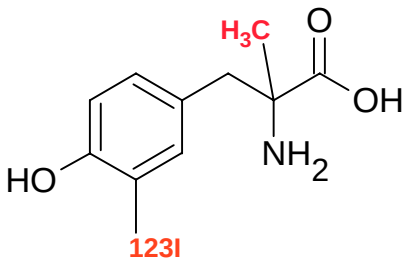

In 1979 Kloss and Leven firstly considered IMT as a potential tracer for nuclear medicine, but initial clinical studies for the detection of melanomas and imaging of the pancreas by planar imaging with gamma cameras were not convincing. A continuation of research on IMT started in the late 1980s stimulated by the promising results of PET studies in brain tumors using amino acids and the general availability of SPECT.

During the last decade, IMT has generated much interest, especially after the demonstration that the uptake of the tracer specifically reflects the amino acid transport in tumour cells. Up until today, IMT is intensively studied and it is the first and the only routinely used amino acid tracer for oncologic imaging with SPECT.

The synthesis of IMT is easy and fast: electrofilic substitution using iodogen, followed by Sep-Pak purification results in a radiochemical yield and purity of over 90% and 99%, respectively. IMT can be produced in a Kit formulation. The synthesis produces a metabolically stable product: no side products are formed and IMT is subject to only minor deiodination (4% deiodination at 90 min p.i.).

IMT is rapidly taken up by brain tumours: at 30 min p.i. the steady state for tumour uptake is reached. The tracer is not incorporated into the cell proteins and washes out relative slowly (approximately 30% at 1h p.i.). Dependent upon the tumour type, in brain mean tumour-to-background ratios of 1.5 up to 2.5 are reached. Moreover, this tumour uptake is specific since up to 53% of the initial uptake can be blocked by administering a mixture of naturally occurring amino acids. The latter observation, made by Langen et al., is now frequently used as proof that IMT, despite the presence of a methyl group and the bulky

iodine atom, is still a substrate for the amino acid transporters in the tumour but also in the blood brain barrier (74).

The role of IMT SPECT for the determination of tumour grading of cerebral tumours is controversial. While some authors reported a high accuracy of IMT SPECT for the separation of high grade from low grade, others could not identify such a difference and observed a wide overlap of IMT uptake. However, several studies did demonstrate that IMT SPECT is a valuable tool to differentiate recurrences of brain tumours from necrotic areas.

During a long time, research about IMT was focussed on the imaging of brain tumours. It was Jager et al. who first described the feasibility of IMT to detect tumours outside the brain (75). Similar results were found for a variety of tumours: breast cancer, lung cancer, soft-tissue sarcoma, head and neck cancer and lymphoma showed similar kinetics as compared to brain tumours. However, based on the still limited data in extracranial tumours, the diagnostic value of IMT SPECT is not convincing and inferior to FDG PET in general. Moreover, a major drawback of IMT for imaging extracranial tumours is its marked long-term renal accumulation.

Similar to other radiolabelled amino acids, IMT is rapidly eliminated from the body and the radiation burden is low. After intravenous injection about 90% of IMT leaves the plasma compartment within 10 min and is predominantly excreted by the urinary tract. Data on renal excretion of IMT range from 40–70% within the first 3 h post injection. While in mice high pancreas uptake was reported, in patients only a minor pancreatic uptake was observed in 35% of the subjects during the first hour which is hardly to separate from background.

Later on, when tumour uptake was proven, in vitro and in vivo studies in animals were performed to reveal the transport mechanisms and the toxicity of IMT uptake. Although IMT is not significantly incorporated into any metabolic pathway the uptake appears to be specific and related to amino acid transport. In vivo studies in mice and rats as well as in vitro studies revealed that IMT transport across the blood brain barrier is similar to its parent L-tyrosine and occurs for over 70% via system L, more specifically LAT1. In general, IMT is non-toxic and no side effects have been reported after intravenous injection of the tracer (58,74-79).

1.7.2.2. [^{123}I]-2-iodo-L-tyrosine

The structure of [^{123}I]-2-iodo-L-tyrosine is shown in figure 1.6.

FIGURE 1.6: Structure of [^{123}I]-2-iodo-L-tyrosine. The modifications in comparison with the native L-tyrosine are printed in red.

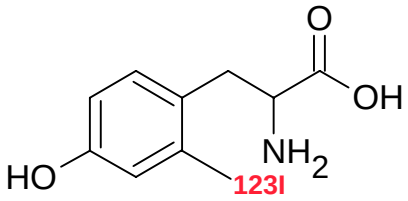

The synthesis is easy and can be performed in a Kit-formulation within 60 minutes. The radioiodination of the precursor occurs through Cu^{1+} assisted isotopic nucleophilic exchange under acidic and reducing conditions. The synthesis results in a radiochemical yield of >98% with a radiochemical purity of >98% and no purification is needed.

Until today, the only reported experiments with [^{123}I]-2-iodo-L-tyrosine are performed in vitro and in tumour bearing rats.

In vitro, [^{123}I]-2-iodo-L-tyrosine showed the same uptake affinity for the LAT1 transporter in comparison to the native L-tyrosine, suggesting that the large iodine atom does not hinder the uptake of [^{123}I]-2-iodo-tyrosine by LAT1.

In vivo in tumour bearing rats, [^{123}I]-2-iodo-L-tyrosine illustrates high and fast tumour accumulation (steady state within 30 minutes), low renal accumulation and minor accumulation in areas of acute inflammation. The low physiologic brain uptake will allow to image brain tumours (80).

1.7.2.3. [^{123}I]-3- iodo-L-tyrosine and [^{123}I]-iodo-Aza-tyrosine

The structures of these amino acids are shown in figure 1.7.

FIGURE 1.7: Structure of [^{123}I]-3-iodo-L-tyrosine and [^{123}I]-iodo-Aza-tyrosine. The modifications in comparison with the native L-tyrosine are printed in red.

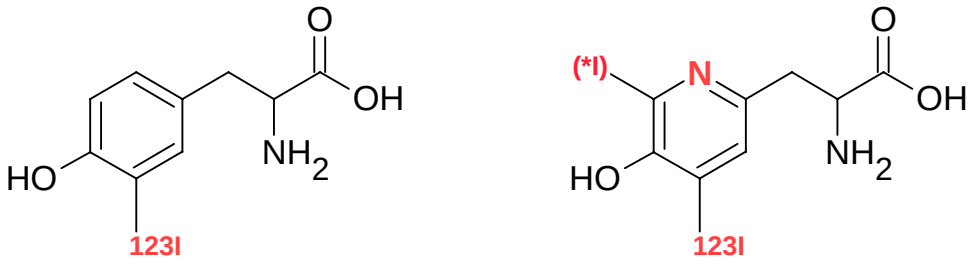

^{123}I-3-iodo-L-tyrosine ^{123}I-iodo-Aza-tyrosine

Radioiodination and purification of [^{123}I]-3-iodo-L-tyrosine and [^{123}I]-iodo-Aza-tyrosine is performed as described for IMT. The radiosynthesis yields > 95 % and > 98 % for [^{123}I]-3-iodo-L-tyrosine and [^{123}I]-iodo-Aza-tyrosine, respectively. A radiochemical purity of > 99 % is obtained for both amino acids.

The only reports found about these tracers describe the in vitro uptake of [^{123}I]-3-iodo-L-tyrosine (81) and the in vivo uptake of both tracers in tumour bearing rats (80).
The transport of [^{123}I]-3-iodo-L-tyrosine in vitro in Xenopus Leavis oocytes is isoform specific and occurs through LAT1.

Both amino acid tracers illustrate low tumour uptake and low renal accumulation. Bloodpool activity is high for [^{123}I]-iodo-Aza-tyrosine. Both tracers were rejected for further analyses because of their low tumour accumulation.

1.7.2.4. [^{123}I]-4-iodo-L-phenylalanine

The structure of [^{123}I]-4-iodo-L-phenylalanine is shown in figure 1.8.

FIGURE 1.8: Structure of [^{123}I]-4-iodo-L-phenylalanine. The modifications in comparison with the native L-phenylalanine are printed in red.

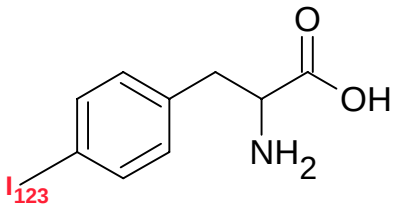

Currently, two methods are used for the radioiodination of 4-iodo-L-phenylalanine:

- Cu^{1+} assisted isotopic nucleophilic exchange as described above, yielding 98 % with a radiochemical purity of > 98% (80)
- Non-isotopic Cu^{2+} assisted [^{123}I]-iododebromination of 4-bromo-L-phenylalanine in the presence of ascorbic acid. This radioiodination method results in a 90 % radiochemical yield after HPLC isolation and a radiochemical purity of > 99 % (82)

This tracer is studied predominantly by Samnick, et al. in pancreatic tumours, in vitro as well as in vivo in tumour engrafted mice:

- In vitro: the uptake of [^{123}I]-4-iodo-L-phenylalanine in pancreas tumour cells is mediated by transport systems L and ASC. The tracer shows minor (8 %) protein incorporation and thus reflects the amino acid transport in the tumour cells.
- In vivo: [^{123}I]-4-iodo-L-phenylalanine showed high tumour uptake but the rate of tracer entering the tumour was slower in comparison to the other abovementioned amino acids. Low brain and abdominal uptake and low renal accumulation are demonstrated and are comparable to those of [^{123}I]-2-iodo-L-tyrosine. However, together with the earlier mentioned [^{123}I]-iodo-Aza-tyrosine, [^{123}I]-4-iodo-L-phenylalanine shows a high bloodpool activity (almost 2 times higher in comparison to [^{123}I]-2-iodo-L-tyrosine and IMT). Moreover, [^{123}I]-4-iodo-L-phenylalanine illustrates significant accumulation in regions of acute inflammation and thus is less tumour specific. The latter observation might be due to the high bloodpool activity of this tracer (80;82-84).

1.7.2.5. [^{123}I]-4-amino-3-iodo-phenylalanine (IAPA) and [^{123}I]-L-Iodo-1,2,3,4-tetrahydro-7-hydroxyisoquinoline-3-carboxylic acid (ITIC)

The structure of these amino acids is shown in figure 1.9.

FIGURE 1.9: Structure of [^{123}I]-4-amino-3-iodo-phenylalanine (IAPA) and [^{123}I]-L-Iodo-1,2,3,4-tetrahydro-7-hydroxyisoquinoline-3-carboxylic acid (ITIC). The modifications in IAPA in comparison with the native L-phenylalanine are printed in red.

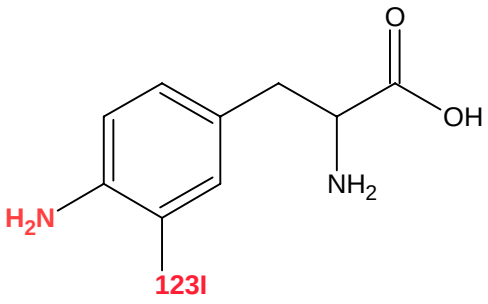

IAPA

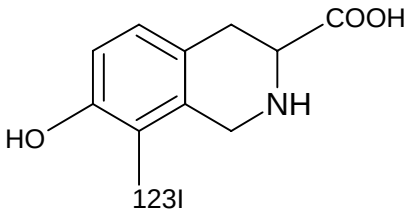

ITIC

IAPA and ITIC are prepared using the Iodogen technique followed by HPLC resulting in a radiochemical yield of 80% and a radiochemical purity of 98% for both tracers.

In vitro characterisation of IAPA and ITIC transport in gliomablastoma cells shows that IAPA is predominantly taken up by system L and ASC while system A is not involved.

By contrast, none of these three principal neutral amino acid transport systems appear to be significantly involved in the cellular uptake of ITIC. The uptake mechanism of ITIC remains unclear. Both tracers are not incorporated into the cell proteins.

In vivo in glioma bearing rats, both tracers are taken up by the tumour. While IPA showed comparable values to IMT, ITIC demonstrated significantly lower tumour uptake levels. Moreover, the initial uptake of ITIC in the tumour decreased significantly by time, suggesting an efflux from the tumour.

General biodistribution studies revealed the ITIC shows a marked renal accumulation with comparable values to IMT (83,85).

1.7.2.6. Overview of the developed radiolabelled amino acids for SPECT

TABLE 1.2: presents an overview of the characteristics of the radiolabelled L-amino acids for oncologic imaging with SPECT.

Tracer	**IMT**	**2IT**	**3IT**	**AzaTyr**	**4IPhe**	**IAPA**	**ITIC**
Synthesis	Iodogen	Cu^{1+}	Iodogen	Iodogen	Cu^{1+} or Cu^{2+}	Iodogen	Iodogen
Radiochemical yield	90%	98%	98%	95%	98% or 90%	80%	80%
Radiochemical purity	99%	98%	99%	99%	98% or 99%	98%	98%
Major transport system used	LAT1	LAT1	Not tested	Not tested	LAT1	L and ASC	Unclear
Tumour accumulation	Good	Good	Poor	Poor	Good	High	Poor
Blood clearance	Fast	Fast	Fast	Slow	Slow	Fast	Fast
Kidney accumulation	High	Low	Low	Low	Low	Low	High
Tumour specificity	High	High	Not tested	Not tested	Low	Not tested	Not tested

1.8 STATUS OF RADIOLABELLED D-AMINO ACIDS

As mentioned before, most naturally occurring amino acids possess the L-configuration. It was long believed that only L-amino acids are present in higher animals and that the D-isomers are only utilized in lower species such as micro-organisms and bacteria. However, recent studies revealed a substantial amount of D-amino acids present in mammals, more precisely D-serine and D-aspartate. The presence of other D-amino acids is negligible and mostly due to ingestion of D-amino acids.

Much attention has been paid to the physiological functions and origin of D-amino acids. D-serine is now thought to have an important role in the central nervous system to modulate the N-methyl-D-aspartate (NMDA) subtype of the glutamate receptor and D-aspartate is reported to regulate the hormonal release in endocrine glands such as testis, pituitary gland and pineal gland. Moreover, D-aspartate could have a role in ontology and

differentiation since D-aspartate increases in each tissue corresponding to the morphological and functional maturation of the tissue.

Many research groups report on the relationship between pathophysiological processes and D-amino acids. For example: not only some brain regions in Alzheimer's disease show altered D-amino acid levels but also renal disease demonstrates elevated D-amino acid levels in serum.

The use of D-amino acids in oncology might find some applications. Tamamesa et al. were the first to report on D-amino acids as potential tumour specific imaging tools. They showed the preferential uptake of some natural radiolabelled D-amino acids in comparison to the L-isoforms in tumor bearing mice. Moreover, Yanagida and co-workers showed in vitro in tumour cells that system L seems to lack stereospecificity: D-amino acids are transported with high affinity by LAT1.

Exogenous uptake of D-amino acids (by ingestion or from micro-organisms) will lead to the metabolization by D-amino acid oxidase, present in liver and kidneys, resulting in the formation of the corresponding α-keto acid and ammonium. The latter together with the stereospecificity of the translational machinery will result in the formation of proteins uniquely consisting of L-amino acids.

Regarding these characteristics, D-amino acids, transported by LAT1, will clear faster from the blood, will not incorporate into the cell proteins, and will be transported by the LAT1 transporter with high affinity, as compared to the corresponding L-isomers. As a result, promising D-amino acid tracers for in vivo oncologic imaging could be developed leading to better tumour to background contrast and less radiation burden (86-92).

1.9 AIM OF THIS THESIS

With the increasing clinical application of ^{18}F-FDG, clinical oncologic imaging through radiolabelled amino acids is also gaining interest. These amino acid tracers may help in imaging areas in which ^{18}F-FDG imaging is limited. In contrast, amino acid uptake has been demonstrated to be increased relative to normal grey and white matter in the majority of low- and high grade tumours in the brain. Moreover, amino acids appear to play a marginal role in the metabolism of inflammatory cells. Furthermore, amino acid transport is a relative rapid process and therefore tumour imaging based on amino acid transport can be performed within 20 minutes post injection (^{18}F-FDG imaging occurs generally at 60 min p.i.). Radiolabelled amino acids may thus be more suited than ^{18}F-FDG for tumour imaging (58,72,93).

Our research group focussed on the development of phenylalanine analogues, more specifically on the substitution of the iodine atom on the 2 position in phenylalanine allowing the 4 position to be free for enzymatic interaction.

It is very important to synthesize the new molecule 2-iodo-L-phenylalanine with a high and reproducible yield and without the formation of undesired side products. Moreover, if this goal could be accomplished, 2-iodo-L-phenylalanine could be used as a precursor for Kit radioiodination using the Cu^{1+}-assisted nucleophilic exchange by analogy with the radiolabelling of 2-iodo-L-tyrosine (80).

As mentioned before, two major transporter systems are over-expressed in tumours for providing the cells with nutrients. One of these systems is LAT1, a member of the L transporter family which is restricted to highly proliferating tissues. This system is responsible for the uptake of neutral branched chain and aromatic amino acids and shows a high affinity

and broad substrate selectivity. L-phenylalanine is one of those amino acids which are transported with high affinity by LAT1. However, the introduction of the large iodine atom could alter not only its uptake but also its affinity towards the transporter. In vitro characterisation of the new tracer [^{125}I]-2-iodo-L-phenylalanine could answer these questions. The R1M cell model, as used for the evaluation of [^{125}I]-2-iodo-L-tyrosine, could be applied.

Once it is demonstrated that the new tracer is transported with high affinity through the LAT1 system, the following step in the evaluation of the tracer as a tumour diagnostic tool for SPECT could be undertaken. In vivo evaluation of [^{123}I]-2-iodo-L-phenylalanine will not only elucidate the tracer behaviour in terms of biodistribution and clearance but will also demonstrate its tumour specificity. The same tumour cell line as used for the in vitro evaluation will be applied for the generation of a tumour bearing athymic mouse model.

As mentioned before, a few decades ago it was shown that both L and D amino acids are taken up in tumours and that both the L and D form of the [^{11}C]-methionine could accumulate in human brain tumours. However, the development of and the studies with radioactively labelled amino acids for tumour diagnosis were focused on the L-enantiomers as it was supposed that the amino acid tracers had to be incorporated into the tumour cell proteins. Today, it has been demonstrated that the LAT1 system is not stereoselective and that the transport of amino acids reflects the malignancy of tumours.

Regarding the latter aspects and the unnatural character of D-amino acids, our research group additionally developed [^{123}I]-2-iodo-D-phenylalanine. However, the same in vitro and in vivo evaluation as for the L-analogue should be performed to answer the question whether this [^{123}I]-2-iodo-D-phenylalanine could present additional benefits for diagnosing cancerous lesions with SPECT.

As a valorisation of the tracer characteristics for tumour imaging, the evaluation of and the comparison between both [^{123}I]-2-iodo-L-phenylalanine and [^{123}I]-2-iodo-D-phenylalanine in various tumours, representing those tumour families with highest prevalence in humans, should be performed. Moreover, an additional comparison with the recently developed tumour tracer [^{123}I]-2-iodo-L-phenylalanine would allow us to choose the optimal analogue for clinical practice.

Before introducing [^{123}I]-2-iodo-L-phenylalanine in human clinical practice, a few applications of the tumour tracer could be highlighted. On the one side veterinarian nuclear oncologic imaging is improving since the owners are prepared to give their pets the best care and on the other side, therapy evaluation is a very important topic in curing patients from cancer.

1.10. REFERENCES

1. Beutel J, Kundel HL and Van Metter RL. Handbook of Medical Imaging Volume I Physics and Psychophysics. Spie Press (2000). P375-378, 465 and 512.
2. Khalkhali I, Maublant JC and Goldsmith SJ. Nuclear Oncology Diagnosis and therapy. Lippencott Williams & Wilkins (2001). P3-12.
3. Weissleder M, Mahmood U. Molecular Imaging. *Radiology* 2001; 219:316–333
4. Jager PL. PhD Thesis 2001: Tumor imaging using L-3-[^{123}I]Iodo-alfa-methyl-tyrosine.
5. Rohren EM, Turkington TG, Coleman RE. Clinical Applications of PET in Oncology. *Radiology*:2004;231:305–332.
6. Perkins A and Frier M. Nuclear Medicine in Pharmaceutical Research. Taylor and Francis (1999)p15-28.
7. Thrall JH and Ziessman HA. Nuclear medicine: The requisites. Mosby (1995) p3-37

8. Fyles AW, Milosevic M, Wong R, et al. Oxygenation predicts radiation response and survival in patients with cervix cancer. *Radiother Oncol* 1998;48:149-156.
9. Hockel M, Schlenger K, Hockel S, et al. Association between tumor hypoxia and malignant progression: the clinical evidence in cancer of uterine cervix. *In*: Vaupel P, Kelleher DK, eds. Tumour hypoxia. Stuttgart: Wissenschafte Verlagsgesellschaft;1999:65-74.
10. Wiebe LI. PET radiopharmaceuticals for metabolic imaging in oncology. *International Congress Series* 2004;1264:53– 76
11. Van de Wiele C. Molecular imaging in oncology by means of nuclear medicine: fact or fiction? Eur J Nucl Med Mol Imaging 2004;31:151-154.
12. Lahorte CMM, Vanderheyden JL, Steinmetz N, et al. Apoptosis detecting radioligands: current state of the art and future perspectives. Eur J Nucl Med Mol Imaging 2004;31:887-919.
13. Wald LL, Nelson SJ, Day MR, et al. Serial proton magnetic resonance spectroscopy imaging of glioblastoma multiforme after brachytherapy. *J Neurosurg* 1997;87:525–34.
14. Tedeschi G, Lundbom N, Raman R, et al. Increased choline signal coinciding with malignant degeneration of cerebral gliomas: a serial proton magnetic resonance spectroscopy imaging study. *J Neurosurg* 1997;87:516–24.
15. Hara T. 18F-fluorocholine: a new oncologic PET tracer. *J Nucl Med* 2001;42:1815–6.
16. Wyss MT, Weber B, Honer M, et al. 18F-choline in experimental soft tissue infection assessed with autoradiography and high-resolution PET. *Eur J Nucl Med Mol Imaging* 2004;31:312–6.
17. Inoue T, Kim EE, Wallace S, et al: Positron emission tomography using [18F]fluorotamoxifen to evaluate therapeutic responses in patients with breast cancer: Preliminary study. *Cancer Biother Radiopharm* 11:235-245, 1996
18. Van den Bossche and Van de Wiele C. Receptor imaging in oncology by means of nuclear medicine: current status. *J Clin Oncol* 2004;22:3593-3607.
19. Blum J, Handmaker H, Lister-James J, et al. A multicenter trial with a somatostatin analog (99m)Tc depreotide in the evaluation of solitary pulmonary nodules. *Chest* 2000;117:1232–1238.
20. Thakur ML, Kolan H, Li J, et al. Radiolabeled somatostatin analogs in prostate cancer. *Nucl Med Biol* 1997; 24:105–113.
21. Decristoforo C, Mather SJ, Cholewinski W, et al. 99mTc-EDDA/HYNIC-TOC: a new 99mTc-labelled radiopharmaceutical for imaging somatostatin receptor-positive tumours; first clinical results and intra-patient comparison with 111In-labelled octreotide derivatives. *Eur J Nucl Med* 2000; 27:1318–1325.
22. Virgolini I, Raderer M, Kurtaran A, et al. 123I-vasoactive intestinal peptide (VIP) receptor scanning: update of imaging results in patients with adenocarcinomas and endocrine tumors of the gastrointestinal tract. *Nucl Med Biol* 1996; 23:685–692.
23. Nguyen DC, Parsa B, Close A, et al: Overexpression of cell cycle regulatory proteins correlates with advanced tumor stage in head and neck squamous cell carcinomas. *Int J Oncol* 22:1285-1290, 2003.
24. Klijn JGM, Berns PMJJ, Schmitz PIM, et al: The clinical significance of epidermal growth factor receptor (EGF-R) in human breast cancer: A review on 5232 patients. *Endocr Rev* 13:3-17, 1992
25. Glennie MJ and Van de Winkel GJ. Renaissance of cancer therapeutic antibodies. *Drug discovery today* 2003;8:503-510.
26. Gura T. Therapeutic antibodies: magic bullets hit the target. *Nature* 2002;417:584-586.
27. Jain M and Batra SK. Genetically engineered antibody fragments and PET imaging: a new era of radioimmunodiagnosis. *J Nucl Med* 2003;44:1970-1972.

28. Alavi A, Reivich M. Guest editorial: the conception of FDG-PET imaging. *Semin Nucl Med* 2002;32:2–5.
29. Warburg O. On the origin of cancer cells. *Science* 1956;123:309–14.
30. Rigo P, Paulus P, Kaschten BJ, et al. Oncological applications of positron emission tomography with fluorine-18 fluorodeoxyglucose. *Eur J Nucl Med* 1996;23:1641–1674.
31. Gambhir SS, Czernin J, Schwimmer J, et al. A Tabulated Summary of the FDG PET Literature. *J Nucl Med* 2001; 42:1S–93S
32. Glaser M, Luthra SK and Brady F. Applications of positron-emitting halogens in PET oncology (Review). *Int J Oncology* 2003;22: 253-267
33. Zuang H, Pourdehnad M, Lambright ES, et al. Dual Time Point 18F-FDG PET Imaging for Differentiating Malignant from Inflammatory Processes. *J Nucl Med* 2001; 42:1412–1417.
34. Yamada S, Kubota K, Kubota R et al. High accumulation of Fluorine-18-fluorodeoxyglucose in turpentine-induced inflammatory tissue. *J Nucl Med* 1995;36:1301-1306.
35. Kubota R, Kubota K, Yamada S, et al. Microautoradiographic study for the differentiation of intratumoural macrophages, granulation tissues and cancer-cells by the dynamics of Fluorine-18-fluorodeoxyglucose uptake. *J Nucl Med* 1994;35:104-112.
36. Been LB, Suurmeijer AJH, Cobben DCP, et al. [18F]-FLT-PET in oncology: current status and opportunities. *Eur J Nucl Med Mol Imaging* 2004;31:1659-1672.
37. Shields AF, Dohmen BM, Mangner TJ, et al. Use of F-18-FLT for imaging gastrointestinal tumors. *J Nucl Med* 2001;42:108.
38. Olivier P. Nuclear oncology, a fast growing field of nuclear medicine. *Nucl Instr Methods Phys Res* A 2004;527:4-8.
39. Pashankar FD, O' Dorisio S, Menda Y. MIBG and Somatostatin Receptor Analogs in Children: Current Concepts on Diagnostic and Therapeutic Use. *J Nucl Med* 2005;46:55S-61S.
40. Glasspool RM and Evans TRJ. Clinical imaging of cancer metastasis. *Eur J Cancer* 200;36:1661-1670.
41. Stryer L. biochemistry 4th edition. W.H. Freeman and Co (1995) p18-23.
42. Lodish H, Baltimore D, Berk A et al. Molecular Cell Biology, 3rd edition. Scientific American Books (1995) p52-56.
43. Christensen NC. Role of amino acid transport and countertransport in nutrition and metabolism. *Phys Rev*. 1990;70:43–77
44. Palacin M, Estevez RL, Bertran J et al. Molecular Biology of Mammalian Plasma Membrane Amino Acid Transporters. *Phys Reviews* 1998;78:969-1054.
45. Johnstone RM, Scholefield PG. Amino acid transport in tumour cells. Adv Cancer Res 1965;9:143-226.
46. Wagner CA, Lang F and Broer S. Function and structure of heterodimeric amino acid transporters. *Am J Physiol Cell Physiol* 2001;281:C1077-C1093.
47. MackEnzie B and Erickson JD. Sodium-coupled neutral amino acid (System N/A) transporters of the SLC38 gene family. *Pflugers Arch - Eur J Physiol* 2004;447:784–795.
48. Sugawara M, Nakanishi T, Fei YJ, et al. Cloning of an Amino Acid Transporter with Functional Characteristics and Tissue Expression Pattern Identical to That of System A. *J Biol Chem* 2000;275:16473–16477.
49. Sutinen E, Jyrkkiö S, Grönroos T, et al. Biodistribution of [11C]methylaminoisobutyric acid, a tracer for PET studies on system A amino acid transport in vivo. *Eur J Nucl Med* 2001; 28:847–854
50. Weiss MD, Derazi S, KilbergMS, et al. Ontogeny and localization of the neutral amino acid transporter ASCT1 in rat brain. *Developmental Brain Research* 2001;130:183–190.

51. Zerangue N, Kavanaugh MP. ASCT-1 Is a Neutral Amino Acid Exchanger with Chloride Channel Activity. *J Biol Chem* 1996;271:27991-27994.
52. Yanagida O, Kanai Y, Chairoungdua A, et al. Human L-Type amino acid transport system 1 (LAT1): characterisation of function and expression in tumour cell lines. *Biochim Biophys Acta.* 2001;1514:291–302.
53. Uchino H, Kanai Y, Kim DK, et al. Transport of Amino Acid-Related Compounds Mediated by L-Type Amino Acid Transporter 1 (LAT1): Insights Into the Mechanisms of Substrate Recognition. *Mol Pharmacol* 2002;61:729–737.
54. Pineda M, Fernandez E, Torrents D, et al. Identification of a Membrane Protein, LAT-2, That Co-expresses with 4F2 Heavy Chain, an L-type Amino Acid Transport Activity with Broad Specificity for Small and Large Zwitterionic Amino Acids. *J Biol Chem* 1999;274:19738–19744.
55. Kanai Y, Segawa H, Miyamoto KI, et al. Expression Cloning and Characterization of a Transporter for Large Neutral Amino Acids Activated by the Heavy Chain of 4F2 Antigen (CD98). *J Biol Chem* 1998;273:23629–23632.
56. Babu E, Kanai Y, Chairoungdua A, et al. Identification of a Novel System L Amino Acid Transporter Structurally Distinct from Heterodimeric Amino Acid Transporters. *J Biol Chem* 2003: 278:43838–43845.
57. Segawa H, Fukasawa Y, Miyamoto KI, et al. Identification and Functional Characterization of a Na1- independent Neutral Amino Acid Transporter with Broad Substrate Selectivity. *J Biol Chem* 1999:274:19745-19751.
58. Jager PL, Vaalburg W, Pruim J, et al. Radiolabelled amino acids: basic aspects and clinical applications in oncology. *J Nucl Med*. 2001;42:432–445.
59. Isselbacher KJ. Sugar and amino acid transport by cells in culture – differences between normal and malignant cells. *Seminars in medicine of the Beth Israel Hospital* 1972; 286:929-933.
60. Bush H, Davis JR, Honig GR, et al. The uptake of a variety of amino acids into nuclear proteins of tumors and other tissues. *Cancer Res* 1959;19:1030-1039.
61. Saier MH. Families of transmembrane transporters selective for amino acids and their derivatives. *Microbiology* 2000;146:1775–1795.
62. Daemen B, Elsinga PH, Ishiwata K, et al. A Comparative PET Study Using Different I1 C-labelled Amino Acids in Walker 256 Carcinosarcoma-bearing Rats. Nucl Med Biol 1991;12:197-204.
63. Kuwert T, Morgenroth C, Woesler B, et al. Uptake of iodine-123-alpha-methyl-tyrosine by gliomas and non-neoplastic brain lesions. *Eur J Nucl Med* 1996;23:1345-1353.
64. Roelcke U, Radu E, Ametamey S, Pellikka R, Steinbrich W, Leenders KL. Association of rubidium and C-methionine uptake in brain tumors measured by positron emission tomography. *J Neurooncol*. 1996;27:163–171.
65. Kubota K, Ishiwata K, Kubota R, et al. Tracer feasibility for monitoring tumor radiotherapy: a quadruple tracer study with fluorine-18-fluorodeoxyglucose or fluorine-18-fluorodeoxyuridine, L-[methyl-14C]methionine, [6-3H]thymidine, and gallium-67. *J Nucl Med*. 1991;32:2118–2123.
66. Derlon JM, Petit-Taboue MC, Chapon F, et al. The in vivo metabolic pattern of low-grade brain gliomas: a positron emission tomographic study using 18F-fluorodeoxyglucose and 11C-L-methylmethionine. *Neurosurgery*. 1997;40:276–287.
67. Ogawa T, Shishido F, Kanno I, et al. Cerebral glioma: evaluation with methionine PET. *Radiology*. 1993;186:45–53.
68. Wester HJ, Herz M, Weber W, et al. Synthesis and radiopharmacology of O-(2-[18F]fluoroethyl)-L-tyrosine for tumor imaging. *J Nucl Med* 199;40:205-212.

69. Heiss P, Mayer S, Herz M, Wester HJ, Schwaiger M, Senekowitsch-Schmidtke R. Investigation of transport mechanism and uptake kinetics of O-(2-[18F]fluoroethyl)-l-tyrosine in vitro and in vivo. *J Nucl Med* 1999; 40:1367–1373.
70. Weber WA, Wester HJ, Grou AL, Herz M, Dzewas B, Feldmann HJ, Molls M, Stocklin G, Schwaiger M. O-(2-[18F]-Fluoroethyl)-l-tyrosine and l-[methyl-11C]methionine uptake in brain tumours: initial results of a comparative study. *Eur J Nucl Med* 2000; 27:542–549.
71. Coenen HH, Kling P, Stocklin G. Cerebral metabolism of L-[2-18F]fluorotyrosine, a new PET tracer of protein synthesis. *J Nucl Med* 1989;30:1367–72.
72. Hustinx R, Lemaire C, Jerusalem G, et al. Whole-body tumor imaging using PET and 2-18F-fluoro-L-tyrosine: preliminary evaluation and comparison with 18F-FDG. J Nucl Med 2003;44:533–9.
73. Watanabe H, Inoue T, Shinozaki T, et al. PET imaging of musculoskeletal tumours with fluorine-18-methyltyrosine: comparison with fluorine-18 fluorodeoxyglucose PET. *Eur J Nucl Med* 2000;27:1509–17.
74. Langen KJ, Pauleit D, Coenen HH. 3-[^{123}I]iodo-alpha-methyl-L-tyrosine: uptake mechanisms and clinical applications. *Nucl Med Biol*. 2002;29:625–631.
75. Jager PL, Franssen EJ, Kool W, et al. Feasibility of tumor imaging using L-3-[iodine-123]-iodo- alpha-methyl-tyrosine in extracranial tumors. *J Nucl Med*. 1998;39:1736–1743.
76. Jager PL, De Vries EGE, Piers DA, et al. Uptake mechanisms of L-3-[125I]-iodo-alfa-methyl-tyrosine in human small-cell lung cancer cell line: comparison with L-1-[14C]-tyrosine. *Nucl Med Comm* 2001;22:87-96.
77. Schmidt D, Gottwald U, Langen KJ, et al. 3-[123I]Iodo-α-methyl-L-tyrosine uptake in cerebral gliomas: relationship to histological grading and prognosis. *Eur J Nucl Med* 2001; 28:855–861.
78. Schmidt D, Langen KJ, Herzog H, et al. Whole-body kinetics and dosimetry of L-3-[123I]iodo-a-methyltyrosine. *Eur J Nucl Med* 1997;24:1162–1166.
79. Shikano, N, Kanai Y, Kawai K, et al. Isoform Selectivity of 3-125I-Iodo-alfa-Methyl-LTyrosine Membrane Transport in Human L-Type Amino Acid Transporters. *J Nucl Med* 2003; 44:244–246
80. Lahoutte T, Mertens J, Caveliers V, et al. Comparative biodistribution of iodinated amino acids in rats: selection of the optimal analog for oncologic imaging outside the brain. *J Nucl Med.* 2003;44:1489–1494.
81. Shikano N, Aisawa Y, Miyamoto T, et al. Transcellular transport of 4-[I-125]-L-meta-Tyrosine across monolayers of kidney epithelial cell line LLC-PK1. *J Label Compd Radiopharm* 2003;46:S340.
82. Samnick S, Schaefer A, Siebert S, et al. Preparation and investigation of tumor affinity, uptake kinetic and transport mechanism of iodine-123-labelled amino acid derivatives in human pancreatic carcinoma and glioblastoma cells. *Nucl Med Biol.* 2001;28:13–23
83. Samnick S, Hellweg D, Schneider G et al. Establishment of an in vivo model of human pancreatic tumor for preclinical studies and evaluation of radioiodinated phenylalanine-analogues as radiopharmaceuticals to image pancreatic carcinomas. *J Label Compd Radiopharm* 2003;46:S78.
84. Samnick S, Hellwig D, Bader JB, et al. Evaluation of the feasibility of Photon Emission Tomography with L-p-[123I]iodophenylalanine for routinely brain tumor imaging. *J Label Compd Radiopharm* 2003;46:S398.
85. Samnick S, Richter S, Romeike BF, et al. Investigation of iodine-123-labelled amino acid derivatives for imaging cerebral gliomas: uptake in human glioma cells and evaluation in stereotactically implanted C6 glioma rats. *Eur J Nucl Med* 2000;27:1543–1551.

86. D'Annielo A, D'Onofrio G, Pischetola M, et al. Biological role of D-amino oxidase and D-aspartate oxidase. *J Biol Chem* 1993; 268:26941-26949.
87. Hamase K, Morikawa A, Zaitsu K. D-amino acids in mammals and their diagnostic value. *J Chromatogr B* 2002; 781:73-91.
88. Yang H, Zheng G, Peng X, et al. D-Amino acids and D-Tyr-tRNATyr deacylase: stereospecificity of the translation machine revisited. *FEBS letters* 2003; 552:95-98.
89. Tamemasa O, Goto R, Suzuki T. Preferential incorporation of some 11C-labeled D-amino acids into tumor bearing animals. *Gann* 1978;69:517-523
90. Tamamesa O, Goto R, Takeda A, et al. high uptake of 11C-labelled D-amino acids by various tumours. *Gann* 1982;73:147-152.
91. Fisher GH, Torres D, Bruna J, et al. Presence of D-aspartate and D-glutamate in tumour proteins. Cancer Biochem Biophys 1995;15:79-82.
92. Fisher GH. Appearance of D-amino acids during aging: D-amino acids in tumor proteins. In: D-amino acids in sequences of secreted proteins of multicellular organisms. Eds P Jolles. Birkhauser verlag, Basel/Switserland (1998) P109-118.
93. Kubota K, Yamada S, Kubota R, et al. Intramural distribution of fluorine-18-fluorodeoxyglucose in vivo: high accumulation in macrophages and granulation tissues studied by microautoradiography. *J Nucl Med*. 1992;33:1972–1980

CHAPTER 2:

Synthesis and evaluation of [$^{123/125}$I]-2-iodo-L-phenylalanine as a tumour tracer for SPECT.

CHAPTER INTRODUCTION

The first goal in this thesis is the development and evaluation of [^{123}I]-2-iodo-L-phenylalanine as a tumour tracer for SPECT.

This chapter starts with the synthesis of the cold precursor 2-iodo-L-phenylalanine and optimization of the reaction by experimental design. Precursor synthesis was performed using a new approach on the nucleophilic exchange mechanism: the Cu^{1+} assisted nucleophilic exchange in acidic and reducing conditions. The influence and relationship between selected factors and the response (yield), as well as the optimal conditions for 2-iodo-L-phenylalanine precursor synthesis using factorial design were determined. Moreover, using the cold iodo-precursor, a Kit radio-iodination based on the same principle was performed to render [$^{123/125}$I]-2-iodo-L-phenylalanine. The optimised reaction conditions together with the Kit formulation could be applied, at a later stadium of this thesis, for the precursor synthesis and radiolabelling of 2-iodo-D-phenylalanine.

Once the new tracer [$^{123/125}$I]-2-iodo-L-phenylalanine is developed, in vitro evaluation of the amino acid analogue could be carried out in a R1M rabdomyosarcoma cell model. This cell model was previously used to characterize the transport mechanism of other labelled amino acids such as [^{123}I]-2-iodo-L-tyrosine and showed that the in vitro uptake is a good representation of the in vivo uptake in rodents bearing a R1M tumour. The transport characteristics for [^{125}I]-2-iodo-L-phenylalanine uptake were examined in different buffer systems and in the presence of several inhibitors. Michaelis-Menten and Lineweaver Burk plots were applied to obtain K_m and K_i values for [^{125}I]-2-iodo-L-phenylalanine cell uptake, respectively. Moreover, the incorporation into the cell proteins of the new amino acid analogue was investigated.

Due to the promising in vitro characteristics, in vivo evaluation of [^{123}I]-2-iodo-L-phenylalanine was performed in a R1M athymic mouse model. The potential application as tumour diagnosticum was investigated by means of dynamic planar imaging and dissection. Not only tumour uptake was examined but also the excretion route of the tracer and its metabolic stability. The specificity of tumour uptake was determined by (1) a displacement study using amino acids which are predominantly transported by the LAT1 system and by (2) a biodistribution study of the tracer in NMRI mice bearing an acute inflammation. In the latter setting, the uptake of [^{123}I]-2-iodo-L-phenylalanine in the inflamed tissue was compared to that of ^{18}F-FDG. The initial uptake kinetics in the tumour are modelled by a rectangular hyperbola as used to represent saturable-pathway absorption in the in vitro experiments. These experiments were performed by analogy with the evaluation of several other amino acids such as [^{123}I]-2-iodo-L-tyrosine and IMT in rodents bearing a R1M tumour.

Additionally, the effect of sedation and data-acquisition method (dissection or planar imaging) on [^{123}I]-2-iodo-L-phenylalanine distribution in R1M-bearing athymic mice was investigated. Indeed, non-invasive animal imaging experiments require that movements of the animal should be minimized to reduce artefacts. To accomplish the latter setting, the animals were sedated using pentobarbital. However, in order to interpret the results correctly, it is important to identify the influence of sedation on tracer distribution since these preclinical data are used for human extrapolation. Kinetic modelling of the initial biodistribution kinetics was performed and statistical analyses were used to compare on the one hand the treated groups and on the other hand the data-acquisition methods.

2.1 Optimization by experimental design of precursor synthesis of 2-iodo-L-phenylalanine, a novel amino acid for tumour imaging.

Veerle Kersemans[1*]; Ken Kersemans[2]; Bart Cornelissen[1]; Ludovicus Staelens[1]; Bart De Spiegeleer[1]; John Mertens[2] and Guido Slegers[1].

[1] Laboratory for Radiopharmacy, Universiteit Gent, Harelbekestraat 72, B-9000 Gent, Belgium
[2] Laboratory for Medical Imaging and Physics, Vrije Universiteit Brussel, Laarbeeklaan 103, B-1090 Brussel, Belgium

Key words: 2-iodo-L-phenylalanine, Cu^{1+}-assisted nucleophilic exchange, DOE-optimisation of synthesis, amino acid analogue

Submitted for the Journal of Labelled Compounds and Radiopharmaceuticals

2.1.1 ABSTRACT

Various radiolabelled amino acids show promising results in tumour detection as applied in the management of cancer patients. We synthesised the precursor 2-iodo-L-phenylalanine for easier Kit labelling of [$^{123/125}$I]-2-iodo-L-phenylalanine using the Cu^{1+}-assisted nucleophilic halogen exchange. Precursor synthesis was optimised by experimental design: 8 parameters were initially screened by a quarter fractional design. The resulting most important parameters (i.e. temperature, $CuSO_4$, NaI) were further optimized using a full 3-factor 3-level factorial design. The final conclusion for the optimal values for temperature, reaction time and concentration of 2-bromo-L-phenylalanine, NaI, $CuSO_4$, $SnSO_4$, $C_6H_6O_7$ and $C_7H_6O_4$ were 180°C, 24h, 61mM, 485mM, 10mM, 90mM, 90mM and 100mM, respectively. The yield was increased from 39% to consistently more than 74% 2-iodo-L-phenylalanine. Structure confirmation and quality control was performed by ^{1}H-NMR, MS and HPLC (RP and chiral). No phenylalanine-related impurities or racemisation was detected. Subsequent radioiodination of the obtained 2-iodo-L-phenylalanine was performed in Kit conditions with n.c.a. Na$^{123/125}$I resulting in a labelling yield of >98%. After Ag-membrane filtration, a radiochemical purity of >99% was obtained. The Cu^{1+}-assisted nucleophilic exchange reaction allows both routine kit preparation and "cold" synthesis of 2-iodo-L-phenylalanine from 2-bromo-L-phenylalanine. The reaction presents an interesting alternative for a cumbersome multi-step stereospecific synthesis.

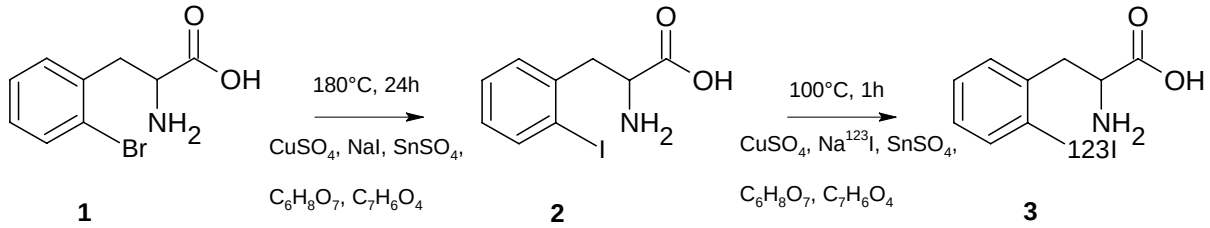

1 **2** **3**

2.1.2 INTRODUCTION

Although conventional imaging techniques such as Magnetic Resonance Imaging (MRI) are widely used as golden standards in detecting tumours, they are not reliable to distinguish normal tissue from tumour lesions after surgical resection and/or radiotherapy of the tumour. Therefore, those techniques are not optimal for monitoring the effectiveness of therapy or detecting tumour recurrence [1].

During the last decade, Positron Emission Tomography (PET) and Single Photon Emission Computed Tomography (SPECT) have become essential tools in the management of cancer patients. [^{18}F]-Fluorodeoxyglucose ([^{18}F]-FDG) is by far the most widely used PET radiopharmaceutical for oncologic imaging. However, there are several well-known disadvantages about the use of [^{18}F]-FDG: glucose metabolism is not significantly increased in all tumour types and the tracer is also accumulated in infection, inflammation, granulomatous diseases [2-3]. Moreover, due to its high brain accumulation, [^{18}F]-FDG is less sensitive in brain tumours.

Besides upregulation of the glucose metabolism, amino acid transport and protein metabolism are also increased in tumour cells. At present, [^{123}I]-3-Iodo-α-methyltyrosine (*I-IMT) is the only routinely used SPECT amino acid tumour tracer for diagnosis. This tracer has major advantages in comparison to [^{18}F]-FDG such as high and fast tumour uptake and rather low uptake in grey matter and inflammatory lesions. However, its marked long term renal accumulation limits its use for oncologic imaging outside the brain and leads to dosimetry exposure problems [4]. Recently, 2-iodo-L-tyrosine and 4-Iodo-L-phenylalanine have been developed and evaluated to overcome this problem but either difficult precursor synthesis or sourcing and high bloodpool activity, respectively, restricts their clinical application.

Recently, we developed a new analogue, i.e. [$^{123/125}$I]-2-iodo-L-phenylalanine, which shows promising characteristics for the study of residual and recurrent tumours [5].Its synthesis was performed by a Cu^{1+} assisted nucleophilic exchange under acidic and reducing conditions, as developed by Mertens et al., with the unlabelled 2-iodo-L-phenylalanine as precursor [6]. Although numerous reports described radiolabelling of aromatic substrates using the latter method, no report published its application for “cold” precursor synthesis and none investigated its optimisation using experimental design. The aim of this study was to examine the influence and the relationship between selected factors and the response (yield) as well as to determine the optimal conditions for 2-iodo-L-phenylalanine precursor synthesis using factorial design.

Other nucleophilic exchange reactions are also widely used. However, often low and irreproducible reaction yields are obtained together with the generation of undesired side products resulting in cumbersome purification procedure. The described Cu^{1+} assisted nucleophilic exchange not only provides an easy 1-step, stereospecific, reaction but also the possibility to establish a Kit-formulation for fast and quantitative routine radioiodination of [$^{123/125}$I]-2-iodo-L-phenylalanine without the need of an extra purification procedure, which is a great added value for everyday clinical practice.

2.1.3 MATERIALS AND METHODS

All reagents used were obtained from commercially available sources. All of the conventional products mentioned were at least analytic or clinical grade and obtained from Sigma-Aldrich. The solvents were of HPLC quality (Chemlab, Belgium). The Na[$^{123/125}$I] was purchased from Bristol-Myers-Squibb, Belgium.

2.1.3.1. Preparation of the precursor 2-iodo-L-phenylalanine (2)

2.1.3.1.1. Optimisation of the reaction parameters

2-iodo-L-phenylalanine (**2**) was synthesized as a precursor for Cu^{1+}-assisted radioiodine labelling. 2-bromo-L-phenylalanine (**1**) was obtained by Peptech Corp, USA.

At first, 2-iodo-L-phenylalanine was prepared from 2-bromo-L-phenylalaline in testing conditions using the Cu^{1+}-assisted nucleophilic exchange under acidic and reducing conditions taken into account the optimal substrate to Cu^{1+} molar ratio range of 5 à 10 as reported by Gysemans et al.: equimolar quantities of substrate and nucleophile, together with an excess (duplicate molar quantities in comparison to Cu^{1+}) of reducing agents and a substrate to catalyst (Cu^{1+}) molar ratio range of 5 à 10 [7,8]. This resulted in 30.0mM 2-bromo-L-phenylalanine, 4.6 mM $CuSO_4$ anhydrous, 9.0mM citric acid anhydrous, 9mM gentisic acid, 9.0mM $SnSO_4$ and 45mM NaI dissolved in 13.5 mL distilled water. The mixture was flushed for 15 minutes with N_2 and a sample was analyzed by RP-HPLC and chiral chromatography. Next, the reaction mixture was placed at 130°C for 15 hours. After the reaction, the mixture was cooled down and a sample was analyzed by RP-HPLC and chiral chromatography.

The reaction yield was calculated as: concentration of 2-iodo-L-phenylalanine divided by the sum of the concentrations of 2-iodo-L-phenylalanine and 2-bromo-L-phenylalanine, using the HPLC relative response factor of 4.66, representing the ratio of the UV-absorption of 2-iodo-L-phenylalanine divided by that of the bromo-derivative.

The reaction was performed in a closed (solid top cap) pyrex single-neck round-bottom flask of 25mL with screw thread neck (Glassware-system-45; Sigma-Aldrich, Belgium). The reaction yield of the synthesis was determined by RP-HPLC as described below. 2-iodo-L-phenylalanine was purified by preparative RP-HPLC as mentioned below and the product was identified by ^{1}H-NMR and mass spectroscopy. The UV molar extinction coefficients were determined as described below.

Starting from the abovementioned reaction parameters, an optimisation of these reaction parameters was performed. The experimental design construction and its statistical analysis were performed using Statgraphics 5.1. At first, the parameters of most influence on the reaction yield were determined using a quarter-fractional factorial screening design. The parameters tested were: reaction temperature, reaction time, [$CuSO_4$], [$SnSO_4$], [gentisic acid], [citric acid], [2-bromo-phenylalanine] and [NaI]. The intervals for testing are shown in Table 2.1.1.

TABLE 2.1.1: Quarter fractional screening design for main effects

Parameters	Levels		ANOVA-results
	Low	High	P-value
Time	1h	24h	0.145
Temperature	50°C	180°C	0.000
2-bromo-L-phenylalanine	1 mM	60.6 mM	0.952
$CuSO_4$	1 mM	50 mM	0.115
Citric acid	1 mM	90 mM	0.888
$SnSO_4$	1 mM	90 mM	0.732
Gentisic acid	1 mM	100 mM	0.963
NaI	1 mM	500 mM	0.076

The maximum temperature was set at 180°C due to physical limitations (pressure in pyrex recipient was to high) and the concentration of substrate was set at a maximum of 61mM due to financial limitations. A second optimisation was performed using a 3-level full factorial design. The intervals are shown in Table 2.1.2.

TABLE 2.1.2: Full factorial 3-factor 3-level design

Parameters	Levels		
	Low	Center	High
Temperature	80°C	130°C	180°C
$CuSO_4$	1 mM	25.5 mM	50 mM
NaI	1 mM	250.5 mM	500 mM

At last, the reaction was performed using the optimised reaction conditions in order to confirm the high reaction yield, to proof the identity and to confirm the absence of possible related byproducts (incl. racemisation) of the product under these conditions.
Moreover, the reaction yield as a function of pH under the optimised conditions was determined.

2.1.3.1.2. Purification of 2-iodo-L-phenylalanine

The solvent of the reaction mixture was removed by rotatory evaporation after reaction. The dry residu was solubilised in 10mL mobile phase used for preparative HPLC purification and the pH was adjusted with NaOH to pH 5.5. After centrifugation at 800g for 5 minutes in a Heraeus Christ Labofuge A Centrifuge, the supernatans was removed and filtered over a Millex HA 0.45µm filter (Millipore). Preparative RP-HPLC was used to purify 2-iodo-L-phenylalanine from 2-bromo-L-phenylalanine and consisted of a Hibar Lichrosorb RP-select B column (250 x 25mm, 7µm) (Merck, Belgium), a Shimadzu LC-8A preparative liquid chromatograph pump and a Waters 486 Tunable Absorbance Detector for UV-detection at λ=254 nm. As mobile phase, a 20/80 MeOH/H_2O containing 1mM ammoniumacetate eluens adjusted to pH 5.5 with HCl was used at a flow rate of 13 mL/min. The eluate corresponding with 2-iodo-L-phenylalanine was collected after which the mobile phase was removed by means of rotatory evaporation. The dry residu was solubilised in 10 ml methanol, filtered and

evaporated. After repeating these last manipulations three times, 2-iodo-L-phenylalanine could be isolated as an off-white powder.
Retention times on this preparative RP-HPLC system: 2-iodo-L-phenylalanine = 27.2 min and 2-bromo-L-phenylalanine = 20.2 min.

2.1.3.2. Preparation of [$^{123/125}$I]-2-iodo-L-phenylalanine (3)

Radiolabelling of the precursor 2-iodo-L-phenylalanine with $^{123/125}$I was performed using the Cu^{1+}-assisted isotopic exchange, by analogy with the radiosynthesis of [^{123}I]-MIBG and [^{123}I]-iodo-L-tyrosine [8,9]. Radioiodination with $^{123/125}$I (37 MBq, no carrier added; 10µl) of 1.0 mg 2-I-L-phenylalanine was performed under acidic and reducing conditions (0.2 mg $CuSO_4$, 2.5 mg citric acid, 0.5 mg $SnSO_4$, 1.3 mg gentisic acid in 565 µl) in a closed conical glass vial (Perbio Science, Belgium). Before the Na[$^{123/125}$I] solution was added, the vial was purged for 15 minutes with nitrogen gas. Subsequently, the radioactivity was injected and the vial was placed into a specially designed stainless steel container. The closed container was placed into boiling water. After 60 minutes, the reaction was stopped by cooling the system with cold water. The reaction mixture was drawn up in a syringe containing the appropriate amount of "make-up solution" (tri-sodium citrate dihydrate, 71 mM) to render the solution isotonic and to adjust the pH to at least 4. The reaction mixture was sent through a 0.22 µm Ag-filter (Millipore, Belgium) to remove free $^{123/125}I^-$ and a sterile 0.22 µm filter (Millipore, Belgium) into a sterile vacuum vial. Identification and quality control was achieved as mentioned below by HPLC and Sep-Pak C18 classic (Waters, Belgium). Chiral chromatography (described below) was used to confirm the absence of 2-I-D-phenylalanine.

2.1.3.3. Identification and quality control

2.1.3.3.1. Chiral chromatography:

Chiral chromatography was used to check the absence of 2-iodo-D-phenylalanine and consisted of a Chirobiotic T column (150 x 4.6 mm, 5µm) (Astec, Belgium), a Waters 515 HPLC Pump, UV-VIS detector at λ=254 nm (Waters 486 Tunable Absorbance Detector).
As eluens for the separation of the stereoisomers, a 20/80 EtOH/H_2O containing 1mM NH_4Ac buffer adjusted with HCl to pH5.5 was used at a flow rate of 1 mL/min.
The HPLC capacity factors (k' values): 2-iodo-D-phenylalanine = 4.8 en 2-iodo-L-phenylalanine = 3.4 (retention times are 4.6 min and 3.5 min repectively; t_0 = 0.8 min).

2.1.3.3.2. RP-HPLC

Reversed-phase HPLC consisted of a Lichrocart RP-8 column (125 x 4 mm, 5µm) (Merck, Belgium) and a Gilson 307 pump, UV-VIS detector at λ=254 nm (2487 dual λ absorbance detector, Waters). To analyze radiolabelled compounds, a NaI detector (Bicron FrisktechTM, probe 1×1 inch) was used. As eluens for the separation of the radiolabelled compound, a 20/80 MeOH/H_2O solution containing 1mM NH_4Ac buffer adjusted with HCl to pH5.5 was used at a flow rate of 1 mL/min.

The retention time of each product used was determined in order to identify the additional peak of the sample after heating.

The HPLC capacity factors (k' values): 2-iodo-L-phenylalanine = 5.6 and 2-bromo-L-phenylalanine = 4.0 (retention times are 5.9 min and 4.5 min, respectively with t_0 = 0.9 min).

2.1.3.3.3. Sep-Pak C18

Additionally to RP-HPLC, Sep-Pak C18 classic (Waters, Belgium) was used to determine the yield of radioiodination. The Sep-pak was preconditioned with 8 ml MeOH followed by 4 ml 0.9% NaCl solution and 4 ml of 0.1M KH_2PO_4 buffer at pH6. Subsequently, 10 µl of the reaction mixture was eluted slowly with 6ml of 0.1M KH_2PO_4 buffer at pH6. Both eluens, which contains the free $^{123/125}I^-$, and Sep-Pak, which contains the radioiodinated 2-iodo-L-phenylalanine, were counted on radioactivity using a Capintec CRC-15R, Ramsey, NJ, USA and the radiochemical yield was calculated.

2.1.3.3.4. Structural confirmation of 2-iodo-L-phenylalanine

The melting point of 2-iodo-L-phenylalanine was determined in a Büchi Melting Point 510. ^{1}H nuclear magnetic resonance (NMR) spectra were recorded on a Bruker AMX-500 NMR Spectrometer at the High Resolution NMR Centre of the VUB. Mass spectra were determined on a VG Quattro II triple quadropole mass spectrometer with electrospray ionisation (ESI) interface in the positive mode (Micromass, Manchester,UK).

The precursor 2-iodo-L-phenylalanine was identified by mass spectroscopy and ^{1}H NMR. In the mass spectrum, a base peak at m/z of 292 (M+1) and a smaller fragment at 293 (M+2) was observed, with no fragmentation under the experimental analytical conditions. The peaks observed in the ^{1}H-NMR were attributed to N**H$_2$** (δ 2.9), NH_2-C**H**-COOH (δ 3.8), phenyl-C**H$_2$** (δ 3.2 and 3.4), phenyl-C**H** (ortho) (δ 7.1), phenyl-C**H** (meta) (δ 7.4 and 7.9), phenyl-C**H** (para) (δ 4.8). Moreover, both spectra showed that the end-product did not contain decomposition products. The melting point was 243.7°C and confirmed on the one hand the identification by mass and ^{1}H-NMR spectra and on the other hand the purity of the product.

UV spectral data, recorded on a UV-VIS detector (LKB Biochrom ULTROSPEC K 4053 kinetics spectrometer), of 2-bromo-L-phenylalanine and 2-iodo-L-phenylalanine dissolved in aqueous methanol (i.e. mobile phase of HPLC system) showed the typical substituted benzene-aromatic maxima around 210-233 (K-band; ε = 2.8 resp. 4.8 x 10^3 l.mol^{-1}.cm^{-1}) and 263-265 nm (B-band; ε = 0.198 resp. 0.570 x 10^3 l.mol^{-1}.cm^{-1}) (Figure 2.1.2). A bathochromic shift from 2-bromo-L-phenylalanine to 2-iodo-L-phenylalanine is observed, consistent with the mesomeric differences between the 2 aromatic auxochromic halogen-substituents.

2.1.4. RESULTS

Eight parameters were initially considered as potentially significant factors influencing the yield (Table 2.1.1).

The pH was not defined as a separate factor in this experimental design, because this parameter was itself a function of the reagents and their concentrations. Moreover, it was already known that an acidic medium was required. The pH of the 67 experimental units showed indeed a mean value of 1.94±0.30 (n=67). After the optimisation, the influence of pH was demonstrated by a simple one-factor-at-a-time experiment, confirming the acidity requirement of this reaction (Figure 2.1.1).

FIGURE 2.1.1: Influence of the pH on the reaction yield of the precursor 2-iodo-L-phenylalanine.

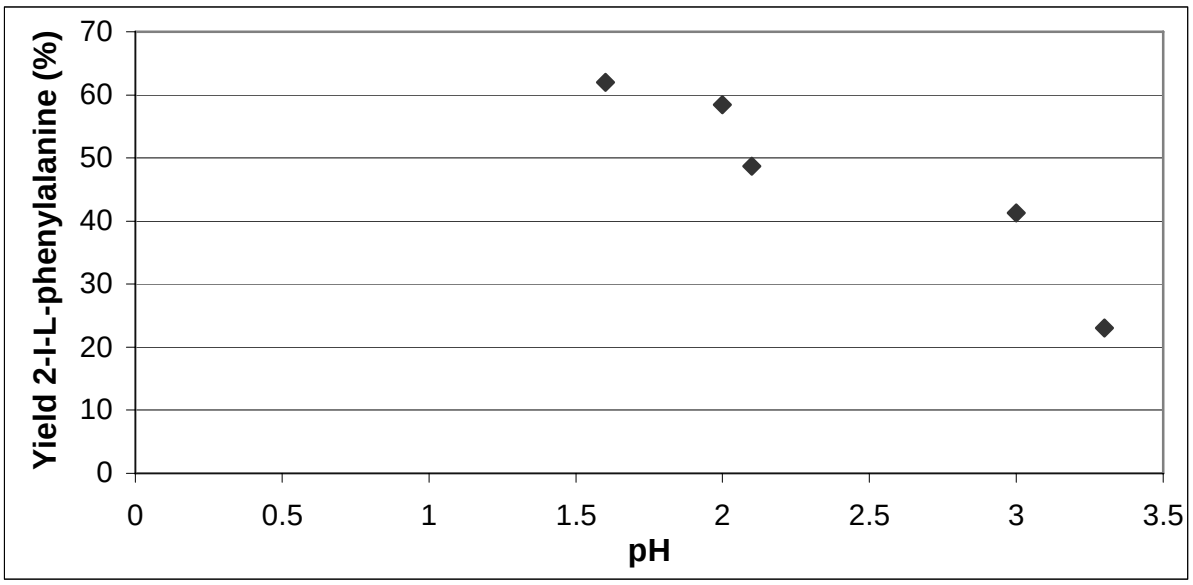

The response was the percentage yield (% molar conversion), defined as:
(mmoles 2-iodo-L-phenylalanine formed / mmoles initial 2-bromo-L-phenylalanine)*100%.

The response was so defined because the major objective of this study was the optimisation of the 2-iodo-L-phenylalanine synthesis, allowing one to obtain as economically as possible this precursor at high quality, where the commercially available 2-bromo-L-phenylalanine was the cost-driver and not the unlabelled NaI. It was obtained by RP-HPLC peak area integration, taking into account the relative response factor of the iodo-derivative versus the bromo-derivative at the detection wavelength of 254 nm (Figure 2.1.2). The mass balance was verified by comparing the initial molar quantity of 2-bromo-L-phenylalanine with the sum of the resultant reaction mixture of 2-iodo-L-phenylalanine and 2-bromo-L-phenylalanine. A mean value percentage deviation of -0.18 % (st.dev. = 1.77 %; n = 67) was obtained, in agreement with the observation that no phenyl-alanine related impurities were detected in the chromatograms.

FIGURE 2.1.2: UV spectra of both 2-bromo-L-phenylalanine (1) and 2-iodo-L-phenylalanine (2) at 1.07 x 10^{-3} mol.l^{-1} and 4.8 x 10-4 mol.l^{-1}, respectively in aqueous methanol.

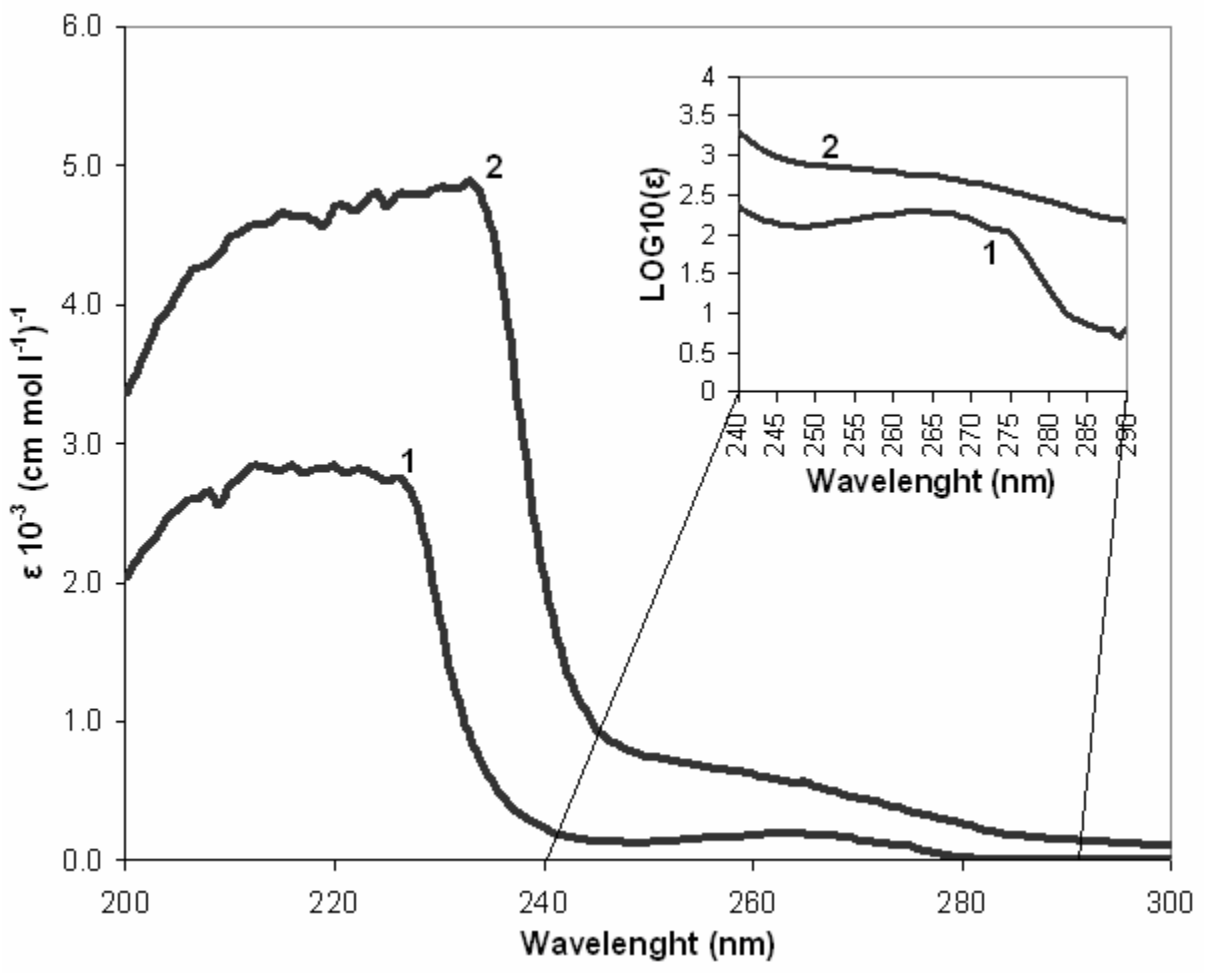

Seen the number of parameters, a quarter-fractional factorial design was used for the initial screening to estimate the main effects of the eight factors. This design requires minimally only $2^{(8-2)}$ which equals 64 runs. To avoid bias, the runs were performed in a totally random order. The fractional factorial design consisting of 64 factorial points was supplemented with triplicate centre points which were located in the middle of the experimental region.

Among the various treatments in the screening design, the highest molar conversion (90%) was obtained with the highest temperature (180°C) for 1 hour, while all other reagents were at 1mM concentration. Several experimental units showed no HPLC-detectable molar conversion and these yield-results were set equal to zero.

The experimental results of this screening design were analyzed by ANOVA to estimate the main effects, fitting the following model:

$$Y = \beta_0 + \sum_{i=1}^{8} \beta_i X_i + \sum_{i=1}^{7} \sum_{j=i+1}^{8} \beta_{ij} X_i X_j$$

where Y is the response (% molar conversion), β_i are the coefficients and X_i are the uncoded independent variables. The main effects together with the most important two-factor interaction terms (P-value <0.2) were retained in the final evaluation. The levels of the

parameters, as well as the ANOVA significance conclusions for the main effects are given in Table 2.1.1. Graphical representation of the main effects is visualised in Figure 2.1.3.

FIGURE 2.1.3: Main effects plot, resulting from the screening design. Temp: temperature; Phe: 2-bromo-L-phenylalanine; CA: citric acid and GA: gentisic acid.

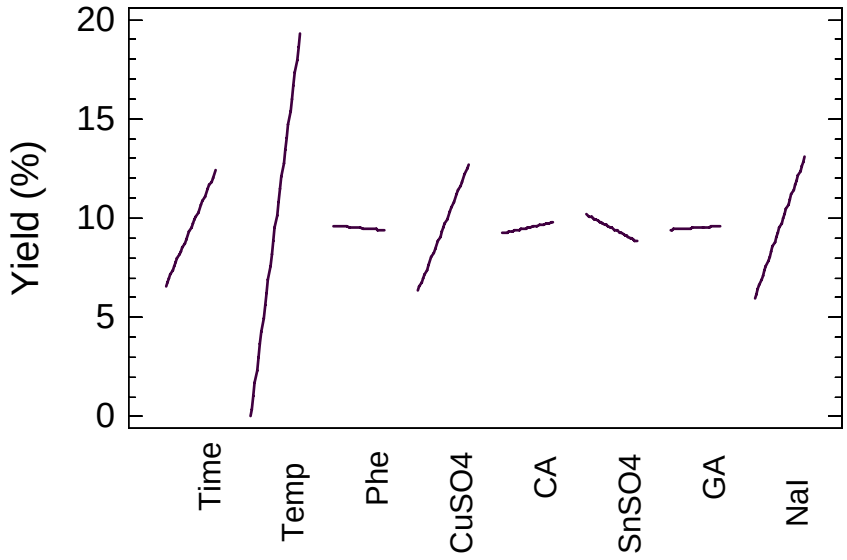

Clearly, the energy-input (time and temperature), as well as cupper-catalyst and NaI-substrate concentration are the most important factors. Several interaction terms (data not shown) were also statistically significant. As cupper occurred most frequently in these interaction terms, it was decided to include this parameter also in the full-factorial design, despite its non-significant main effect (P-value of 0.115). Although time occurred also in five interaction terms, this parameter was not included in the full factorial design for practical, experimental reasons as well as its known energy-input relation with temperature.

Having established the most important factors as temperature, $CuSO_4$ and NaI concentrations from the initial screening design, second order quadratic effects were estimated by a 3-level factorial design, allowing to measure the curvature of the response. In this second-order model, squared terms are thus also included:

$$Y = \beta_0 + \sum^{3}_{i=1} \beta_i X_i + \sum^{3}_{i=1} \beta_{ii} X_i^2 + \sum^{2}_{i=1} \sum^{3}_{j=i+1} \beta_{ij} X_i X_j$$

The 3 variables together with their levels applied are given in Table 2.1.2. The other reaction parameters were set fixed at 24 hours (reaction time) 61mM 2-bromo-L-phenylalanine, 90mM citric acid, 90mM $SnSO_4$ and 100mM gentisic acid. Twenty-seven (i.e. 3^3) experimental units were performed and the experimental yields were fitted to the second order polynomial:

$$\text{Yield} = 5.28\text{x}10^{1} - 1.08\ \text{Temp} + 4.61\text{x}10^{-3}\ CuSO_4 - 9.39\text{x}10^{-3}\ \text{NaI} + 8.44\text{x}10^{-4}\ \text{Temp}.CuSO_4 + 1.75\text{x}10^{-3}\ \text{Temp}.\text{NaI} + 6.13\text{x}10^{-4}\ CuSO_4.\text{NaI} + 4.64\text{x}10^{-3}\ (\text{Temp})^2 - 1.09\text{x}10^{-3}\ (CuSO_4)^2 - 3.65\text{x}10^{-4}\ (\text{NaI})^2.$$

A coefficient of determination of 0.85 was obtained with temperature and NaI as the statistically significant factors (main as well as interaction and quadratic terms of both). $CuSO_4$ concentration was not statistically significant, nor is interaction and quadratic terms. Figure 2.1.4 shows the comparison between the experimental data and the predictions given by the previous equation.

FIGURE 2.1.4: Predicted (from full factorial design) versus experimental values of yield (%).

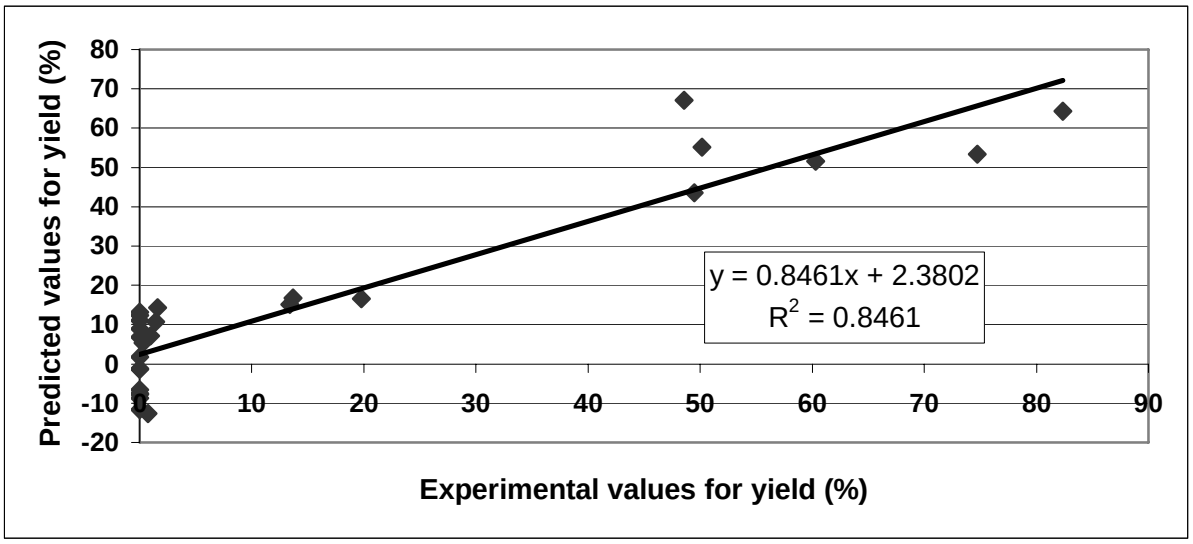

Using this 3-level factorial design, the optimal reaction conditions for temperature, CuSO4 and NaI concentration were 180°C, 49mM and 500mM, respectively. Due to the physical limitations of the glassware used, the optimum for reaction temperature was not reached. As mentioned previously, no statistically significant influence of the tested $CuSO_4$ concentrations within the experimental region on the reaction yield could be demonstrated. Figure 2.1.5 shows the response surface plot for the two remaining significant factors temperature and NaI.

FIGURE 2.1.5: Response surface plot for the significant factors temperature and NaI concentration, obtained from the full factorial design (level of $CuSO_4$: 25.5 mM).

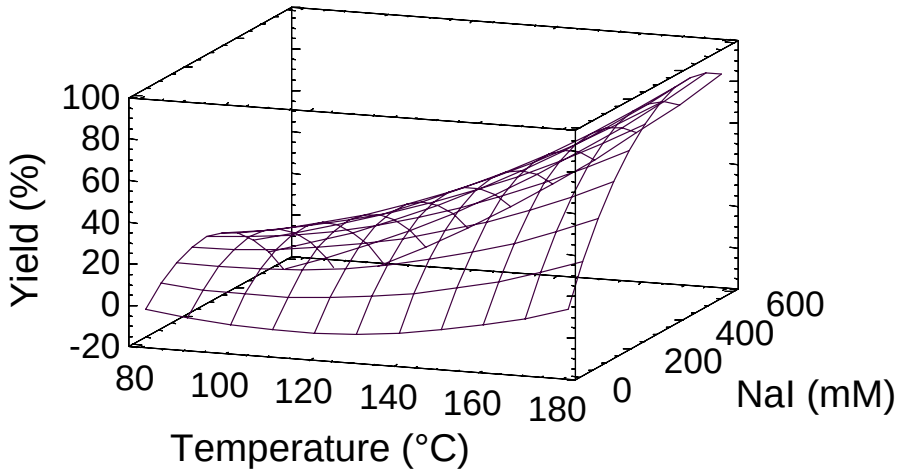

Chemical identity as well as its chemical purity was confirmed by melting point, ^{1}H-NMR, spectroscopy and chromatography (see experimental section). Chiral chromatography demonstrated the absence of 2-iodo-D-phenylalanine when performing the reaction at optimal conditions.

Subsequent radioiodination with [Na^{123}I] of 2-I-L-phenylalanine by Cu^{1+}-assisted isotopic exchange showed a labelling yield of over 98% [^{123}I]-2-iodo-L-phenylalanine (**3**) (expressed on original quantity of Na^{123}I). This radio-chemical synthesis was followed by Ag-membrane filtration, obtaining a radiochemical purity of >99% and a specific activity of 11 GBq/mmol. Thus, additional purification of the reaction mixture is not necessary which allowed us to conduct the radio-synthesis as a Kit. It was shown by chiral radio-chromatography that there was no detectable amount of D-analogues. No optimisation of the radioiodination of 2-iodo-L-phenylalanine was necessary since the radiochemical yield and purity was already very high using the conditions as described for 2-iodo-L-tyrosine [9].

2.1.5. DISCUSSION

Mertens et al. first described the Cu^{1+}-assisted nucleophilic exchange radioiodination method with a minimal quantity of side products [10]. Cu^{2+} was in situ reduced into Cu^{1+} in an acidic and reducing medium with an excess of Sn^{2+} ions and gentisic acid. Evidence was given that the Cu^{1+}-assisted nucleophilic exchange radioiodination proceeds by the formation of an intermediate organo-copper complex (Figure 2.1.6) with a suggested optimal substrate to Cu^{1+} molar ratio range of 5 à 10 under the applied experimental conditions [8].

FIGURE 2.1.6: Proposed mechanistic model for the Cu^{1+} assisted nucleophilic exchange in acidic and reducing conditions. Ar = aromatic phenylalanine moiety; Y = Br or I; X = I.

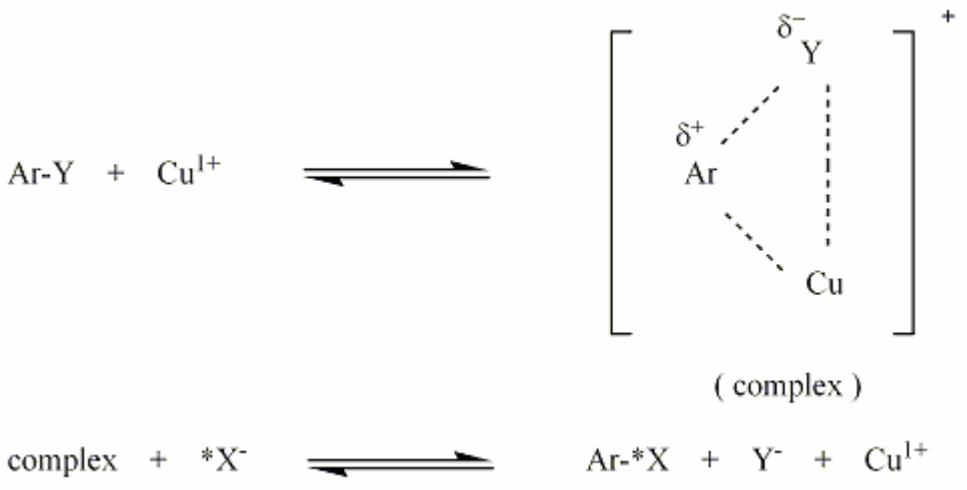

In this study, this Cu^{1+} nucleophilic exchange reaction was applied and optimised for the "cold" precursor synthesis of 2-amino-3-(2-iodophenyl)propanoic acid or 2-iodo-L-phenylalanine (**2**) from 2-amino-3-(2-bromophenyl)propanoic acid or 2-bromo-L-phenylalanine (**1**).

Mertens et al. indicated that the acidic pH of the reaction mixture was important to avoid the hydrolysis of Sn^{2+} and thus avoiding precipitation [7]. A separate experiment was performed to verify this and the results confirmed that an increase of pH resulted in a decrease of the reaction yield (Figure 2.1.1).

The optimal molar substrate to Cu^{1+} ratio range of 5 à 10, proposed by Mertens and co-workers, was not confirmed using optimisation by experimental design: no interaction between the latter factors was observed. This discrepancy could be explained by the analysis method. Indeed, a one-factor-at-a-time analysis does not take into account the interaction between the fixed factors.

2.1.6. CONCLUSION:

The Cu^{1+}-assisted nucleophilic exchange synthesis of 2-iodo-L-phenylalanine occurs without changing the stereospecificity and presents an interesting alternative for a cumbersome multi-step stereospecific synthesis. High yields and radiochemical purities were obtained. The following conditions are proposed as optimal for the "cold" synthesis of the 2-iodo-L-phenylalanine precursor from 2-bromo-L-phenylalanine: reaction time of 24hours, reaction temperature of 180°C, 61mM 2-bromo-L-phenylalanine, 90mM citric acid, 100mM gentisic acid, 90mM $SnSO_4$, 48mM $CuSO_4$ and 500 mM NaI.

2.1.7. REFERENCES:

1. Buonocore E: Comparison of PET with conventional imaging techniques. *In*: Hubner KF, Collmann J, Buonocore E, et al (eds): Clinical Positron Emission Tomography. St Louis MO, Mosby Year Book, 1992, pp 17-27.
2. Strauss LG. Flourine-18-deoxyglucose and false-positive results: a major problem in the diagnostics of oncological patients. *Eur J Nucl Med* 1996;23:1409-1415.
3. Kubota K, Yamada S, Kubota R, Ishiwata K, Tamahashi N and Ido T. Intramural distribution of fluorine-18-fluorodeoxyglucose in vivo: high accumulation in macrophages and granulation tissues studied by microautoradiography. *J Nucl Med*. 1992;33:1972–1980
4. Jager PL, Vaalburg W, Pruim J, de Vries EGE, Langen KJ and Piers DA. Radiolabelled amino acids: basic aspects and clinical applications in oncology. *J Nucl Med*. 2001;42:432–445
5. Kersemans V, Cornelissen B, Kersemans K, Bauwens M, Achten E, Dierckx RA, Mertens J and Slegers G. In Vivo Characterization of 123/125I-2-iodo-LPhenylalanine in an R1M Rhabdomyosarcoma Athymic Mouse Model as a Potential Tumour Tracer for SPECT. *J Nucl Med* 2005;46:532-539.
6. Gysemans M, Mertens JJR. Cu(I) assisted nucleophilic exchange radiohalogenation – application and mechanistic approach.
7. Mertens J, Gysemans M; Cu^{1+}-assisted nucleophilic exchange radiohalogenation: application and mechanistic approach. In: *New Trends In Radiopharmaceutical Synthesis, Quality Assurance And Regulatory Control*. New York: Plenum Press; 1991:53–65.
8. Wafelman AR, Konings MCP, Hoefnagel CA, Maes RAA, Beijnen JH. Synthesis, radiolabelling and stability of radioiodinated of m-Iodobenzylguanidine: a review. *Appl Radiat Isot* 1994;45:997-1007.
9. Lahoutte T, Mertens J, Caveliers V, Franken PR, Everaert H and Bossuyt A. Comparative biodistribution of iodinated amino acids in rats: selection of the optimal analog for oncologic imaging outside the brain. *J Nucl Med.* 2003;44:1489–1494.
10. Mertens JJR, Vanryckeghem W, Carlsen L. Cu(I) supported isotopic exchange of arylbound iodide, new future for fast high yield labelling. In: *Progress in Radiopharmacy, Proceedings of the Second European Symposium on Radiopharmacy and Radiopharmaceuticals* (Cox P., Ed.), 1986, p101, Martinus Nijhoff, The Hague.

2.2 Synthesis, Radiosynthesis and In vitro characterisation of [^{125}I]-2-iodo-L-phenylalanine in a R1M rhabdomyosarcoma cell model as a new potential tumour tracer for SPECT.

J. Mertens[13]*, V. Kersemans[2], M. Bauwens[1], C. Joos[1], T. Lahoutte[1], A. Bossuyt[1], G. Slegers[2,3].

[1] Nuclear Medicine Department/BEFY, Vrije Universiteit Brussel, Laarbeeklaan 103, 1090 Brussel, Belgium,
[2] Radiopharmacy Department, Universiteit Gent, Harelbekestraat 72, B9000 Gent, Belgium
[3]Inter University Institute for Radiopharmaceutical Chemistry

Keywords: [^{125}I]-2-iodo-L-phenylalanine, Kit preparation, LAT1 transport uptake, specific tumour tracer, SPECT

Nuclear medicine and Biology 2004; 31:739-746

2.2.1. ABSTRACT

[^{125}I]-2-iodo-L-phenylalanine, a new radioiodinated phenylalanine analogue was evaluated as a potential specific tumour tracer for SPECT. The tracer is obtained with an overall radiochemical yield of at least 98 %, a purity of > 99 % and a specific activity of 11 MBq/mmole in one pot Kit conditions using the Cu^{1+} assisted isotopic exchange. The tracer is evaluated in vitro using R1M rat rabdomyosarcoma cells in HEPES buffer with and without Na^+ ions and in MEM buffer. The uptake of [^{125}I]-2-iodo-L-phenylalanine follows a reversible pseudo first order reaction which is the same in presence and absence of Na^+ ions, but the compound is not incorporated into the cell-proteins. The reversible uptake is proven to occur with the same affinity as L-phenylalanine by a saturable transport system which is competitively inhibited by BCH, a L transport type selective molecule. Trans-stimulation of the efflux by BCH and typical L transported amino acids shows that the transporter is of the anti-port type and fulfils all the properties of the LAT1 heterodimer transport system. [^{125}I]-2-iodo-L-phenylalanine is thus a phenylalanine analogue that for the uptake uses for the major part the LAT1 transport system which is known to be over-expressed in tumour cells. This, together with the easy Kit preparation, makes [^{123}I]-2-iodo-L-phenylalanine a promising tumour specific tracer for SPECT.

2.2.2. INTRODUCTION

[^{11}C]-labelled and [^{18}F]-labelled L-amino acid analogues show a better tumour selectivity in comparison to [^{18}F]-FDG which is considerably taken up in inflammatory tissue [1,2,3].

Amino acid transport across the cell membrane is mediated via amino acid transport systems. Among the different amino acid transport systems, the Na^+-independent L-type LAT amino acid transport system 1 (LAT1 system) is a major route for providing cells with large amino acids including branched or aromatic amino acid analogues. The LAT1 transport system is a capacitive limited transport system functioning through a 1:1 anti-port exchange of amino acids [4,5]. The subtype LAT1, covalently bound by a disulfide bridge to the heavy chain type II glycosylated membrane protein 4F2hc, required for functional surface expression, is highly expressed in proliferating tissue to support the high-level protein synthesis for continuous growth and proliferation and shows a broad selectivity for large neutral amino acid analogues like L-phenylalanine, L-tyrosine [5,6,7] and iodo-alfa-methyl-L-tyrosine [8,9,10]. This amino acid transport system is heavily up-regulated in tumour tissue and has only a very limited expression in normal tissue [5]. The over-expression of this type of transport system in R1M cells was proven by the uptake of [^{3}H]-L-phenylalanine , [^{3}H]-L-tyrosine and of [^{125}I]-2-iodo-L-tyrosine which occurred for the largest part (> 85 %) by the Na^+ independent L system, more specifically the LAT1 system [11]. The aim of this study is to characterise *in vitro* in the same cell model [^{125}I]-2-iodo-L-phenylalanine ([^{125}I]-2-I-L-Phe), with the bulky iodine atom at the 2-position, as a potential new tracer for tumour diagnosis with SPECT.

2.2.3. MATERIALS AND METHODS

All the conventional products mentioned were at least analytical or clinical grade. The solvents were of HPLC quality.

2.2.3.1 Synthesis of the precursor

2-iodo-L-phenylalanine (2-I-L-Phe) was prepared using the Cu^{1+} non-isotopic exchange method [12,13]. Briefly, in a reaction vial, a 10 ml aqueous solution containing 30.3 mM 2-bromo-L-phenylalanine (Peptech Corp., Burlington, Ma,USA), 4.46 mM $CuSO_4$ (Merck), 8.9 mM citric acid (Merck), 9.0 mM $SnSO_4$ (Merck), 10.7 mM gentisic acid (Merck) and 44.5 mM NaI (Merck) was added. The solution is flushed with N_2 for 10 minutes and heated at 160 °C for 16 hours under N_2 atmosphere. After centrifugation the solution containing the product was transferred to a new flask and the water was evaporated. After reuptake in an appropriate volume of mobile phase, purification was performed by HPLC using a 7 µm Hibar Lichrosorb RP-select column (250 x 25 µm) and 20/ 80 MeOH (Merck)/ H2O containing 1 mM NH_4Ac (Merck) (pH 5.5, λ = 261 nm) at

13 ml/min. Further purification was performed by repeated dissolving of the remaining precipitate in MeOH coupled to evaporation of the MeOH fraction.

2.2.3.2. Radiochemistry

[^{125}I]-2-iodo-L-phenylalanine ([^{125}I]-2-I-L-Phe) was prepared using the Cu^{1+} assisted Kit preparation method [12,13]. In a 1 ml septum-closed vial, 28 µl of a $CuSO_4.5H_20$ (Merck) solution ($1.3x10^{-8}$ mol/µl) was added to a mixture of 2-I-L-Phe (1 mg), $SnSO_4$ (0.5 mg), gentisic acid (Merck) (1.25 mg) and citric acid (Merck) (2.5 mg) in 500 µl H_2O. This solution was flushed with N_2 for 10 minutes. 37 MBq Carrier-free sodium [^{125}I] iodide in 10^{-2} M NaOH (Bristol-Meyers Squibb Pharma, Belgium) was added. The reaction vial placed in a septum-closed closed safety container was heated at 100 °C during 60 minutes. The reaction mixture followed by 500 µl of a 71 mM Na_3-citrate solution was passed through a sterile 0.22 µm Ag-membrane filter (Millipore).

2.2.3.3. Quality Control

Quality control of 2-I-L-Phe and the radioiodinated analogue was achieved by HPLC, using a C8-column (LichrosPher 100RP8 (5 µm), Lichrocart 125-4) and 10/90 MeOH/H_2O (v/v) containing 1 mM NH_4Ac as mobile phase at 1.0 ml /minute while monitoring UV absorption (Shimadsu UV detector, 280 nm) and radioactivity (NaI-detector).
Chiral chromatography was performed on a 5µm Chirobiotic T (Astec) column (150 mm x 4.6 mm) using 80/20 Methanol/H_2O (v/v) containing 20 mM ammonium acetate at a flow of 1 mL/ minute. In these conditions a complete separation of the chiral isomers was obtained.
The capacity values (k') of L-2-I-Phe and D-2-I-Phe were 2.7 and 3.8, respectively.

2.2.3.4. Cell model

2.2.3.4.1. Cell cultures

R1M rhabdomyosarcoma cells (VUB) were cultivated in cell culture flasks (NUNC) at 37 °C and a 5% CO_2 atmosphere in MEM (Minimum Essential Medium with Earl's salts and with L-glutamine) (Invitrogen) in the presence of 10 % (v/v) Foetal Bovine Serum (FBS) (Invitrogen), 100 IU/mL Penicilline (Invitrogen) and 100µg/mL Streptomycine (Invitrogen). For in vitro experiments cells were cultivated in 6-well-plates (NUNC) for 2 days until adhesive mono-layers, containing about 4 (± 0.2) million cells per well were obtained.

2.2.3.4.2. In vitro evaluation

All in vitro experiments were carried out in 6-well-plates, using three wells for each data-point. Influx and efflux were studied both in a Na^+ containing buffer (HEPES+ (Sigma), 100 mM NaCl (Merck), 2 mM KCl (Sigma), 1 mM $MgCl_2$ (Merck), 1 mM $CaCl_2$ (Merck), 10 mM Hepes (Sigma), 5 mM Tris (Merck), 1 g/L glucose (Merck) and 1 g/L Bovine Serum Albumine (Sigma), pH = 7,4), a Na^+ free buffer (HEPES-, 100 mM Choline-Cl (Sigma), 2 mM KCl, 1 mM $MgCl_2$,1 mM $CaCl_2$, 10 mM Hepes, 5 mM Tris, 1 g/L glucose and 1 g/L Bovine Serum Albumin, pH = 7,4) and MEM buffer (pH 7.2, containing essential and non essential amino acids of which 1.2 mM of amino acids known to be transported by the L transport system). The process was terminated by physical withdrawal of the buffer and washing three times with ice-cold phosphate-buffered saline (PBS). Subsequently, the cells were detached from the well with 2 mL of 0, 1 M NaOH. The radioactivity of the samples was counted using a gamma-counting-system (Cobra-inspector 5003, Canberra Packard, Meriden, CT, USA).

This cell model was already used for the evaluation of several radioiodinated amino acids which were later on tested in vivo in tumour bearing rats. It was shown that the *in vitro* uptake results could accurately predict the uptake obtained later *in vivo* in rodents. [14,15].

2.2.3.4.3. Time and concentration dependency

The cells were incubated for times ranging from 1 to 20 minutes in 1 ml of 0.1 mM 2-I-L-Phe in HEPES+ and HEPES- or MEM containing 37 KBq [^{125}I]-2-I-L-Phe. [^{3}H]-L-phenylalanine (Amersham Biosciences) or [^{3}H]-L-tyrosine (Perkin Elm, Canberra) were used as reference products. Saturation of the uptake was measured at 15 min with concentrations of 2-I-L-Phe varying from 0.01 to 0.2 mM. The data were fit to the Michaelis-Menten relation and the $K_{m,apparent}$, V_{max} and K_i values were calculated from Eady-Hofstee and Hanes-Woolf and Lineweaver-Burk (LWB) plots. "$K_{m\ apparent}$" is the combination of the K_m values related to the transport system(s) involved.

2.2.3.4.4. Inhibition of [^{125}I]-2-I-L-Phe influx

In these inhibition experiments the cells were incubated with 37 KBq [^{125}I]-2-I-L-Phe for 15 minutes in HEPES+ and HEPES- buffer supplemented with 5 mM L-phenylalanine or BCH (2-Amino-2-norbornane-carboxylic acid). LWB plots were used for the calculation of Ki.

2.2.3.4.5. Trans- stimulation of [^{125}I]-2-I-L-Phe efflux

The cells were incubated with 37 KBq [^{125}I]-2-I-L-Phe for 15 minutes in HEPES+ and HEPES- buffer. The incubation medium was removed and the cells were washed three times with ice-cold PBS. Subsequently HEPES buffer containing 5 mM L-phenylalanine or 5mM BCH or MEM buffer was added. The efflux medium was removed after 20 minutes; the cells were washed three times with ice-cold PBS, detached with 0.1 M NaOH, suspended and counted.

2.2.3.4.6. Incorporation into cell proteins

The cells were incubated with the radioactive amino acid for a period ranging from 15 minutes up to 18 hours in MEM under constant CO_2 partial pressure (5%) using the GENBOX system. After removal of the radioactive solution, the cells were submitted twice to efflux conditions in fresh MEM solution and washed with ice cold PBS buffer. Precipitation of proteins was performed by adding 2 mL of 20 % trichloroacetic acid, intense mixing (vortex) followed by cooling during 30 minutes at 0 °C. After two times of repeated centrifugation and washing, 2 ml of 0.1 M NaOH was added and radioactivity was counted.

2.2.4. RESULTS

2.2.4.1. Chemistry and radiochemistry

The mean yield of the precursor-synthesis of 2-I-L-Phe under the applied experimental conditions was 65 %. Chiral chromatography showed that the reaction conditions involved did not induce chiral modification leading to the formation of 2-iodo-D-phenylalanine

The labelling yield in Kit conditions was at least 98 %. The final product showed a radiochemical purity of > 99 %. The specific activity was 10.9 GBq/mmol. Chiral chromatography showed that no chiral modification occurred during labelling leading to the formation of [^{125}I]-2-iodo-D-phenylalanine. The product was stored at 4 °C. HPLC analysis during the long time course of the experiments revealed the quality of the preparation to be stable for at least a month. After that period a few percent of free radioiodide was observed. This was quantitatively removed by passing the solution through a sterile 0.22 µm Ag-membrane filter (Millipore). [^{125}I]-2-I-L-Phe also remained stable in the “cell model” conditions.

2.2.4.2. In vitro evaluation

2.2.4.2.1. Kinetic model

The change of radioactivity (*AA) inside the cells reflects the change of specific activity of the "tracer amino acid" as related to the transported amino acids inside and outside the cells using the same transport system(s) as the radioactive amino acid analogue.

The uptake of radioactivity $(*AA,t)_{in}$ as a function of time for cells in equilibrium with the medium shows a rectangular hyperbolic shape reaching an equilibrium $(*AA,eq)_{in}$.

The “uptake as function of the time” kinetics can be represented by:

$$1/(*AA_t)_{in} = 1/(*AA_{eq})_{in} + [t_{1/2} /(*AA_{eq})_{in}] \; 1/t \qquad (1)$$

The velocity at initial conditions with $t << t_{1/2}$ is

$$V_0 = [d(AA_{t=o,in}) /dt]_{t=o} \sim *AA_{eq,in}/ t_{1/2} \qquad (2)$$

$$= 1/*AA_{eq} + (1/V_0) \; 1/t \qquad (3)$$

It allows an accurate estimation of V_0 from a 3 points uptake - time curve around $t_{1/2}$.

The time kinetics equation for a reversible first order reaction is given by:

$$*(AA_t)_{in} / (*AA_{eq})_{in} = 1\text{-}e^{-K_R .t} \text{ with } K_R = k \text{ influx} + k \text{ efflux} \qquad (4)$$

Applying series expansion and assuming that $K_R t >>> (K_R t)^2$ equation *(4)* can be approximated by:

$$*(AA_t)_{in} / (*AA_{eq})_{in} = 1/(*AA_{eq})_{in} + [1/(*AA_{eq})_{in} . K_R] \; 1/t \qquad (5)$$

The reversible exchange of *AA, ruled by an anti-port transport system (see transport type characteristics), represented by the rectangular hyperbole, can be assumed theoretically to behave as a reversible pseudo first order reaction.

In equations *(1)* and *(5)* $[*AA_t]_{in}$ and $[*AA_{eq}]_{in}$ reflect the specific activity respectively related to the amount of free neutral amino acid exchanged and the amount present in the tumour cells.
At equilibrium, per unit of volume:

$$[*AA_{i,eq} / \Sigma \kappa i \; . \; mAA_i]_{out} = [*AA_{i,eq} / \Sigma \kappa i \; . \; mAA]_{in} \qquad (6)$$

with:
- m amount in moles in outer (out) compartment or in the cells (in)
- $\Sigma \kappa i \; . \; mAAi$ representing all the amino acids using the same transport system(s) and κi their relative Km values (for the LAT anti-porter system it is assumed that $[\kappa i]_{in} \neq [\kappa i]_{out}$ [7]) .

Equation *(6)* shows that as long as the amount of tracer is negligible as compared to the amount of natural amino acids using the same transport system(s), there is no need for extremely high specific activity.

2.2.4.2.2. Uptake-time kinetics

The uptake of [^{125}I]-2-I-L-Phe/2-I-L-Phe increases with time following a hyperbole to reach an equilibrium value of 4.5 ± 0.2% per million cells up from 15 minutes (Figure 2.2.1).

FIGURE 2.2.1: Uptake of [^{125}]-2-I-L-Phe/ 2-I-L-Phe as function of time in different buffer systems. Calculated time course based on mean data from HEPES$^-$ and HEPES$^+$. Data expressed as mean ± SD (n = 3).

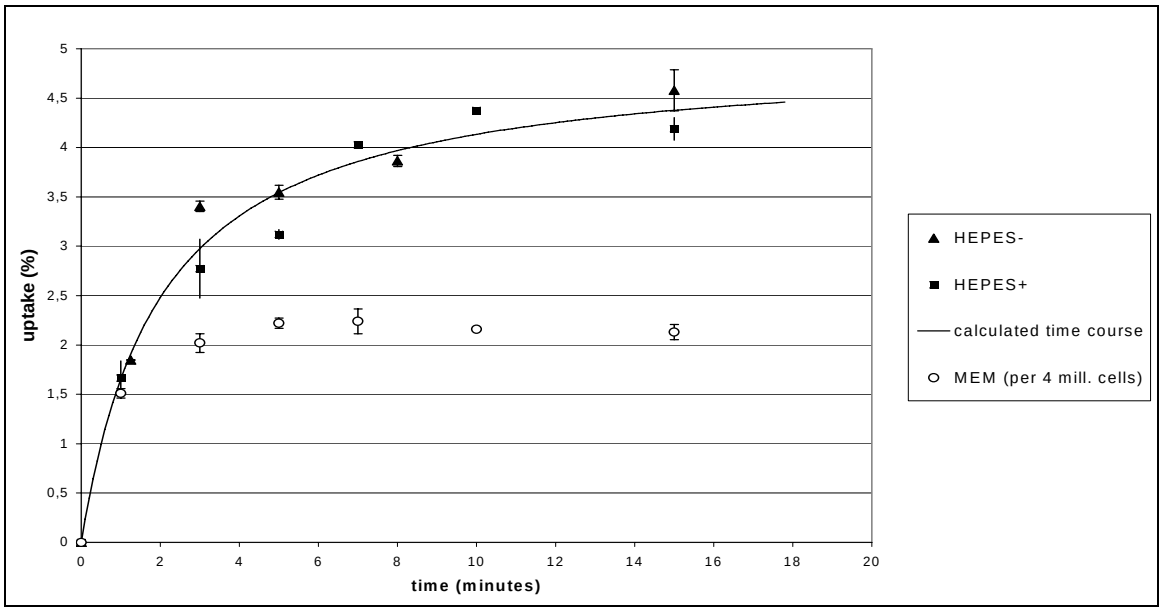

When plotting $1/(*AA_t)_{in}$ as a function of 1/t for the uptake of 2-[^{125}I]-L-Phe the same linear relationship ($R^2 > 0.97$) was obtained in both buffer systems (Figure 2.2.2).

FIGURE 2.2.2: Uptake of [^{125}I]-2-I-L-Phe/2-I-L-Phe: plot of $1/(*AA_t)_{in}$ as function of 1/t. Data are expressed as mean ± SD (n=3).

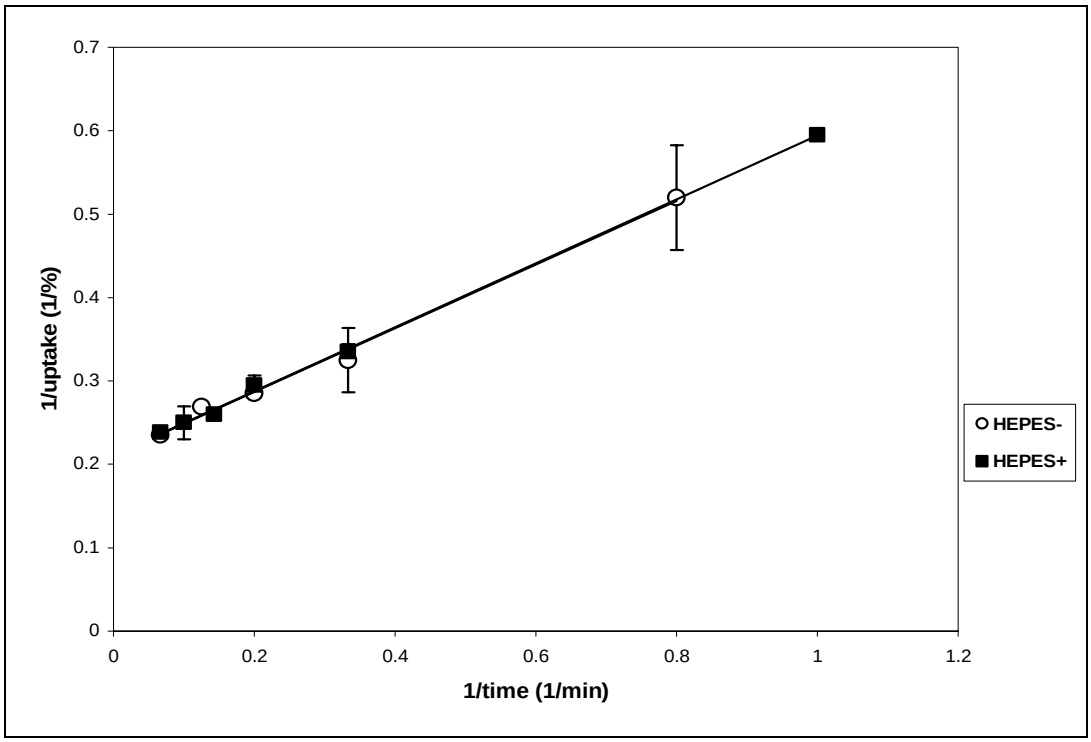

The results obtained when applying equations (1) and (3) are represented in Table 2.2.1.

TABLE 2.2.1: Calculated kinetic parameter values applying equations *(1), (3) and (5)*.

	Vo (% uptake/minute)	$t_{1/2}$: hyperbole (minutes)	$(*AAeq)_{in}$ (% uptake)	$t_{1/2}$: rev.1st order (minutes)
HEPES+	2.6	1.82	4.76	2.6
HEPES-	2.6	1.80	4.74	2.6

Figure 2.2.1 shows that the theoretical time course hyperbole calculated from these values fits the experimental data. The uptake kinetics of [^{125}I]-2-I-L-Phe are the same as the short time kinetics (up to 15 minutes) obtained for [^{3}H]-L-phenylalanine ($[^{*}AA_{in}]_{eq}$ = 4.8 % per million of cells and $t_{1/2}$ = 1.9 minutes). The uptake of [^{125}I]-2-I-L-Phe in MEM is lower in comparison to the uptake in HEPES^{-} and HEPES^{+}.

In figure 2.2.3, the linear relation between $Ln\{([*AA_{eq}]_{in} - [*AA_t]_{in}) / *AA_{eq,in}\}$ and the time shows that the apparent capacitively limited uptake, represented by the rectangular hyperbole, can be approached by a reversible pseudo first order reaction (equation *(6)*).

FIGURE 2.2.3: Uptake of [^{125}I]-L-2-I-Phe as function of time: Pseudo reversible first order fit. Data expressed as individual points.

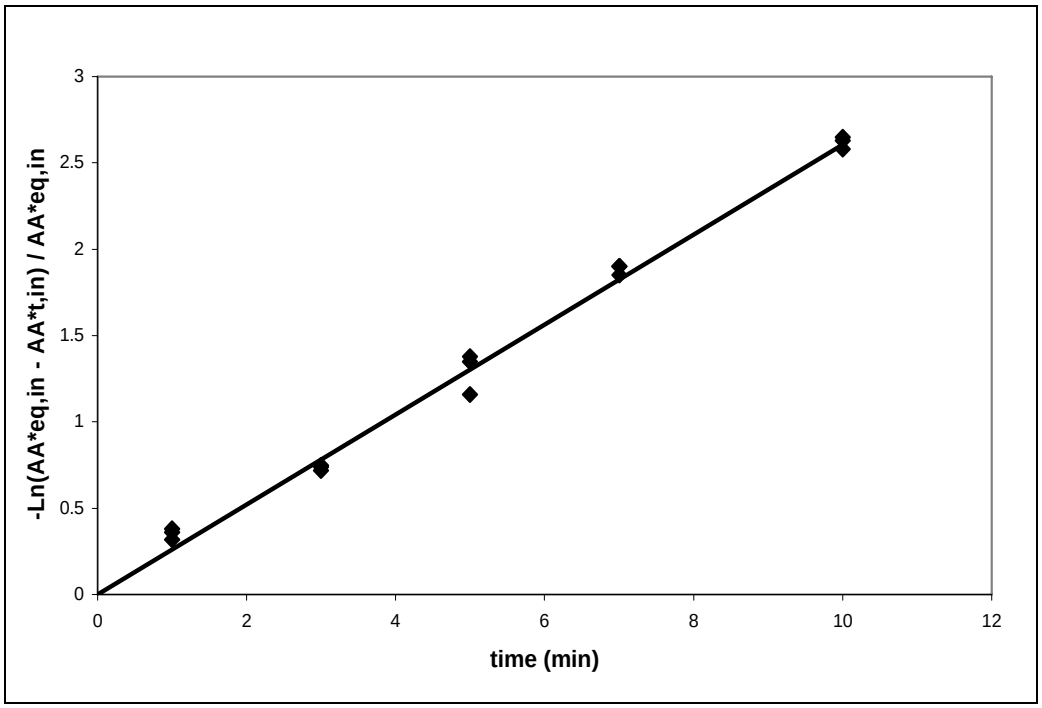

2.2.4.2.3. Concentration depending kinetics

The uptake at the 15 minutes time point (exchange rate at equilibrium) of [^{125}I]-2-I-L-Phe/2-I-L-Phe for concentrations ranging from 0.1 to 2 mM in HEPES+ was measured. The uptake as a function of concentration is saturable and follows the Michaelis-Menten relation (Fig 2.2.4).

FIGURE 2.2.4: Uptake of [^{125}I]-2-I-L-he2-I-L-Phe in HEPES+: Michaelis-Menten plot. Data: mean ± SD (n=3). Calculated curve based on generated K_m and V_{max} data.

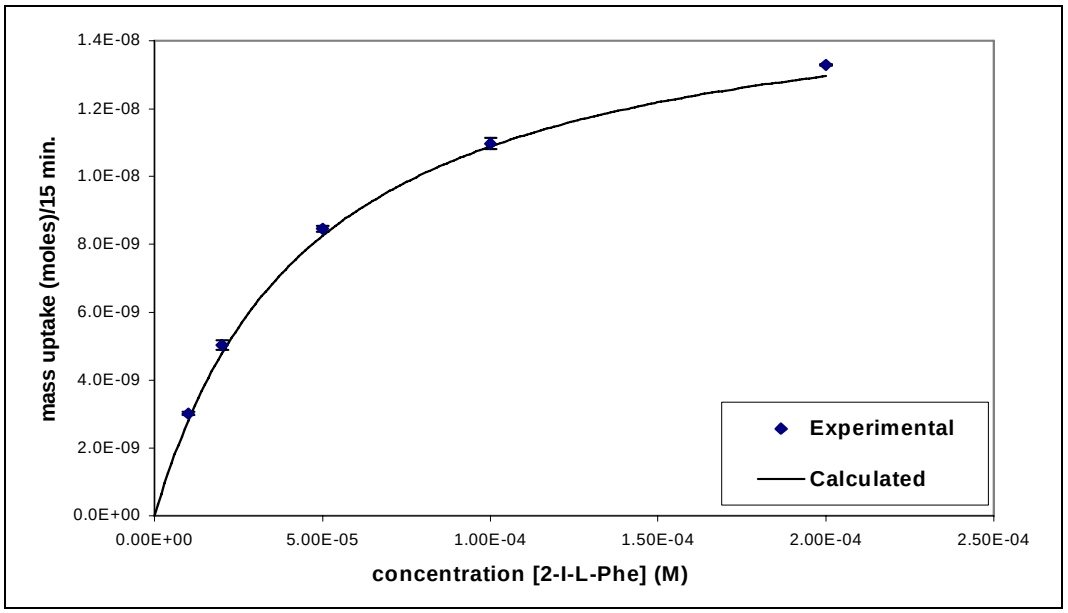

The related Eady-Hofstee (Fig. 2.2.5) shows a single substrate – transport system interaction. The resulting apparent Km value is 46 µM and is comparable to these of [^{3}H]-L-tyrosine (Km: 39 µM) and [^{3}H]-L-phenylalanine (Km: 55 µM) in the same conditions. The calculated simulation using the experimental $Km_{,apparent}$ and Vmax values fits the experimental curve completely (R^2 >0.97) (Fig. 2.2.4).

FIGURE 2.2.5: Uptake of [^{125}I]-2-I-L-Phe/2-I-L-Phe in HEPES+: Eady-Hofstee plot. Data: mean ± SD (n = 3).

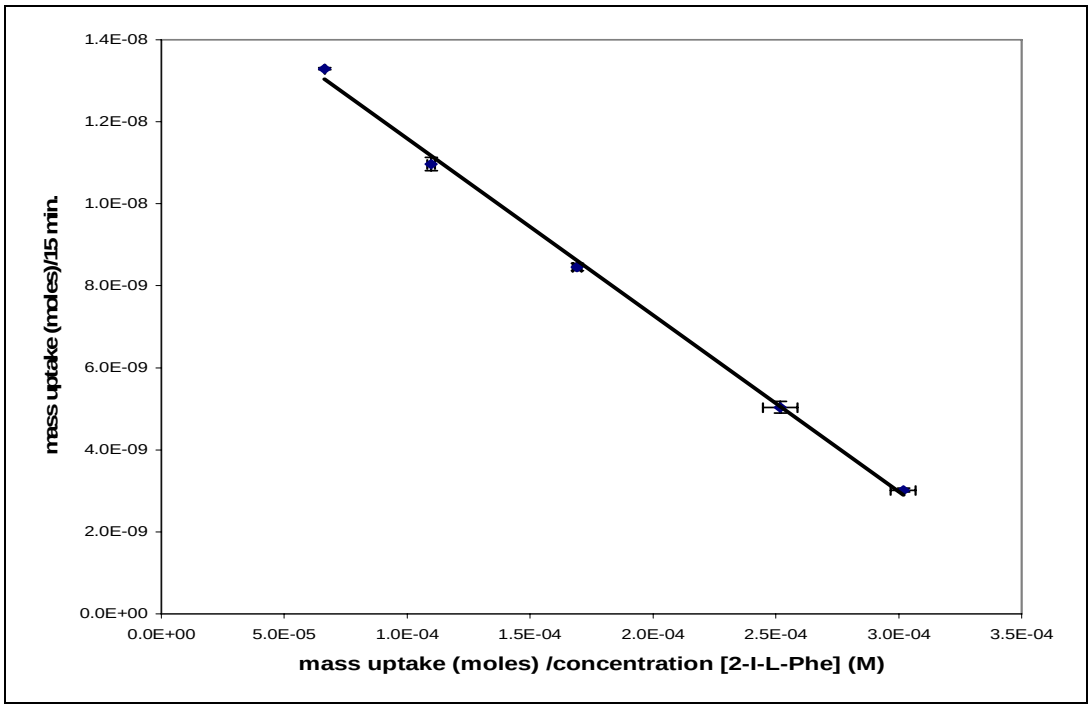

3.4.2.4. Transport Type Characterisation

The uptake of [^{125}I]-2-I-L-Phe was reduced to 15 % of the original value by the presence of 5 mM BCH, and to 3 % by 5 mM L-phenylalanine in both HEPES- and HEPES+. Moreover, the inhibition of [^{125}I]-2-I-L-Phe uptake by BCH, phenylalanine and tyrosine was competitive as revealed from a double-reciprocal Lineweaver-Burk plot showing different lines for different concentrations of inhibiting compound with different slopes but the same intercept on the 1/mass-uptake axis. Inhibition of ^{3}H-L-phenylalanine/L-phenylalanine concentration dependent uptake by 2-I-L-Phe related Lineweaver-Burk plots also showed a typical competitive inhibition pattern (Fig. 2.2.6) resulting in an apparent Ki value of 57 μM for 2-I-L-Phe.

FIGURE 2.2.6: Inhibition of the uptake of ^{3}H-L-phenylalanine/L-phenylalanine (lower) by 2-I-L-Phe (upper): Lineweaver- Burk plots. Data are expressed as mean ± SD (n=3).

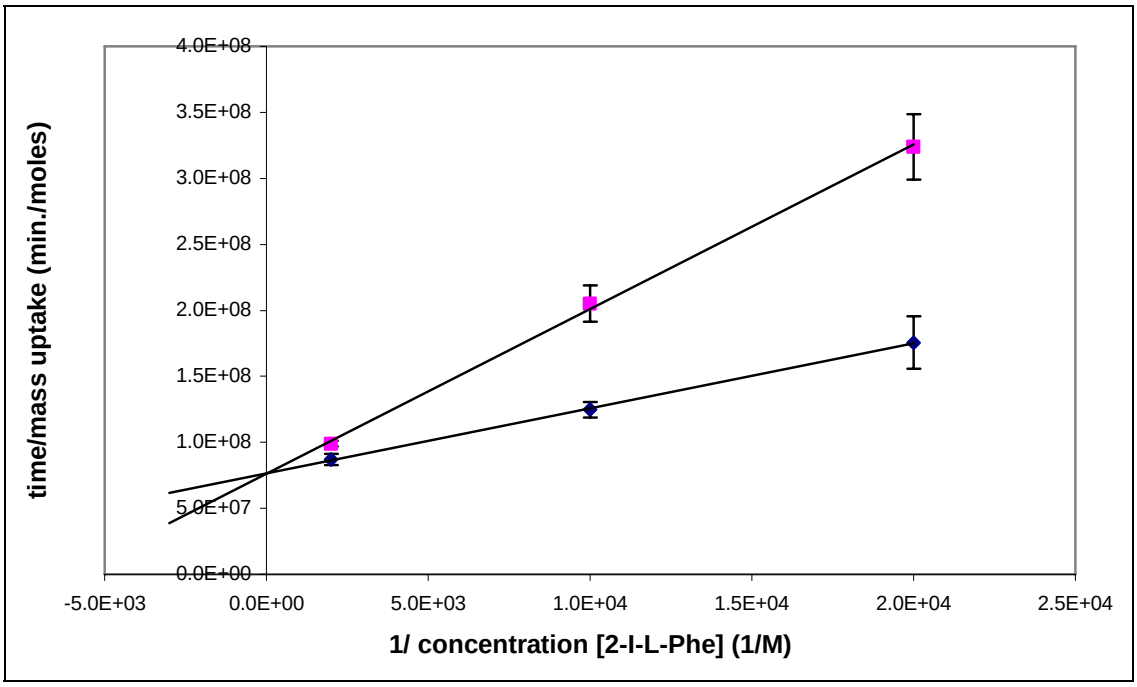

3.4.2.5. Protein incorporation paradigm

[^{125}I]-2-I-L-Phe is not significantly (< 1% of the uptake) incorporated into the R1M cell proteins. A slight apparent accumulation after repeated stimulated effluxes in MEM can be explained by the fact that the huge excess of natural amino acids inside the cell compete for transport with [^{125}I]-2-I-L-Phe resulting in an apparent bounded aspect.

Fig. 2.2.7 shows the total uptake as well as the incorporated fraction of [^{3}H]-L-phenylalanine in R1M cells as function of time.

FIGURE 2.2.7: Uptake (upper curve) and incorporation (lower curve) of [^{3}H]-L-phenylalanine/ L-phenylalanine as function of time. Data are expressed as mean ± SD (n = 3).

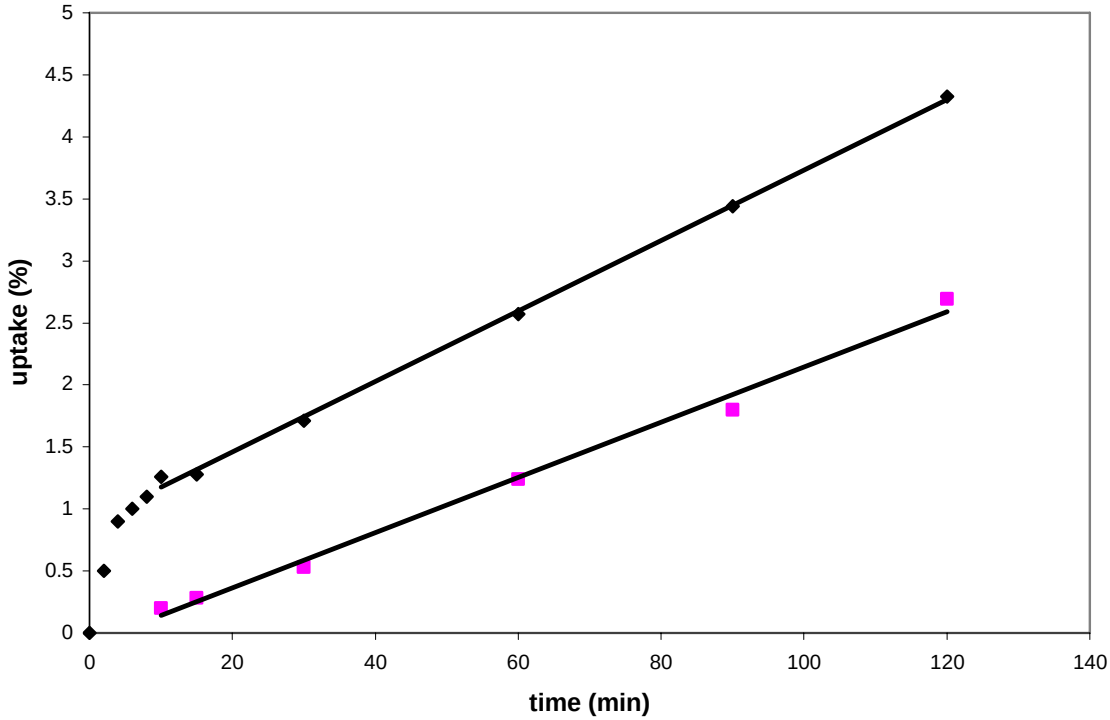

It indicates that the incorporation rate in vitro is very much slower (0.03 %/min.) than the short time reversible uptake kinetics (2.6 % / min.) and that incorporation follows a pseudo zero order reaction pattern. Both linear parts of the time related curves, representing respectively the total uptake (upper) and the incorporation fraction (lower), show the same slope up from 20 minutes.

2.2.5. DISCUSSION

Amino acid transport across the cell membrane is mediated via amino acid transport systems. Among the different amino acid transport systems, the Na^{+}-independent L-type LAT amino acid transport system 1 (LAT1 system) is a major route for providing cells with large amino acids including branched or aromatic amino acid analogues. This amino acid transport system is heavily up-regulated in tumour tissue and has only a very limited expression in normal tissue [5]. In view of the latter characteristics, [^{125}I]-2-I-L-Phe was developed as a potential tumour tracer for SPECT.

There is no significant difference between the uptake patterns of [^{125}I]-2-I-L-Phe in presence of 0.1 mM 2-I-L-Phe in HEPES+ and HEPES- (Fig. 2.2.1 and Table 2.2.1). The inverse relationship between $*AA_t$ and time revealed the same linear straight line (R^2 > 0.97) both buffer systems (Fig. 2.2.2) meaning that in the two buffer systems 2-I-L-Phe

is transported by the same transport system. However, the uptake of [^{125}I]-2-I-L-Phe in MEM is lower in comparison to the uptake in HEPES$^-$ and HEPES$^+$. This could be due to the competition of other natural amino acids. MEM mimics in vivo conditions in blood and contains about 1.2 mM amino acids which are known to be transported by the L transport system.

The uptake of [^{125}I]-2-I-L-Phe was reduced to 15 % of the original value by the presence of the specific inhibitor of L transport system BCH, and to 3 % by the native L-phenylalanine in both HEPES- and HEPES+. This points to the fact that the major part of the uptake is ruled by the same transport system belonging to the L type. Moreover, the competitively [^{125}I]-2-I-L-Phe uptake inhibition BCH, phenylalanine and tyrosine as revealed from a double-reciprocal Lineweaver-Burk plot proves that radioiodinated 2-I-L-Phe shows a high affinity for the transport system involved.

The fact that the stimulated efflux in HEPES+ and HEPES- buffer in presence of 5 mM L-Phe or 5 mM BCH amounted to about 80 % of the initial uptake while in absence of amino acids this was limited to < 10%, points to an anti-port transport system. This means that the uptake occurs through obligatory exchange by a parallel functioning unidirectional transport system which transports specifically BCH. The transport system type that fulfils all these properties is the LAT1 heterodimer transport system [4,5,6,7]. 2-I-L-Phe is thus a phenylalanine analogue that for the major part uses this LAT1 transport system for reversible exchange in the R1M cell model.

Protein incorporation studies indicate that the incorporation rate in vitro is much slower than the short time reversible uptake kinetics. This means that the uptake in the growing cells by a reversible exchanging mechanism (equation *(6)*) remains constant and that the LAT coupled influx of radioactivity is directly related to the requirement of amino acids for protein synthesis or the cell metabolism. Related to equations *(1)* and *(6)* the uptake at equilibrium of [^{125}I]-2-I-L-Phe, even not incorporated into the proteins, reflects the total "amino acid turn-over" of the tumour cells. Several authors [16] presumed that radioactive labelled amino acid analogues could only be useful as an appropriate tracer for emission tomography when they are recognised by the natural amino acid related t-RNA and incorporated into the cell proteins. More recent articles about the application of ^{123}I, ^{11}C and ^{18}F labelled amino acids in vivo in humans [14,17,18] proved that the increased uptake, due to over-expression of amino acid transporters, was directly related to the metabolic requirements of the tumour cells.

2.2.6. CONCLUSION

A new promising tumour specific tracer for SPECT is proposed. Radioiodinated 2-I-L-Phe can be obtained with an almost quantitative yield in a one-pot Kit preparation. This tracer is shown to be taken up in a high amount using the LAT1 transport system which is over-expressed in the major part of cancer cells.

2.2.7 REFERENCES

1. Kubota R, Yamada S, Kubota R, Ishiwata K, Tamahashi N, Ido T. Intramural distribution of fluorine-18-fluorodeoxyglucose in vivo: high accumulation in macrophages and granulation tissues studied by microautoradiography, J Nucl Med 1992, Vol. 33, 1972-1980
2. Langen KJ, Ziemons K, Kiwit JC et al. 3-[123I]Iodo-alpha-methyltyrosine and [methyl-11C]-methionine uptake in cerebral gliomas: a comparative study using SPECT and PET, J Nucl Med, 1997, Vol. 38, p. 517-522
3. Rau FC, Weber WA, Wester HJ, et al. O-(2-[(18)F]fluoroethyl)-L-tyrosine (FET): a tracer for differentiation of tumor from inflammation in murine lymph nodes, Eur J Nucl Med, 2002, Vol. 29, p. 1039-1046
4. N. H. Christensen, Role of Amino Acid Transport and Countertransport in Nutrition and metabolism, Physiol Rev, Vol. 70, Nr.1, 1990, p. 43-71
5. O. Yanagida, Y. Kanai, A. Chairoungdua, D. K. Kim, H. Segawa, T. Nii, S.H. Cha, H. Matsuo, J. Fukushima, Y. Fukasawa, Y. Tani, Y. Taketani, H. Uchino, J.Y. Kim, J. Inatomi, I. Okayasu, K. Miyamoto, E. Takeda, T. Goya, H. Endou, Human L-Type amino acid transport system 1 (LAT1) : characterisation of function and expression in tumour cell lines, Biochim Biophys Acta, Vol. 1514, 2001, p. 291-302
6. H. Ohkame, H. Masuda, Y. Ishii, Y. Kanai, Expression of L-type amino acid transporter 1 (LAT1) and 4F2 heavy chain in liver tumor lesions of rat models, Journal of Surgical oncology, 2001, Vol. 78, p. 265-272
7. C. Meier, Z. Ristic, S. Klauser, F. Verrey, Activation of system L heterodimeric amino acid exchangers by intracellular substrates, The EMBO Journal, Vol. 21 Nr. 4, 2002, p. 580-589
8. N. Shikano, Y. Kanai, K. Kawai, J. Inatomi, D. K. Kim, N. Ishikawa, H. Endou, Isoform Selectivity of 3-[^{125}I]-α-Methyl-L-Tyrosine Membrane Transport in Human L-Type amino acid transport systems, J Nucl Med, Vol. 44, N° 2, 2003, p. 244-246
9. T. Lahoutte, V. Caveliers, L. Dierickx, M. Vekeman, H. Everaert, J. Mertens, A. Bossuyt, In vitro characterisation of the influx of 3-[^{125}I]-iodo-L-Tyrosine and 2-[^{125}I]-iodo-L-Tyrosine into U266 human myeloma cells : Evidence for system T transport, Nucl Med Biol , Vol 28, Issue 2, 2001, p. 129-134
10. T. Lahoutte, V. Caveliers, P.R. Franken, A. Bossuyt, J. Mertens, H. Everaert, Increase tumor uptake of 3-[^{123}I]-Iodo-L-alpha-methyltyrosine after preloading with amino acids, an in vivo animal imaging study, J Nucl Med, Vol 43(9), 2002, p. 1201-1206
11. J. Mertens, T. Lahoutte, C. Joos, A. Bossuyt, New approach of cell uptake kinetics of L-2-123I-Tyr and L-2-123I-Phe, new potential tumour tracers for SPECT, Eur J Nucl Med Mol Imag, Vol 29, 2002, S377-P722
12. J. Mertens, M. Gysemans, Cu^{1+}-assisted nucleophilic exchange radiohalogenation: application and mechanistic approach. In: New trends in Radiopharmaceutical Synthesis, Quality Assurance and Regulatory Control, Plenum Press, New York, 1991, p. 53-65

13. J. Yu, I. Zolle, J. Mertens, F. Rakias, Synthesis of 2-[131I]iodoPhenyl-metyrapone using Cu(I)-assisted nucleophilic exchange labelling: study of the reaction con2-I-L-Pheions, Nuclear Med Biol, 1995, p. 257-262
14. Tony Lahoutte, John Mertens, Vicky Caveliers et al., Biodistribution of Iodinated Amino Acids in Rats: Selection of the Optimal Analog for Oncologic Imaging Outside the Brain, J Nucl Med 2003, Vol 44, p. 1489-1494
15. J. Mertens, T. Lahoutte, C. Joos, A. Bossuyt, In vivo evaluation of 2-123I-Tyr and 2-123I-Phe as tumour specific tracers for SPECT, European Journal of Nuclear Medicine and molecular imaging, Volume 29, Supplement 1, August 2002
16. PET Studies on Amino Acid Metabolism and Protein Synthesis, Editors B.M.Mazoyer, W.D.Heissand D.Comar, 1993, Kluwer Academic Publishers
17. Jager PL, Franssen EJ, Kool W, et al. Feasibility of tumor imaging using l-3-[iodine-123]-iodo-alpha-methyltyrosine in extracranial tumors. J Nucl Med 1998, Vol. 39, p. 1736-1743
18. Weber WA, Dick S, Reidl G, et al. Correlation between postoperative 3-[(123)I]iodo-L-alpha-methyltyrosine uptake and survival in patients with gliomas. J Nucl Med 1998, Vol. 42, p. 1144-1150

2.3 In Vivo Characterization Of [$^{123/125}$I]-2-iodo-L-phenylalanine In A R1M Rabdomyosarcoma Athymic Mice Model As A Potential Tumour Tracer For SPECT.

Veerle Kersemans, MSc[1]; Bart Cornelissen, MSc[1]; Ken Kersemans, MSc[2]; Erik Achten, PhD[3]; Rudi A. Dierckx, PhD[4]; John Mertens, PhD[2,5] and Guido Slegers, PhD[1,5].

[1] Laboratory for Radiopharmacy, Universiteit Gent, Harelbekestraat 72, B-9000 Gent, Belgium
[2] BEFY, Vrije Universiteit Brussel, Belgium
[3] Department of Radiology and Magnetic Resonance Imaging, Gent University Hospital, Belgium
[4] Division of Nuclear Medicine, Gent University Hospital, Belgium
[5] Inter University Institute for Radiopharmaceutical Chemistry

Key words: [^{123}I]-2-iodo-L-phenylalanine; radiolabeled amino acids; tumour imaging; inflammation; biodistribution; ^{18}F-FDG

Journal of Nuclear Medicine 2005 (46): 532 – 539.

2.3.1. ABSTRACT

The application of [^{123}I]-3-Iodo-α-methyltyrosine is limited to diagnosis of brain tumours due to its marked long term uptake in kidneys. In vitro evaluation of [^{125}I]-2-iodo-L-phenylalanine showed high uptake in R1M cells by LAT1 transport. This study evaluates [^{123}I]-2-iodo-L-phenylalanine as a new specific tumour tracer for SPECT. **Methods**: [$^{123/125}$I]-2-iodo-L-phenylalanine is prepared as a one pot Kit using the Cu^{1+}-assisted isotopic exchange method. The characteristics of [^{125}I]-2-iodo-L-phenylalanine were examined in vivo in R1M tumour bearing athymic mice and in acute inflammation bearing NMRI mice. The uptake of [$^{123/125}$I]-2-iodo-L-phenylalanine in tumour and other organs of interest were measured by dynamic planar imaging (DPI) and gamma counting after dissection. Displacement of [^{123}I]-2-iodo-L-phenylalanine radioactivity by L-phenylalanine, L-methionine and L-cysteine was measured. [^{123}I]-Iodo-HSA planar imaging was performed to correct for bloodpool activity and MRI to delineate the tumour in DPI. [^{18}F]-FDG uptake was measured with an animal PET. [^{125}I]-2-iodo-L-phenylalanine and [^{18}F]-FDG uptake in inflamed muscle were compared. **Results**: [$^{123/125}$I]-2-iodo-L-phenylalanine showed a high and fast tumour uptake and followed a reversible first order pattern allowing to calculate $t_{1/2}$ and t_R (time to reach equilibrium). Net tumour-to-background ratios up to 6.7 at 60 min were obtained. This radioactivity was significantly displaced by L-phenylalanine, L-methionine and L-cysteine pointing to reversible LAT transport. When plotting t_R of the tumour uptake as a function of tumour volume, a rectangular hyperbolic curve was obtained. The almost constant t_R values at higher tumour volumes (> 4ml) could be linked to increased necrotic tissue. Fast blood clearance of the tracer through the kidneys to the bladder and low tracer activity in abdomen and brain was observed.

The inflamed muscle showed only a slight increase of [^{125}I]-2-iodo-L-phenylalanine uptake (inflammation to background ratio RIB=1.30±0.02), in contrast to the high [^{18}F]-FDG uptake (RIB=11.1±1.7). The in vivo stability of [$^{123/125}$I]-2-iodo-L-phenylalanine was good: only 7% of free radioiodide and no other labelled metabolites were observed after 90 min. **Conclusions:** [$^{123/125}$I]-2-iodo-L-phenylalanine is quickly taken up by the overexpressed LAT1-system in R1M tumours with high tumour specificity. The availability of a Kit and the specificity of the tracer make [^{123}I]-2-iodo-L-phenylalanine a promising tool for oncologic SPECT imaging.

2.3.2 INTRODUCTION

Both amino acid transport across the cell membrane and protein synthesis rate are early features of malignant transformation. A and L type amino acid transport have been shown to be increased in tumour cells relative to normal tissue and these transport systems have been the major focus of the development of amino acid tumour tracers for oncologic imaging *(1,2)*.

At present, [^{123}I]-3-Iodo-α-methyltyrosine is the only routinely used amino acid tracer for Single Photon Emission Computed Tomography (SPECT) tumour diagnosis. This tracer has major advantages in comparison to ^{18}F-Fluorodeoxyglucose (^{18}F-FDG) such as high and fast tumour uptake and rather low uptake in grey matter and inflammatory lesions. However, its marked long term renal accumulation limits its use for oncologic imaging outside the brain *(2-5)*. Recently, other L-system transported radiolabelled amino acids for SPECT have been developed and evaluated to overcome this problem: 2-iodo-L-tyrosine *(6)*, 4-iodo-L-phenylalanine *(7)* and 2-iodo-L-phenylalanine. The latter was developed in our research group and showed high accumulation in vitro by L type amino acid transport (more specific LAT1) in R1M (rabdomyosarcoma) tumour cells without incorporation in the cell proteins *(8)*. Recent articles proved that incorporation of radiolabelled amino acids is not necessary and that the increased uptake is directly related to the metabolic requirements of the tumour cells *(8)*. Therefore we evaluated in vivo in rodent [^{123}I]-2-iodo-L-phenylalanine as a potential SPECT tracer to detect brain as well as periphery tumours.

2.3.3 MATERIALS AND METHODS

All the conventional products mentioned were at least analytical or clinical grade and obtained from Sigma-Aldrich. The solvents were of HPLC quality (Chemlab, Belgium).

2.3.3.1. Synthesis of Precursor 2-iodo-L-phenylalanine

2-iodo-L-phenylalanine was prepared from 2-bromo-L-phenylalanine (PepTech Corp, USA) using the Cu^{1+} assisted nucleophilic exchange under acidic and reducing conditions (30.3 mM 2-bromo-L-phenylalanine, 4.4 mM $CuSO_4$, 8.9 mM citric acid, 9.0 mM $SnSO_4$, 10.7 mM gentisic acid, 44.5 mM NaI) at 160°C for 16 hours *(9)*. 2-iodo-L-phenylalanine and 2-bromo-L-phenylalanine were recovered separately from RP-HPLC separation (Hibar Lichrosorb RP-select 7μm; λ = 261 nm; Merck, Belgium) with 20/80 MeOH/H_2O containing 1mM NH_4Ac (pH 5.5, 13 ml/min) and 2-iodo-L-phenylalanine was purified from methanol by evaporation. Identification and quality control was achieved by NMR, LC-MS, TLC and

HPLC. Chiral chromatography (5 µm Chirobiotic T, 150 x 4.6 mm; Astec) with 20/80 MeOH/H_2O containing 20 mM NH_4Ac (pH 5.5, 1 ml/min) was used to check chiral modification to 2-iodo-D-phenylalanine.

2.3.3.2. Radiochemistry

2.3.3.2.1. [^{123}I/^{125}I]-2-iodo-L-phenylalanine.

Radioiodination with ^{123}I (222 MBq; 10 – 20 µl) or ^{125}I (37 MBq; 10µl) (Nordion Europe, Belgium) of 1.0 mg 2-iodo-L-phenylalanine was performed by Cu^{1+} assisted isotopic exchange *(9)* under acidic and reducing conditions (0.2 mg $CuSO_4$, 2.5 mg citric acid, 0.5 mg $SnSO_4$, 1.3 mg gentisic acid in 565 µl; 60 min at 100°C). The reaction mixture was drawn up in a syringe containing the appropriate amount of "make-up solution" (Tri-sodium Citrate dihydrate, 71 mM) to render the solution isotonic and to adjust the pH to at least 4. The reaction mixture was sent through a 0.22 µm Ag-filter (Millipore, Belgium) and a sterile 0.22 µm filter (Millipore, Belgium) into a sterile vacuum penicillin vial to remove the free $^{123/125}I^-$. Identification and quality control was achieved by HPLC and Sep-pak C18 (Waters, Belgium). Chiral chromatography was used to check the absence of 2-iodo-D-phenylalanine.

2.3.3.2.2. [^{123}I]-iodo-Human Serum Albumin.

Radioiodination of Human Serum Albumin (HSA) with ^{123}I (Nordion Europe, Belgium) was performed by electrophilic substitution using the Iodogen technique. Iodogen (1, 3, 4, 6-tetrachloro-3α, 6α-diphenylglycouracil; Pierce, Belgium) was coated on the wall of polypropylene vials using 70 µg of Iodogen per 200 µl of chloroform per vial. The solvent was evaporated by airflow at room temperature. In the Iodogen vial, the ^{123}I (111 MBq) solution was added to HSA (50 µg) in 140 µl 0.1 M potassium phosphate buffer at pH 8.5. After 15 min at room temperature the mixture was removed from the Iodogen coated vial to stop the reaction and was sent through a 0.22 µm Ag-filter to remove the free $^{123}I^-$ from [^{123}I]-iodo-HSA. The specific activity was 1.5 10^5 GBq/mmol. Quality control was achieved using a standard prepacked PD-10 SEC column (Size Exclusion Chromatography, Amersham Pharmacia Biotech, Sweden) using PBS/HSA as the eluting agent.

2.3.3.3. In Vivo Experiments

2.3.3.3.1. Laboratory Animals.

Water and food was freely available during the experimental period.

For the tumour model, male SWISS~nu/nu mice (n=33) (Bioservices, The Netherlands) were injected subcutaneously in the right flank (armpit region) with 5.10^6 R1M rabdomyosarcoma cells. Tumours were grown and normal tumour growth curves were obtained using sliding caliper measurement and the estimate volume formula $V = 0.4\ a^2.b$, a and b being the short and the long axis of the tumour respectively *(10)*. Imaging experiments with [^{123}I]-2-iodo-L-phenylalanine, [^{123}I]-iodo-HSA and ^{18}F-FDG and dissection experiments with [^{125}I]-2-iodo-L-phenylalanine were performed.

For the inflammation model, male NMRI mice (n=9) (in house breeding program) were injected in the right biceps brachii with 25 µl of turpentine. Imaging ([^{123}I]-2-iodo-L-phenylalanine, [^{123}I]-iodo-HSA and ^{18}F-FDG) and dissection ([^{125}I]-2-iodo-L-phenylalanine

and ^{18}F-FDG) experiments with the inflamed mice were performed 24 hours after turpentine injection.

During all imaging experiments, the animals were anesthetized intraperitoneal (IP) with 75 µl (1.5 mg) of solution containing 20 mg pentobarbital per ml (Nembutal, 60 mg/ml, Ceva Santé Animale, Belgium). For the biodistribution experiments by dissection, the animals were killed without sedation by cervical dislocation and the organs of interest were dissected.

All tracers ([$^{123/125}$I]-2-iodo-L-phenylalanine, ^{18}F-FDG and [^{123}I]-iodo-HSA) were injected intravenously (IV) in the lateral tail vein. The study protocol was approved by the ethical committee for animal studies of our institution. Guidelines of the National Institute of Health principles of laboratory animal care (NIH publication 86-23, revised 1985) were followed.

2.3.3.3.2. Dynamic Planar Imaging (DPI).

Imaging was performed using a gamma camera (Toshiba GCA-9300A/hg) in planar mode equipped with a high-resolution parallel-hole collimator. All images were acquired into 128 x 128 matrices (FOV: 23.5 x 12.46 cm) and with a photopeak window set at 15 % around 159 keV. Together with the animals, a syringe with a known amount of radioactivity was scanned, to allow the semi-quantification of the results of the ROI analysis. The ROIs were drawn using a MRI maximum intensity projection (MIP) *(10)*. The ROI of the heart was used as a measure for bloodpool activity. Due to partial volume effects, the measured bloodpool data will be overestimated *(11)*. The injected activity (IA) was calculated as the amount of radioactivity in the syringe before and after injection (Capintec CRC-15R, Ramsey, NJ, USA). The tracer uptake was expressed as the percentage IA per Pixel (%IA/P).

At first, a [^{123}I]-HSA study was performed to measure the relative bloodpool distribution to correct the uptake of [^{123}I]-2-iodo-L-phenylalanine in the tumour and the inflammation area as well as the rest of the animal for bloodpool activity. Ten tumour bearing mice and 3 acute inflammation bearing mice were injected with 7.4 MBq [^{123}I]-HSA. Ten dynamic planar images of 1 min were acquired 10 min after injection. ROIs were drawn around the tumour or inflammation area and the contralateral background area. The tumour to contralateral background (RTB) and inflammation to contralateral background (RIB) ratios were calculated and the mean for all animals was determined.

The DPI experiments with [^{123}I]-2-iodo-L-phenylalanine (figure 2.3.1) were started when the tumour reached a volume of 0.30 cm^3. Thirty tumour bearing mice were followed up with the new tracer until the tumour reached a volume of 5.00 cm^3.

FIGURE 2.3.1: Scheme of planar imaging procedure. a: static acquisition to determine background radiation; b: dynamic planar imaging to determine plateau phase (equilibrium) for [^{123}I]-2-iodo-L-phenylalanine uptake; c: dynamic planar imaging to determine displacement of [^{123}I]-2-iodo-L-phenylalanine radioactivity with L-phenylalanine, L-methionine or L-cysteine; d: injection of [^{123}I]-2-iodo-L-phenylalanine at 0 min; e: injection of L-phenylalanine, L-methionine or L-cysteine at 10 min.

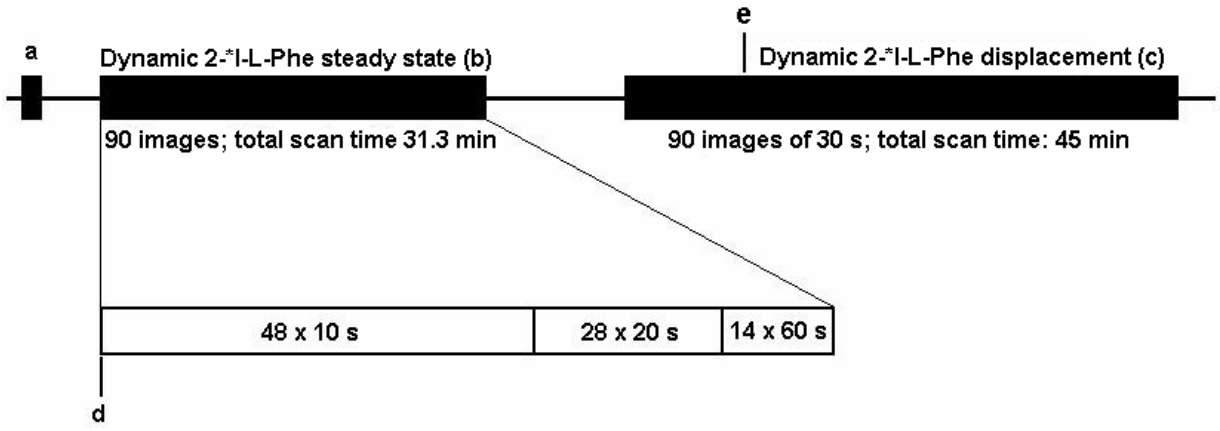

DPI was started immediately after injection of 18.5 MBq [^{123}I]-2-iodo-L-phenylalanine. First, the steady state of tracer uptake in the tumour was determined. Second, at steady state a displacement study with L-phenylalanine, L-methionine and L-cysteine, which all use the L-type transport system *(12)* was performed. For the displacement study, 200 µl of a 145 mM amino acid solution was IV injected in the lateral tail vein.
ROIs were drawn around the tumour, the contralateral background area, the right kidney, the heart, the pancreas, the brain, the thyroid and the total body. In the case of the inflammation model, the ROI for the tumour was replaced by the ROI for the inflammation site. Due to superposition of the pancreas with other organs such as left kidney and stomach, the results will be overestimated, especially during the beginning of the DPI scan.
Tumour [^{123}I]-2-iodo-L-phenylalanine uptake was compared to the uptake in the contralateral background area and RTB calculated. The significance of displacement of [^{123}I]-2-iodo-L-phenylalanine activity by the above mentioned amino acids was calculated for a 95 % confidential interval.
The [^{123}I]-2-iodo-L-phenylalanine tumour uptake as a function of time, obtained from DPI experiments, were fit to a pseudo first order model. The kinetic parameters $t_{1/2}$, time-to-reach-equilibrium (t_R) and theoretical equilibrium for tumour tracer uptake were determined. The latter as well as the pseudo first order fitting were performed in parallel to the in vitro experiments performed by Mertens J et al. *(8)*. The relationship tumour volume as a function of t_R was examined, non linear regression was performed and a theoretical rectangular hyperbole was calculated.
In case of the inflammation model, the uptake of [^{123}I]-2-iodo-L-phenylalanine in the inflammation area was compared to the contralateral background area and the RIB was calculated.

2.3.3.3.3. ^{18}F-FDG Animal PET Imaging.

PET imaging was performed with a high sensitivity animal PET-scanner (VUB-PET, resolution 3 – 4 mm) *(13)*. Three NMRI mice bearing an acute inflammation and 3 R1M

bearing athymic mice were injected with 18.5 MBq of ^{18}F-FDG. Fifteen minutes post injection, one time frame of 15 min was acquired. The images were reconstructed using Fourier rebinning and 2D OSEM *(13)*. The images produced had a matrix size of 128 x 128 x 19.

VOIs were drawn around the tumour (or inflammation site) using a MRI image. The VOI for the tumour was horizontally mirrored to create the contralateral background VOI. The values are expressed as counts per voxel and the ratios tumour to background (RTB) and inflammation to background (RIB) were calculated.

2.3.3.3.4. Magnetic resonance imaging (MRI)

The tumour bearing animals were anaesthetized as mentioned above. After sedation, the animals were placed in a specially designed restrainer box in which sterile conditions could be retained. 3D Dess-weighted images, being hybrid T1-T2 weighted images, were generated on a 1 Tesla whole-body system (Magnetom SP; Siemens, Erlangen, Germany) *(10)*. The animals were scanned two at a time using a small surface flex coil.

2.3.3.3.5. Dissection: Biodistribution Of [^{123}I]-2-iodo-L-phenylalanine.

The IA was calculated by weighing the syringes before and after injection of the tracer and by the use of a dilution series of the injected tracer solution which was also weighed and counted for radioactivity using the auto gamma-counting system (CobraII Series, Canberra Packard, Meriden, CT, USA Cobra).

Thirty R1M bearing athymic mice were injected with 7.4 kBq [^{125}I]-2-iodo-L-phenylalanine, six days after the last imaging experiment was performed. At various time points (2, 30, 45, 60 and 180 min) post injection 6 animals per time point were sacrificed. The organs and tissues were removed, washed and weighted. The blood was collected in an EDTA coated vial. The radioactivity of the samples was counted by use of an auto gamma-counting system (CobraII Series, Canberra Packard, Meriden, CT, USA Cobra). The amount of radioactivity in the organs and tissues was calculated as the differential absorption rate (DAR): $[(\%IA/g)_{tumour}]/[(\%IA/g)_{total\ body}]$.

Inflammation bearing NMRI mice (n=3) were injected with 7.4 kBq of [^{125}I]-2-iodo-L-phenylalanine together with 16 MBq of ^{18}F-FDG through the lateral tail vein. After 30 min, the mice were sacrificed and organs and tissues were removed, washed and weighted. Muscle tissue was collected from the inflamed left leg and the non-inflamed right leg. The ^{18}F activity was counted on day 1 and the ^{125}I activity in the same samples was counted three days later. The amount of radioactivity in the organs and tissues was calculated as DAR.

2.3.3.3.6. Metabolization Study:

In vivo stability of [^{125}I]-2-iodo-L-phenylalanine. The blood, collected in the tumour model biodistribution study, was used for a metabolization study of [^{125}I]-2-iodo-L-phenylalanine as a function of time. Five hundred microlitres of blood was centrifuged at 1800 g for 10 min and the supernatant (plasma) was removed from the pellet. First, 200 µl of plasma was diluted three times with 9 ‰ NaCl. Second, 200 µl of this "plasma – NaCl – solution" was added to the same volume of 20 % Trichloroacetic acid to denaturize the protein content. After 5 min centrifugation at 1800 g, the supernatant was collected and filtered with a 0.22 µm filter. The samples were analysed on RP-HPLC (C18 Hypersil BDS, 5 µm, 250 x 46 mm; λ = 254 nm) (Alltech, Belgium) with 20/80 MeOH/H_2O containing 1mM NH_4Ac (pH 5.5, 1 ml/min)

and fractions of 0.5 ml were collected and counted by use of a gamma counting system (CobraII Series, Canberra Packard, Meriden, CT, USA Cobra).

To determine the influence of EDTA on the formation of [^{125}I]-2-iodo-L-phenylalanine metabolites, 2 control experiments were performed. First, 7.4 kBq of [^{125}I]-2-iodo-L-phenylalanine was added to an EDTA coated vial and treated identical to the blood samples. Secondly, mouse blood was recovered from a wild type NMRI mouse and 7.4 kBq of [^{125}I]-2-iodo-L-phenylalanine was added. After 90 min of incubation at 37°C, the sample was treated as mentioned above.

2.3.4. RESULTS

2.3.4.1. Synthesis And Radiolabeling of 2-iodo-L-phenylalanine

Yields up to 65 % were obtained under the applied reaction conditions for the presursor synthesis of 2-iodo-L-phenylalanine from 2-bromo-L-phenylalanine using the Cu^{1+} assisted nucleophilic exchange method.

Radioiodination of 2-iodo-L-phenylalanine by Cu^{1+} assisted isotopic exchange, followed by Ag-membrane filtration, resulted in a radiochemical purity of > 99% and a specific activity of 65 GBq/mmol ([^{123}I]-labeling) and 11 GBq/mmol ([^{125}I]-labeling).
In both cases, it was shown by chiral HPLC that there was no detectable amount of D analogues.

2.3.4.2. In Vivo Results

2.3.4.2.1. In Vivo Stability Of [^{125}I]-2-iodo-L-phenylalanine.

HPLC analysis of the mouse blood showed a dehalogenation of 7.3 % of [^{125}I]-2-iodo-L-phenylalanine 90 minutes post injection. No other metabolites were detected. EDTA did not show any influence on the deiodination of [^{125}I]-2-iodo-L-phenylalanine.

2.3.4.2.2. Planar Imaging.

DPI with [^{123}I]-HSA showed no significant difference between the blood flow in the tumour or inflammated muscle and the contralateral reference leg (RTB = 1.1 ± 0.2 and RIB = 1.1 ± 0.2).
The [^{123}I]-2-iodo-L-phenylalanine uptake – time kinetics in R1M tumours in vivo is shown in Figure 2.3.2 and follows a rectangular hyperbolic shape.

FIGURE 2.3.2: Uptake of [^{123}I]-2-iodo-L-phenylalanine (%IA/P) in tumour and contralateral background region as functions of time by dynamic planar imaging for tumour volumes ranging from 0.3 cm^3 to 5.0 cm^3.

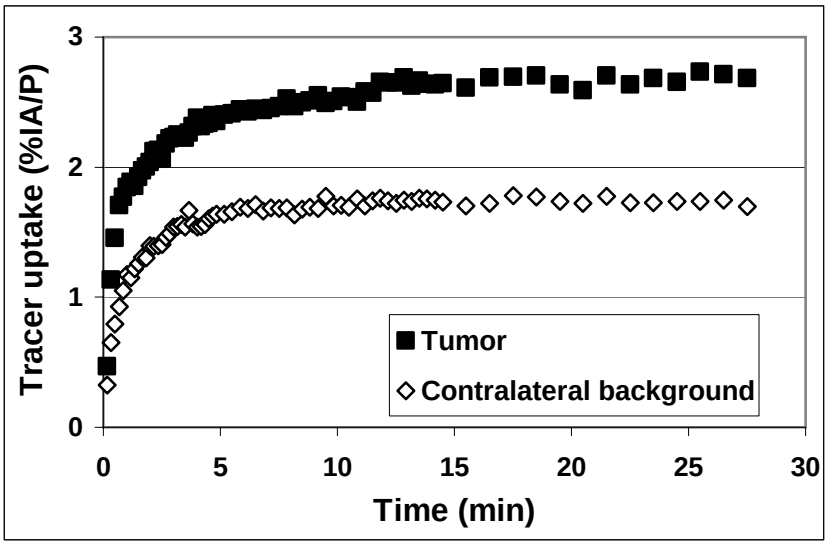

When plotting 1/ (net tumour uptake) as a function of 1/t, a linear relationship ($R^2 > 0.95$) is obtained (Fig. 2.3.3A). This means that important kinetic parameters such as $t_{1/2}$, velocity at initial conditions and the theoretical equilibrium of tumour tracer uptake can be determined. This results in the calculated values for [^{123}I]-2-iodo-L-phenylalanine of: (net tumour uptake)$_{equilibrium}$ = 2.7 %IA/P, $t_{1/2}$ = 0.5 min. Figure 2.3.3B indicates that [^{123}I]-2-iodo-L-phenylalanine uptake in R1M tumours follows a pseudo reversible first order reaction ($R^2 > 0.90$) *(8)*.

FIGURE 2.3.3: (A) Uptake of [^{123}I]-2-iodo-L-phenylalanine: plot of $1/(AA_t)$ as function of 1/t. Equation of fitted curve: y=0.17x+ 0.37 (R^2=0.9784) resulting in AA_{eq}(*)=2.73 %IA/P and $t_{1/2}$=0.46 min. (B) Uptake of [^{123}I]-2-iodo-L-phenylalanine as a function of time by dynamic planar imaging: pseudo first order fit (R^2 = 0.9764). (*) Net [^{123}I]-2-iodo-L-phenylalanine tumour uptake at equilibrium (%IA/P); (†) Net [^{123}I]-2-iodo-L-phenylalanine tumour uptake when equilibrium is not reached (%IA/P).

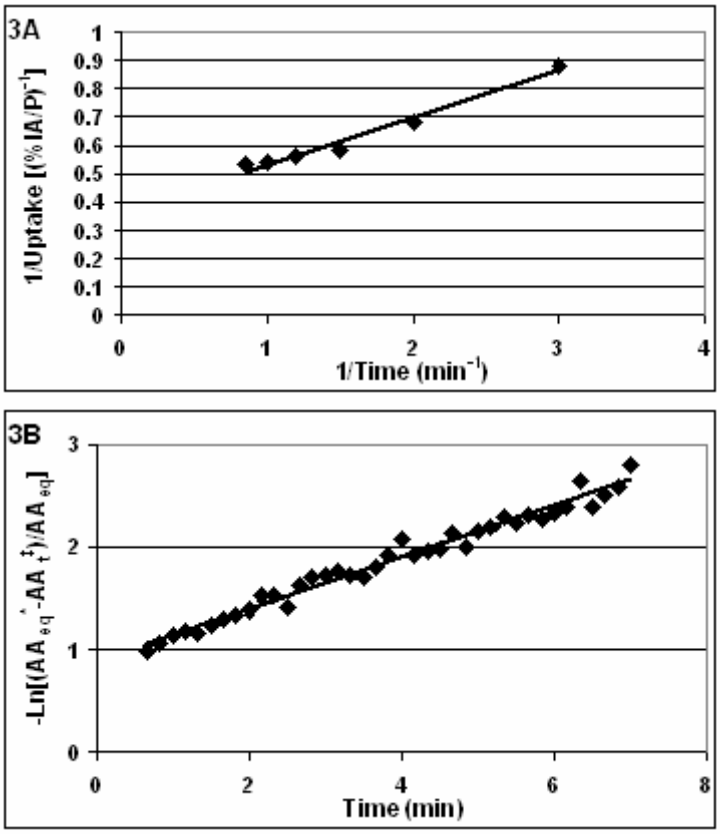

At equilibrium (plateau phase), net [^{123}I]-2-iodo-L-phenylalanine uptake in the tumour was high. It increased from 0.60 ± 0.03 %IA/P up to 5.7 ± 0.4 %IA/P for tumour volumes ranging from 0.3 cm^3 to 5.0 cm^3 (Fig. 2.3.2, 2.3.4A and 2.3.4B). When plotting the [^{123}I]-2-iodo-L-phenylalanine tumour uptake at equilibrium as a function of tumour volume a large spread of the results (R^2 = 0.11) and no correlation between tumour uptake and tumour volume was observed.

FIGURE 2.3.4: (A) Uptake of [^{123}I]-2-iodo-L-phenylalanine uptake in the rabdomyosarcoma tumour model as functions of time by dynamic planar imaging for a tumour volume of 0.50 cm^3. Each image is the result of the summation of 11 consecutive frames. Relative scaling was used (see coloured tool bars). (B) Uptake of [^{123}I]-2-iodo-L-phenylalanine at steady state. B = Bladder; P = Pancreas-zone; K = Kidney; T = Tumour; C = Calibration syringe.

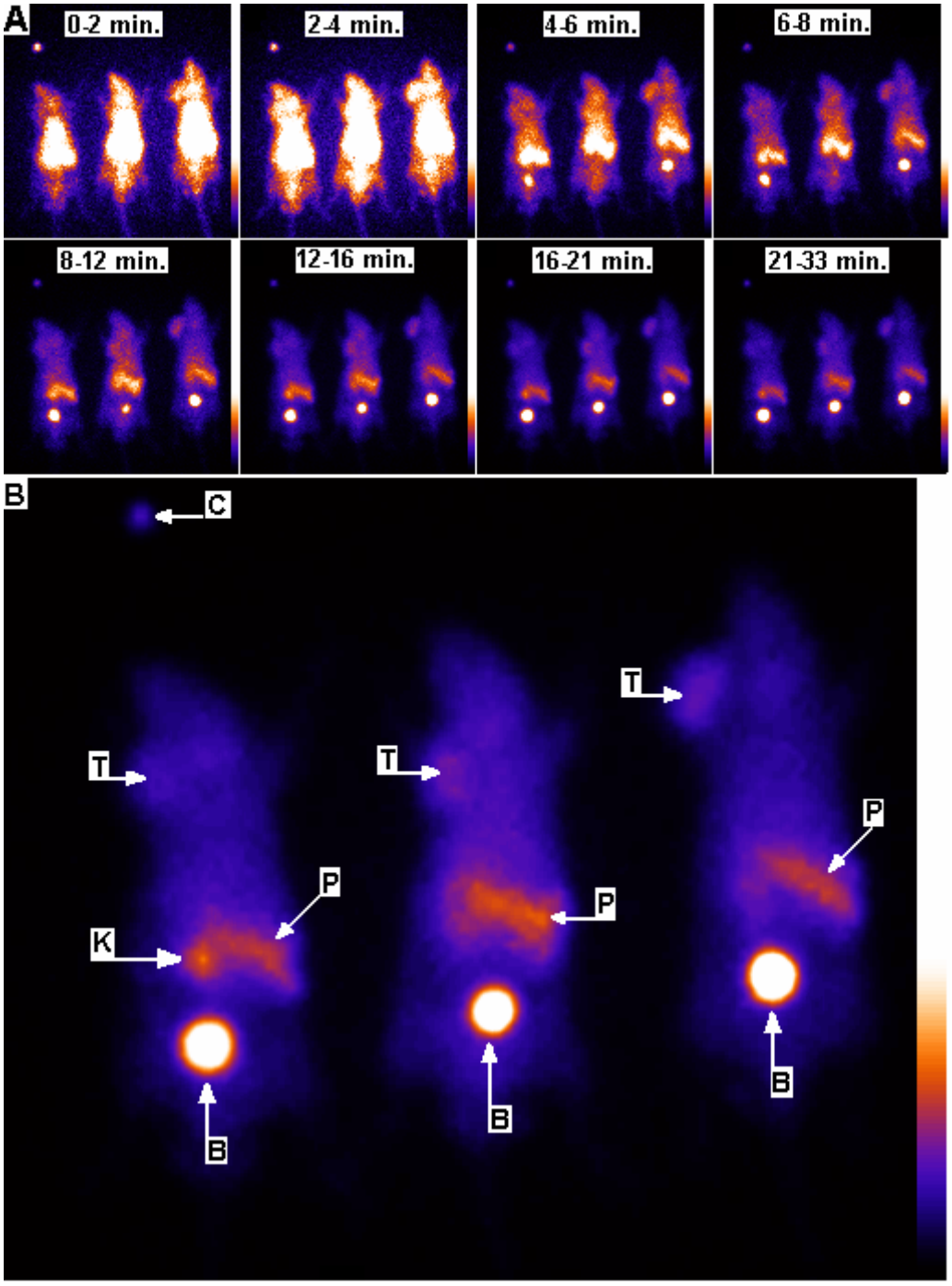

When plotting the "time to reach equilibrium" t_R as a function of tumour volume a hyperbolic curve ($R^2 > 0.90$) reaching a plateau up from a tumour volume of 4.0 cm^3 was obtained (Fig. 4.5). Non-linear regression of a theoretical hyperbolic curve to the experimental values shows a top value of 15.3 ± 0.7 min. The experimental curve fitted the theoretical rectangular hyperbole ($R^2 = 0.91$) (Fig. 2.3.5).

FIGURE 2.3.5: The "time to reach equilibrium" (t_R) as a function of tumour volume. t_R = time to reach equilibrium; NLR = Non Linear Regression

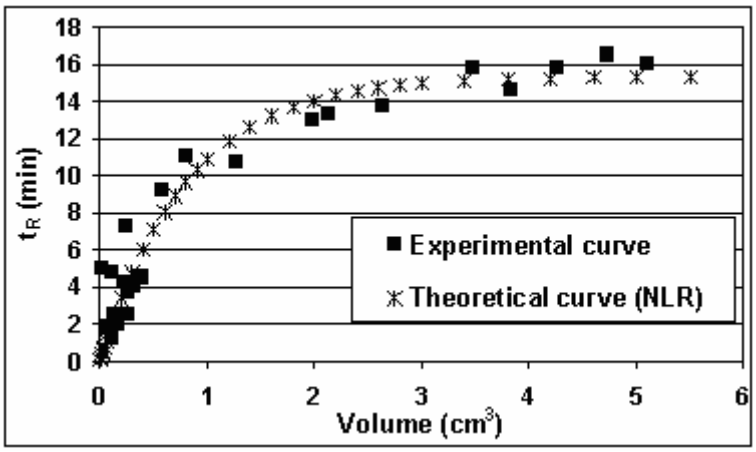

The displacement of [^{123}I]-2-iodo-L-phenylalanine activity in the tumour with L-phenylalanine, L-methionine and L-cysteine is summarized in Table 2.3.1. The radioactivity in the tumour decreased rapidly for a small but significant amount ($p<0.05$) after IV administration of those amino acids and reached a new plateau within 2 min.

TABLE 2.3.1: Displacement study of [^{123}I]-2-iodo-L-phenylalanine activity in the tumour using planar gamma scintigraphy.
(*) % of all animals in which a significant displacement of radioactivity was observed (n = 25); (†) amount (%) of tracer decrease by administering the amino acid (mean ± SD); (‡) L-type transporter system; (§) ASC-type transporter system; (‖) other systems; (¶) A-type transporter system

Amino acid used	Contribution of Transport Systems	% P *	% D†
L-phenylalanine	L ‡ (70%), ASC § (25%), O ‖ (5%)	72	12.3 ± 4.2
L-methionine	L (50%), ASC (20%), A ¶ (10%), O (20%)	80	16.0 ± 4.2
L-cysteine	L (30%), ASC (55%), A (10%), O (5%)	57	11.5 ± 7.8

[^{123}I]-2-iodo-L-phenylalanine was cleared quickly through the kidneys, without accumulation, to the bladder (Fig. 2.3.6). This is confirmed by the fact that the first order fits of the activity as a function of time were almost the same for kidneys and the heart (Fig. 2.3.6). High tracer uptake (3.3 ± 1.5 %IA/P) was noticed in the zone of the pancreas but due to superposition of the pancreas with other organs such as left kidney and stomach, the results are overestimated *(14)*. Low uptake of radioactivity in the thyroid (2.1 ± 1.1 %IA/P), brain (1.5 ± 0.8 %IA/P) or abdominal organs was observed (Fig. 2.3.7).

FIGURE 2.3.6: Uptake of [^{123}I]-2-iodo-L-phenylalanine uptake (%IA/P) as a function of time by dynamic planar imaging: clearance of the tracer through the kidneys to the bladder.

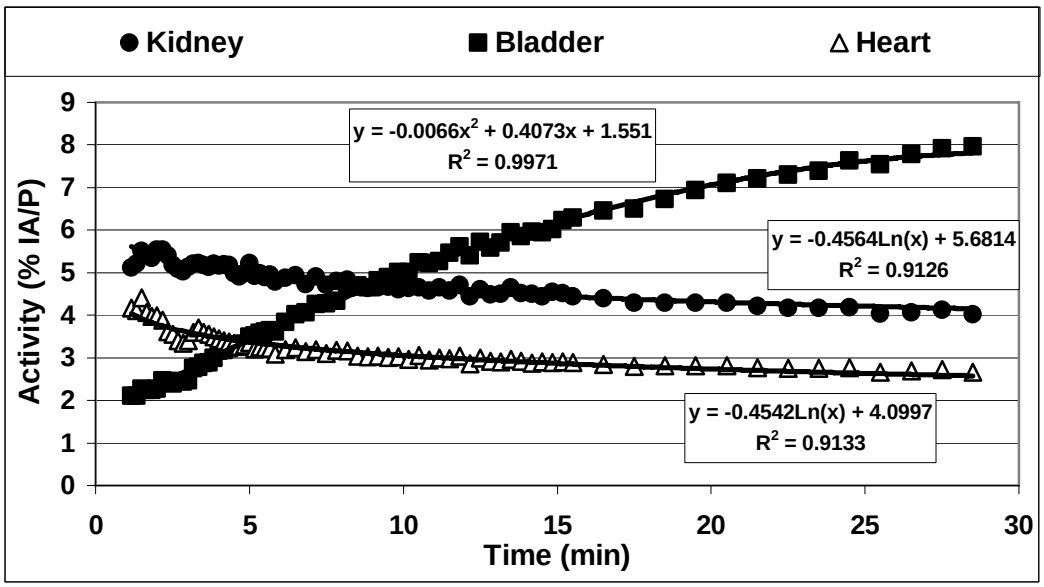

FIGURE 2.3.7: Uptake of [^{123}I]-2-iodo-L-phenylalanine uptake (%IA/P) in heart, pancreas, brain and thyroid as functions of time by dynamic planar imaging.

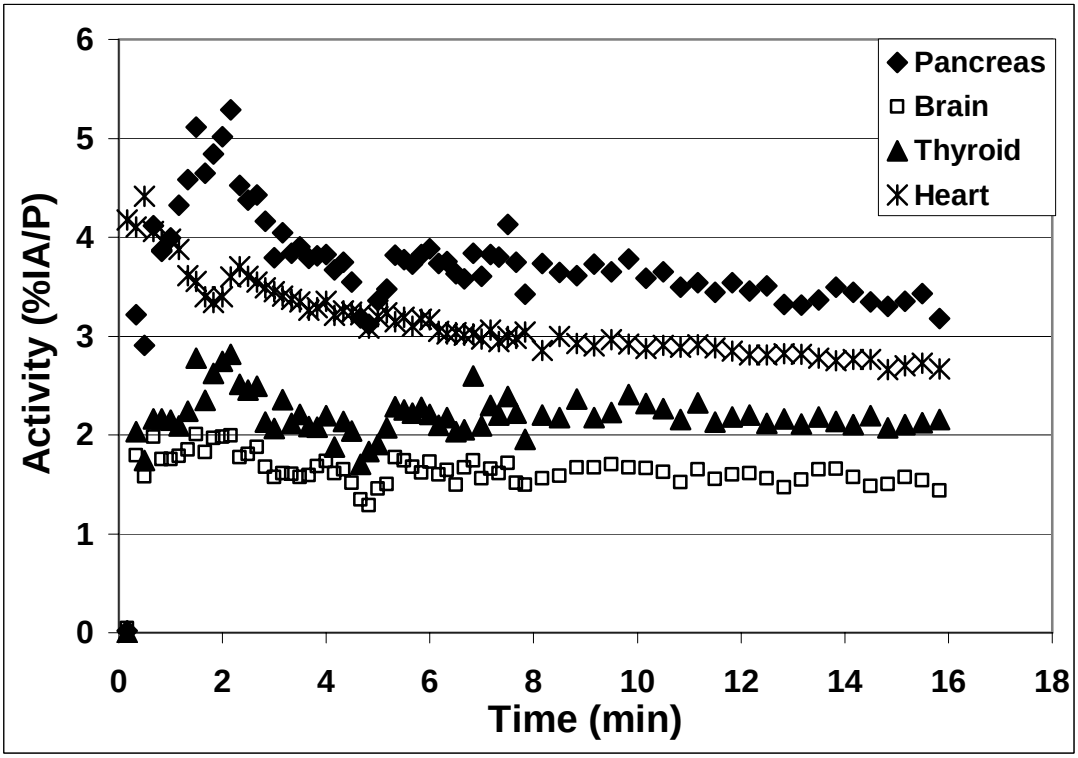

Important was that there was no significant (detectable) increased uptake of [^{123}I]-2-iodo-L-phenylalanine in the inflammation area. The RIB was 0.97 ± 0.14. This results in an apparent tumour to inflamed tissue ratio (ratio T/I) of 5.9 ± 0.42.

2.3.4.2.3. ^{18}F-FDG Animal PET Imaging.

The uptake of ^{18}F-FDG was high in the tumour but also in the inflammation area. A RTB of 3.6 ± 1.6 and a RIB of 2.3 ± 0.6 were obtained. The resulting apparent ratio T/I is 1.6 ± 1.2.

2.3.4.2.4. Biodistribution By Dissection.

The biodistribution data of [^{125}I]-2-iodo-L-phenylalanine in R1M tumour bearing athymic mice are shown in Table 2.3.2.

TABLE 2.3.2: Biodistribution study by dissection of [^{123}I]-2-iodo-L-phenylalanine in R1M bearing athymic mice expressed as DAR (n = 6).

Tissue	Mean ± SD				
	2	30	45	60	180
Blood	1.76±0.94	1.46±0.37	1.39±0.28	1.06±0.31	1.16±0.21
Brain	0.34±0.01	0.49±0.09	0.55±0.18	0.63±0.16	0.47±0.07
Heart	1.31±0.15	0.84±0.23	0.65±0.09	0.82±0.04	0.74±0.18
Lung	1.33±0.28	1.11±0.50	0.69±0.24	0.80±0.07	0.86±0.25
Stomach	0.88±0.20	1.98±1.23	2.60±1.25	3.34±0.24	2.61±1.59
Liver	0.88±0.08	0.52±0.17	0.42±0.08	0.53±0.08	0.56±0.10
Kidneys	4.81±2.16	1.73±0.51	1.79±0.46	1.45±0.10	1.03±0.28
Small intestine	0.57±0.05	0.61±0.08	0.59±0.20	0.76±0.12	0.70±0.23
Large intestine	0.41±0.13	0.29±0.03	0.18±0.07	0.32±0.08	0.44±0.13
Pancreas	5.37±1.03	4.71±1.00	4.56±1.98	7.87±2.61	8.64±1.74
Front leg	0.77±0.23	0.43±0.38	0.64±0.36	0.56±0.24	0.47±0.12
Tumour	1.13±0.11	2.58±0.61	2.70±0.23	3.76±0.52	3.02±0.39
RTB	1.61±0.72	3.58±0.97	5.02±2.20	6.71±1.26	6.35±1.05

The net [^{125}I]-2-iodo-L-phenylalanine tumour uptake reached equilibrium up from 60 min with a mean DAR value of 3.8 ± 1.5. At the same time point, [^{125}I]-2-iodo-L-phenylalanine activity in the blood and in the contralateral leg tissue reached a DAR of 1.1 ± 0.3 and 0.6 ± 0.2 respectively.

[^{125}I]-2-iodo-L-phenylalanine was cleared very fast through the kidneys, without accumulation, to the bladder. A significant uptake of radioactivity in the pancreas was observed. No significant accumulation of radioactivity was observed in other abdominal organs such as liver, lungs, small intestine and large intestine, neither in the brain.

The biodistribution data of [^{125}I]-2-iodo-L-phenylalanine and ^{18}F-FDG in inflammation bearing NMRI mice are shown in Table 2.3.3. A marked high ^{18}F-FDG uptake in the inflamed muscle with a RIB value of 11.1 ± 1.7 is observed while only a small increase of [^{125}I]-2-iodo-L-phenylalanine uptake in the inflammation site vis à vis the contralateral muscle was noticed with a RIB value of 1.30 ± 0.02. This results in a ratio T/I of 8.5 ± 1.7.

TABLE 2.3.3: Biodistributon study by dissection of [^{125}I]-2-iodo-L-phenylalanine and [^{18}F]-FDG in NMRI mice bearing an inflammation expressed as DAR (n = 3).

Tissue	Mean ± SD	
	[^{18}F]-FDG	[^{125}I]-2-iodo-L-phenylalanine
Blood	0.92±0.09	1.10±0.11
Brain	2.10±0.17	0.57±0.20
Heart	0.50±0.28	1.00±0.10
Lung	0.61±0.28	0.80±0.15
Stomach	0.88±0.25	0.29±0.16
Liver	0.37±0.20	0.42±0.53
Kidneys	1.92±1.14	1.92±0.37
Small intestine	0.34±0.05	0.68±0.19
Large intestine	0.17±0.10	0.36±0.09
Pancreas	3.51±1.03	4.22±1.30
Muscle	1.85±0.01	0.65±0.07
Inflamed muscle	20.50±3.30	0.84±0.10
Ratio inflammation/muscle	11.06±1.72	1.29±0.02

The discrepancies between results obtained by dynamic planar imaging and the dissection could not only be explained by biodiversity but could also be due to the well known differences in resolution and counts acquisition between the used methods.

2.3.5. DISCUSSION

[^{123}]-2-iodo-L-phenylalanine was developed as an alternative SPECT tumour tracer to [^{123}]-4-iodo-L-phenylalanine, [^{123}]-2-iodo-L-tyrosine and [^{123}]-3-iodo-α-methyltyrosine to overcome the high bloodpool and inflammation activity, the difficult precursor synthesis and the marked long term renal accumulation, respectively *(15-17)*.

The Cu^{1+} assisted nucleophilic exchange not only provides an easy 1-step reaction for precursor synthesis but also the possibility to establish a Kit-formulation for fast and quantitative routine radioiodination of 2-iodo-L-phenylalanine without the need of an extra purification procedure.

In vitro in R1M cells, the uptake kinetics and the K_m values of [^{125}I]-2-iodo-L-phenylalanine and the natural amino acid L-phenylalanine are both similar and both amino acids are transported by the obligatory exchange LAT1 system. Moreover, our research group revealed that [^{125}I]-2-iodo-L-phenylalanine is not incorporated into the cell proteins and that the uptake of the tracer at equilibrium reflects the total "amino acid turn-over" of the R1M tumour cells. Recent articles proved that incorporation of radiolabelled amino acids is not necessary for tumour imaging and that the increased uptake is directly related to the metabolic requirement of the tumour cells *(8)*.

Regarding the abovementioned characteristics, the new tracer [$^{123/125}$I]-2-iodo-L-phenylalanine, which has a free para position and is some less lipophilic than 4-iodo-L-phenylalanine, was evaluated in vivo in view of its potential application for oncologic imaging with SPECT.

The planar imaging experiments with the new tracer showed that the same uptake kinetics, compared to the in vitro experiments, could be applied: the uptake as a function of time followed a rectangular hyperbolic curve and Figure 2.3.3B indicated that for the uptake a pseudo reversible pseudo first order reaction was followed *(8)*. These observations strongly suggest that in vivo, [$^{123/1225}$I]-2-iodo-L-phenylalanine is also transported by the LAT1 system.

The latter hypothesis is confirmed by the displacement study. Although the displaced [^{123}I]-2-iodo-L-phenylalanine radioactivity in the tumour by L-phenylalanine, L-methionine and L-cysteine was small, it was significant (Table 2.3.1). This shows that the transporter system involved is of the "obligatory exchanger" type such as LAT1. The rather small amount of displaced radioactivity can be explained by the fact that the blood plasma is continuously filtered in the kidneys by the glomerulus and the Bowman's capsule. When a huge excess of amino acids, such as L-phenylalanine and L-methionine, is administered to the animals, the excess will be immediately excreted to the urinary tractus.

[$^{123/125}$I]-2-iodo-L-phenylalanine accumulated quickly to reach high amounts in the R1M tumours and only a very small part did show dehalogenation after 90 minutes (Fig. 2.3.5, Table 2.3.2). Moreover, low abdominal background, fast blood clearance, low brain uptake and almost negligible uptake in inflammatory tissue (ratio T/I of 1.3 and 1.6), in comparison to ^{18}F-FDG (ratio T/I of 5.9 and 8.5), was observed. These findings are also confirmed in literature for another radiolabelled amino acid, 2-iodo-L-tyrosine, which showed a much lower uptake in the site of inflammation in comparison to ^{18}F-FDG *(17)*.

Just like [^{123}I]-2-iodo-L-tyrosine, [^{123}I]-4-iodo-L-phenylalanine and [^{123}I]-3-iodo-α-methyltyrosine uptake in rodents *(17,18)*, [^{125}I]-2-iodo-L-phenylalanine showed high uptake in the pancreas. This is typical for labelled amino acid analogues in rodent. In patients, no significant pancreatic uptake was observed for 2-iodo-L-tyrosine and [^{123}I]-3-iodo-α-methyltyrosine *(15,17)*.

The relationship "time to reach the steady state for [^{123}I]-2-iodo-L-phenylalanine tumour uptake in vivo" versus "tumour volume", reached a plateau phase at tumour volume of 4 cm^3 which could be due to the higher level of necrosis in the larger tumours. It is shown that, even when the radiolabeled synthetic amino acid tumour tracer is not incorporated into cell proteins, the uptake reflects the total "amino acid turn-over" of the tumour cells *(8)*.

2.3.6. CONCLUSION

[^{123}I]-2-iodo-L-phenylalanine is a promising tracer for intracranial as well as extracranial oncologic imaging with SPECT because of its high and fast tumour accumulation, low renal and brain uptake, and minor accumulation in acute inflammatory lesions. Furthermore, its chemical synthesis is easy and allows a kit formulation which is a benefit for transferring the tracer to clinical use.

2.3.7. REFERENCES

1. Yanagida O, Kanai Y, Chairoungdua A, et al. Human L-Type amino acid transport system 1 (LAT1): characterisation of function and expression in tumour cell lines. *Biochim Biophys Acta.* 2001;1514:291–302.
2. Jager PL, Vaalburg W, Pruim J, et al. Radiolabelled amino acids: basic aspects and clinical applications in oncology. *J Nucl Med*. 2001;42:432–445.

3. Weber W, Bartenstein P, Gross MW, et al. Fluorine-18F-FDG PET and iodine-123-IMT SPECT in the evaluation of brain tumours. *J Nucl Med*. 1997;38:802–808.
4. Langen KJ, Ziemons K, Kiwit JC, et al. 3-[^{123}I]-iodo-alpha-methyltyrosine and [methyl-^{11}C]-L-methionine uptake in cerebral gliomas: a comparative study using SPECT and PET. *J Nucl Med*. 1997;38:517–522.
5. Kubota K, Yamada S, Kubota R, et al. Intramural distribution of fluorine-18-fluorodeoxyglucose in vivo: high accumulation in macrophages and granulation tissues studied by microautoradiography. *J Nucl Med*. 1992;33:1972–1980.
6. Mertens JR, Lahoutte T, Joos C et al. In vivo evaluation of 2-123I-Tyr and 2-123I-Phe as tumour specific tracers for SPECT [abstract]. *Eur J Nucl Med.* 2002;29:S76.
7. Samnick S, Schaefer A, Siebert S, et al. Preparation and investigation of tumour affinity, uptake kinetic and transport mechanism of iodine-123-labelled amino acid derivatives in human pancreatic carcinoma and glioblastoma cells. *Nucl Med Biol.* 2001;28:13–23.
8. Mertens JR, Lahoutte T, Joos C et al. New approach of cell uptake kinetics of L-2-123I-Tyr and L-2-123I-Phe, new potential tumour tracers for SPECT [abstract]. *Eur J Nucl Med.* 2002;29:S377.
9. Mertens J, Gysemans M; Cu^{1+}-assisted nucleophilic exchange radiohalogenation: application and mechanistic approach. In: *New Trends In Radiopharmaceutical Synthesis, Quality Assurance And Regulatory Control*. New York: Plenum Press; 1991:53–65.
10. Waterton JC, Alott CP, Pickfort R, et al; Assessment of mouse tumour xenograft volumes in vivo by ultrasound imaging, MRI and calliper measurement. In: *Proceedings of the 19th LH Gray Conference: Quantitative imaging in oncology.* London: Eds Faulkner K, Carey B, Crellin A, Harisson RM; 1997:146–149.
11. Hoffman AJ, Huang SC, Phelps ME. Quantitation in positron emission computed tomography: 1. effect of object size. *J of Comput Assist Tomogr.* 1979;3:299-308.
12. Christensen NC. Role of amino acid transport and countertransport in nutrition and metabolism. *Phys Rev*. 1990;70:43–77.
13. Xuan L, Rajeswaran S, Smolik W, et al. Design and physical characteristics of a small animal PET using BaF2 crystals and a photosensitive wire chamber. *Nucl Instr Meth*. 1996;A382:589-600.
14. Cook, MJ; *The Anatomy of the Laboratory Mouse*. New York: Academic Press; 1965:55-78.
15. Langen KJ, Pauleit D, Coenen HH. 3-[^{123}I]iodo-alpha-methyl-L-tyrosine: uptake mechanisms and clinical applications. *Nucl Med Biol*. 2002;29:625–631.
16. Jager PL, Franssen EJ, Kool W, et al. Feasibility of tumour imaging using L-3-[iodine-123]-iodo- alpha-methyl-tyrosine in extracranial tumours. *J Nucl Med*. 1998;39:1736–1743.
17. Lahoutte T, Mertens J, Caveliers V, et al. Comparative biodistribution of iodinated amino acids in rats: selection of the optimal analog for oncologic imaging outside the brain. *J Nucl Med.* 2003;44:1489–1494.
18. Vekeman M, Chavatte K, Lahoutte T, et al. L-[2-radioiodo] tyrosine, a new potential protein synthesis and tumour tracer for spect: radiosynthesis and biodistribution in rodent [abstract]. *Eur J Nucl Med.* 1999;26:S43.

2.4 Influence of sedation and data-acquisition-method on tracer uptake in animal models: [^{123}I]-2-iodo-L-phenylalanine in pentobarbital sedated tumour bearing athymic mice.

Veerle Kersemans[1], Bart De Spiegeleer[1], John Mertens[2] and Guido Slegers[1].

1 Laboratory for Radiopharmacy, Universiteit Gent, Gent, Belgium
2 Laboratory for Medical Imaging and Physics, Vrije Universiteit Brussel, Brussel, Belgium

Key words: 2-iodo-L-phenylalanine, pentobarbital, tumour, biodistribution, amino acid analogue, athymic mice, dissection, imaging.

Submitted for British Journal of Pharmacology

2.4.1. ABSTRACT

Objectives. To minimize movement artefacts during tracer imaging studies, the animals are generally sedated. Although many reports describe the effect of barbiturates on brain function, less is published about the general impact on the extra-cerebral metabolism and tracer biodistribution. This report describes the influence of pentobarbital on tumour [^{123}I]-2-iodo-L-phenylalanine uptake using dissection and nuclear imaging. **Methods**. R1M tumour bearing athymic mice were divided in 2 populations: untreated and pentobarbital-treated. Each group was subjected to dynamic and static planar imaging and dissection after [^{123}I]-2-iodo-L-phenylalanine injection. Two-compartment blood-modelling of the blood kinetics was performed. ANOVA, t-test and clustered boxplot analyses were used to compare the results between the treatment groups and the data-acquisition methods. **Results**. Two-compartment blood-modelling demonstrated that pentobarbital slowed down the elimination velocity and the distribution towards the peripheral compartment organs. The same results were obtained when performing initial saturable-pathway absorption kinetics. Both observations lead to higher bloodpool and kidney activities after administering pentobarbital. The dependence of the DAR/DUR results on organ, method and treatment demonstrated that all factors had a significant effect. Moreover, a significant effect for method and treatment was observed for each organ separately and the RTB showed additionally an ordinal interaction. Although the tumour uptake values were lower when using nuclear imaging and sedation, the tumour could still be visualized. **Conclusions**. An effect of sedation-treatment and data-acquisition method was demonstrated for 2-iodo-phenylalanine, currently under development as tumour tracer. More generally, it is recommended that animal experiments should include quantitative investigation of sedation and the data-acquisition method.

2.4.2. INTRODUCTION

Non-invasive animal imaging experiments require that movements of the animal should be minimized to reduce artefacts. To accomplish the latter setting, the animals are generally sedated over varying periods of time, according to the characteristics of the tracer being studied. When dissection is used to obtain Absorption-Distribution-Metabolism-Excretion data, the animals are generally not sedated to the same extent. Both experimental animal settings aims at obtaining preclinical data, which can be used for human extrapolations as applied in physiologic kinetic modelling. However, the influence of the sedation as well as of the data-acquisition method (imaging or dissection) is most often not investigated or taken into consideration.

Many reports described the effects of barbiturates on the neuronal system (1,2) and clinical pharmacology studies describe a thorough analysis of their influence on the central nervous system. However, less is published about the general impact of pentobarbital anaesthesia on the extra-cerebral metabolism. Zanelli et al. described the influence of pentobarbital on the blood perfusion in transplanted mouse tumours (3). Using ^{86}Rb, ^{125}I-human serum albumin and ^{51}Cr-labelled red blood cells, this anaesthetic was found on the one hand to increase the relative blood perfusion in tumours and kidneys, and to decrease the relative muscle perfusion but on the other hand it reduced the blood volume of the tumour and kidneys. Only a few investigations, designed to assess the influence of pentobarbital on the metabolism, are reported but either they did not use nuclear medicine imaging techniques (4,5) and/or the influence of sedation was only described for the biodistribution of a specific platinum drug (6).

In order to interpret correctly the planar imaging and dissection results of [^{123}I]-2-iodo-L-phenylalanine (7), the influence of pentobarbital on tumour tracer uptake was examined in vivo in rabdomyosarcoma tumour bearing athymic mice. Moreover, the differences between biodistribution by nuclear imaging and by dissection are investigated.

2.4.3. MATERIALS AND METHODS

2.4.3.1. Animal model

Male Swiss *nu/nu* mice (20-25g) obtained from Bio-Services (The Netherlands) were housed under sterile conditions with free access to food (SSNIFF® special treated, Bio-Services, The Netherlands) and water. They were accommodated in sterile conditions in a standard controlled environment. All animal studies were approved by the local ethical committee and were conform to the Belgian legislation.
Twelve athymic mice were subcutaneously inoculated with 1 million R1M rabdomyosarcoma tumour cells in the right armpit region. All mice grew tumours with a volume of approximately 1 ml after about 28 days. The mouse population was divided into groups with each group, anaesthetised and conscious, consisted of 6 animals at the start of the experiment.

Each group was subjected to dynamic planar imaging immediately after intravenous (IV) injection of the tracer 2-iodo-L-phenylalanine followed by static

planar imaging and dissection. [^{123}I]-2-iodo-L-phenylalanine ([^{123}I]-2-I-L-Phe) was prepared as previously published (7).

2.4.3.2. Anaesthesia

Nembutal sodium solution (Pentobarbital sodium; Ceva Santé Animale, Belgium) was administered intraperitoneally at a dose of 30 mg/kg, following the recommendations of the drug information insert. The animals used as the control group did not receive any sedation or a placebo.

2.4.3.3. Planar imaging

Imaging was performed using a gamma camera (Toshiba GCA-9300A/hg) in planar mode equipped with a high-resolution parallel-hole collimator. After the IV bolus injection of the [^{123}I]-labelled product in the lateral tail vein, the data were recorded on a 128 x 128 matrix (field of view: 23.5 x 12.5 cm) and with a photopeak window set at 15 % around 159 keV. Dynamic planar imaging was performed to visualize the kinetics of tracer distribution in the organs of interest. The same time schedule as described for [^{123}I]-2-iodo-L-phenylalanine was used (7). Time activity curves were obtained from region of Interest (ROI) analysis using a MRI intensity projection and the tracer uptake data were expressed as differential uptake ratio (DUR) and as % Injected dose per Pixel (%ID/P). DUR was defined as: [(counts per ROI $_{tissue}$ * Pixels per ROI $_{total\ body}$)/(Pixels per ROI $_{tissue}$ * counts per ROI $_{total\ body}$)]. The percentage injected dose per pixel was defined as: [(counts/pixel)$_{tissue}$/(Injected dose)*100%] (%ID/P) with the injected dose (ID) calculated as [(counts$_{calibration}$ * pixels$_{calibration}$ * activity in µCi $_{injection\ syringe}$)/(activity in µCi $_{calibration}$)], respectively. Dose calibration was performed with a syringe with known activity (measured on a calibrated NaI counting system; Capintec, CRC-15R; Ramsey, USA). The latter calculations were performed to meet the conclusions made by Boellaard and Thie et al. (8,9). The DURs for the dynamic planar imaging were extrapolated to 90 min using a Log scale.

Secondly, a static image was recorded in a 1024 x 1024 matrix at 90 min p.i. and the results of the static and dynamic planar imaging, both expressed as DURs, were compared. Due to the high amount of counts recorded in the bladder ROI, the latter ROI was masked and the results before and after masking were compared.

2.4.3.4. Dissection

The biodistribution by dissection was carried out immediately after the static planar imaging (at 90 min p.i.).

The injected dose (ID) was calculated by weighing the syringes before and after injection of the tracer and by the use of a dilution series of the injected tracer solution which was also weighed and counted for radioactivity using the auto gamma-counting system (CobraII Series, Canberra Packard, Meriden, CT, USA Cobra).

The animals were sacrificed by cervical dislocation. The organs and tissues of interest were removed, washed with 9‰ NaCl solution, dried and weighted. The blood was collected and weighted. The radioactivity of the samples was counted by

use of an auto gamma-counting system (CobraII Series, Canberra Packard, Meriden, CT, USA Cobra). The amount of radioactivity in the organs and tissues was calculated as the differential absorption ratio (DAR): [($activity_{tissue}$ * total body weight)/($weight_{tissue}$ * $activity_{injected\ dose}$)], or concentration in tissue (Bq/g)/injected dose per body weight (Bq/g). The ratio tumour to background (=frontleg) (RTB) was calculated.

2.4.3.5. Statistics

ANOVA and t-test statistical analysis was used to compare the results obtained by static and planar imaging at 90 min p.i. as well as the results obtained before and after masking of the bladder ROI.

A clustered boxplot analysis was performed to compare both imaging versus dissection and conscious versus sedation with Nembutal. Univariate ANOVA analyses was used to check the latter results.

2.4.3.6. Two-compartment modelling

Two-compartment modelling of the blood kinetics, obtained by dynamic planar imaging, for [^{123}I]-2-iodo-L-phenylalanine were fit to a two-compartment model with IV-bolus injection, without a lag time and with first order elimination, using WinNonlin 4.0.1. The primary parameters V_1, $k_{1,0}$ (elimination velocity), $k_{1,2}$ (distribution velocity to the peripheral compartment) and $k_{2,1}$ (distribution velocity from the peripheral to the blood compartment) were determined.

2.4.4. RESULTS

The dynamic planar imaging results of the different organs were extrapolated by linear regression from the first-order elimination phase (log-lin 10-30 minutes p.i.) to the 90 minute time-point. The results are given in Table 2.4.1.

TABLE 2.4.1: Extrapolated dynamic versus experimental static imaging results at 90 min p.i., expressed as DUR-values (mean ± std.dev.; n = 4 and 5 for the conscious and anaesthetized group, respectively).

Organ	Extrapolated dynamic		Experimental static	
	Anaesth	Conscious	Anaesth	Conscious
Heart	1.27±0.11	1.16±0.09	1.19±0.08	1.06±0.10
Kidney	1.76±0.09	1.81±0.16	1.89±0.14	1.67±0.18
Tumour	1.12±0.13	1.09±0.17	0.95±0.15	1.16±0.23
Contralateral background	0.69±0.12	0.51±0.08	0.57±0.07	0.45±0.07

ANOVA as well as the paired t-test (n=8) analysis of these results demonstrated that no statistically significant difference (at $\alpha = 0.05$) was obtained between the extrapolated dynamic and experimentally-obtained static planar imaging

DUR-values at 90 min p.i. As a consequence, the static planar imaging results were used for the equilibrium comparisons while the initial kinetics of tracer distribution were characterized with the dynamic planar imaging data. This analysis is important concerning the experimental setup for [^{123}I]-2-I-L-Phe imaging since the extrapolated dynamic study did not differ significantly from the static image at 90 minutes p.i. These results recommend using at all times the static imaging device if the initial tracer kinetics are not required. Indeed, the mice are easier to inject, the method is less time consuming and it is easier to conduct the experiments without sedation which will lead to higher tumour uptake values and lower bloodpool activity.

The imaging DUR-data of each organ obtained 90 min. p.i. from the static imaging experiment were obtained before and after masking of the bladder-ROI due to (1) differences in urinary excretion pattern between sedated and non-sedated mice and (2) to the high bladder accumulation together with the normalisation of these recorded data to the "bladder hot spot" by the data reconstruction procedure. Comparison using ANOVA demonstrated no statistically significant difference ($p = 0.451$) between both imaging modes related to the inclusion/exclusion of the bladder-ROI. Therefore, for all experiments, the imaging DUR's for heart, kidney, tumour and contralateral background were obtained with the bladder-ROI not eliminated in the imaging mode. This study demonstrated that the high bladder accumulation and thus the high activity concentration did not affect the results. This implicates that no saturation of the counting system took place and that the linearity of the calculations was not lost.

The initial uptake kinetics in the tumour and its contralateral background tissue, as well as the elimination-organ (kidney) are modelled by a rectangular hyperbola as used to represent saturable-pathway absorption (10). Similar to the biochemically well-known Michaelis-Menten and its linearised Lineweaver-Burke equation, this model allows the calculations of the initial velocity (V_0), the equilibrium activity (A_{eq}) and the time corresponding to reach half the A_{eq} ($t_{1/2}$). The data of the imaging up to 2.5 minutes p.i. were used in the calculations. The results are given in Table 2.4.2.

TABLE 2.4.2: Initial uptake kinetics of [^{123}I]-2-I-L-Phe by dynamic imaging (0 to 2.5 min) presented as mean ± std.dev. (n = 4 untreated and n = 5 for Nembutal treated).

	Tumour		**Contr. Background**		**Kidney**	
	Nemb	Untreated	Nemb	Untreated	Nemb	Untreated
V_0 (%ID/P.min)	0.66 ± 0.023	0.79 ± 0.10	0.49 ± 0.09	0.19 ± 0.06	1.62 ± 0.22	2.43 ± 0.36
A_{eq} (%ID/P)	0.08 ± 0.00	0.08 ± 0.00	0.04 ± 0.00	0.02 ± 0.00	0.17 ± 0.00	0.10 ± 0.00
$t_{1/2}$ (min)	0.123 ± 0.01	0.10 ± 0.01	0.09 ± 0.02	0.12 ± 0.01	0.10 ± 0.01	0.04 ± 0.01

The blood kinetics obtained by dynamic imaging of the heart are shown in Figure 2.4.1. Two-compartment modelling demonstrated that Nembutal slowed down the elimination velocity ($k_{1,0}$). Moreover, kinetic modelling indicated a slower

distribution of the tracer towards the peripheral compartment organs ($k_{1,2}$) but an equal release velocity of the tracer from the peripheral compartment ($k_{2,1}$).

FIGURE 2.4.1: Representation of the blood kinetics by 2-compartmentmodelling on the dynamic imaging results: fitting of the theoretical curve to the observed blood-curve (%ID/P = % injected dose per pixel).

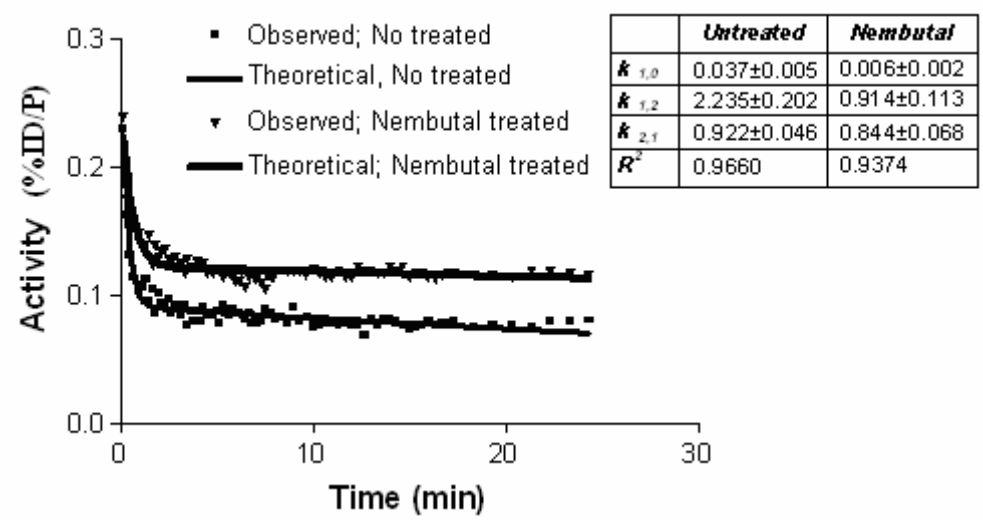

	Untreated	Nembutal
$k_{1,0}$	0.037±0.005	0.006±0.002
$k_{1,2}$	2.235±0.202	0.914±0.113
$k_{2,1}$	0.922±0.046	0.844±0.068
R^2	0.9660	0.9374

The results at 90 min p.i. obtained by dissection and static imaging, each with Nembutal-treated and untreated animals, are given in Table 2.4.3, representing a 2 x 2 factorial experimental design. Values given for each combination method-treatment are mean values ± std.dev. (n = 4 for untreated and 5 for Nembutal-treated mice).

TABLE 2.4.3. Equilibrium DUR/DAR results of [^{123}I]-2I-L-PA at 90 min. p.i.

Organ	Method	Nembutal-treated	Untreated
Heart	Imaging	1.19 ± 0.08	1.06 ± 0.10
	Dissection	0.89 ± 0.07	0.73 ± 0.10
Kidney	Imaging	1.89 ± 0.14	1.67 ± 0.18
	Dissection	1.04 ± 0.10	0.97 ± 0.15
Tumour	Imaging	0.95 ± 0.15	1.16 ± 0.33
	Dissection	2.40 ± 0.10	3.13 ± 0.33
Contr Bckgr	Imaging	0.57 ± 0.07	0.45 ± 0.07
	Dissection	0.72 ± 0.05	0.61 ± 0.09
Ratio RTB	Imaging	1.67 ± 0.21	2.54 ± 0.44
	Dissection	3.32 ± 0.20	5.13 ± 0.24

The dependence of the DAR/DUR results on the three factors (organ, method and treatment) was analysed by a 3-factor ANOVA analysis, demonstrating all three factors had a significant effect. Post-hoc testing for organ clustering showed each organ to be treated as a separate group, indicating each of the investigated organs behaves differently with respect to the equilibrium tracer uptake. The tumour is the disease target-organ, while the contralateral background is not only the control but is

representing the general body-tissues as well. The heart is representative for the blood-activity, while the kidney is the main elimination organ.

Therefore, a 2-factor ANOVA analysis was performed for each organ separately (Table 2.4.4).

TABLE 2.4.4: ANOVA results for heart, kidney, tumour and contralateral frontleg.

Source	heart	kidney	tumour	Contr.bckgr
Treatment	0.003	0.053	0.001	0.004
Method	< 0.001	< 0.001	< 0.001	< 0.001
Treatment x Method	0.697	0.299	0.036	0.891

For the kidney, heart and contralateral background, the method and the treatment showed a statistically significant effect (although marginal treatment effect for kidney), but the interaction was not significant. For the tumour and the RTB, the effect of the individual factors as well as their interaction was highly significant. The detailed ANOVA results for the ratio RTB, the ultimate response in tumour tracer development, is given in Table 2.4.5.

TABLE 2.4.5: ANOVA results for RTB

Source	SS	df	MS	F	P
Treatment	7.992	1	7.992	103.5	0.000
Method	19.975	1	19.975	258.7	0.000
Treatment x Method	0.966	1	0.966	12.5	0.003
Error	1.081	14	0.077		
Total	29.287	17			

The difference of RTB-results between dissection (mean value of 4.22) and imaging (mean value of 2.10) is thus statistically significant (at $\alpha = 0.05$). Similarly, the RTB-results of Nembutal-treated (mean value of 2.49) and untreated mice (mean value of 3.83) are also statistically significant different. An ordinal interaction is observed between sedation-treatment and data-acquisition-method, indicating that the difference between the RTB means for Nembutal-treated and the untreated mice depends on the data-acquisition-method. For example, with dissection, the difference between the RTB means for Nembutal-treated and untreated mice is 1.81. But when we look at the difference obtained by imaging, a mean value of 0.87 is obtained. The interaction is clearly observed in the graphical representation by clustered box-plots (Figure 2.4.2).

FIGURE 2.4.2. Clustered boxplots of the 90 min p.i. results, expressed as differential absorption ratio (DAR), respectively differential uptake ratio (DUR).

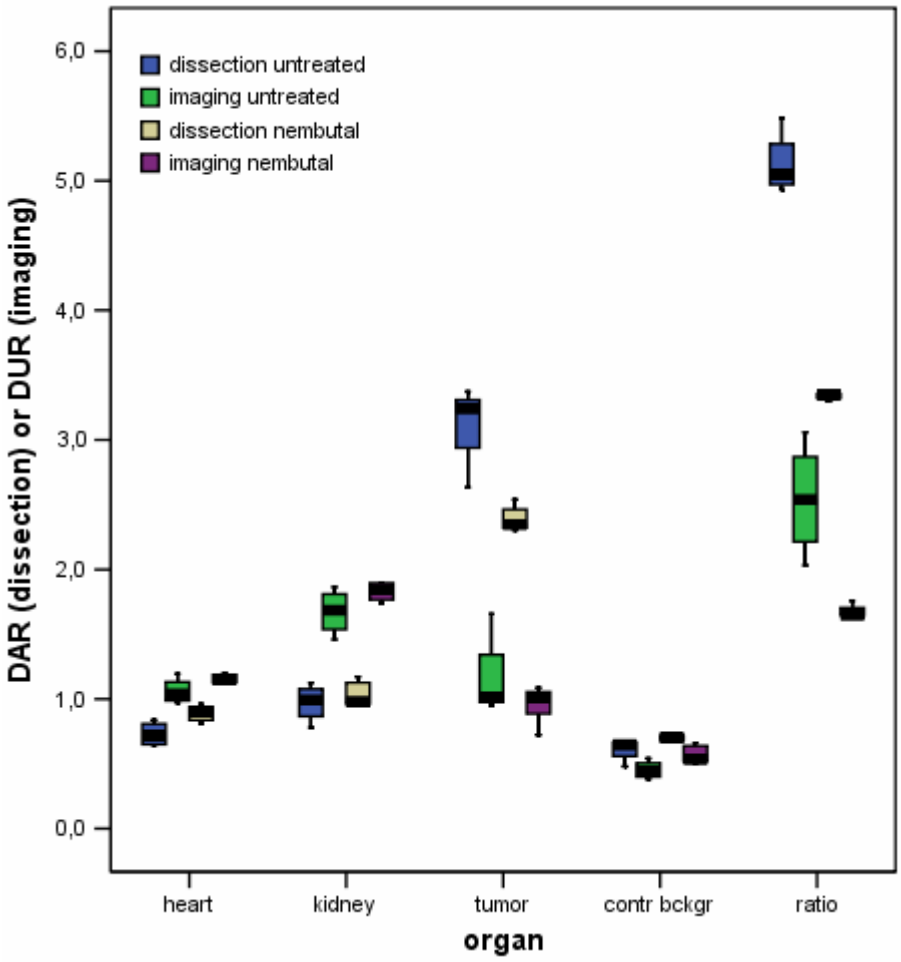

2.4.5. DISCUSSION

Barbiturates interact with the gamma-aminobutyric acid (GABA) transmission. GABA is the most common inhibitory transmitter in the mammalian nervous system. Activation of the postsynaptic GABA receptors results in hyperpolarization, thereby inhibiting the postsynaptic neuron. The GABA receptor is an oligomeric complex which includes i.a. a barbiturate binding site. Binding of barbiturates to this receptor decreases the rate of dissociation of GABA from its receptor, thus prolonging the duration of GABA-induced hyperpolarization.

The barbiturates are negative inotropic agents. They produce dose-dependent decreases in ventricular *dP/dt* and the force-velocity relationship of ventricular muscle (11). The main hemodynamic effect of parenteral barbiturates is a decrease in arterial blood pressure that is compensated for by an increase in heart rate. This decrease in arterial pressure is due to peripheral vasodilation induced by depression of the medullary vasomotor center and decreased sympathic outflow. Alterations in liver or kidney function associated with their use are considered secondary to hemodynamic effects of the drugs and altered perfusion.

Barbiturates, e.g. pentobarbital, are quite often used as sedating agent in animal experiments. When performing tracer animal studies, it is important to identify the influence of sedation on tracer distribution since these preclinical data are used for human extrapolation. As reported earlier, barbiturates may affect the relative blood perfusion and the blood volume of the studied organs and consequently may alter the elimination velocity of the compound. In nuclear medicine and radiopharmology, the influence of the sedation may be well confounded with the data-acquisition method (dissection or imaging).

Kinetic two-compartment modelling demonstrated that Nembutal both decreases the elimination velocity ($k_{1,0}$), and thus blood clearance of [^{123}I]-2-I-L-Phe, and the biodistribution velocity ($k_{1,2}$) of the compound to the peripheral compartment. Both observations will lead to higher bloodpool and kidney activities after administering the pentobarbital solution which confirmed by the equilibrium organ data as given in Table 2.4.3 and Figure 2.4.2.

Besides the two-compartment blood modelling, the initial uptake kinetics of the tissues and organs of interest could also be investigated using the model as described by Mertens et al (10). This analysis confirmed the 2-compartment modelling as it demonstrated a higher initial uptake velocity and a lower $t_{1/2}$ value for [^{123}I]-2I-L-PA in the tumour and the kidneys of the untreated mice. Besides kinetic information, a prediction of the steady state (= equilibrium for tracer uptake) values could be performed. Although the initial kinetics for tracer uptake differed between the 2 experimental treatment-groups, they demonstrated the same tumour uptake at equilibrium but a higher kidney uptake in the Nembutal treated group. The latter could be due to the presence of urine in the kidneys: as both kinetic modelling procedures illustrated a slower elimination of the tracer, it would take relatively a longer time to clear the tracer from the blood when the mice are sedated. This explanation is supported by the comparison between the 2 data-acquisition methods. Indeed, the differences of tracer uptake in the kidneys are much smaller when using dissection, when the organs are washed and dried to remove the urine and blood fraction, as compared to imaging, where the ROI for the kidney includes the tissue, the blood and urine. The same rationale explains the higher imaging results for heart and kidneys as compared to the dissection (Figure 2.4.2).

The method and the treatment showed both a highly significant effect on the individual organs: the target tumour organ showed significant lower [^{123}I]-2-I-L-Phe uptake values after sedation while the blood and kidney values were elevated. This will result not only in a higher radiation burden for the animal, but also in lower tumour to blood ratios and thus a more difficult tumour detection with imaging techniques. However, the tumour could still be visualized using this non-invasive imaging method in combination with Nembutal despite its worst case scenario. The influence of Nembutal on tumour detection is also well illustrated by the RTB: both data-acquisition procedures result in a 1.5 fold lower ratio when sedation was administered.

2.4.6. CONCLUSION

The data-acquisition method (dissection versus imaging) as well as sedation-treatment (Nembutal-treated versus untreated animals) significantly influence the organ uptake results of [^{123}I]-2-I-L-Phe.

It is recommended that animal experiments should always include a quantitative investigation of these two factors, so that the results can be correctly interpreted.

2.4.7. REFERENCES

1. Hodes JE, Soncrant TT, Larson DM, Carlson SG, Rapoport SI.Selective changes in local cerebral glucose utilization induced by phenobarbital in the rat. *Anesthesiology* 1985;63:633–639.
2. Nilsson L, Siesjo BK. The effect of phenobarbitone anaesthesia on blood flow and oxygen consumption in the rat brain. Acta Anesthesiol Scand Suppl 1975;57:18–24.
3. Zanelli GD, Lucas PB and Fowler JF. The effect of anaesthetics on blood perfusion in transplanted mouse tumours. *Br J cancer* 1975;32:380-390.
4. Baudelet C and Gallez B. Effect of anesthesia on the signal intensity in tumours using BOLD-MRI: Comparison with flow measurements by laser Doppler flowmetry and oxygen measurements by luminiscence-based probes. *Magnetic resonance Imaging* 2004;22:905-912.
5. Okinieff P, Rummeny E, Vaupel P, et al. Effects of pentobarbital-anesthesia on the energy-metabolism of murine tumours studied by in vivo P-31 nuclear magnetic resonance imaging. *Radiation research* 1988;115:361-372.
6. Sancho AR, Dowell JA and Wolf W. The effects of anesthesia on the biodistribution of drugs in rats: a carboplatin study. *Cancer Chemother Pharmacol* 1997;40:521-525.
7. Kersemans V, Cornelissen B, Kersemans K, et al. In vivo characterisation of 2-iodo-L-phenylalanine in a R1M rabdomyosarcoma mouse model as a potential tumour tracer for SPECT. *J Nucl Med* 2005;46:532-539.
8. Boellaard R, Nanda CK, Hoekstra OS, et al. Effects of noise, image resolution and ROI definition on the accuracy of Standard Uptake Values: a simulation study. *J Nucl Med* 2004;45:1519-1527.
9. Thie JA. Understanding the standarized uptake value, its methods and implications for usage. *J Nucl Med* 2004;45:1431-1434.
10. Mertens J, Kersemans V, Bauwens M, et al. Synthesis, radiosynthesis, and in vitro characterization of [125I]-2-iodo-L-phenylalanine in a R1M rhabdomyosarcoma cell model as a new potential tumour tracer for SPECT. J Nucl Med Biol 2004;31:739-746
11. Stowe DF, Bosnjak ZJ, Kampine JP: Comparison of etomidate, ketamine, midazolam, propofol, and thiopental on function and metabolism of isolated hearts. *Anesth Analg* 1992; 74: 547.

CHAPTER CONCLUSION

The precursor 2-iodo-L-phenylalanine was synthesized from its bromo-derivative 2-bromo-L-phenylalanine using the Cu^{1+}-assisted nucleophilic exchange in acidic and reducing conditions. An experimental design allowed us to determine the optimal reaction conditions resulting in a yield of at least 60% without the formation of undesired side products or stereoisomers and with an easy purification procedure. A Kit-formulation based on the same principle allowed fast and quantitative routine radioiodination of 2-iodo-L-phenylalanine without the need for extra purification which is a great added value for everyday clinical practice.

The in vitro studies in the R1M cell model illustrated that, although a bulky iodine atom was incorporated at the 2 position of the molecule, 2-iodo-L-phenylalanine is still transported by the L-amino acid transporter subtype 1 (LAT1). Moreover, the new amino acid analogue illustrated almost the same affinity for this transporter system as compared to the native L-phenylalanine and L-tyrosine. RT-PCR and inhibition experiments showed that 2-iodo-L-phenylalanine is transported for the largest part by LAT1. Additionally, 2-iodo-L-phenylalanine is not incorporated into the cell proteins and LAT1 coupled influx of radioactivity is directly related to the requirement of amino acids for protein synthesis or cell metabolism. Thus, even not incorporated, 2-iodo-L-phenylalanine uptake reflected the total "amino acid turn-over" of the tumour cells.

In vivo, tumour uptake of [^{123}I]-2-iodo-L-phenyalanine demonstrated fast, high and specific tumour accumulation. As compared to the in vitro studies, the same kinetic approach could be applied: the uptake as a function of time followed a rectangular hyperbolic curve and a pseudo reversible pseudo first order reaction was followed. These observations, together with the displacement [^{123}I]-2-iodo-L-phenylalanine radioactivity in the tumour by L-phenylalanine, strongly indicated that in vivo, [$^{123/1225}$I]-2-iodo-L-phenylalanine is also transported by the LAT1 system, an "obligatory exchanger" transport system.

Regarding the general biodistribution characteristics, 2-iodo-L-phenylalanine was cleared fast from the blood through the kidneys to the bladder. No accumulation was noticed in the kidneys, brain and the abdominal organs with an exception of the pancreas which is typical in rodents. Moreover, the new tracer showed negligible uptake in inflammatory lesions in comparison to ^{18}F-FDG.

Additionally, the effect of sedation and data-acquisition method (dissection or planar imaging) on [^{123}I]-2-iodo-L-phenylalanine distribution in R1M-bearing athymic mice was investigated. Kinetic modelling of the initial biodistribution kinetics revealed that pentobarbital both decreases the elimination velocity ($k_{1,0}$), and thus blood clearance of [^{123}I]-2-iodo-L-phenylalanine, and the biodistribution velocity ($k_{1,2}$) of the compound to the peripheral compartment. Moreover, the method and treatment showed both a highly significant effect on the individual organs: the target tumour organ showed significant lower [^{123}I]-2-iodo-L-phenylalanine uptake values after sedation while the blood and kidney values were elevated. However, the tumour could still be visualized using this non-invasive imaging method in combination with Nembutal despite its worst case scenario.

CHAPTER 3:

Evaluation of [$^{123/125}$I]-2-iodo-D-phenylalanine as a tumour tracer for SPECT.

CHAPTER INTRODUCTION

During the last decades, the development of radioisotope labelled amino acids for tumour diagnosis was focused on the L-enantiomers as it was supposed that the amino acid tracers had to be incorporated into the tumour cell proteins. Today, the latter hypothesis is refuted and regarding the unnatural character of D-amino acids, our research group additionally developed [^{123}I]-2-iodo-D-phenylalanine

The use of D-amino acids in oncology might find some applications due to their unnatural character. Exogenous uptake of D-amino acids (by ingestion or from micro-organisms) will lead to the metabolization by D-amino acid oxidase, present in liver and kidneys, resulting in the formation of the corresponding α-keto acid and ammonium. The latter together with the stereospecificity of the translational machinery will result in the formation of proteins uniquely consisting of L-amino acids. Moreover, regarding these characteristics, D-amino acids, transported by LAT1, will clear faster from the blood, will not incorporate into the cell proteins, and will be transported by the LAT1 transporter with high affinity, as compared to the corresponding L-isomers. As a result, promising D-amino acid tracers for in vivo oncologic imaging could be developed.

The cold precursor 2-iodo-D-phenylalanine was synthesized by analogy with its L-isomer: the optimal reaction conditions for 2-iodo-L-phenylalanine precursor synthesis using the Cu^{1+} assisted nucleophilic exchange in acidic and reducing conditions were applied. Moreover, the same Kit-formulation could be used for the radioiodination of the precursor 2-iodo-D-phenylalanine leading to the same radiochemical yield and purity.

Just like the L-analogue, [^{123}I]-2-iodo-D-phenylalanine was first evaluated in vitro in the R1M rhabdomyosarcoma cell model. The time course for tracer uptake was examined in MEM up 24 hours to determine the long time kinetics. Transport characterisation was performed in the presence of several inhibitors. Michaelis-Menten and Lineweaver Burk plots were applied to obtain K_m and K_i values for [^{125}I]-2-iodo-L-phenylalanine cell uptake, respectively. Moreover, the incorporation into the cell proteins of the new amino acid analogue was investigated.

Subsequently, in vivo characterisation was performed of [^{123}I]-2-iodo-D-phenylalanine as a tumour tracer by means of dynamic planar imaging and dissection in the R1M athymic mouse model. Just like the in vivo evaluation of the L-isomer, the tumour uptake, the excretion route and the metabolic stability of [^{123}I]-2-iodo-D-phenylalanine was examined. The specificity of tumour uptake was determined by (1) a displacement study and by (2) a biodistribution study of the tracer in NMRI mice bearing an acute inflammation. In the latter setting, the uptake of [^{123}I]-2-iodo-L-phenylalanine in the inflamed tissue was compared to that of ^{18}F-FDG. Two-compartment blood modelling was applied to investigate the short time kinetics. Moreover, tumour retention and tumour contrast were examined up to 31 hours post tracer injection. Additionally, dosimetric calculations were performed on the dissection data of [^{123}I]-2-iodo-D-phenylalanine, [^{123}I]-2-iodo-L-phenylalanine and [^{123}I]-2-iodo-L-tyrosine in order to compare the extrapolated effective dose of both new amino acid analogues with the tyrosine analogue. These results were compared to the initial kinetic two-compartment modelling and the consistency of the results was checked.

3.1 In vitro characterisation of [^{125}I]-2-iodo-D-phenylalanine in a R1M rhabdomyosarcoma cell model as a new potential tumour tracer for SPECT.

Keywords: [^{125}I]-2-iodo-D-phenylalanine, LAT1 transport uptake, accumulation, SPECT, radionuclide therapy .

Performed in corporation with and at the Free University of Brussels.

3.1.1. ABSTRACT

The aim of this study was the in vitro evaluation of [$^{123/125}$I]-2-iodo-D-phenylalanine. **Methods:** The radioactive product was prepared in one pot Kit with a yield and radiochemical purity exceeding 98%. *In vitro*, time course and concentration dependency and the cellular uptake mechanism were assessed in R1M rat rhabdomyosarcoma cells. Also, the efflux mechanism was studied. **Results:** The uptake of [^{125}I]-2-iodo-D-phenylalanine was high, Na^+ independent, saturable (Km = 32 μM) and competitively and quantitatively inhibited by BCH and L-phenylalanine, while its efflux from the cells was stimulated by these same compounds pointing to an anti-port type LAT1 system. The compound was not incorporated into proteins. **Conclusion:** The typical LAT1 uptake mechanism makes [^{123}I]-2-iodo-D-phenylalanine a promising tracer for specific tumour imaging in and outside the brain with SPECT.

3.1.2. INTRODUCTION

Already in 1978, 1982 and 1984 Tamessa and Goto et al. and Takeda et al. (1-3) showed uptake of [^{14}C]-labelled D-leucine, D-alanine and D-tryptophane in mice tumour and human tumour derived tumour cells induced in nude mice, without being able to explain this phenomenon at that time. They suggested that D-leucine was transported by the same transporter as L-leucine, but that the isomers were supposed to bind to different parts of the transporter. This transporter was later defined as the L-transporter. In 1985 Meyer et al. (4) showed that both the L and D form of the [^{11}C]-methionine could accumulate in human brain tumours. Since then all the development of and studies with radioactively labelled amino acids for tumour diagnosis with PET and SPECT were focused on the L-enantiomeric form as it was supposed that the amino acid tracers had to be incorporated into the tumour cell proteins. More recently Langen et al. (5) and Lahoutte et al. (6-9) showed that it is the increased L-mediated transport of amino acid analogues into tumour cells and not necessary the incorporation that is needed for efficient tumour imaging and follow up. Moreover, Langen et al. (5) have

demonstrated that the expression of L transporters and related reversible uptake depended on the proliferation rate of human glioma cells.

This L transporter is a major nutrient transport system responsible for Na^+- independent transport of large neutral amino acids including synthetic amino acids by an obligatory exchange mechanism coupled to an anti-port system (10, 11). The heterodimeric LAT transporter contains 2 subunits, a heavy chain 4F2/CD98 and a light chain named LAT1 or LAT2. LAT1 expression was scarcely detected in non-tumour areas (12-14) but highly expressed (up-regulated) in proliferating tissues, in particular malignant tumours, as it plays a critical role in cell growth and proliferation (14,15). A remarkable characteristic of system L and the hLAT-1 amino acid uptake is its broad substrate selectivity, which enables the transporter to accept amino acid related compounds, such as D-amino acids and cancer drugs like Melphalan (1, 12). LAT2 on the other hand has a high level of expression in small intestine, kidney, placenta, brain and in epithelia and blood-tissue barriers. It transports all of the isomers of neutral alpha-amino acids by facilitated diffusion; however it does not transport D-amino acids.

2-iodo-L-tyrosine and 2-iodo-L-phenylalanine (6-9, 16-21) show a very high tumour selectivity when compared to [^{18}F]-FDG which is taken up considerably in brain and inflammatory tissue (22-24). We have shown that [^{14}C]-D-phenylalanine and D-phenylalanine were taken up in R1M cells by the LAT transport system (25, 26). R1M cells are proposed to evaluate [$^{123/125}$I]-2-iodo-D-phenylalanine in vitro.

3.1.3. MATERIALS AND METHODS

All the conventional products mentioned were at least analytical or clinical grade and obtained from Sigma-Aldrich. The solvents were of HPLC quality (VWR, Belgium).

3.1.3.1. Precursor synthesis and radiolabelling

The synthesis of 2-iodo-D-phenylalanine/2-iodo-L-phenylalanine and the labelling were achieved as earlier described (20). Quality control was achieved by HPLC, using a C8-column (LichrosPher 100RP8 (5 µm), Lichrocart 125-4) and 10/90 MeOH/H_2O containing 1 mM NH_4Ac as mobile phase at 1.0 ml/min while monitoring UV absorption (Hitachi UV detector, 254 nm) and radioactivity (NaI(Tl)-detector (Harshaw chemie)).

Chiral chromatography was performed on a chiral column (5µm Chirobiotic T (Astec) column (150 mm x 4.6 mm)) using 80/20 Methanol/H_2O (v/v) containing 20 mM NH_4Ac at a flow of 1 mL/ minute. In these conditions a complete separation of the chiral isomers was obtained. The capacity values (k') of 2-iodo-L-phenylalanine and 2-iodo-D-phenylalanine were 2.7 and 3.8, respectively.

3.1.3.2. Reverse Transcriptase – PCR

Primers were designed as shown in Table 3.1.1 (27).

TABLE 3.1.1: Primer sequences of the LAT specific mRNA

Primer	Sense	
LAT1	Forward	5'- TGTGCTGGCATTATACAGCG - 3'
	Backward	5'- AGGTGATAGTTCCCGAAGTC - 3'
LAT2	Forward	5'- TTTCCAGGAACCTGACATCG - 3'
	Backward	5' - ACATTGCAGTACATAAGCG - 3'
4F2hc	Forward	5'- GAATGAGTTAGAGCCCGAGA - 3'
	Backward	5'- CGATTATGACCACGGCACCA - 3'

Reverse Transcriptase PCR was performed on the R1M cell line using BioTaq RED (Bioline) according to manufacturer guidelines. The amplification of the cDNA strands was performed using the following conditions:

- Pre-cycle: 94°C during 3', 60°C during 1', 72°C during 2'
- 26 cycles of: 94°C during 1', 60°C during 1', 72°C during 2'
- Hold: 72°C during 10'

Gel-electrophoresis was performed on a 1.5% agarose/EtBr gel at 250V and 250mA during 15 minutes. The entire PCR product was loaded onto the gel, Hyperladder IV (Bioline) was used as a marker. Actin was used as a positive control of the method, while as a positive control cell line (4), HeLa cell line was used to confirm the validity of the RT-PCR method.

3.1.3.3. Cell model.

3.1.3.3.1. Cell cultures.

R1M rhabdomyosarcoma cells (VUB) were cultivated as described before (14).

3.1.3.3.2. In vitro experiments.

All in vitro experiments were carried out in 6-well-plates (VWR), using three wells for each data-point. Influx and efflux were studied both in a Na^+ containing buffer (pH 7,4; HEPES+ (Sigma), 100 mM NaCl (VWR), 2 mM KCl (Sigma), 1 mM $MgCl_2$ (VWR), 1 mM $CaCl_2$ (VWR), 10 mM Hepes (Sigma), 5 mM Tris (VWR), 1 g/l glucose (VWR) and 1 g/l Bovine Serum Albumine (Sigma)), a Na^+ free buffer (pH 7,4; HEPES-, 100 mM Choline-Cl (Sigma), 2 mM KCl, 1 mM $MgCl_2$,1 mM $CaCl_2$, 10 mM Hepes, 5 mM Tris, 1 g/l glucose and 1 g/l Bovine Serum Albumin) and MEM buffer (pH 7.2, containing essential and non essential amino acids of which 1.2 mM of amino acids known to be transported by the L transport system). The process was terminated by physical withdrawal of the buffer and washing three times with ice-cold phosphate-buffered saline (PBS). Subsequently, the cells were detached from the well with 2 ml of 0, 1 M NaOH. The radioactivity of the samples was counted using a gamma-counting-system (Cobra-inspector 5003, Canberra Packard, Meriden, CT, USA).

3.1.3.4. Time and concentration dependency:

For the kinetic studies the cells were incubated for times ranging from 1 to 20 minutes in 1 ml of 0.1 mM 2-iodo-D-phenylalanine or 2-iodo-L-phenylalanine respectively in HEPES+, HEPES- or MEM containing 37 kBq [^{125}I]-2-iodo-D-phenylalanine or 37 kBq [^{125}I]-2-iodo-L-phenylalanine respectively. [^{3}H]-L-phenylalanine (Amersham Biosciences), [^{3}H]-L-tyrosine (Perkin Elm, Canberra) or [^{14}C]-D-phenylalanine were used as reference products.

For concentration dependency, uptake was measured at 1 min uptake with concentrations of 2-iodo-D-phenylalanine varying from 0.01 to 0.2 mM. The data were fit to the Michaelis-Menten relation and the apparent K_m, V_{max} and K_i values were calculated from Eady-Hofstee and Hanes-Woolf and Lineweaver-Burk (LWB) plots. "Apparent K_m" is calculated from V_o conditions, i.e. uptake after 1 minute where only influx has to be considered.

Using [^{3}H]-L-phenylalanine/L-phenylalanine as a reference molecule, the type of competition and K_i value of 2-iodo-D-phenylalanine, 2-iodo-L-phenylalanine and D-phenylalanine were determined using a double-reciprocal Lineweaver-Burk plot. Concentrations of L-phenylalanine varied from 0.01 to 0.2 mM, while inhibitor concentrations were set at 0.1 mM.

3.1.3.5. Inhibition of [^{125}I]-2-iodo-D-phenylalanine influx

In these inhibition experiments the cells were incubated with 37 kBq [^{125}I]-2-iodo-D-phenylalanine for 1 minute in HEPES+ and HEPES- buffer supplemented with 8 mM L-phenylalanine (a LAT transport system inhibitor, BCH (2-Amino-2-norbornane-carboxylic acid, a LAT transport system specific inhibitor) or MeAIB (Methyl amino isobutyric acid, a A/ASC transport system specific inhibitor).

3.1.3.6. Incorporation into cell proteins

The cells were incubated with the radioactive amino acid for a period ranging from 15 minutes up to 18 hours in MEM under constant CO_2 partial pressure (5%) using the GENBOX system. After removal of the radioactive solution, the cells were submitted twice to efflux conditions in fresh MEM solution and washed with ice cold PBS buffer. Precipitation of proteins was performed by adding 2 mL of 20 % trichloroacetic acid, intense mixing (vortex) followed by cooling during 30 minutes at 0 °C. After two times of repeated centrifugation and washing, 2 ml of 0.1 M NaOH was added and radioactivity was counted.

3.1.3.7. Trans- stimulation of [^{125}I]-2-iodo-D-phenylalanine or [^{125}I]-2-iodo-L-phenylalanine efflux.

The cells were incubated with 37 kBq [^{125}I]-2-iodo-D-phenylalanine or 37 kBq [^{125}I]-2-iodo-L-phenylalanine for 15 minutes in HEPES- buffer. The incubation medium was removed and the cells were washed three times with ice-cold PBS. Subsequently HEPES- buffer

containing 0.1 mM L-phenylalanine was added. The efflux medium was removed after 30 seconds or 1 minute, after which the cells were washed three times with ice-cold PBS, detached with 0.1 M NaOH, suspended and counted.

3.1.4 RESULTS

3.1.4.1. Chemistry and radiochemistry

2-iodo-D-phenylalanine and 2-iodo-L-phenylalanine were pure for at least 99%. The labelling yield in Kit conditions (2 component Kit) was at least 98%. The final injection ready product showed a radiochemical purity of > 99% and was sterilised with a sterile 0.22 μm Ag-membrane filter (Millipore). At the end of labelling the specific activity of both [^{125}I]-2-iodo-L-phenylalanine and [^{123}I]-2-iodo-D-phenylalanine was 10.9 GBq/mmol. Chiral chromatography showed that no chiral modification occurred during the labelling. The sterile and isotonic [^{123}I]-2-iodo-D-phenylalanine solution was injected in the rats within 2 - 4 hours after the preparation. The [^{125}I]-labelled compound was stored at 4°C. HPLC analysis during the long time course of the experiments revealed the quality of the preparation to be stable for at least a month. After that period a small amount of free radioiodide was observed (2-3%). This was quantitatively removed by filtering the solution through a sterile 0.22 μm Ag-membrane filter.

3.1.4.2. In vitro evaluation.

3.1.4.2.1. RT-PCR

The RT-PCR result, as obtained by gel-electrophoresis for the R1M cell line is depicted in Figure 3.1.1.

FIGURE 3.1.1: RT-PCR as obtained by gel-electrophoresis of the R1M cell line.

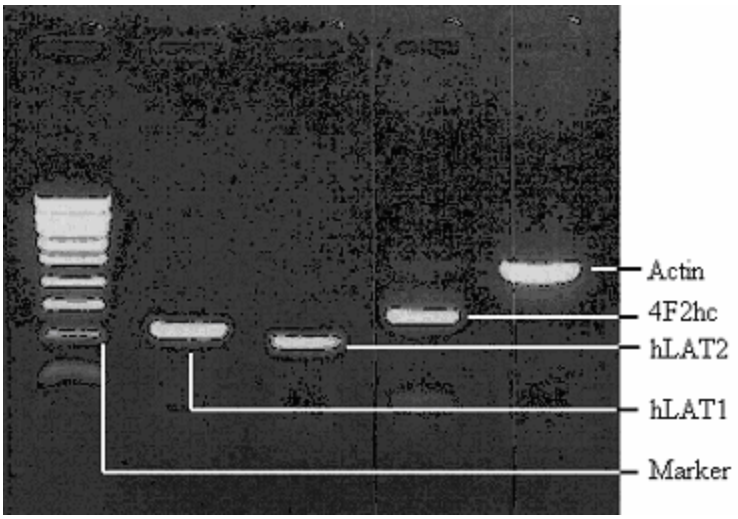

3.1.4.2.2. Time and concentration depending kinetics and affinity

Within the first hour, the uptake of [^{125}]-2-iodo-D-phenylalanine in R1M cells in MEM buffer is about 25% lower than that of [^{125}I]-2-iodo-L-phenylalanine (Figure 3.1.2). The uptake of both compounds at longer times, up to 24 hours, shows a slight accumulation which is not due to incorporation (the iodinated phenylalanine analogues are not incorporated into the cell proteins) nor to cell growth (the results are expressed per million cells).

FIGURE 3.1.2: [^{125}]-2-iodo-D-phenylalanine and [^{125}]-2-iodo-L-phenylalanine Uptake-time kinetics in R1M cells in MEM buffer: mean ± SD (n = 9).

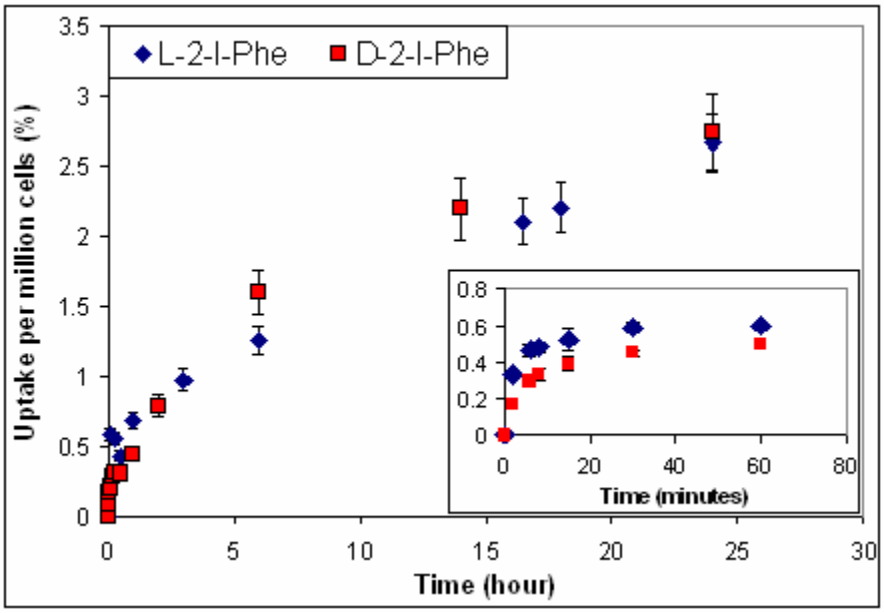

The uptake in V_o conditions (at the 1 minute) of [^{125}]-2-iodo-D-phenylalanine as a function of 2-iodo-D-phenylalanine concentration (0.01 – 0.2 mM) is saturable and follows the Michaelis-Menten relation. The related Eady-Hofstee plot shows a single substrate – transport system interaction (Figure 3.1.3).

FIGURE 3.1.3: Eady-Hofstee plot of uptake of [^{125}I]-D-2-iodo-phenylalanine/D-2-iodo-phenylalanine in R1M cells at Vo Data expressed as mean ± SD (n = 3).

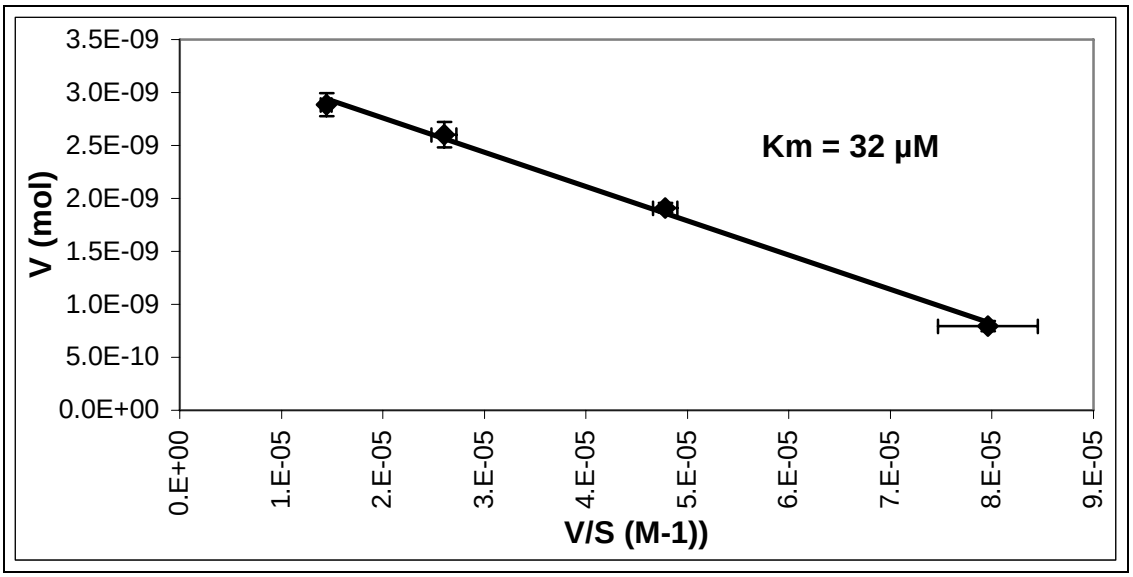

The resulting apparent Km value is 32 ± 10 µM. The Ki calculated from the inhibition of the uptake of [^{3}H]-L-phenylalanine/L-phenylalanine in R1M cells in HEPES- medium resulted in a value of 50 ± 10 µM (Figure 3.1.4). In the same conditions 2-iodo-L-phenylalanine and D-phenylalanine showed Ki values of 35 ± 10 µM and 124 ± 10 µM respectively.

FIGURE 3.1.4: Inhibition of [^{3}H]-L-phenylalanine/L-phenylalanine uptake by D-2-iodo-phenylalanine, D-phenylalanine and 2-iodo-L-phenylalanine: Lineweaver-Burke plot Data expressed as mean ± SD (n = 3).

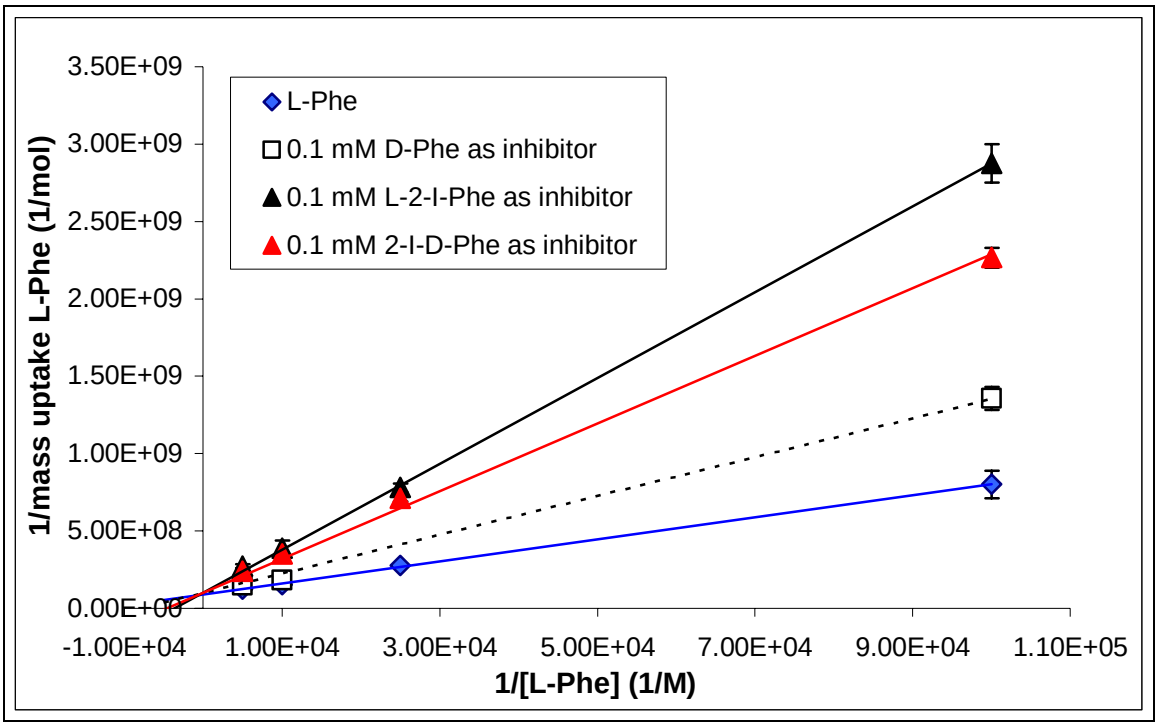

3.1.4.3.3. Transport Type Characterisation.

There was no significant difference between the uptake of [^{125}I]-2-iodo-D-phenylalanine in HEPES+ (Na^+ presence) and HEPES- (Na^+ absence) and the uptake was reduced to 2 % of the original value by both the presence of 8 mM of L-phenylalanine and of 8 mM BCH, a specific inhibitor of L transport system (Figure 3.1.5). Moreover, the inhibition by 8 mM MeAIB (a specific inhibitor of the Na+ dependent A/ASC transport system) is negligible. Figure 3.1.4, representing a double-reciprocal Lineweaver-Burk plot, reveals that the inhibition of [^{3}H]-L-phenylalanine by 2-iodo-D-phenylalanine, 2-iodo-L-phenylalanine and D-phenylalanine (the latter both proven LAT transported amino acids) is competitive. 0.1 mM 2-iodo-D-phenylalanine caused a net efflux of 26 % within 1 minute of the initial uptake of [^{3}H]-L-phenylalanine and the efflux of [^{125}I]-2-iodo-D-phenylalanine from the cells is stimulated by L-phenylalanine and BCH.

FIGURE 3.1.5: Uptake of [^{125}I]-2-iodo-D-phenylalanine in presence and absence of Na+ and the inhibition by 8 mM L-phenylalanine, 8 mM BCH and 8 mM MeAIB. Data expressed as mean ± SD (n = 3).

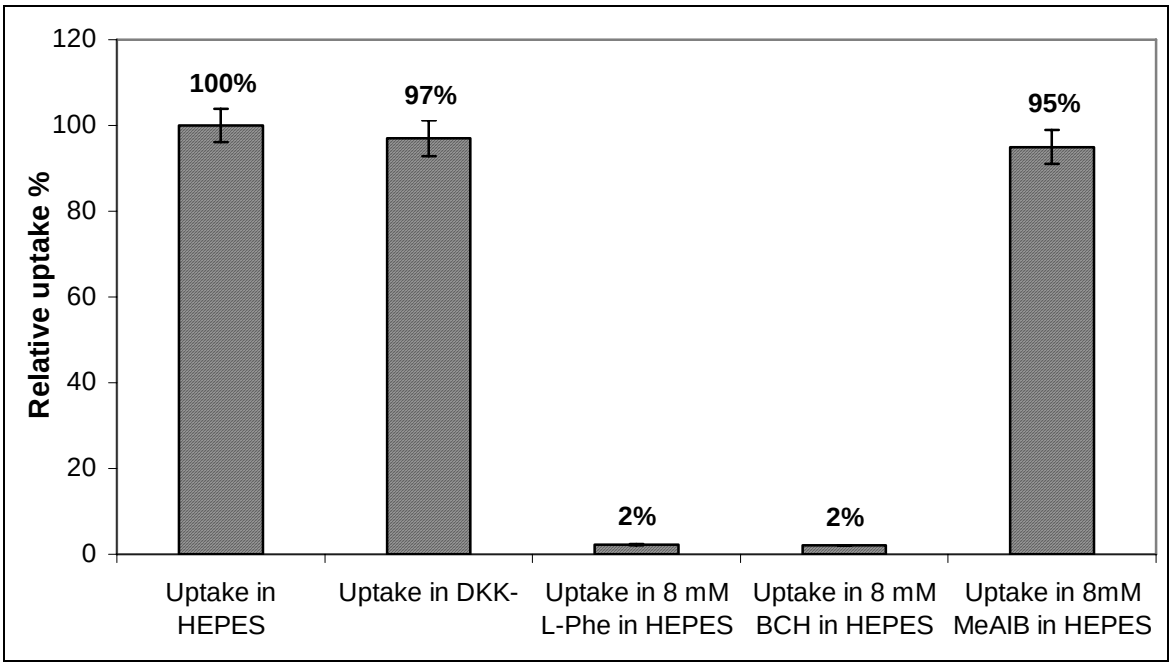

3.1.5. DISCUSSION

Reverse Transcripase PCR gel electrophoresis (Fig. 3.1.1) clearly shows the presence of the mRNA of hCD98hc, hLAT1 and hLAT2 in the R1M cell line, allowing a functional LAT1 and LAT2 transport system. The band width and brightness indicate a greater presence of the LAT1 transport system compared to the LAT2 transport system.

The Lineweaver-Burk plot (Figure 3.1.2) reveals from the same intercept of the different lines obtained for L-phenylalanine, D-phenylalanine, 2-iodo-D-phenylalanine and 2-iodo-L-phenylalanine that all these compounds enter the R1M cells *in vitro* by the same transport system(s). The influx of [^{125}I]-D-2-I-phenylalanine was completely inhibited by 8 mM BCH, whereas no Na^+ dependence could be found. The influx of 0.1 mM 2-iodo-D-phenylalanine caused an efflux of 26% of the initial [^{3}H]-L-phenylalanine uptake while [^{125}I]-2-iodo-D-phenylalanine efflux, although in a smaller amount, was stimulated by 0.1 mM L-phenylalanine and BCH. These characteristics are compliant with the utilization of the LAT system as an obligatory 1/1 antiport system.

The difference in uptake kinetics (Fig. 3.1.1) and affinity for influx (Fig.3.1.4) between 2-iodo-D-phenylalanine and 2-iodo-L-phenylalanine might be due to the fact that the D-form only shows a high affinity for the LAT1 system and much lower affinity for LAT2 while 2-iodo-L-phenylalanine shows a high affinity for both transporter types. BCH is highly "general L transport" specific but with low affinity so it does not allow to differentiate the LAT types in the current conditions.

The small difference in affinity between the L and D iodinated phenylalanine analogues, if expressed as Ki values L about 30% more than D, is less than observed for the non-substituted

phenylalanines (L about 250% more potent). This can be due by the fact that the increase in the lipophilicity due to the substituted iodine atom, in the amino acid – transporter interaction reduces the relative influence of the chiral α carbon atom on the recognition sites of the transport system.

It is stated in literature (5, 10, 21) that the LAT systems show a relatively symmetrical broad selectivity but strongly asymmetrical substrate affinity, such that the intracellular amino acid concentration controls their exchange activity. The increase in non-incorporated uptake in vitro as well as a less stimulated efflux than L-phenylalanine can be due to a significant difference in affinity between the radioiodinated D analogue and the natural L amino acid present in the tumour cells

3.1.6. CONCLUSION

It is shown that the uptake of 2-iodo-D-phenylalanine in R1M cells is significantly slower then the uptake of 2-iodo-L-phenylalanine, as would be expected for the "unnatural" D-amino acid analogue. The K_m (32 μM) and K_i (50 μM) values for 2-iodo-D-phenylalanine however indicate a good affinity to the uptake system involved. The uptake of 2-iodo-D-phenylalanine is Na^+ independent and is quantitatively inhibited by 8 mM L-phenylalanine and 8 mM BCH and competitive with well known LAT amino acids indicating transport via the LAT transport system. As the difference in affinity, as compared to the L analogue and natural L amino acids ,of the new tracer inside the R1M cells is larger than in the outer medium a "pseudo" accumulation effect is generated.
The rather fast uptake and the accumulation effect over longer times make [^{123}I] labelled 2-iodo-D-phenylalanine a promising SPECT tracer for tumour specific imaging and potentially for radionuclide therapy with [^{131}I].

3.1.7. REFERENCES

1. Tamemasa O, Goto R, Suzuki T. Prefential incorporation of some 14C-labeled D-amino acids into tumour-bearing animals. *Gann* 1978 ; 69:517-523
2. Takeda A, Goto R, Tamemasa O, et al. Biological evaluation of radiolabelled D-Methionine as a parent compound in potential Nuclear imaging. *Radioisotopes* 1984 ; 33: 213-217
3. Goto R. Charateristics of D-Leucine uptake by Mouse Ehrlich cells ascites tumour cells. *J Biochem* 1979 ; 86:363-36
4. Fisher GH, Torres D, Bruna J, et al. Presence of D-aspartate and D-glutamate in tumour proteins. *Cancer Biochem Biophys* 1995 ; 15:79-82
5. Segawa H, Fukasawa Y, Miyamoto K, et al. Identification and functional characterisation of a Na+-independent neutral L-amino acid transporter with broad substrate selectivity. *The Journal of Biological Chemistry* 1999 ; 274:19745-19751
6. Lahoutte T, Caveliers V, Camargo SM, et al. SPECT and PET amino acid tracer influx via system L (h4F2hc-hLAT1) and its transstimulation. *J Nucl Med* 2004 ; 45:1591-1596

7. Lahoutte T, Mertens J, Caveliers V, Franken PR, Everaert H, Bossuyt A. Comparative biodistribution of iodinated amino acids in rats: selection of the optimal analog for oncologic imaging outside the brain. *Nucl Med* 2003 ; 44:1489-1494
8. Lahoutte T, Caveliers V, Dierickx L, Vekeman M, Everaert H, Mertens J, Bossuyt A. In vitro characterisation of the influx of 3-[^{125}I]-iodo-L-Tyrosine and 2-[^{125}I]-iodo-L-Tyrosine into U266 human myeloma cells : Evidence for system T transport. *Nucl Med Biol* 2001 ; 28:129-134
9. Lahoutte T, Caveliers V, Franken PR, Bossuyt A, Mertens J, Everaert H. Increase tumour uptake of 3-[^{123}I]-Iodo-L-alpha-methyltyrosine after preloading with amino acids, an in vivo animal imaging study, *J Nucl Med* 2002 ; 43:1201-1206
10. Fukasawa, Y., et al. Identification and characterisation of a Na+-independent neutral amino acid transporter that associates with the 4F2 heavy chain and exhibits substrate selectivity for small neutral D- and L- amino acids. *J Biol Chem* 2000 ; 31:9690-9698
11. Snyder, SH, Kim PM. D-amino acids as putative neurotransmitters: focus on D-serine. *Neurochem res* 2000 ; 25: 553-560
12. Hamase K, Morikawa A, Zaitsu K. D-amino acids in mammals and their diagnostic value. *Journal of Chromatography* 2002 ; 781:73-91
13. Ercal N, Luo X, Matthews RH, et al. In vitro study of the metabolic effects of D-amino acids. *Chirality* 1996 ; 8:24-29
14. Friedmann, M. Formation, nutrional value and safety of D-amino acids. *Adv Exp Med Biol* 1991 ; 289:448-481
15. Imai K, Fukushima T, Santa T, et al. Distribution of free D-amino acids in tissues and body fluids of vertebrates. *Enantiomer* 1997 ; 2:143-145
16. Christensen NH. Role of Amino Acid Transport and Countertransport in Nutrition and metabolism. *Physiol Rev* 1990 ; 70:43-71
17. Ohkame H, Masuda H, Ishii Y, et al. Expression of L-type amino acid transporter 1 (LAT1) and 4F2 heavy chain in liver tumour lesions of rat models. *J Surg Oncol* 2001 ; 78:265-272
18. Meier C, Ristic Z, Klauser S, et al. Activation of system L heterodimeric amino acid exchangers by intracellular substrates. *EMBO* 2002 ; 21:580-589
19. Shikano N, Kanai Y, Kawai K, et al. Isoform Selectivity of 3-[^{125}I]-α-Methyl-L-Tyrosine Membrane Transport in Human L-Type amino acid transport systems, *J Nucl Med*, 2003 ; 44:244-246
20. Mertens J, Kersemans V, Bauwens M, Joos C, Lahoutte T, Bosuyt A, Slegers G. Synthesis, radiosynthesis and in vitro characterisation of [125I]-2-iodo-L-phenylalanine in a R1M rhabdomyosarcoma cell model as a new potential tumour tracer for SPECT, *Nucl Med Biol* 2004 ; 31:739-746
21. Yanagida O, Kanai Y, Chairoungdua A, et al. Human L-Type amino acid transport system 1 (LAT1): characterisation of function and expression in tumour cell lines. *Biochim Biophys Acta* 2001 ; 1514:291-302
22. Kubota R, Yamada S, Kubota R, et al. Intramural distribution of fluorine-18-fluorodeoxyglucose in vivo: high accumulation in macrophages and granulation tissues studied by microautoradiography. *J Nucl Med* 1992 ; 33:1972-1980
23. Langen KJ, Ziemons K, Kiwit JC, et al. 3-[123I]Iodo-alpha-methyltyrosine and [methyl-11C]-methionine uptake in cerebral gliomas: a comparative study using SPECT and PET. *J Nucl Med* 1997 ; 38:517-522

24. Rau FC, Weber WA, Wester HJ, et al. O-(2-[(18)F]fluoroethyl)-L-Tyrosine (FET): a tracer for differentiation of tumour from inflammation in murine lymph nodes. *Eur J Nucl Med* 2002 ; 29:1039-1046
25. Mertens J, et al. Radioactive labelled D-amino acid analogues, a new perspective for tumour therapy and diagnosis: an in vitro evaluation model. *Eur J Nucl Med* 2003 ; 30S2:P530
26. Kersemans V., et al. In vivo evaluation of [123I]-2-iodo-D-Phenylalanine in tumour inoculated athymic mice by means of SPECT as a potential diagnostic and radionuclide therapy tool. *Eur J Nucl Med and Mol Imaging* 2004 ; 31S2:67
27. Kudo Y and Boyd CAR. Heterodimeric amino acid transporters: expression of heavy but not light chains of CD98 correlates with induction of amino acid transport systems in human placental trophoblast. *J Physiol* 200;523:13-18.

3.2 In Vivo Evaluation and dosimetry of [$^{123/125}$I]-2-iodo-D-phenylalanine in a R1M Rabdomyosarcoma Athymic Mice Model by Means of Dynamic Planar Imaging as a Potential Diagnostic Tool.

Veerle Kersemans, MSc[1]; Bart Cornelissen, PhD[1,2]; Klaus Bacher, PhD[4]; Ken Kersemans, MSc[3]; Hubert Thierens, PhD[4]; Rudi A. Dierckx, PhD[5]; Bart De Spiegeleer, PhD[1]; Guido Slegers, PhD[1] and John Mertens, PhD[3].

[1] Laboratory for Radiopharmacy, Universiteit Gent, Harelbekestraat 72, B-9000 Gent, Belgium
[2] Laboratory for Molecular Imaging and Targeted Radiotherapy, University of Toronto, Canada.
[3] Laboratory for Medical Imaging and Physics, Vrije Universiteit Brussel, Belgium
[4] Laboratory for anatomy, embryology, histology and medical physics, Universiteit Gent, Belgium
[5] Division of Nuclear Medicine, Gent University Hospital, Belgium

Key words: [^{123}I]-2-iodo-D-phenylalanine; radiolabeled amino acid analogue; tumour imaging; D-amino acid; biodistribution

Submitted for the Journal of Nuclear Medicine

3.2.1. ABSTRACT

Objectives. Tamamesa et al. reported the preferential uptake of D-amino acids in tumour bearing mice (4,5). Moreover, Yanagida et al. showed in vitro in tumour cells that the LAT transporter seemed to lack stereospecificity. According to the successful results of [^{125}I]-2-iodo-L-phenylalanine, [^{125}I]-2-iodo-D-phenylalanine was developed and its tumour detecting characteristics were evaluated in vivo. **Methods**. [^{123}I]-labelling of 2-iodo-D-phenylalanine was performed in Kit formulation using the Cu^{1+} assisted nucleophilic exchange. [^{123}I]-2-iodo-D-phenylalanine was evaluated in R1M tumour bearing athymic mice using dynamic planar imaging (DPI) and dissection and the stability of the tracer in vivo was tested. Tumour tracer retention and tracer contrast were evaluated as a function of time. Two-compartment blood modelling and dosimetric calculations were performed on the biodistribution results. Moreover, [^{125}I]-2-iodo-D-phenylalanine and ^{18}F-FDG uptake in acute inflammation was investigated by dissection. **Results**. [^{123}I]-2-iodo-D-phenylalanine was metabolically stable. Fast, high and highly specific tumour accumulation was observed. Two-compartment modelling confirmed the fast clearance of the tracer through the kidneys to the bladder as observed by DPI and dissection. Moreover, when compared to the L-isomer, [^{123}I]-2-iodo-D-phenylalanine demonstrated a faster clearance and a faster uptake in the peripheral compartment. No accumulation in the abdomen or in the brain was noticed. Dosimetry revealed that, compared to [^{123}I]-2-iodo-L-phenylalanine and [^{123}I]-2-iodo-L-tyrosine, [^{123}I]-2-iodo-D-phenylalanine demonstrated the lowest radiation burden. Although, [^{123}I]-2-iodo-D-phenylalanine showed a tumour retention of only 4%, the tumour contrast increased up to 350 % at 19 hours p.i. **Conclusions**. [^{123}I]-2-iodo-D-phenylalanine is a promising tracer for diagnostic oncologic imaging due to its high, fast and specific tumour

uptake and fast blood clearance. Moreover, the new tracer possessed better diagnostic imaging characteristics regarding the enhanced tumour contrast in comparison to its L-analogue.

3.2.2. INTRODUCTION

At present, more and more interest exists in nuclear medicine based tumour detection by Positron Emission Tomography (PET) and Single Photon Emission Computed Tomography (SPECT). The most prominent example is [^{18}F]-Fluorodeoxyglucose (^{18}F-FDG), which is routinely used for oncologic imaging, but due to its high brain and inflamed tissue uptake, new more specific oncologic imaging tracers are required (1).

Both increased amino acid transport across the cell membrane and protein synthesis rate are early features of malignant transformation. A and L type amino acid transport have been shown to be increased in tumour cells relative to normal tissue and these transport systems have been the major focus of the development of amino acid tumour tracers for oncologic imaging (1,2*)*

Recently, various radiolabelled L-amino acids have been developed successfully to overcome the limitations of ^{18}F-FDG. Moreover, it was demonstrated that membrane transport of the amino acids reflects the malignancy of the cell and that incorporation of radiolabelled amino acids into the cell proteins is not necessary. The increased amino acid uptake is directly related to the metabolic requirements of the tumour cells (1,3). [^{123}I]-3-Iodo-α-methyltyrosine is at present the only routinely used amino acid tracer for SPECT but due to its marked long term renal accumulation, the development of other radiolabelled amino acid tumour tracers is necessary.

Tamamesa et al. (4) suggested the use of D-amino acids as specific tumour detecting agents. They showed the preferential uptake of some unnatural radiolabelled D-amino acids in comparison to the L-isoforms in tumour bearing mice. Moreover, Yanagida et al. showed in vitro in tumour cells that system L seems to lack stereospecificity: D-amino acids are transported with high affinity by LAT1 (2). The latter, together with the slower excretion of D-amino acids from the tumour cells could be an important rationale to develop D-amino acids as tumour diagnostic agents (5). Moreover, a lower radiation burden is expected from D-amino acids in comparison to the L-isoforms because of their faster blood clearance due to both negligible tissue distribution and incorporation into cell proteins.

Our research group developed [$^{123/125}$I]-2-iodo-D-phenylalanine and demonstrated its uptake in vitro in a R1M (rabdomyosarcoma) cell model (6). The D-isomer was taken up by the L amino acid transporter system subtype 1 (LAT1), overexpressed in many tumours, and accumulated slower but in the same amounts as compared to [^{125}I]-2-iodo-L-phenylalanine. This paper evaluated [$^{123/125}$I]-2-iodo-D-phenylalanine as a potential new tumour diagnosticum in vivo in a R1M athymic mouse model by means of dissection and dynamic planar imaging.

3.2.3. MATERIALS AND METHODS

All the conventional products mentioned were at least of analytical or clinical grade and obtained from Sigma-Aldrich. The solvents were of HPLC quality (Chemlab, Belgium).

3.2.3.1. Synthesis of Precursor 2-iodo-D-phenylalanine

2-iodo-D-phenylalanine was prepared from 2-bromo-D-phenylalanine (PepTech Corp, USA) by analogy with 2-iodo-L-phenylalanine as mentioned before (3). Briefly, the Cu^{1+} assisted nucleophilic exchange under acidic and reducing conditions was used (30.3 mM 2-bromo-D-phenylalanine, 4.4 mM $CuSO_4$, 8.9 mM citric acid, 9.0 mM $SnSO_4$, 10.7 mM gentisic acid, 44.5 mM NaI; at 160°C for 16 hours). 2-iodo-D-phenylalanine and 2-bromo-D-phenylalanine were recovered separately from RP-HPLC (Hibar semi-preparative Lichrosorb RP-select 7µm; λ = 261 nm; Merck, Belgium) with 20/80 MeOH/H_2O containing 1mM NH_4Ac (adjusted to pH 5.5 with HCl, 13 ml/min). 2-iodo-D-phenylalanine was obtained from methanol by evaporation of the mobile phase. Identification and quality control were achieved by LC-MS, TLC and HPLC. Chiral chromatography (5 µm Chirobiotic T, 150 x 4.6 mm; Astec) with 20/80 MeOH/H_2O containing 20 mM NH_4Ac (adjusted to pH 5.5 with HCl, 1 ml/min) was used to confirm the chiral purity.

3.2.3.2. Radiochemistry

3.2.3.2.1. [^{123}I/^{125}I]-2-iodo-D-phenylalanine

Radioiodination with $^{123}I^-$ (222 MBq; 10 – 20 µl) or $^{125}I^-$ (37 MBq; 10 µl) (Nordion Europe, Belgium) on 1.0 mg 2-iodo-D-phenylalanine was performed by Cu^{1+} assisted isotopic exchange under acidic and reducing conditions as described before. The reaction mixture was drawn up in a syringe containing the appropriate amount of "make-up solution" (Tri-sodium Citrate dihydrate, 71 mM) to render the solution isotonic and to adjust the pH to at least 4. The reaction mixture was filtered by 0.22 µm Ag-filter (Millipore, Belgium) to remove free $^{123}I^-$ and by a sterile 0.22 µm filter (Millipore, Belgium) for sterilisation into a sterile vacuum vial. Quality control was achieved by HPLC and Sep-pak C18 (Waters, Belgium). Chiral chromatography was used to confirm the chiral purity.

3.2.3.2.2. [^{123}I]-iodo-Human Serum Albumin.

Radioiodination of Human Serum Albumin (HSA) with ^{123}I (Nordion Europe, Belgium) was performed by electrophilic substitution using the Iodogen technique as described before (3). The reaction mixture was sent through a 0.22 µm Ag-filter to remove the free $^{123}I^-$ from [^{123}I]-iodo-HSA and through a sterile 0.22 µm filter for sterilisation. The specific activity was 4.10^4 GBq/mmol. Quality control was achieved using a standard prepacked PD-10 SEC column (Size Exclusion Chromatography, Amersham Pharmacia Biotech, Sweden) using PBS/HSA as the eluting agent.

3.2.3.3. In Vivo Experiments

3.2.3.3.1. Laboratory Animals.

The study protocol was approved by the local ethical committee for animal studies and was within the rules of Belgian legislation. Guidelines of the National Institute of Health principles of laboratory animal care were followed.

Water and food were freely available during the experimental period.

Male SWISS~nu/nu mice (n=30) (Bioservices, The Netherlands) were injected subcutaneously in the right flank (armpit region) with 5.10^6 R1M rabdomyosarcoma cells. Normal tumour growth curves were obtained using sliding caliper measurement and the estimate volume formula $V = 0.4\ a^2.b$, a and b being the short and the long axis of the tumour respectively (3,7). For the inflammation model, male NMRI mice (n=5) (in house breeding program) were injected in the right biceps brachii with 25 µl of turpentine to create an acute inflammation.

During all imaging experiments, the animals were anesthetized by intraperitoneal injection (IP) with 75 µl (1.5 mg) of a solution containing 20 mg/ml pentobarbital (Nembutal, 60 mg/ml, Ceva Santé Animale, Belgium). For the biodistribution experiments by dissection, the animals were sacrificed by cervical dislocation without sedation and the organs of interest were dissected.

[$^{123/125}$I]-2-iodo-D-phenylalanine, ^{18}F-FDG and [^{123}I]-iodo-HSA were injected intravenously (IV) in the lateral tail vein.

3.2.3.3.2. Dynamic Planar Imaging (DPI).

Imaging was performed as described before using a gamma camera (Toshiba GCA-9300A/hg) in planar mode equipped with a high-resolution parallel-hole collimator (3). All experiments were conducted within the same mouse population to limit the number of animals needed.
In order to perform semi-quantitative analysis, a syringe with known [^{123}I]-2-iodo-D-phenylalanine activity (measured on a calibrated ionisation chamber; Capintec, CRC-15R; Ramsey, USA) was used as dose calibration. The syringes, containing [^{123}I]-2-iodo-D-phenylalanine were counted by the same Capintec before injection. The tracer uptake was expressed the differential uptake ratio (DUR): $[(counts_{tissue} * pixels_{total\ body})/(pixels_{tissue} * counts_{total\ body})]$. The latter calculations are performed to meet the conclusions and guidances of Boellaard and Thie (8,9).

At first, a [^{123}I]-iodo-HSA study was carried out to measure the relative bloodpool distribution to correct the uptake of [^{123}I]-2-iodo-D-phenylalanine in the studied organs for bloodpool activity. Ten tumour bearing mice were injected with 7.4 MBq [^{123}I]-iodo-HSA. Of each animal, ten dynamic planar images of 1 min were acquired starting 10 min p.i. ROIs were drawn around the tumour, heart and the contralateral background area. The tumour to contralateral background (RTB) ratio was calculated and the overall mean for the animals determined.

DPI experiments were started when the tumour reached a volume of 1 cm^3. Immediately after injection of 18.5 MBq [^{123}I]-2-iodo-D-phenylalanine, a dynamic acquisition was performed to determine the steady state of tracer uptake in the tumour. Subsequently, at steady state a displacement study with L-phenylalanine (200 µl IV of a 145 mM solution) was performed. Regions of interest (ROI's) were drawn using a MRI maximum intensity projection as described before (3). [^{123}I]-2-iodo-D-phenylalanine tumour uptake was compared to the uptake in the contralateral background area and RTB calculated. The significance of displacement of [^{123}I]-2-iodo-D-phenylalanine activity by L-phenylalanine was calculated for a 95% confidential interval.

To test the tumour retention of [^{123}I]-2-iodo-D-phenylalanine, 3 R1M bearing athymic mice were injected with 37 MBq of the tracer. One, 6.5, 16, 19, 21, 24 and 31 hours p.i., a static image of 15 min was acquired (1024 x 1024 matrix; FOV 23.5 x 12.46 cm and with a photopeak window set at 15% around 159 keV). Tumour retention of the tracer was calculated relatively to the time-point 1h p.i.. The tumour contrast was defined as DUR relative to the 1 hour time-point: relative DUR = $(\%IA/P_{tumour}/\%IA/P_{total})$ at 1, 6.5, 16, 19, 21, 24 or 24 hours divided by DUR at steady state (1h).

3.2.3.3.3. MRI.

The tumour bearing animals were anaesthetized as mentioned above. After sedation, 3D Dess-weighted images, being hybrid T1-T2 weighted images, were generated on a 1 Tesla whole-body system (Magnetom SP; Siemens, Erlangen, Germany) as mentioned before (3,7).

3.2.3.3.4. Dissection: Biodistribution of [^{123}I]-2-iodo-D-phenylalanine in tumour model.

The injected dose (ID) was calculated by weighing the syringes before and after injection of the tracer and by the use of a dilution series of the injected tracer solution which was also weighed and counted for radioactivity using the auto gamma-counting system (CobraII Series, Canberra Packard, Meriden, CT, USA Cobra).

The same mouse population as applied for the DPI experiments was used. Twelve R1M bearing athymic mice were injected with 7.4 kBq [^{123}I]-2-iodo-D-phenylalanine, six days after the last imaging experiment was performed. At various time points (2, 5, 10, 15, 30, 45, 60, 90, 120 and 180 min) post injection 3 animals per time point were sacrificed. The organs and tissues were removed, washed and weighted. The blood was collected in an EDTA coated vial. The radioactivity of the samples was counted by use of an auto gamma-counting system (CobraII Series, Canberra Packard, Meriden, CT, USA Cobra). The amount of radioactivity in the organs and tissues was calculated as the differential absorption rate (DAR): [(activity$_{tissue}$ * total body weight)/(weight$_{tissue}$ * activity$_{injected\ dose}$)].

3.2.3.3.5. Two-compartment modelling.

The data obtained by DPI and dissection for [^{123}I]-2-iodo-D-phenylalanine were fit to a two-compartment model with IV-bolus injection, without a lag time and with first order elimination, using WinNonlin 4.0.1 (Figure 3.2.1). This kinetic model was chosen by analogy with [^{123}I]-3-iodo-α-methyltyrosine (10) The primary parameters V_1, $k_{1,0}$, $k_{1,2}$ and $k_{2,1}$ were determined.

FIGURE 3.2.1.: Graphic presentation and kinetic parameters of the 2-compartment model applied on blood dynamic imaging data of [^{123}I]-2-iodo-D-phenylalanine. (*) [^{123}I]-2-iodo-D-phenylalanine or (‡) [^{123}I]-2-iodo-L-phenylalanine. (A) DPI results and (B) dissection results.

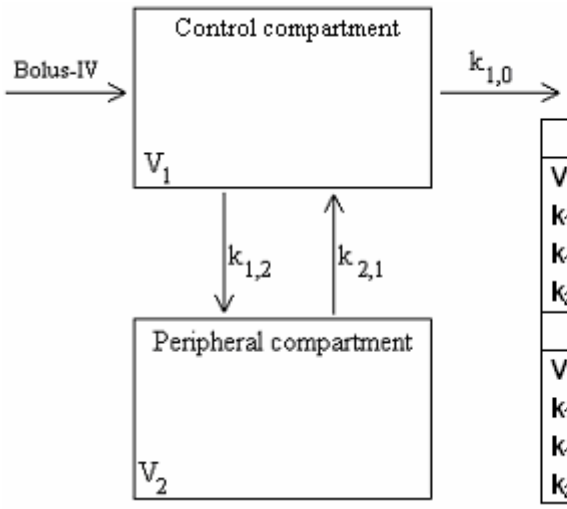

Kinetic parameters (mean±SD)			
A	**units**	**2-I-D-Phe***	**2-I-L-Phe‡**
V_1	Activity$_{total}$/DUR	7.10±0.10	9.65±0.20
$k_{1,0}$	1/min	0.075±0.004	0.035±0.003
$k_{1,2}$	1/min	1.09±0.04	0.80±0.04
$k_{2,1}$	1/min	0.41±0.01	0.42±0.02
B	**units**	**2-I-D-Phe***	**2-I-L-Phe‡**
V_1	Activity$_{total}$/DUR	6.66±0.18	18.78±0.62
$k_{1,0}$	1/min	0.0025±0.0003	0.0014±0.0002
$k_{1,2}$	1/min	0.060±0.010	0.009±0.003
$k_{2,1}$	1/min	0.030±0.006	0.019±0.007

3.2.3.3.6. Dissection: Biodistribution of [^{125}I]-2-iodo-D-phenylalanine in inflammation model.

Inflammation bearing NMRI mice (n = 5) were injected with 7.4 kBq of [^{125}I]-2-iodo-D-phenylalanine together with 16 MBq of ^{18}F-FDG 24h post terpentine injection. After 30 min, the mice were sacrificed and the blood, muscle from the inflamed and non-inflamed leg was removed, washed and weighted. The ^{18}F activity was counted on day 1 and the $^{125}I^-$ activity in the same samples was counted three days later. The amount of radioactivity in the organs and tissues was calculated as DAR.

3.2.3.3.7. Metabolization Study: in Vivo Stability of [^{125}I]-2-iodo-D-phenylalanine.

The blood, collected in the dissection study, was used for a metabolization study of [^{125}I]-2-iodo-D-phenylalanine as a function of time as described before (3).

3.2.3.4. Dosimetric calculations

Mean time–activity curves (expressed as %Injected Activity/weight$_{tissue}$ or %Injected Activity$_{tissue}$) were generated for the organs of interest from the dissection experiment. Source organ residence times were determined from time-integration of the bi-exponential fit to the experimental biodistribution data. Fitting was performed in SPSS 12.0 software package. In order to fit the experimental data, 2 extra time points were generated at 792 min and 2376 min p.i. (1x and 3x the half life of iodine-123, respectively) by only considering the physical decay of the tracer and thus assuming the worst case scenario. The latter was performed because the dissection was only conducted until 180 min p.i. of the tracer. Extrapolation of the animal biodistribution to the human reference adult was performed by assuming that either the %IA/weight$_{tissue}$ or %IA$_{tissue}$ in mice and humans was equal. Absorbed radiation dose estimates were then calculated for the target organs applying the MIRD methodology (11) for healthy adults using the MIRDOSE 3.0 software package. The absorbed-dose estimate for the urine bladder wall was determined according to the dynamic bladder model as described by Cloutier et al. using a bladder voiding interval of 4.8 hours (12). The dosimetric calculations were not only performed on the data mentioned in this report but also on the dissection data of 2-iodo-L-phenylalanine and 2-iodo-L-tyrosine, as reported earlier, in order to compare the new D-isomer tracer to other newly developed amino acid analogues.

The parameters of the exponential fitted curves in SPSS were applied for hierarchical clustering of the organs using the average linkage algorithm. This analysis was performed to discover which organs exhibit the same behaviour for [^{123}I]-2-iodo-D-phenylalanine tracer biodistribution.

3.2.4. RESULTS

3.2.4.1. Synthesis and Radiolabeling of 2-iodo-D-phenylalanine

Yields up to 65 % were obtained for the presursor synthesis of 2-iodo-D-phenylalanine from 2-bromo-D-phenylalanine using the Cu^{1+} assisted nucleophilic exchange method.

Radioiodination of 2-iodo-D-phenylalanine by Cu^{1+} assisted isotopic exchange, followed by Ag-membrane filtration, resulted in a radiochemical purity of > 99 % and a specific activity of 65 GBq/mmol ([^{123}I]-labeling) and 11GBq/mmol ([^{125}I]-labeling).

In both cases, it was shown by chiral HPLC that there was no detectable amount of L analogues

3.2.4.2. In Vivo Results

3.2.4.2.1. In Vivo Stability of [^{125}I]-2-iodo-D-phenylalanine.

HPLC analysis of the mouse blood showed 4.8 % of free iodide 90 minutes post injection. No other metabolites were detected. EDTA did not show any influence on the deiodination of [^{125}I]-2-iodo-D-phenylalanine.

3.2.4.2.2. Planar Imaging.

DPI with [^{123}I]-iodo-HSA showed no significant difference between the blood flow in the tumour and the contralateral reference leg: RTB = 1.1 ± 0.2.

At equilibrium (plateau phase), net [^{123}I]-2-iodo-D-phenylalanine uptake in the tumour was high. An overall mean of [^{123}I]-2-iodo-D-phenylalanine tumour uptake of 1.00 ± 0.02 was obtained (Figure 3.2.2). Administration of L-phenylalanine resulted in a significant displacement of the [^{123}I]-2-iodo-D-phenylalanine activity from the tumour: the radioactivity in the tumour showed a decrease of 9.6 % ± 2.3 % as compared to the initial uptake values ($p<0.05$) after IV administration of L-phenylalanine.

FIGURE 3.2.2: Overall mean for [^{123}I]-2-iodo-D-phenylalanine uptake (DUR) in tumour and contralateral background region as functions of time by dynamic planar imaging.

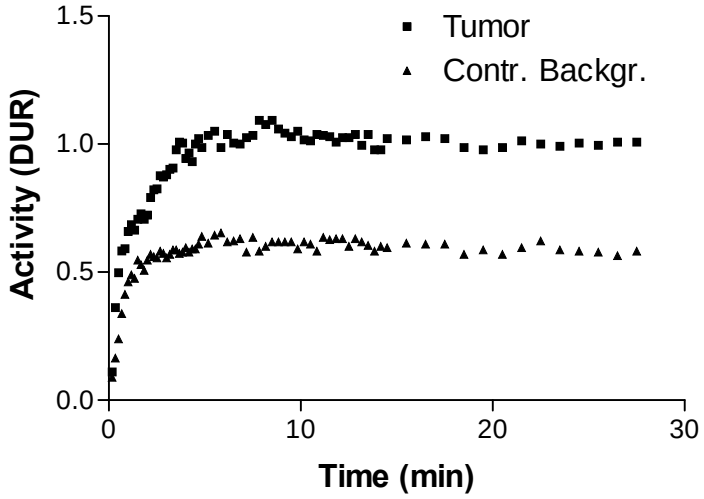

[^{123}I]-2-iodo-D-phenylalanine blood elimination showed a renal clearance to the bladder (Fig. 3.2.3). High tracer uptake was noticed in the zone of the pancreas: it reached a peak value of 3.3 ± 0.2, 2 min p.i. but decreased rapidly (Figure 3.2.4). Due to superposition of the pancreas with other organs such as left kidney and stomach, the results of pancreas uptake are overestimated (13). Low uptake of radioactivity in the thyroid (1.08 ± 0.06) or brain (0.76 ± 0.05) was observed (Figure 3.2.4).

FIGURE 3.2.3: Uptake of [^{123}I]-2-iodo-D-phenylalanine (DUR) as a function of time by dynamic planar imaging: clearance of the tracer through the kidneys to the bladder. Kinetic fitting of the observed blood curve for [^{123}I]-2-iodo-D-phenylalanine tracer distribution with the theoretical (line) curve using a two-compartment model.

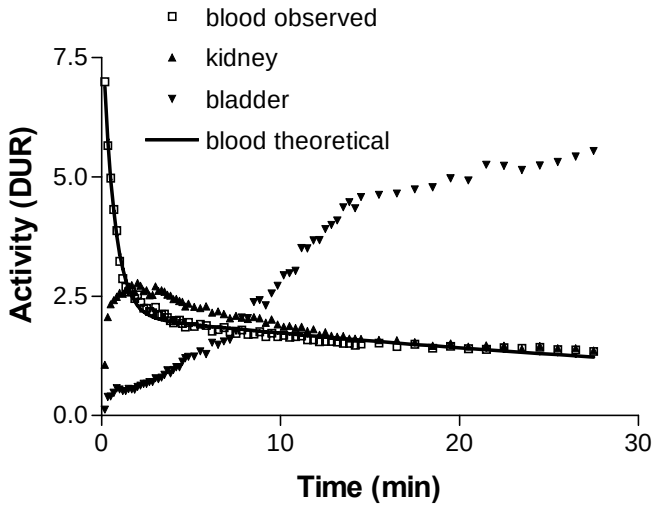

FIGURE 3.2.4: Uptake of [^{123}I]-2-iodo-D-phenylalanine (DUR) pancreas zone, brain and thyroid.

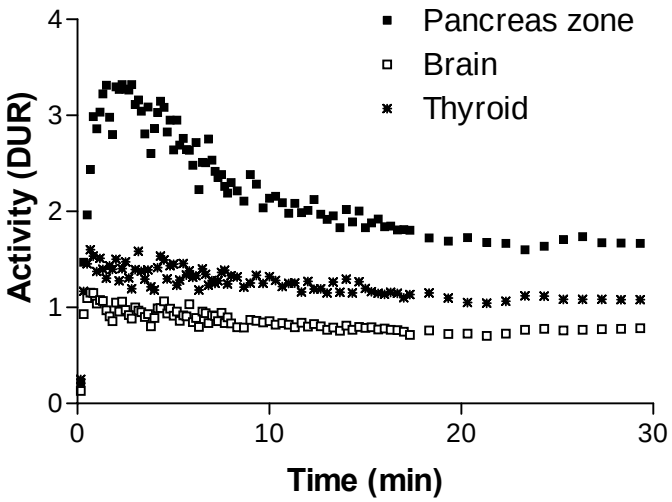

The retention study of [^{123}I]-2-iodo-D-phenylalanine showed that only 4% of the initial [^{123}I]-2-iodo-D-phenylalanine uptake remained in the tumour 31 hours p.i.. However, when concerning tumour contrast, an increase of 352% 19 hours p.i. was observed (Table 3.2.1).

TABLE 3.2.1: Retention study of [^{123}I]-2-iodo-D-phenylalanine activity in the tumour using planar gamma scintigraphy. (*) % contrast enhancement in comparison to the initial [^{123}I]-2-iodo-D/L-phenylalanine tumour contrast; (†) % of the initial [^{123}I]-2-iodo-D/L-phenylalanine uptake that remained in the tumour; (§) [^{123}I]-2-Iodo-L-phenylalanine; (‖) [^{123}I]-2-Iodo-D-phenylalanine.

	Tumour contrast (%±SD)*		Tumour retention (%±SD)†	
Time (h)	2-I-L-Phe§	2-I-D-Phe‖	2-I-L-Phe	2-I-D-Phe
1	100±0	100±0	100.0±0.0	100.0±0.0
6.5	100±2	120±22	67.8±2.5	52.6±10.7
16	75±19	314±36	23.2±5.6	15.5±1.6
19	71±17	352±31	23.1±7.9	6.7±2.1
21	95±25	213±34	21.1±8.5	5.0±1.7
24	91±16	251±36	17.1±6.3	5.0±2.0
31	86±16	197±10	11.6±3.9	4.0±1.1

3.2.4.2.3. Biodistribution By Dissection.

Biodistribution data of [^{125}I]-2-iodo-D-phenylalanine for the selected time-points 2, 30, 60 and 120 minutes p.i. in R1M tumour bearing athymic mice are shown in Table 3.2.2. Those of [^{125}I]-2-iodo-L-Phenylalanine were reported earlier (3).

TABLE 3.2.2: Biodistributon study by dissection of [^{125}I]-2-iodo-D-Phenylalanine in R1M bearing athymic mice (n = 3).

	Differential Absorption Ratio (DAR) Mean ± SD			
Time (min)	2	30	60	120
Blood	***3.10±0.12***	***1.25±0.21***	***1.08±0.12***	***1.06±0.05***
Brain	***0.33±0.07***	***0.36±0.06***	***0.42±0.05***	***0.38±0.10***
Heart	2.13±0.07	1.04±0.29	0.81±0.10	0.73±0.04
Lung	2.17±0.12	0.91±0.20	0.75±0.07	0.71±0.09
Stomach	0.68±0.20	1.87±1.13	2.14±1.15	2.83±1.75
Milt	2.20±0.28	0.99±0.28	0.81±0.20	0.95±0.12
Liver	2.21±0.23	0.91±0.16	1.02±0.25	1.07±0.33
Kidneys	***17.65±2.55***	***6.88±3.27***	***2.97±0.24***	***2.05±0.04***
Small intestines	1.33±0.13	1.02±0.31	1.20±0.14	1.88±0.71
Large intestines	0.64±0.07	0.40±0.20	0.50±0.11	1.73±0.20
Fatty tissue	0.73±0.39	0.66±0.45	0.19±0.02	0.32±0.10
Contr. Bckgr.	***1.10±0.21***	***1.06±0.19***	***0.68±0.12***	***0.66±0.04***
Pancreas	***10.52±3.63***	***10.68±5.18***	***6.84±1.07***	***6.17±0.53***
Tumour	***2.05±0.82***	***3.89±1.22***	***2.30±0.39***	***2.09±0.54***
RTB	***1.86±0.36***	***3.64±0.48***	***3.38±0.52***	***3.13±0.73***

The net [^{125}I]-2-iodo-D-phenylalanine tumour uptake reached equilibrium from 30 min with a mean DAR value of 3.9 ± 1.2. At the same time point, [^{125}I]-2-iodo-D-phenylalanine activity in the blood and in the contralateral leg tissue reached a DAR of 1.3 ± 0.2 and 1.1 ± 0.2 respectively.

[^{125}I]-2-iodo-D-phenylalanine was cleared very fast through the kidneys, without accumulation. A high uptake of radioactivity in the pancreas was observed. Very low accumulation of radioactivity was observed in other abdominal organs such as liver, lungs, stomach, small intestine and large intestine, neither in the brain.

Comparison of ^{18}F-FDG with [^{125}I]-2-iodo-D-phenylalanine uptake in the inflammation site resulted in a "ratio inflamed muscle to contralateral muscle" of 10.5 ± 2.1 and 1.43 ± 0.09, respectively.

3.2.4.2.4. Two-compartment modelling.

The results obtained by two-compartment modelling are given in Figure 3.2.1 and 3.2.4. They showed that [^{123}I]-2-iodo-D-phenylalanine biodistribution by DPI and dissection fitted the theoretical curve for the proposed kinetic model (all $R^2 > 0.95$). When compared to its L-isomer, [^{123}I]-2-iodo-D-phenylalanine was cleared almost two times faster from the blood. Moreover, [^{123}I]-2-iodo-D-phenylalanine was taken up faster in the peripheral compartment but its elimination velocity from this compartment was comparable to that of [^{123}I]-2-iodo-L-phenylalanine. Both biodistribution methods showed the same kinetic pattern.

3.2.4.3. Dosimetry

Mean radiation dose estimates were calculated for the human reference adult using time–activity curves and organ residence times derived from mice biodistribution data. The MIRDOSE 3.0 program was applied assuming that either the %IA/g tissue values or the %IA values for [^{123}I]-2-iodo-D-phenylalanine, [^{123}I]-2-iodo-L-phenylalanine and [^{123}I]-2-iodo-L-tyrosine in mice are equal to those in humans. Dosimetry results according to both estimates are summarized in Table 3.2.3. They show that the highest equivalent organ dose was reached for the pancreas and stomach. When selecting the highest equivalent organ dose for each organ out of both dosimetry estimations, this worst-case scenario would result in an effective dose of 0.0330, 0.0375 and 0.0542 mSv/ MBq for [^{123}I]-2-iodo-D-phenylalanine, [^{123}I]-2-iodo-L-phenylalanine and [^{123}I]-2-iodo-L-tyrosine, respectively. Although no statistically significant difference was observed between the two phenylalanine analogues ($p = 0.378$), the tyrosine analogue differed significantly from the latter tracers ($p = 0.041$).

TABLE 3.2.3: Dosimetric calculations and estimation of the "worse-case" effective dose for [^{123}I]-2-iodo-D-phenylalanine, [^{123}I]-2-iodo-L-phenylalanine and [^{123}I]-2-iodo-L-tyrosine.

	2-iodo-D-phenylalanine		2-iodo-L-phenylalanine		2-iodo-L-tyrosine	
Organs	Dose %ID	Dose %ID/g	Dose %ID	Dose %ID/g	Dose %ID	Dose %ID/g
Adrenals	1.56E-02	9.24E-03	1.39E-02	1.04E-02	2.38E-02	1.26E-02
Brain	4.95E-03	5.18E-03	4.37E-03	6.37E-03	1.14E-02	1.30E-02
Breasts	6.23E-03	5.59E-03	5.95E-03	6.46E-03	6.07E-03	6.26E-03
Gallbladder Wall	1.78E-02	9.61E-03	1.52E-02	1.09E-02	2.66E-02	1.33E-02
LLI Wall	2.46E-02	8.98E-03	2.85E-02	2.02E-02	4.92E-02	1.94E-02
Small Intestine	3.41E-02	1.15E-02	2.59E-02	1.42E-02	4.02E-02	1.48E-02
Stomach	1.28E-01	1.92E-02	5.49E-02	1.30E-02	5.83E-02	1.36E-02
ULI Wall	2.88E-02	9.20E-03	2.21E-02	1.16E-02	4.55E-02	1.28E-02
Heart Wall	1.32E-02	1.01E-02	1.05E-02	9.36E-03	1.81E-02	1.49E-02
Kidneys	2.07E-02	8.02E-03	9.07E-03	6.00E-03	5.20E-02	1.84E-02
Liver	1.69E-02	8.29E-03	1.24E-02	6.92E-03	3.64E-02	1.62E-02
Lungs	8.89E-03	9.44E-03	6.99E-03	8.08E-03	1.18E-02	1.49E-02
Muscle	8.94E-03	7.00E-03	1.07E-02	1.06E-02	1.14E-02	9.92E-03
Ovaries	1.51E-02	9.34E-03	2.19E-02	2.00E-02	2.50E-02	1.80E-02
Pancreas	1.98E-01	4.27E-02	2.14E-01	4.91E-02	5.41E-01	1.24E-01
Red Marrow	8.77E-03	6.87E-03	9.35E-03	9.28E-03	1.07E-02	8.91E-03
Bone Surfaces	1.47E-02	1.28E-02	1.56E-02	1.65E-02	1.65E-02	1.57E-02

Skin	5.49E-03	4.92E-03	6.03E-03	6.53E-03	5.84E-03	5.95E-03
Spleen	2.32E-02	8.90E-03	2.37E-02	1.03E-02	3.93E-02	1.40E-02
Testes	6.85E-03	6.63E-03	1.36E-02	1.46E-02	1.19E-02	1.26E-02
Thymus	7.93E-03	7.50E-03	7.77E-03	8.68E-03	7.72E-03	8.36E-03
Thyroid	7.44E-03	7.42E-03	7.60E-03	8.85E-03	6.79E-03	8.00E-03
Urin Bladder Wall	9.93E-03	9.29E-03	3.02E-01	3.03E-01	2.61E-01	2.60E-01
Uterus	1.33E-02	9.40E-03	3.64E-02	3.55E-02	3.49E-02	3.12E-02
Total Body	1.03E-02	7.50E-03	1.14E-02	1.09E-02	1.38E-02	1.08E-02
"worse-case" dose	**3.30E-02**	**mSv/MBq**	**3.75E-02**	**mSv/MBq**	**5.42E-02**	**mSv/MBq**

The clustering results of the coefficients of the exponential models as used in the dosimetric calculations are visually presented by the dendrogram in Figure 3.2.5. It presents the closeness of the different organs with respect to the [^{123}I]-2-iodo-L-phenylalanine tracer pharmacokinetic behaviour. The dendrograms for [^{123}I]-2-iodo-D-phenylalanine and [^{123}I]-2-iodo-L-tyrosine are not shown but they demonstrate the same behaviour. Clearly, the tumour, remainder of the body, kidneys and stomach are separate groups, with 2 additional clusters: (1) blood-group containing blood, lungs, spleen, heart and liver and (2) other organs group containing the organs left. When looking at the elimination coefficients only (dendrogram not shown), an identical, even more pronounced, pattern was observed, with exception of the stomach which belongs to the blood-group. Indeed, the elimination kinetics from the stomach was similar to the blood-group organs, which however did not show uptake kinetics under the applied experimental conditions. These clustering results indicate that not every organ is to be considered separately in full pharmacokinetic modelling, due to similar pharmacokinetic behaviour within the groups. Five different groups can be defined.

FIGURE 3.2.5: Hierarchical clustering using average linkage algorithm for the exponential curve parameters obtained by non-linear regression of the dissection data of 2-iodo-L-phenylalanine.

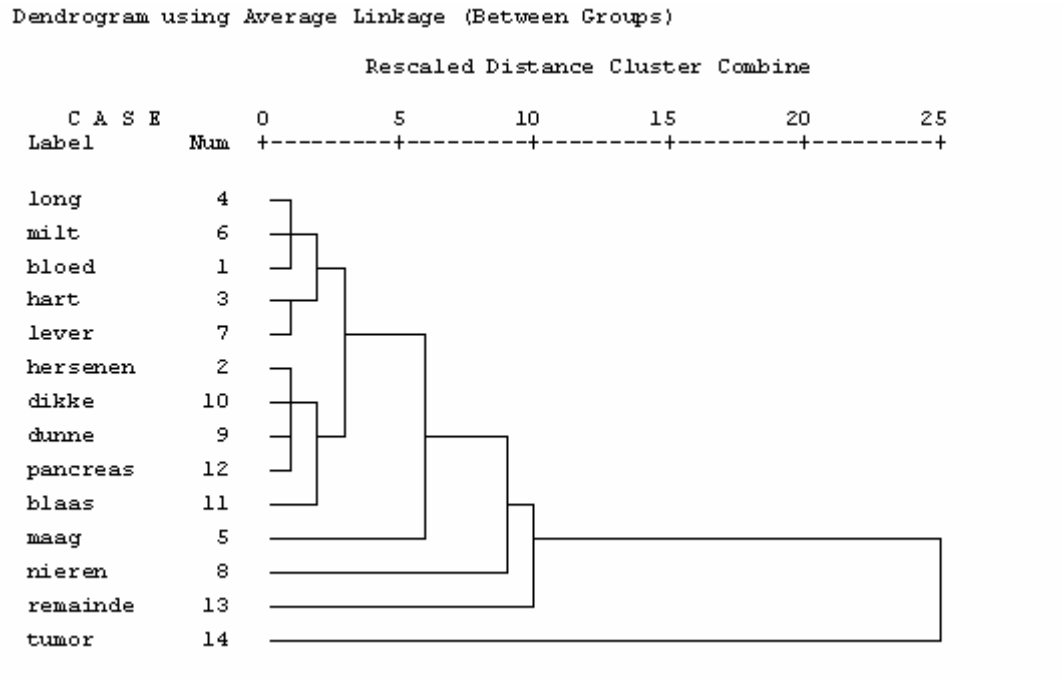

3.2.5. DISCUSSION

Tamamesa et al. reported the preferential uptake of D-amino acids in tumour bearing mice (4,5). Moreover, Yanagida and co-workers showed in vitro in tumour cells that the LAT transporter seemed to lack stereospecificity: D-amino acids were transported with high affinity by LAT1 (2). Accordign to the succesful results of [^{125}I]-2-iodo-L-phenylalanine, [^{125}I]-2-iodo-D-phenylalanine was developed and its tumour detecting characteristics were evaluated.

In vitro in R1M cells, the K_m values of [^{125}I]-2-iodo-D-phenylalanine, [^{125}I]-2-iodo-L-phenylalanine and the natural amino acid L-phenylalanine were similar. All compounds were transported by the same obligatory exchange LAT1 system (6), confirming the hypothesis made by Yanagida et al. In vitro (full MEM buffer) accumulation of [^{125}I]-2-iodo-D-phenylalanine in R1M cells over a longer period of time (up to 24 hours) was noticed although no incorporation e into the cell proteins was found, just like the L-isomer (2,14).

Given the abovementioned characteristics, the new tracer [^{123}I]-2-iodo-D-phenylalanine was evaluated in vivo using dynamic planar imaging in view of its potential application for oncologic diagnostic imaging.

Identical to 2-iodo-L-phenylalanine, the D-isomer could be synthesised easily and radio-iodinated quantitatively in a Kit formulation using the Cu^{1+} assisted nucleophilic exchange method (3). The same precursor yields and the same tracer specific activities were obtained for both tracers. No metabolization of [^{125}I]-2-iodo-D-phenylalanine took place. Only a minor dehalogenation was observed, which was somewhat lower in comparison to the L-isomer and which is reflected by the low radioactivity uptake in the thyroid. Thus, oral administration of stable potassium iodide before injection of [^{123}I]-2-iodo-D-phenylalanine shall protect the thyroid from radioiodine poisoning.

Concerning the planar imaging data of [^{123}I]-2-iodo-D-phenylalanine, tracer kinetics were in accordance with the proposed 2-compartment model. Moreover, due to its higher $k_{1,0}$ velocity and thus faster tracer elimination from the blood, 2-iodo-D-phenylalanine will demonstrate better tumour contrast at the same time-point in comparison to its L-isomer. Additionally, 2-iodo-D-phenylalanine was taken up faster by the peripheral compartment as compared to 2-iodo-L-phenylalanine ($k_{1,2}(D) \approx 1.4 \times k_{1,2}(L)$) but both tracers were eliminated at equal velocities from the peripheral compartment ($k_{2,1}(D) \approx k_{2,1}(L)$). These findings together with the very fast [^{123}I]-2-iodo-D-phenylalanine wash out from the pancreas will lead to faster and higher tumour uptake and thus better tumour contrast as compared with the L-analogue. This hypothesis is confirmed by the [^{123}I]-2-iodo-D-phenylalanine tumour retention study. Although only 4 % of the initial [^{123}I]-2-iodo-D-phenylalanine uptake remained in the tumour after 31 hours, the tumour contrast became much more favourable for oncologic imaging in comparison to [^{123}I]-2-iodo-L-phenylalanine with a retention of 11%: whereas the latter showed a decrease in tumour contrast, [^{123}I]-2-iodo-D-phenylalanine demonstrated an contrast increase of 352 % 19 hours p.i. (Table 3.2.1). These results demonstrate the capability of 2-iodo-D-phenylalanine as a tumour detecting agent by SPECT and opens perspectives as a radiotherapeutic agent. Indeed, meta-iodobenzylguanidine (MIBG), which showed only a tumour uptake of 2 % of the ID, has become an effective anti-neuroblastoma agent, besides its diagnostic tumour imaging application. Apart from its tumour-targeting properties, our new tracer 2-iodo-D-phenylalanine is metabolically stable but shows lower liver uptake and accumulation than MIBG and is rapidly cleared from the circulation via the kidneys, being an ideal starting point for systemic radiotherapy (15-17).

Although the kinetic modelling of both tracers showed similar trends for DPI and dissection, the values differed significantly from each other. This could be explained by the difference in data-acquisition: the ROI for the blood in DPI includes besides the blood also the heart muscle. Although the dissection results showed that no accumulation of the tracer took

place in the heart-muscle (primary energy source = glucose), the latter tissue could have an additional effect on the total counts in the ROI resulting in higher values.

Regarding the tumour uptake, DPI showed that [^{123}I]-2-iodo-D-phenylalanine accumulated quickly to reach a high level in the R1M tumours. The specificity of this [$^{123/125}$I]-2-iodo-D-phenylalanine tumour uptake was confirmed by: (1) a low contribution of the blood flow to tumour activity, (2) by the small but significant amount of radioactivity displaced by L-phenylalanine coupled to the obligatory exchange by LAT1 and (3) by a minor uptake in inflamed tissue.

Moreover, low abdominal background, fast blood clearance and low brain uptake were observed (Figure 3.2.3, 7.4 and Table 3.2.2) which is favourable for brain tumour detection as well as peripheral tumour detection. As compared to 2-iodo-L-phenylalanine, the net tumour uptake and RTB of 2-iodo-D-phenylalanine are similar but the D-isomer was cleared two times faster from the blood (Figure 3.2.1, 3.2.3) (3). The latter will result in better tumour to blood ratios and less radiation burden to the animal.

Exogenous uptake of D-amino acids (by ingestion or from micro-organisms) will lead to the metabolization by D-amino acid oxidase, present in liver, kidneys and pancreas parenchym. The latter together with the stereospecificity of the translational machinery will result in the formation of proteins uniquely consisting of L-amino acids (18,19). Although 2-iodo-D-phenylalanine showed high uptake in the pancreatic zone, it was excreted very fast. This observation could implicate that the D-isomer, just like [^{123}I]-2-iodo-L-phenylalanine, is not incorporated into the cell proteins since the pancreas in rodent demonstrates a high protein turn over. In human, this high uptake of radiolabelled amino acids in the pancreas does not occur (20).

The abovementioned characteristics of [^{123}I]-2-iodo-D-phenylalanine, make this tracer a potential diagnostic tool for oncologic imaging. The rapid blood clearance together with the high, fast and specific tumour uptake shall lead to specific targeting of the tumour with minor radiation burden to other organs and tissues.

The dissection study presented more detailed, but equal, results about the tracer distribution as compared to DPI. It confirmed the high tumour uptake but low abdominal uptake of [^{123}I]-2-iodo-D-phenylalanine and its renal clearance. Regarding dosimetry, important differences between the three amino acid analogues were observed: of the three tracers, 2-iodo-L-tyrosine showed the highest effective dose followed by 2-iodo-L-phenylalanine and 2-iodo-D-phenylalanine, respectively. These results confirm the predictions made by 2-compartment modelling where a slower elimination and distribution to the peripheral compartment was observed for the L-analogue in comparison to 2-iodo-D-phenylalanine which results in slower clearance of 2-iodo-L-phenylalanine from the blood and thus a higher radiation burden. The extrapolation of the animal dosimetric data to humans indicate that the administration of 30 MBq of [^{123}I]-2-iodo-D-phenylalanine to healthy volunteers in a study of the human biodistribution will result in an effective dose of less than 1 mSv, limit for category IIb studies involving a risk of 10^{-5} according to the ICRP Publication 62 (21). Moreover, pancreas accumulation is typical in rodents and does not appear in humans what will additionally lead to lower effective doses. The low effective doses and biodistribution data obtained in present study assure that the use of [^{123}I]-2-iodo-D-phenylalanine in patients for medical diagnostics will not be restricted by radiation burden concerns.

Using hierarchical classification for [^{123}I]-2-iodo-L-phenylalanine for the exponential fitted parameters, a first step towards physiological modelling could be undertaken. This analysis indicated that not every organ is to be considered separately in full pharmacokinetic modelling, due to similar pharmacokinetic behaviour within the groups. Five different groups can be defined: tumour, remainder of the body, stomach, blood-group and other organs group. The stomach as an individual group can be explained by the uptake of free $^{123}I^-$ after dehalogentaion.

The abovementioned characteristics of [^{123}I]-2-iodo-D-phenylalanine make this tracer a potential diagnostic tool for oncologic imaging. The rapid blood clearance together with the high, fast and specific tumour uptake shall lead to specific targeting of the tumour with minor radiation burden to other organs and tissues.

3.2.6. CONCLUSION

[^{123}I]-2-iodo-D-phenylalanine is a promising tracer for diagnostic oncologic imaging due to its high, fast and specific tumour uptake and fast blood clearance. Moreover, the new tracer possessed better diagnostic imaging characteristics regarding the enhanced tumour contrast in comparison to its L-analogue.

3.2.7. REFERENCES

1. Jager PL, Vaalburg W, Pruim J, et al. Radiolabelled amino acids: basic aspects and clinical applications in oncology. *J Nucl Med*. 2001;42:432–445.
2. Yanagida O, Kanai Y, Chairoungdua A, et al. Human L-Type amino acid transport system 1 (LAT1): characterisation of function and expression in tumour cell lines. *Biochim Biophys Acta.* 2001;1514:291–302.
3. Kersemans V, Cornelissen B, Kersemans K, et al. In vivo characterisation of 2-Iodo-L-phenylalanine in a R1M rabdomyosarcoma mouse model as a potential tumour tracer for SPECT. *J Nucl Med* 2005;46:532-539.
4. Tamemasa O, Goto R, Suzuki T. Preferential incorporation of some 11C-labeled D-amino acids into tumour bearing animals. *Gann* 1978;69:517-523.
5. Tamemasa O, Goto R, Taketa A, et al. High uptake of 11C-labelled D-amino acids by various tumours. *Gann* 1982; 73:147-152.
6. Mertens JJR, Kersemans V, Lahoutte T, et al. Radioiodo-D-2-I-Phenylalanine a new tumour specific tracer for diagnosis and systemic radionuclide therapy. *Eur J Nucl Med 2004*; 31:S220
7. Waterton JC, Alott CP, Pickfort R, et al; Assessment of mouse tumour xenograft volumes in vivo by ultrasound imaging, MRI and calliper measurement. In: *Proceedings of the 19th LH Gray Conference: Quantitative imaging in oncology.* London: Eds Faulkner K, Carey B, Crellin A, Harisson RM; 1997:146–149
8. Boellaard R, Nanda CK, Hoekstra OS, et al. Effects of noise, image resolution and ROI definition on the accuracy of Standard Uptake Values: a simulation study. *J Nucl Med* 2004;45:1519-1527.
9. Thie JA. Understanding the standarized uptake value, its methods and implications for usage. *J Nucl Med* 2004;45:1431-1434.
10. Langen KJ, Pauleit D, Coenen HH, et al. 3-[(123)I]Iodo-alpha-methyl-L-tyrosine: uptake mechanisms and clinical applications. Nucl Med Biol 2002;29:625-631.
11. Loevinger R, Budinger T, Watson E. MIRD Primer for Absorbed Dose Calculations. New York, NY: The Society of Nuclear Medicine; 1991:1–17.
12. Cloutier RJ, Smith SA, Watson EE, Snyder WS, Warner GG. Dose to the fetus from radionuclides in the bladder. Health Phys. 1973;25:147–161.
13. Cook, MJ; *The Anatomy of the Laboratory Mouse*. New York: Academic Press; 1965:55-78.

14. Mertens J, Kersemans V, Bauwens M, et al. Synthesis, Radiosynthesis and In vitro characterisation of [125I]-2-Iodo-L-phenylalanine in a R1M rhabdomyosarcoma cell model as a new potential tumour tracer for SPECT. *Nucl Med Biol* 2004;31:739-746.
15. Rutgers M, Buitenhuis CKM, Hoefnagel CA, et al. Targeting of meta-iodobenzylguanidine to SK-N-SH human neuroblastoma xenografts: tissue distribution, metabolism and therapeutic efficacy. *Int J Cancer* 2000;87:412-422.
16. Hoefnagel CA and Lewington VJ. MIBG Therapy *In:* I.P.C. Murray and P.J. Ell (eds), Nuclear medicine in clinical diagnosis and treatment (2n ed) pp 1067-1081. Churchill Livingstone, London (1998).
17. Matthay KK, Desantes K, Hasegawa B, et al. Phase I dose escalation of 131I-metaiodobenzylguanidine with autologous bone marrow support in refractory neuroblastoma. *J Clin Oncol*. 1998;16:229-236
18. Langen KJ, Pauleit D, Coenen HH. 3-[^{123}I]iodo-alpha-methyl-L-tyrosine: uptake mechanisms and clinical applications. *Nucl Med Biol*. 2002;29:625–631.
19. Yang H, Zheng G, Peng X et al. D-Amino acids and D-Tyr-tRNA^{Tyr} deacylase: stereospecificity of the translation machine revisited. *FEBS Letters* 2003;552:95-98.
20. Langen KJ, Pauleit D, Coenen HH. 3-[^{123}I]iodo-alpha-methyl-L-tyrosine: uptake mechanisms and clinical applications. *Nucl Med Biol*. 2002;29:625–631.
21. Beekhuis H. Population radiation absorbed dose from nuclear medicine procedures in the Netherlands. Health Phys. 1988;54:287–291.

CHAPTER CONCLUSION

The precursor 2-iodo-D-phenylalanine was synthesized by analogy with its L-isomer: the optimal reaction conditions for 2-iodo-L-phenylalanine precursor synthesis using the Cu^{1+} assisted nucleophilic exchange in acidic and reducing conditions were applied. Moreover, the same Kit-formulation could be used for the radioiodination of the precursor 2-iodo-D-phenylalanine leading to the same radiochemical yield and purity.

In vitro evaluation of [^{125}I]-2-iodo-D-phenylalanine in the R1M rabdomyosarcoma cell model revealed a difference in uptake kinetics and affinity for influx between [^{125}I]-2-iodo-D-phenylalanine and [^{125}I]-2-iodo-L-phenylalanine which might be due to the fact that that the D-form only shows a high affinity for the LAT1 system and much lower affinity for LAT2 while [^{125}I]-2-iodo-L-phenylalanine demonstrates a high affinity for both transporter types. BCH is highly "general L transport" specific but with low affinity so it does not allow to differentiate the LAT types in the current conditions. Concentration depending kinetics illustrated that [^{125}I]-2-iodo-D-phenylalanine was transported into the cells by a single substrate-transport system interaction and that the K_m value for the latter amino acid analogue was comparable to that of L-phenylalanine and 2-iodo-L-phenylalanine.

[^{123}I]-2-iodo-D-phenylalanine showed in many aspects comparable characteristics to [^{123}I]-2-iodo-L-phenylalanine. Indeed, besides the same general biodistribution characteristics, such as renal clearance of the tracer and the absence of accumulation in the abdominal and brain regions, [^{123}I]-2-iodo-D-phenylalanine tumour accumulation was high and specific and occurred through the same transporter system LAT1. Moreover, the two-compartment modelling and the excretion as function of time both revealed that [^{123}I]-2-iodo-D-phenylalanine was cleared 2 times faster from the blood in comparison with [^{123}I]-2-iodo-L-phenylalanine. However, concerning the long time kinetics, both tracers showed some important differences. In vivo planar imaging revealed that although less [^{123}I]-2-iodo-D-phenylalanine remained in the tumour 19 hours p.i. in comparison with its L-analogue, an increase of 352% in tumour was observed whereas the tumour contrast for the L-isomer decreased to 71%.

The in vivo evaluation of [^{123}I]-2-iodo-D-phenylalanine illustrated that this tracer could be used as tumour diagnosticum for SPECT. Moreover, due to its metabolic stability and its fast clearance from the circulation, [^{123}I]-2-iodo-D-phenylalanine might be an interesting tracer for radionuclide therapy applications.

CHAPTER 4:

Comparative biodistribution between [^{123}I]-2-iodo-L-phenylalanine, [^{123}I]-2-iodo-L-tyrosine and [^{123}I]-2-iodo-L-phenylalanine.

CHAPTER INTRODUCTION

As a valorisation of the tracer characteristics for tumour imaging, the evaluation of and the comparison between both [^{123}I]-2-iodo-L-phenylalanine and [^{123}I]-2-iodo-D-phenylalanine in various tumours, representing those tumour families with highest prevalence in humans, should be performed. Moreover, an additional comparison with the recently developed tumour tracer [^{123}I]-2-iodo-L-phenylalanine would allow us to choose the optimal analogue for clinical practice.

At the moment, several amino acids have been developed for SPECT tumour imaging. Of these amino acid analogues, 2-iodo-L-tyrosine has made the largest progressions towards clinical application. Literature illustrated that the latter tracer showed no kidney accumulation and good tumour specificity characteristics.

As a consequence, we compared [^{123}I]-2-iodo-L-phenylalanine to [^{123}I]-2-iodo-L-tyrosine in the R1M athymic mouse model whether the former showed comparable or even better characteristics. Dynamic planar imaging and dissection were performed to study on the one hand the general tracer characteristics and on the other hand the tracer uptake kinetics. The latter was achieved using two compartment modelling. Moreover, both tracers were compared to ^{18}F-FDG to determine their additional benefits.

Although positive results were obtained using [^{123}I]-2-iodo-L-phenylalanine and [^{123}I]-2-iodo-D-phenylalanine, the question whether those two amino acids analogues could be used as “general tumour detecting agents” was not answered yet. As a consequence, both tumour tracers were evaluated in different tumour cells lines, corresponding with those tumours with high prevalence in human. Moreover, after this comparative biodistribution, the optimal analogue could be identified for further clinical use. Dynamic planar imaging and dissection were performed to study on the one hand the general tracer characteristics

4.1 Comparative Biodistribution Study of the New Tumour Tracer [^{123}I]-2-iodo-L-phenylalanine with [^{123}I]-2-iodo-L-tyrosine.

Veerle Kersemans, MSc[1]; Bart Cornelissen, PhD[1,2]; Rudi A. Dierckx, PhD[3]; Bart De Spiegeleer, PhD[1], John Mertens, PhD[4] and Guido Slegers, PhD[1].

[1] Laboratory for Radiopharmacy, Universiteit Gent, Belgium
[2] Laboratory for Molecular Imaging and Targeted Radiotherapy, University of Toronto, Canada.
[3] Division of Nuclear Medicine, Ghent University Hospital, Belgium
[4] Laboratory for Medical Imaging and Physics, Vrije Universiteit Brussel, Belgium

Key words: [^{123}I]-2-iodo-L-phenylalanine; radiolabeled amino acid analogue; tumour imaging; [^{123}I]-2-iodo-L-tyrosine; ^{18}F-FDG; SPECT.

Submitted for Nuclear Medicine and Biology

4.1.1 ABSTRACT

Introduction. Amino acid tracers are developed to overcome the limitations of ^{18}F-FDG since amino acid transport across the cell membrane is upregulated in tumour cells. The newly developed tracer [^{123}I]-2-iodo-L-phenylalanine showed high and specific tumour uptake and no accumulation in the kidneys and brain. This study compared [^{123}I]-2-iodo-L-phenylalanine with [^{123}I]-2-iodo-L-tyrosine, an [^{123}I]-IMT-analogue, which has recently entered clinical trials. **Methods.** [^{123}I]-2-iodo-L-phenylalanine and [^{123}I]-2-iodo-L-tyrosine were evaluated in rabdomyosarcoma tumour bearing athymic mice by means of dynamic planar imaging (DPI) and dissection. A displacement study with L-phenylalanine was performed to prove the specificity of tracer tumour uptake and kinetic modelling was applied on the DPI results. Moreover, the biodistribution of both tracers was compared with ^{18}F-FDG. **Results**. Both [^{123}I]-2-iodo-L-phenylalanine and [^{123}I]-2-iodo-L-tyrosine showed fast, high and specific tumour accumulation with no significant difference observed between both tracers. However, [^{123}I]-2-iodo-L-phenylalanine was cleared faster from the blood to the bladder in comparison to the tyrosine analogue. Moreover, [^{123}I]-2-iodo-L-phenylalanine tumour uptake equilibrated faster with the blood. Dissection showed that [^{123}I]-2-iodo-L-tyrosine slightly accumulated in the liver, which was not the case for the phenylalanine analogue. Compared to ^{18}F-FDG, both tracers demonstrated better imaging characteristics relating to brain and heart uptake. **Conclusions**. [^{123}I]-2-iodo-L-phenylalanine showed more promising characteristics for oncologic imaging as compared to [^{123}I]-2-iodo-L-tyrosine. The former tracer demonstrated not only faster blood clearance but the tracer uptake in the tumour reached its equilibrium with the bloodpool activity faster which lead to faster and better tumour contrast. Moreover, both tracers could overcome the limitations of ^{18}F-FDG.

4.1.2. INTRODUCTION

During the last decade, amino acid analogues gained much more interest in metabolic tumour imaging. They have put forward beneficial properties over [^{18}F]-fluorodeoxyglucose (^{18}F-FDG) and thus, they may help in imaging areas in which ^{18}F-FDG imaging is limited [1].

Malignant tumours represent a hypermetabolic state: not only glucose metabolism but also protein synthesis and amino acid transport are enhanced in cancer cells [2,3]. A- and L-type amino acid transport has been shown to be upregulated in tumour cells compared to normal tissue and these transport systems have been the major focus of the development of amino acid tumour tracers for oncologic imaging. Earlier studies showed that the enhanced amino acid transport across the cell membrane correlated with the malignancy of the tumour. Therefore, amino acid transport tracers are valuable tracers to reflect the malignancy of tumours [1].

2-amino-3-(4-hydroxy-3-[^{123}I]iodophenyl)-2-methylpropanoic acid (3-[^{123}I]-Iodo-α-methyltyrosine; ^{123}I-IMT) is currently the main and only routinely used amino acid tumour tracer for SPECT. However, its application in the abdominal area is limited by its marked and rapid renal accumulation [4,5]. To overcome these limitations, numerous amino acid analogues were investigated. Most attention was paid to 2-iodo-L-tyrosine which showed no accumulation in the kidneys and demonstrated high tumour specificity [6]. The latter amino acid has recently entered the clinical trial process.

To overcome the limitations of 3-[^{123}I]-Iodo-α-methyltyrosine, our research group focussed on 2-amino-3-(2-[^{123}I]iodophenyl)propanoic acid ([^{123}I]-2-iodo-L-phenylalanine) and described its promising properties as SPECT tumour diagnosticum in a variety of tumours [7,8]. The aim of this study was to compare the in vivo behaviour of [^{123}I]-2-iodo-L-phenylalanine with 2-amino-3-(4-hydroxy-2-[^{123}I]iodophenyl)propanoic acid ([^{123}I]-2-iodo-L-tyrosine) in order to evaluate whether the phenylalanine analogue exhibited better diagnostic imaging characteristics over the tyrosine analogue.

4.1.3. MATERIALS AND METHODS

All the conventional products mentioned were at least of analytical or clinical grade and obtained from Sigma-Aldrich. The solvents were of high-performance liquid chromatography quality (Chemlab, Belgium). The precursor 2-iodo-L-tyrosine was obtained from ABX, Belgium.

4.1.3.1. Synthesis of Precursor 2-iodo-L-phenylalanine

2-iodo-L-phenylalanine was prepared from 2-bromo-L-phenylalanine (PepTech Corp, USA) as described before, using the Cu^{1+} assisted nucleophilic exchange under acidic and reducing conditions [9]. After optimisation, the mean reaction yield was 74 % and no contamination of the D-isomer was detected by chiral chromatography.

4.1.3.2. Radiochemistry

4.1.3.2.1. [^{123}I/^{125}I]-2-iodo-L-phenylalanine and [^{123}I/^{125}I]-2-iodo-L-tyrosine.

Radioiodination of 1.0 mg 2-iodo-L-phenylalanine or 2-iodo-L-tyrosine with $^{123}I^-$ (222 MBq; 10 – 20 µl) or $^{125}I^-$ (37 MBq; 10 µl) (Nordion Europe, Belgium) was performed by Cu^{1+} assisted isotopic exchange (0.2 mg $CuSO_4$, 2.5 mg citric acid, 0.5 mg $SnSO_4$, 1.3 mg gentisic acid in 565 µl; 60 min at 100 °C). Radiolabeling of both tracers with $^{123}I^-$ or $^{125}I^-$ resulted in a radiochemical purity of > 99 % and a specific activity of 65 GBq/mmol ([^{123}I]-labeling) and 11 GBq/mmol ([^{125}I]-labeling) for 2-iodo-L-phenylalanine and a specific activity of 68 GBq/mmol ([^{123}I]-labeling) and 11 GBq/mmol ([^{125}I]-labeling) for 2-iodo-L-tyrosine. Chiral chromatography showed no transformation to the D-isomer.

4.1.3.2.2. [^{123}I]-iodo-Human Serum Albumin.

Radioiodination of Human Serum Albumin (HSA) with $^{123}I^-$ was performed by electrophilic substitution using the Iodogen technique: 50 µg HSA together with 111 MBq $^{123}I^-$ (10 µl) and 140 µl 0.1 M KH_2PO_4 buffer at pH 8.5 was added to a 1, 3, 4, 6-tetrachloro-3α, 6α-diphenylglycouracil (Pierce, Belgium) coated vial for 15 minutes. The reaction mixture was sent through a Ag-filter to remove the free $^{123}I^-$ from [^{123}I]-iodo-HSA. The specific activity was 4.10^4 GBq/mmol.

4.1.3.3. In Vivo Experiments

4.1.3.3.1. Laboratory Animals.

All in vivo studies were carried out in accordance with the Belgian legislation including the approval of the study protocol by the ethical committee for animal studies of the University of Gent. Guidelines of the National Institute of Health principles of laboratory animal care were followed.

Water and feed (SSNIFF® special treated, Bio-Services, The Netherlands) were freely available during the experimental period.

Studies were performed in female SWISS~*nu/nu* mice (n = 36) (weight range: 20 – 25 g) obtained from Bio-Services, The Netherlands. The mice were implanted with a R1M (rabdomyosarcoma) tumour, by subcutaneous injection of 5.10^6 R1M cells (BEFY-VUB, Brussels, Belgium) in the right armpit region. Normal tumour growth curves were obtained using sliding caliper measurement and the estimate volume formula $V = 0.4\ a^2.b$, with a and b being the short and the long axis of the tumour respectively [9,10]. All mice grew tumours with a volume of approximately 1 ml after 28 days. The imaging experiments were started when the tumour reached a volume of 0.5 ml. This R1M tumour model has been used previously to study the behaviour of radioiodinated amino acids [6].

Imaging experiments with [^{123}I]-iodo-HSA, [^{123}I]-2-iodo-L-phenylalanine and [^{123}I]-2-iodo-L-tyrosine were carried out on the same group of mice. The following scanning order was followed with an interval of 6 days in which the injected radioactivity decayed: [^{123}I]-iodo-HSA, [^{123}I]-2-iodo-L-tyrosine and [^{123}I]-2-iodo-L-phenylalanine. All tracers were injected intravenously (IV) in the lateral tail vein.

During all imaging experiments, anaesthesia was induced by intraperitoneal injection of pentobarbital (1.5 mg in 75 µl per animal; prepared by dilution (1:3) of 60 mg/ml Nembutal from Ceva Santé Animale, Belgium). For the biodistribution experiments by

dissection, the animals were killed by cervical dislocation without sedation and the organs of interest were dissected.

4.1.3.3.2. Dynamic Planar Imaging (DPI).

Imaging was performed using a gamma camera (Toshiba GCA-9300A/hg) in planar mode equipped with a high-resolution parallel-hole collimator. After the IV bolus injection of the [^{123}I]-labeled product in the lateral tail vein, the data were recorded in a 128 x 128 matrix (field of view: 23.5 x 12.5 cm) and with a photopeak window set at 15 % around 159 keV. The same time schedule as described for [^{123}I]-2-iodo-L-phenylalanine was used [9]. The tracer uptake was recorded as differential uptake ratio, taking into account a dose calibration and background correction following the guidances of Thie, et al. (16). The DUR was calculated [($counts_{tissue}$ * $pixels_{total\ body}$)/($pixels_{tissue}$ * $counts_{total\ body}$)].

Briefly, a [^{123}I]-iodo-HSA study was performed to measure the relative bloodpool distribution to correct the uptake of [^{123}I]-2-iodo-L-phenylalanine or [^{123}I]-2-iodo-L-tyrosine for bloodpool activity. Ten tumour bearing mice were injected with 7.4 MBq [^{123}I]-iodo-HSA. Ten dynamic planar images of 1 min were acquired starting 10 min p.i. ROIs were drawn around the tumour and the contralateral background area. The tumour to contralateral background (RTB) ratio was calculated and the overall mean for all animals determined.

Subsequently, immediately after injection of 18.5 MBq [^{123}I]-2-iodo-L-phenylalanine or [^{123}I]-2-iodo-L-tyrosine, the steady state of tumour uptake for both tracers was determined followed by a displacement study with L-phenylalanine (200 µl IV of a 145 mM solution). Tumour [^{123}I]-2-iodo-L-phenylalanine or [^{123}I]-2-iodo-L-tyrosine uptake was compared to the uptake in the contralateral background area and the ratio tumour to contralateral background (RTB) was calculated. Other organs, quantitatively assessed by DPI, were kidney, bladder and heart, the latter being representative for the blood activity as similar kinetic profiles xere obtained by dissection. The significance of displacement of [^{123}I]-2-iodo-L-phenylalanine or [^{123}I]-2-iodo-L-tyrosine activity by L-phenylalanine was calculated at a 95 % confidential interval.

Time activity curves were obtained from ROI analysis using a MRI maximum intensity projection as described before [9].

The data (= ROI of the heart) obtained by DPI for [^{123}I]-2-iodo-L-phenylalanine and [^{123}I]-2-iodo-L-tyrosine were fit to a two-compartment model with IV-bolus injection, without a lag time and with first order elimination, using WinNonlin 4.0.1. The primary parameters V_1, $k_{1,0}$, $k_{1,2}$ and $k_{2,1}$ were determined.

The behaviour of both tumour tracers was studied in the same animal to reduce variability between different animals. The results were submitted to *paired student t* statistical analysis.

4.1.3.3.3. Dissection: tissue distribution in time of [^{125}I]-2-iodo-tyrosine.

The IA was calculated by weighing the syringes before and after injection of the tracer and by the use of a dilution series of the injected tracer solution which was also weighed and counted for radioactivity using the auto gamma-counting system (CobraII Series, Canberra Packard, Meriden, CT, USA Cobra).

Twenty-seven R1M bearing athymic mice of the group of 36 animals used for imaging were injected with 7.4 kBq [^{125}I]-2-iodo-L-tyrosine, six days after the last imaging experiment was performed. At various time points (2, 5, 10, 15, 30, 45, 60, 120 and 180 min) post injection 3 animals per time point were sacrificed. The organs and tissues were removed, washed, dried and weighted. The blood was collected and weighted. The radioactivity of the

samples was counted by use of an auto gamma-counting system (CobraII Series, Canberra Packard, Meriden, CT, USA Cobra). The amount of radioactivity in the organs and tissues was calculated as the differential absorption rate (DAR): $[(IA/g)_{tissue}]/[(IA/g)_{total\ body}]$.

4.1.3.3.4. Dissection: Comparison of [^{125}I]-2-iodo-L-phenylalanine with [^{125}I]-2-iodo-tyrosine and ^{18}F-FDG at 90 min p.i.

Of the group of 36 mice used for imaging, 3 R1M bearing athymic mice per tracer were injected with 7.4 kBq [^{125}I]-2-iodo-L-phenylalanine, [^{125}I]-2-iodo-L-tyrosine or ^{18}F-FDG six days after the last imaging experiment was performed. At 90 min post injection, when the steady state for all tracers is reached, the animals were sacrificed. The organs and tissues were removed, washed, dried and weighted. The blood was collected and weighted. The radioactivity of the samples was counted by use of an auto gamma-counting system (CobraII Series, Canberra Packard, Meriden, CT, USA Cobra). The amount of radioactivity in the organs and tissues was calculated as DAR.

4.1.4. RESULTS.

4.1.4.1. Biodistribution by DPI

DPI with [^{123}I]-iodo-HSA showed no significant difference ($p < 0.05$) between the blood flow in the tumour and the contralateral reference leg: overall mean $RTB_{[123I]\text{-iodo-HSA}}$ = 1.1 (st. dev. = 0.2; n = 10; 10 min p.i.; independent of tumour volume).

Both [^{123}I]-2-iodo-L-phenylalanine and [^{123}I]-2-iodo-L-tyrosine showed high and fast tumour accumulation: the equilibrium for tumour uptake for both tracers was reached within 10 min post injection (p.i.) with an overall mean tumour DUR uptake value of 1.19 (st. dev.= 0.05; n = 12) and 1.24 (st. dev.= 0.06; n = 12) for [^{123}I]-2-iodo-L-phenylalanine and [^{123}I]-2-iodo-L-tyrosine, respectively, at equilibrium between 15 min and 30 min p.i. (Figure 4.1.1). The paired student t statistical analysis showed no significant difference in tumour tracer concentration at equilibrium. Administration of L-phenylalanine resulted in a significant ($p<0.05$) displacement of the radioactivity from the tumour for both tracers.

FIGURE 4.1.1: Overall mean uptake of [^{123}I]-2-iodo-L-phenylalanine (A) and [^{123}I]-2-iodo-L-tyrosine (B) in tumour and contralateral background region as a function of time by DPI expressed as DUR.

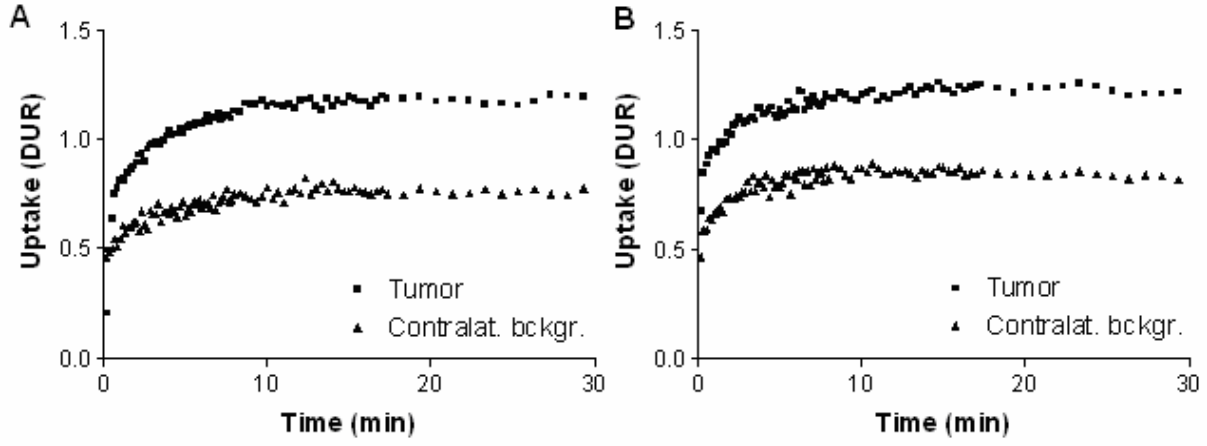

Both amino acid analogues showed a fast clearance from the blood through the kidneys to the bladder (Figure 4.1.2) but [^{123}I]-2-iodo-L-phenylalanine showed higher bladder accumulation at the same time point in comparison to [^{123}I]-2-iodo-L-tyrosine. Blood clearance of both tumour tracers could be described by first order kinetics (Figure 4.1.3).

FIGURE 4.1.2: Overall mean uptake of [^{123}I]-2-iodo-L-phenylalanine (A) and [^{123}I]-2-iodo-L-tyrosine (B) (DUR) as a function of time by dynamic planar imaging: clearance of the tracer through the kidneys to the bladder.

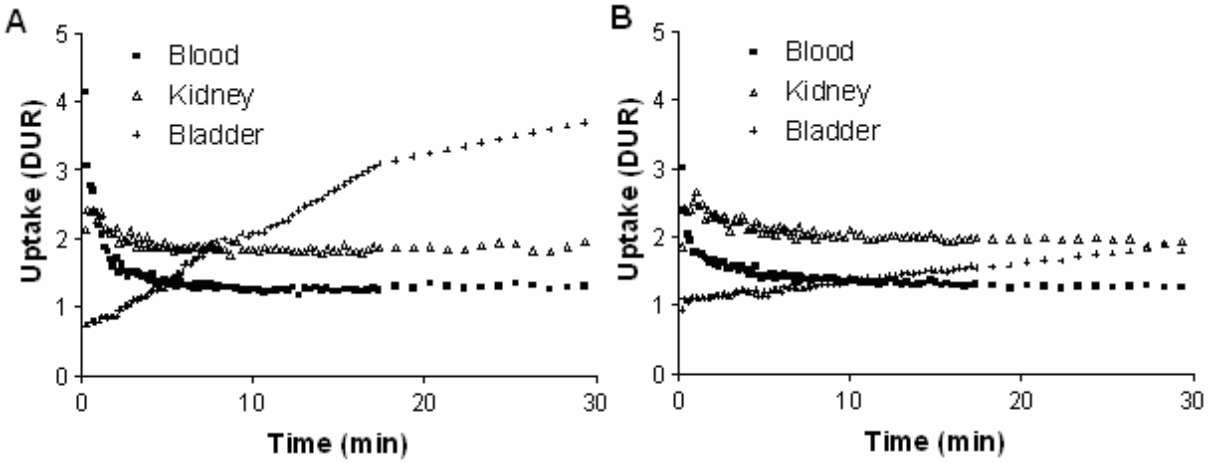

FIGURE 4.1.3: Plot of [^{123}I]-2-iodo-L-phenylalanine and [^{123}I]-2-iodo-L-tyrosine elimination: 1st order kinetic fitting for the blood clearance of both tracers to the bladder. $R^2_{\text{2-I-L-phenylalanine}}$ = 0.99; $R^2_{\text{2-iodo-L-tyrosine}}$ = 0.97

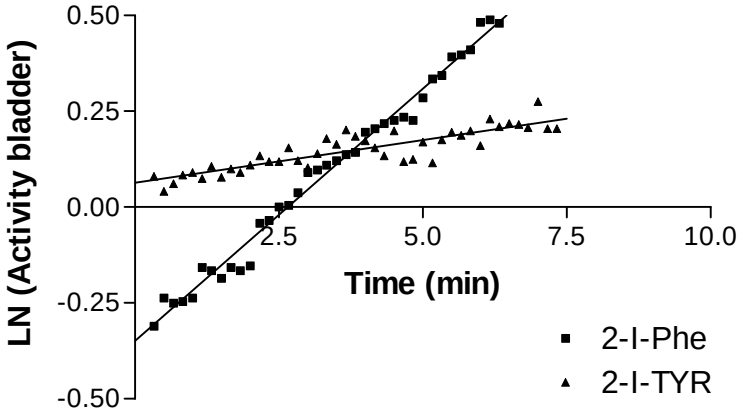

Tumour uptake of [^{123}I]-2-iodo-L-phenylalanine and [^{123}I]-2-iodo-L-tyrosine equilibrated with blood: both tumour-to-blood ratios as a function of time reached a steady state approximately at 15 min. However, the phenylalanine analogue tumour uptake equilibrated faster with the blood as compared to the tyrosine analogue: equilibrium was obtained from 9.7 min, respectively 15.3 min, as measured by the first derivatives of the tumour-to-blood ratio as a function of time becoming zero (Figure 4.1.4).

FIGURE 4.1.4: Plot of inverse relationship of ratio tumour-to-blood as a function of time for [^{123}I]-2-iodo-L-phenylalanine (y = 2.14 [C.I. = 2.08 – 2.21] x + 1.28; R^2 = 0.997) and [^{123}I]-2-iodo-L-tyrosine (y = 0.67 [C.I. = 0.61 – 0.73] x + 1.68; R^2 = 0.974).

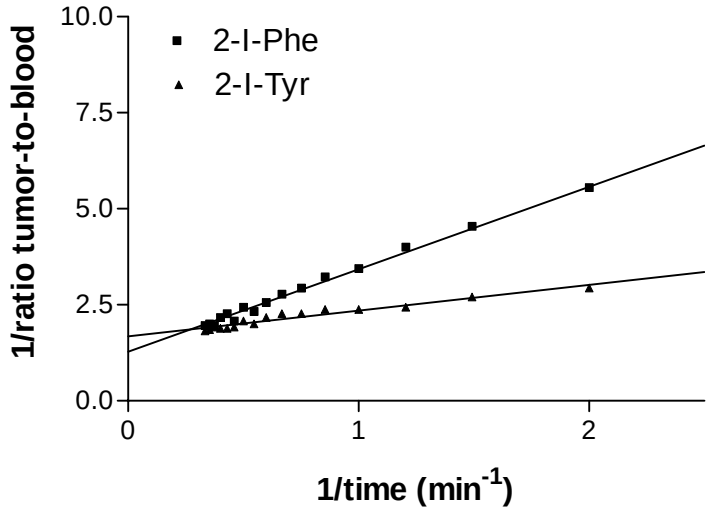

The results obtained by two-compartment modelling are given in Figure 4.1.5 and Table 4.1.1. Both [^{123}I]-2-iodo-L-phenylalanine and [^{123}I]-2-iodo-L-tyrosine biodistribution by DPI fitted the calculated curve for the proposed kinetic model (both $R^2 > 0.95$). Moreover, the pharmacokinetic model illustrated that [^{123}I]-2-iodo-L-tyrosine was cleared almost two times slower from the blood in comparison to the phenylalanine analogue. Although, [^{123}I]-2-iodo-L-tyrosine was taken up faster in the peripheral compartment, this tracer also disappeared faster from this compartment in comparison to [^{123}I]-2-iodo-L-phenylalanine.

FIGURE 4.1.5.: Kinetic fitting of the observed blood curve for [^{123}I]-2-iodo-L-phenylalanine (A) and [^{123}I]-2-iodo-L-tyrosine (B) tracer distribution with the calculated curve using a two compartment model.

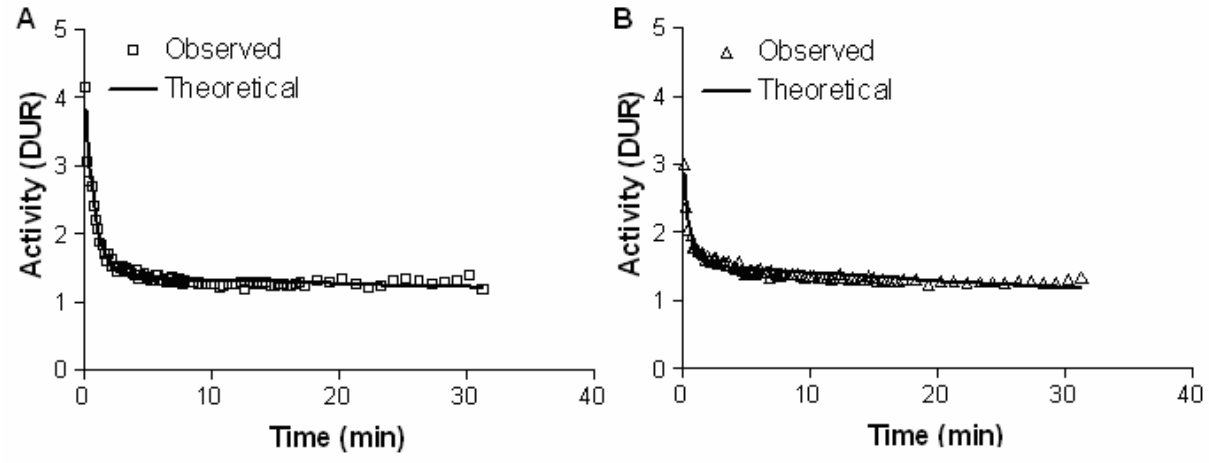

TABLE 4.1.1: Kinetic parameters obtained for (*) [^{123}I]-2-iodo-L-phenylalanine or (†) [^{123}I]-2-iodo-L-tyrosine by 2-compartment modelling. V_1 = Apparent distribution volume of central compartment; $k_{1,0}$ = elimination velocity; $k_{1,2}$ = distribution velocity from the central to the peripheral compartment; $k_{2,1}$ = velocity from the peripheral to the central compartment.

	Kinetic parameters±SD		
	unit	**2-I-L-Phe***	**2-I-L-Tyr†**
V_1	**(activity$_{totalbody}$)/(DUR)**	9.65±0.20	9.89±0.33
$k_{1,0}$	**1/min**	0.035±0.003	0.019±0.002
$k_{1,2}$	**1/min**	0.80±0.04	1.13±0.11
$k_{2,1}$	**1/min**	0.42±0.02	0.92±0.05

4.1.4.2. Biodistribution by dissection

The results of the biodistribution by dissection of [^{125}I]-2-iodo-L-tyrosine are shown in Table 4.1.2; those of the phenylalanine analogue were described earlier by Kersemans, et al. [9].

The biodistribution by dissection confirmed the results obtained by DPI and additionally showed that the plateau for tumour uptake for both tracers was constant, between 45 min and 3 hours p.i.. Slightly elevated liver [^{125}I]-2-iodo-L-tyrosine uptake was detected. No significant accumulation of radioactivity was observed in other abdominal organs such as lungs, stomach, small intestine and large intestine, neither in the brain for both tracers.

The results of the comparative biodistribution by dissection at equilibrium (90 min p.i.) are given in Table 4.1.3. Both amino acid tracers showed better characteristics relating to brain and heart uptake in comparison to ^{18}F-FDG which showed elevated levels in the organ.

TABLE 4.1.2: Biodistribution study by dissection of [^{125}I]-2-iodo-L-tyrosine in R1M bearing athymic mice expressed as DAR (n = 3).

	Mean ± SD			
Time (min)	**2**	**5**	**10**	**15**
blood	1.98±0.04	1.64±0.29	1.57±0.11	1.46±0.15
brain	0.43±0.02	0.69±0.03	0.72±0.19	0.65±0.09
heart	2.01±0.14	1.61±0.26	1.37±0.11	1.35±0.01
lung	1.54±0.04	1.42±0.38	1.22±0.10	1.04±0.01
stomach	0.64±0.28	0.86±0.34	1.53±0.43	1.02±0.25
milt	1.68±0.19	1.50±0.34	1.40±0.19	1.30±0.29
liver	2.66±0.48	2.17±0.88	1.99±0.64	1.92±0.66
kidneys	4.06±0.50	3.67±0.42	3.29±0.59	3.06±0.41
small intestine	1.18±0.04	1.11±0.25	0.94±0.22	0.87±0.06
large intestine	0.65±0.10	0.55±0.10	0.57±0.12	0.54±0.19
contr. Bckgr.	1.01±0.11	1.09±0.15	0.89±0.06	0.98±0.12
pancreas	6.68±3.84	11.21±2.88	10.40±6.07	10.56±8.34
tumour	0.34±0.06	0.36±0.18	0.55±0.11	0.79±0.05
RTB	0.34±0.11	0.33±0.16	0.61±0.14	0.81±0.06

	Mean ± SD				
Time (min)	**30**	**45**	**60**	**120**	**180**
blood	1.41±0.07	1.41±0.03	1.40±0.01	1.23±0.05	1.15±0.08
brain	0.91±0.29	0.96±0.20	0.78±0.02	0.84±0.23	0.72±0.04
heart	1.23±0.01	1.26±0.16	1.30±0.08	1.16±0.05	0.93±0.03
lung	1.02±0.11	1.21±0.14	1.25±0.05	1.01±0.07	0.99±0.11
stomach	1.33±0.87	1.20±0.80	1.58±0.49	1.89±0.62	1.57±0.58
milt	1.24±0.20	1.23±0.25	1.12±0.29	0.89±0.09	1.07±0.18
liver	1.79±0.58	1.75±0.68	1.71±0.39	1.77±0.45	1.95±0.43
kidneys	2.97±0.28	2.77±0.38	2.84±0.47	2.74±0.48	2.41±0.10
small intestine	1.08±0.30	1.00±0.23	1.05±0.32	1.02±0.23	1.08±0.32
large intestine	0.55±0.14	0.50±0.15	0.37±0.13	0.45±0.10	0.34±0.07
contr. Bckgr.	0.83±0.14	0.99±0.15	0.89±0.16	0.62±0.04	0.66±0.19
pancreas	8.15±4.25	10.55±6.88	9.38±4.59	10.85±6.31	10.53±5.80
tumour	0.97±0.06	1.38±0.14	1.33±0.03	1.31±0.18	1.14±0.15
RTB	1.16±0.22	1.40±0.21	1.49±0.19	1.67±0.23	1.74±0.24

TABLE 4.1.3: Biodistribution study by dissection: comparison of [^{125}I]-2-iodo-L-phenylalanine (*), [^{125}I]-2-iodo-L-tyrosine (†) and ^{18}F-FDG biodistribution in R1M bearing athymic mice (DAR values; mean ± st. dev.; n = 3; t = 90 min p.i.).

	Mean ± SD		
Tissue	**^{18}F-FDG**	**2-I-TYR†**	**2-I-PHE***
blood	0.19±0.02	1.76±0.13	1.42±0.36
brain	3.76±0.26	1.05±0.13	1.08±0.15
heart	7.01±1.16	1.37±0.09	1.42±0.04
lung	1.48±0.13	1.22±0.06	1.18±0.08
stomach	1.04±0.11	1.96±0.17	1.49±0.27
milt	1.10±0.11	1.66±0.18	1.33±0.06
liver	0.58±0.03	2.06±0.05	1.32±0.08
kidneys	0.48±0.06	4.93±0.18	2.26±0.17
large intestine	0.97±0.08	1.48±0.06	1.25±0.02
small intestine	1.86±0.03	0.82±0.19	0.78±0.05
contr. Bckgr	1.60±1.11	2.11±0.13	1.19±0.12
pancreas	1.62±0.17	24.72±1.75	16.81±1.59
tumour	1.69±0.29	3.69±0.55	2.18±0.70
RTB	1.18±0.59	1.92±0.26	2.06±0.78

4.1.5. DISCUSSION

Both amino acid analogues showed high and fast tumour accumulation. This fast tumour accumulation implicates that imaging with both amino acid tumour tracers could be performed within a very short period of time which is beneficial for the patient. Moreover, the displacement study with L-phenylalanine demonstrated on the one hand that the tumour uptake of both tracers was specific and on the other side that both amino acid analogues were transported through LAT1, an obligatory amino acid exchanger.

Concerning the general tracer characteristics, both amino acid tumour tracers demonstrated a renal clearance to the bladder without accumulation in the kidneys since both curves showed a parallel decline (Figure 4.1.2). Although they followed the same excretion route, [^{123}I]-2-iodo-L-phenylalanine reached higher accumulation values in the bladder at the same time point post injection (Figure 4.1.2). Moreover, [^{123}I]-2-iodo-L-phenylalanine tumour uptake equilibrated faster with the blood as compared to its tyrosine analogue. Both observations are important concerning radiation burden and imaging.

The results obtained by two-compartment modelling confirmed the first order fittings of the excretion. Moreover, kinetic modelling revealed that [^{123}I]-2-iodo-L-phenylalanine demonstrated better imaging conditions in comparison to [^{123}I]-2-iodo-L-tyrosine if the tumour shows elevated uptake values as compared to the contralateral background. As the latter is observed in our experiments, the faster blood clearance and longer stay in the peripheral compartment will benefit the tumour contrast.

The biodistribution results not only confirmed the general tracer characteristics as observed by DPI but demonstrated also a slightly elevated liver [^{125}I]-2-iodo-L-tyrosine uptake. The latter could be due to the slower blood clearance of the tracer in comparison to [^{125}I]-2-iodo-L-phenylalanine together with the high blood perfusion of this organ.

The comparative biodistribution study demonstrated that both the amino acid analogues are more suitable for brain tumour imaging because of their low uptake in comparison to ^{18}F-FDG. Moreover, earlier experiments illustrated that [^{123}I]-2-iodo-L-phenylalanine and [^{123}I]-2-iodo-L-tyrosine showed only a minor accumulation in inflamed lesions [6]. Comparison of [^{125}I]-2-iodo-L-tyrosine with [^{125}I]-2-iodo-L-phenylalanine revealed once more the slower blood clearance of [^{125}I]-2-iodo-L-tyrosine which is reflected by the longer kidney retention of this tracer.

4.1.6. CONCLUSION

The development of new tumour tracers for SPECT is important to overcome the well known limitations of [^{123}I]-L-3-iodo-α-methyltyrosine. The aim of this study was to compare the recently developed tumour tracer [^{123}I]-2-iodo-L-phenylalanine with [^{123}I]-2-iodo-L-tyrosine to check whether the phenylalanine analogue exhibited better in vivo characteristics over the tyrosine analogue which has recently entered the clinical trial process.

This study illustrated the more promising characteristics of [^{123}I]-2-iodo-L-phenylalanine for oncologic imaging as compared to [^{123}I]-2-iodo-L-tyrosine. The former amino acid analogue showed not only faster blood clearance but the tracer uptake in the tumour reached its equilibrium with the bloodpool activity faster. Both observations lead to faster and better tumour contrast for [^{123}I]-2-iodo-L-phenylalanine. Moreover, high tumour uptake and no significant uptake of [^{123}I]-2-iodo-L-phenylalanine in the abdominal region and brain favours the use of the phenylalanine analogue for tumour imaging with SPECT, whereas [^{123}I]-2-iodo-L-tyrosine tumour imaging shall be slightly hindered by its liver uptake. Both tracers showed no accumulation in the kidneys and thus overcome the limitations of IMT.

4.1.7. REFERENCES

1. Jager PL, Vaalburg W, Pruim J, et al. Radiolabelled amino acids: basic aspects and clinical applications in oncology. *J Nucl Med*. 2001;42:432–445.
2. Isselbacher KJ. Sugar and amino acid transport by cells in culture: differences between normal and malignant cells. *N Engl J Med.* 1972;286:929–933.
3. Ishiwata K, Vaalburg W, Elsinga PH, Paans AM, Woldring MG. Comparison of L-[1-11C]methionine and L-[methyl-11C]methionine for measuring in vivo protein synthesis rates with PET. *J Nucl Med.* 1988;29:1419–1427.
4. Langen KJ, Pauleit D, Coenen HH. 3-[^{123}I]iodo-alpha-methyl-L-tyrosine: uptake mechanisms and clinical applications. *Nucl Med Biol*. 2002;29:625–631.
5. Jager PL, Franssen EJ, Kool W, et al. Feasibility of tumour imaging using L-3-[iodine-123]-iodo- alpha-methyl-tyrosine in extracranial tumours. *J Nucl Med*. 1998;39:1736–1743.
6. Lahoutte T, Mertens J, Caveliers V, et al. Comparative biodistribution of iodinated amino acids in rats: selection of the optimal analog for oncologic imaging outside the brain. *J Nucl Med.* 2003;44:1489–1494.
7. Kersemans V, Cornelissen B, Kersemans K, et al. Detection of Various Tumour types in Athymic mice using [^{123}I]-2-iodo-L-phenylalanine Planar SPECT. *Eur J Nucl Med*. 2004: 31(S2), S380

8. Mertens J, Kersemans V, Bauwens M, et al. Synthesis, radiosynthesis, and in vitro characterization of [125I]-2-iodo-L-phenylalanine in a R1M rhabdomyosarcoma cell model as a new potential tumour tracer for SPECT. *Nucl Med Biol* 2004;31:739-746.
9. Kersemans V, Cornelissen B, Kersemans K, et al. In vivo characterisation of 2-iodo-L-phenylalanine in a R1M rabdomyosarcoma mouse model as a potential tumour tracer for SPECT. *J Nucl Med* 2005;46:532-539.
10. Waterton JC, Alott CP, Pickfort R, et al; Assessment of mouse tumour xenograft volumes in vivo by ultrasound imaging, MRI and calliper measurement. In: *Proceedings of the 19th LH Gray Conference: Quantitative imaging in oncology.* London: Eds Faulkner K, Carey B, Crellin A, Harisson RM; 1997:146–149

4.2 [$^{123/125}$I] Labelled 2-iodo-L-phenylalanine and 2-iodo-D-phenylalanine: Comparative Uptake in Various Tumour Types and Biodistribution in Mice.

Veerle Kersemans, MSc[1]; Bart Cornelissen, PhD[1]; Matthias Bauwens, MSc[2]; Ken Kersemans, MSc[2]; Rudi A. Dierckx, PhD[3]; Bart De Spiegeleer, PhD[1], John Mertens, PhD[2] and Guido Slegers, PhD[1].

[1] Laboratory for Radiopharmacy, Universiteit Gent, Harelbekestraat 72, B-9000 Gent, Belgium
[2] Laboratory for Medical Imaging and Physics, Vrije Universiteit Brussel, Belgium
[3] Division of Nuclear Medicine, Gent University Hospital, Belgium

Key words: [^{123}I]-2-iodo-phenylalanine; radiolabelled amino acids; tumour imaging; D-amino acid; tracer evaluation

Submitted for European Journal of Nuclear Medicine and Molecular Imaging

4.2.1 ABSTRACT

Objectives. In vitro in R1M cells as well as in vivo in the R1M tumour bearing athymic mice, both [^{123}I]-2-iodo-L-phenylalanine and [^{123}I]-2-iodo-D-phenylalanine showed tumour specific uptake. In order to compare both amino acid analogues and to generalize these characteristics, both isomers were evaluated in various tumour cell type. **Methods**. RT-PCR was used to check the presence of LAT1 in A549, A2058, C6, C32, Capan2, EF43fgf4, HT29 and R1M cells. Functional transport type characterisation in vitro with [^{123}I]-2-iodo-L-phenylalanine was performed by analogy with Shotwell, et al. Subsequently, both [^{123}I]-2-iodo-L-phenylalanine and [^{123}I]-2-iodo-D-phenylalanine tumour uptake and biodistribution using dynamic planar imaging and/or dissection was measured in A549, A2058, C6, C32, Capan2, EF43fgf4, HT29 and R1M inoculated athymic mice. **Results**. In vitro testing demonstrated that [^{123}I]-2-iodo-L-phenylalanine was transported in all tumour cell lines by the LAT1 system which presence was shown by RT-PCR. In vivo, both amino acid analogues showed in all tumour cell types the same general biodistribution characteristics: high and specific tumour uptake and a renal clearance. Two-compartment modelling revealed that the D-isomer showed a faster blood clearance together with a faster distribution to the peripheral compartment in comparison to [^{123}I]-2-iodo-L-phenylalanine. **Conclusions**. [^{123}I]-2-iodo-L-phenylalanine as well as its D-isomer are promising tumour diagnostics for dynamic planar imaging. Both showed a high uptake in all tested tumours, except in EF43fgf4.

4.2.2. INTRODUCTION

[^{18}F]-labelled Fluorodeoxyglucose (18F-FDG) is by far the most common radiopharmaceutical in clinical use. However, there are several well known limitations for the use of ^{18}F-FDG in oncology: not all tumours show an elevated glucose metabolism, brain uptake is high and the tracer lacks tumour specificity. The latter property is of utmost importance for the study of residual and recurrent tumour lesions after primary therapy (1-3)
Another interesting target for metabolic tumour imaging is the increased protein metabolism and amino acid uptake in the generally rapidly proliferating cancer cells. Over the past decade, many research groups reported the overexpression of both amino acid transporter systems A and LAT1. The role of LAT1 is to provide cells with essential amino acids for cell growth and tissue development which is reflected in its high upregulation in fetal tissues and tumours. The latter observation led to the development of various radiolabelled amino acids for tumour imaging (2,4).

In contrast to ^{18}F-FDG, amino acids play a marginal role in the metabolism of inflammatory cells. Radiolabelled amino acids may thus be more suited than ^{18}F-FDG for tumour imaging (3,5). Further studies with unnatural amino acids, which could not be incorporated into cell proteins, showed significant correlation between tracer uptake and thus amino acid transport and proliferation. For these reasons, amino acid transport tracers are proved to be valuable to reflect the malignancy of tumour. Moreover, those experiments showed that incorporation of radiolabelled amino acids into the cell proteins was not necessary to image cancer (2).

During the 80s, it was already shown that some D-amino acids, in comparison to their L-analogues, were taken up preferentially in tumours (6). More recently, it was demonstrated that D-amino acids were transported by the same amino acid transporter systems: LAT1 showed a high affinity for radiolabelled D-amino acids (7). These observations together with the highly stereospecific translation machinery and the presence of D-amino acid oxidase in kidneys and liver to metabolize exogenously D-amino acids, could make D-amino acids promising tumour diagnosting tools (8).

Our research group developed besides [$^{123/125}$I]-2-iodo-L-phenylalanine, also [$^{123/125}$I]-2-iodo-D-phenylalanine. Both [$^{123/125}$I]-2-iodo-L-phenylalanine and [$^{123/125}$I]-2-iodo-D-phenylalanine showed uptake in vitro as well as in vivo (nude mice and rats) using the R1M rabdomyosarcoma cell line (9,10,11,17). Both tracers demonstrated high tumour specificity, i.e. minor accumulation in inflammatory regions and no accumulation in the kidneys and thus the possibility to image peripheral tumours outside the brain. Moreover, due to rather slow clearance from the tumours, the tracers might have future perspectives as a systemic radiotherapy tool. These promising characteristics lead to the evaluation of both tracers in tumour cell lines which represent those tumour families with high prevalence in human. This paper evaluated whether the characteristics observed in the R1M tumor cell line could be extended to other tumour cell lines representative for human cancers, and thus whether both tracers could be used as general tumour detecting agents by dynamic planar imaging.

4.2.3. MATERIALS AND METHODS

All the conventional products mentioned were at least of analytical or clinical grade and obtained from Sigma-Aldrich. The solvents were of HPLC quality (Chemlab, Belgium).

4.2.3.1. Synthesis of Precursor 2-iodo-L-phenylalanine and 2-iodo-D-phenylalanine

2-iodo-L-phenylalanine and 2-iodo-D-phenylalanine were prepared from 2-bromo-L-phenylalanine and 2-bromo-D-phenylalanine (PepTech Corp, USA), respectively as described before, using the Cu^{1+} assisted nucleophilic exchange under acidic and reducing conditions. The mean reaction yield obtained for 2-iodo-L-phenylalanine and 2-iodo-D-phenylalanine was 74 % and 65 %, respectively and no contamination of the other isomer was detected by chiral chromatography for each reaction (9,10).

4.2.3.2. Radiochemistry

4.2.3.2.1. [^{123}I/^{125}I]-2-iodo-L-phenylalanine and [^{123}I/^{125}I]-2-iodo-D-phenylalanine.

Radioiodination with $^{123}I^-$ (222 MBq; 10 – 20 µl) or $^{125}I^-$ (37 MBq; 10 µl) (Nordion Europe, Belgium) on 1.0 mg 2-iodo-L-phenylalanine or 2-iodo-D-phenylalanine was performed by Cu^{1+} assisted isotopic exchange under acidic and reducing conditions (0.2 mg $CuSO_4$, 2.5 mg citric acid, 0.5 mg $SnSO_4$, 1.3 mg gentisic acid in 565 µl; 60 min at 100 °C) (9,10). The reaction mixture was drawn up in a syringe containing the appropriate amount of "make-up solution" (Tri-sodium Citrate dihydrate, 71 mM) to render the solution isotonic and to adjust the pH to at least 4. The reaction mixture was sent through a 0.22 µm Ag-filter (Millipore, Belgium) to remove the free $^{123/125}I^-$ and through a sterile 0.22 µm filter (Millipore, Belgium) into a sterile vacuum vial. Quality control was achieved by HPLC and Sep-pak C18 (Waters, Belgium). Radiolabeling of both tracers with $^{123}I^-$ or $^{125}I^-$ resulted in a radiochemical purity of > 99 % and a specific activity of 65 GBq/mmol ([^{123}I]-labeling) and 11 GBq/mmol ([^{125}I]-labeling). Chiral chromatography showed no transformation to the analogous isomer.

4.2.3.2.2. [^{123}I]-Iodo-Human Serum Albumin.

Radioiodination of Human Serum Albumin (HSA) with $^{123}I^-$ was performed by electrophilic substitution using the Iodogen (1, 3, 4, 6-tetrachloro-3α, 6α-diphenylglycouracil) technique: 50 µg HSA together with 111 MBq $^{123}I^-$ (10 µl) and 140 µl 0.1 M KH_2PO_4 buffer at pH 8.5 was added to an Iodogen (Pierce, Belgium) coated vial. After 15 min at room temperature the mixture was removed from the Iodogen coated vial to stop the reaction and was sent through a 0.22 µm Ag-filter to remove the free $^{123}I^-$ from [^{123}I]-Iodo-HSA and through a sterile 0.22 µm filter to sterilize into a sterile vacuum vial. The specific activity was 4.10^4 GBq/mmol. Quality control was achieved using a standard prepacked PD-10 SEC column (Size Exclusion Chromatography, Amersham Pharmacia Biotech, Sweden) using PBS/HSA as the eluting agent.

4.2.3.3. In Vitro Experiments

To check the presence of the L-type amino acid transporter LAT1, we performed a short in vitro evaluation of [^{125}I]-2-iodo-L-phenylalanine uptake in all cell lines used. The applied method has been described by Shotwell, et al and is frequently used to determine the relative contribution of the individual neutral transporter systems involved (11). Using R1M cells and 4F2hc-LAT1 transfected oocytes, respectively, Mertens et al. and Yanagida et al. described in earlier work that [^{125}I]-2-iodo-D-phenylalanine is taken up by the same transporter system with the same affinity for LAT1 as compared to its L-isomer (11,12).

4.2.3.3.1. Cell model.

A549 human non small cellular lung cell carcinoma, C32 human amelanotic melanoma, Capan2 human pancreatic carcinoma and HT29 human colon adenocarcinoma cells were purchased from Janssen Pharmaceutica, Beerse, Belgium. A2058 human melanoma and EF43fgf4 mouse breast carcinoma cells were obtained from the Laboratoire de Biologie des Tumeurs et du Développement, ULg, Liège, Belgium. C6 rat glioma and R1M rabdomyosarcoma cells were purchased from BEFY-VUB, Brussels, Belgium. Cell cultures were maintained and treated according to ATCC recommendations. A549, A2058, C6, C32, Capan2, EF43fgf4, HT29 and R1M cells were cultured in complete medium (Ham's F12 for C6, McCoys 5A for Capan2 and HT29 and DMEM for A549, A2058, C32, EF43fgf4 and R1M), enriched with 10 % of fetal bovine serum (FBS) and supplemented with 1 % penicillin-streptomycin and 1 % L-glutamine. Weekly split ratios were 1:20, 1:10, 1:5, 1:4, 1:20, 1:20, 1:10 and 1:20 for A2058, A549, C32, C6, Capan2, EF43fgf4, HT29 and R1M, respectively. All cell lines grew in an anchorage-dependent manner in tissue culture flasks and Falcon 6-well tissue culture plates.

All in vitro experiments were carried out in 6-well-plates (Novolab, Belgium), using three wells for each data-point. Influx of [^{125}I]-2-iodo-L-phenylalanine radioactivity was studied both in a Na^+ containing buffer ("$HEPES^+$": pH 7.4; 100 mM NaCl, 2 mM KCl, 1 mM $MgCl_2$, 1 mM $CaCl_2$, 10 mM Hepes, 5 mM Tris, 1 g/l glucose and 1 g/l Bovine Serum Albumine) and a Na^+ free buffer ("$HEPES^-$": pH 7.4; 100 mM Choline-Cl, 2 mM KCl, 1 mM $MgCl_2$,1 mM $CaCl_2$, 10 mM Hepes, 5 mM Tris, 1 g/l glucose and 1 g/l Bovine Serum Albumin). The influx was terminated by physical withdrawal of the buffer and by washing 3 times with ice-cold phosphate-buffered saline (PBS). Subsequently, the cells were lysed from the well with 1 ml of 0.1 M NaOH. The radioactivity of the samples was counted using the auto gamma-counting system (CobraII Series, Canberra Packard, Meriden, CT, USA Cobra).

4.2.3.3.2. Time dependency.

Cells were incubated for different times (0.5, 1, 2.5, 5, 7.5, 10, 15, 30 minutes) in 1 ml of $HEPES^+$ or $HEPES^-$ containing 37 kBq [^{125}I]-2-iodo-L-phenylalanine. ANOVA statistical analysis was performed to determine statistical differences in [^{125}I]-2-iodo-L-phenylalanine uptake between the various tumour cell lines.

Inhibition of [^{125}I]-2-iodo-L-phenylalanine influx.

In these inhibition experiments the cells were incubated with 37 kBq [^{125}I]-2-iodo-L-phenylalanine for 10 minutes in $HEPES^+$ buffer supplemented with 1 mM L-phenylalanine (the natural amino acid transported by LAT), 1 mM 2-iodo-L-phenylalanine (the "cold" precursor), 1 mM BCH (2-Amino-2-norbornane-carboxylic acid, a LAT transport system specific inhibitor) or 1 mM MeAIB (Methyl amino isobutyric acid, a A/ASC transport system specific inhibitor).

4.2.3.3.3. RT-PCR.

Oligonucleotide primers were synthesized by Eurogentec (Liège, Belgium). Human LAT1 (hLAT1) specific primers were matched to base pair 781-800 (hLAT1 forward: 5'-TGTGCTGGCATTATACAGCG-3') and base pair 992-1011 (hLAT1 backward: 5'-AGGTGATAGTTCCCGAAGTC-3') of the coding sequence (13). Human CD98 (=4F2hc) specific primers were matched to 151-170 (CD98 forward: 5'-GAATGAGTTAGAGCCCGAGA-3') and base pair 400-419 (CD98 backward: 5'-

CGATTATGACCACGGCACCA-3') of the coding sequence (13). Total RNA was isolated from the cell lines mentioned above by using a total mRNA isolation kit (Qiagen, Belgium) according to manufacturer guidelines. First strand cDNA synthesis is performed using Bioscript (Bioline, Belgium) according to manufacturer guidelines. RT-PCR was performed using BioTaq RED (Bioline, Belgium) according to manufacturer guidelines. The amplification of the cDNA strands was performed using a pre-cycle (94 °C during 3', 60 °C during 1', 72 °C during 2'), an amplification cycle (94 °C during 1', 60 °C during 1', 72 °C during 2', repeated for 26 cycles) and a hold cycle (72 °C during 10'). Gel-electrophoresis was performed on a 1.5% agarose/EtBr gel at 250 V and 250 mA during 15 minutes. The entire PCR product was loaded onto the gel whereby Hyperladder IV (Bioline, Belgium) was used as a marker.

4.2.3.4. In Vivo Experiments

4.2.3.4.1. Laboratory Animals.

The study protocol was approved by the local ethical committee for animal studies and was within the rules of Belgian legislation. Guidelines of the National Institute of Health principles of laboratory animal care were followed.

Water and food was freely available during the experimental period.

SWISS~nu/nu mice (n = 15 per cell line; except R1M: n = 30) (Bioservices, The Netherlands) were injected subcutaneously (SC) in the right flank (armpit region) with 5.10^6 A549, A2058, C6, C32, Capan2, HT29 or R1M cells. Female NMRI mice (n = 15) were injected SC in the right armpit region with 5.10^6 EF43fgf4 cells. These tumour cell lines were chosen as representatives of the tumour families who appear with highest prevalence in humans. Normal tumour growth curves were obtained using sliding caliper measurement and the estimate volume formula $V = 0.4\ a^2.b$, a and b being the short and the long axis of the tumour respectively (9,14). The imaging experiments started when the tumour reached a volume of 0.5 ml. Imaging experiments with [^{123}I]-2-iodo-L-phenylalanine, [^{123}I]-2-iodo-D-phenylalanine and [^{123}I]-iodo-HSA were carried out on the same mouse population (per cell line). Between the different experiments, attention was paid to a decay period of 6 days. Dissection experiments with [^{125}I]-2-iodo-L-phenylalanine were performed on each cell line and in the same mouse population as used for imaging experiments. Additionally, dissection experiments with [^{125}I]-2-iodo-D-phenylalanine were carried out in the R1M athymic mouse model as confirmation of the conclusions obtained by imaging for this isomer.

During all imaging experiments, the animals were anesthetized by intraperitoneal injection of a dilution (1:3) of pentobarbital (1.5 mg in 75 µl of Nembutal 60 mg/ml from Ceva Santé Animale, Belgium). For the biodistribution experiments by dissection, the animals were killed by cervical dislocation without sedation and the organs of interest were dissected.

All tracers (([$^{123/125}$I]-2-iodo-L-phenylalanine, [$^{123/125}$I]-2-iodo-D-phenylalanine and [^{123}I]-iodo-HSA) were injected intravenously (IV) in the lateral tail vein.

4.2.3.4.2. Dynamic Planar Imaging (DPI).

Imaging was performed using a gamma camera (Toshiba GCA-9300A/hg) in planar mode equipped with a high-resolution parallel-hole collimator After the IV bolus injection of the [^{123}I]-labeled product in the lateral tail vein, the data were recorded on a 128 x 128 matrices (field of view: 23.5 x 12.5 cm) and with a photopeak window set at 15 % around 159 keV. The DPI to determine the steady state of tumour tracer uptake consisted of 90 frames (48

x 10sec, 28 x 20sec and 14 x 60sec) and the DPI for the displacement study contained 90 frames of 30 sec.

Time activity curves were obtained by Region Of Interest Analysis (ROI) using a MRI maximum intension projection as described before (15). The tracer uptake was recorded as differential uptake ratio, taking into account a dose calibration and background correction following the guidances of Thie, et al. (16). The DUR was calculated as $[(counts_{tissue} * pixels_{total\ body})/(pixels_{tissue} * counts_{total\ body})]$.

At first, a [^{123}I]-iodo-HSA study was performed to measure the relative bloodpool distribution to correct the uptake of [^{123}I]-2-iodo-D-phenylalanine and [^{123}I]-2-iodo-L-phenylalanine in the tumours for bloodpool activity. For each cell line, ten tumour bearing mice were injected with 7.4 MBq [^{123}I]-iodo-HSA. Ten dynamic planar images of 1 min were acquired starting 10 min p.i. The tumour to contralateral background (RTB) ratio was calculated and the overall mean for all animals determined. Statistical analysis (ANOVA α = 0.05; SPSS 13.0 software package) was performed to compare the [^{123}I]-iodo-HSA uptake in the tumour tissue with the contralateral background tissue.

Immediately after injection of 18.5 MBq [^{123}I]-2-iodo-L-phenylalanine or [^{123}I]-2-iodo-D-phenylalanine, a dynamic acquisition was performed to determine the steady state of tracer uptake in the tumour. Secondly, at steady state a displacement study with L-phenylalanine (200 µl IV of a 145 mM solution) was performed. Regions of interest (ROI's) were drawn using a MRI maximum intensity projection as described before (9). Tumour [^{123}I]-2-iodo-L-phenylalanine or [^{123}I]-2-iodo-D-phenylalanine uptake was compared to the uptake in the contralateral background area and RTB calculated. The significance of displacement of [^{123}I]-2-iodo-L-phenylalanine or [^{123}I]-2-iodo-D-phenylalanine activity by L-phenylalanine was calculated at a 95 % confidential interval.

The data obtained by DPI for the blood curve for [^{123}I]-2-iodo-L-phenylalanine and [^{123}I]-2-iodo-D-phenylalanine were fit to a two-compartment model with IV-bolus injection, without a lag time and with first order elimination, using WinNonlin 4.0.1. This kinetic model was chosen by analogy with [^{123}I]-3-iodo-α-methyltyrosine (17). The primary parameters V_1, $k_{1,0}$, $k_{1,2}$ and $k_{2,1}$ were determined for both tracers in each cell line and the overall mean values and corresponding standard deviations (n=8 tumour cell lines) calculated.

Statistical analysis was performed using a 2-factor ANOVA (tumour-type and [^{123}I]-2-iodo-L-phenylalanine or [^{123}I]-2-iodo-D-phenylalanine) on the DPI results to investigate whether tumour uptake was different amongst the tumour types and both tracers.

4.2.3.4.3. Dissection: Biodistribution of [^{125}I]-2-iodo-L-phenylalanine or [^{125}I]-2-iodo-D-phenylalanine.

The IA was calculated by weighing the syringes before and after injection of the tracer and by the use of a dilution series of the injected tracer solution which was also weighed and counted for radioactivity using the auto gamma-counting system (CobraII Series, Canberra Packard, Meriden, CT, USA Cobra).

For each cell line tested, fifteen mice were injected with 7.4 kBq [^{125}I]-2-iodo-L-phenylalanine or 7.4 kBq [^{125}I]-2-iodo-D-phenylalanine, six days after the last imaging experiment with $^{123}I^-$-tracer was performed. At various time points (2, 30, 60, 120 and 180 min) post injection 3 animals per time point were sacrificed. The organs and tissues were removed, washed and weighted. The blood was collected and weighted. The radioactivity of the samples was counted by use of an auto gamma-counting system (CobraII Series, Canberra Packard, Meriden, CT, USA Cobra). The amount of radioactivity in the organs and tissues was calculated as the differential absorption rate (DAR): $[(activity_{tissue} * total\ body\ weight)/(weight_{tissue} * activity_{injected})]$. ANOVA statistical analysis was used to evaluate

whether the different tumour models showed differences in [^{125}I]-2-iodo-L-phenylalanine organ uptake.

4.2.4. RESULTS

4.2.4.1. In Vitro

Concerning RT-PCR, a single band for each gene was observed at the expected size in all tumour cell lines.

The results of the functional in vitro experiments are summarized in Table 4.2.1. All tested cell lines showed comparable [^{125}I]-2-iodo-L-phenylalanine uptake in HEPES$^+$ and HEPES$^-$. Tracer uptake in all cell lines in HEPES$^+$ was blocked for the largest part by L-phenylalanine, 2-iodo-L-phenylalanine and BCH but only for a minor part by MeAIB. It was confirmed by ANOVA followed by post-hoc analysis (Tukey HSD), that all cell lines demonstrated similar uptake values in Hepes$^+$ or Hepes$^-$, with exception of HT29 and EF453fgf4 which showed significant lower [^{125}I]-2-iodo-L-phenylalanine uptake values. However, the difference between Hepes$^+$ and Hepes$^-$ [^{125}I]-iodo-L-phenylalanine uptake, which is a measure for the investigated sodium dependence, was not significant ($p = 0.696$).

TABLE 4.2.1: In vitro uptake of [^{125}I]-iodo-L-phenylalanine at equilibrium (t=15min). (*) % of tracer uptake that is Na$^+$-independent; (*) L-Phe: L-phenylalanine; (†) 2-I-L-Phe: 2-iodo-L-phenylalanine; (‡) BCH: 2-Amino-2-norbornane-carboxylic acid; (§)MeAIB: Methyl amino isobutyric acid.

	%Uptake/million cells		% inhibition			
Cell line	Hepes-	Hepes+	L-Phe*	2-I-L-Phe†	BCH‡	MeAIB§
A549	12.2±3.6	10.4±2.3	71	77	79	0
A2058	10.3±0.9	10.1±1.3	72	81	83	18
C6	12.3±2.3	12.5±1.7	79	85	87	0
C32	12.9±2.4	15.8±1.7	88	90	85	0
Capan2	13.3±2.2	15.3±1.6	89	90	90	0
EF43fgf4	2.6±0.4	3.8±0.5	79	82	75	9
HT29	5.3±0.8	7.5±1.8	80	83	78	2
R1M	14.1±1.1	14.3±0.9	90	89	93	6

4.2.4.2. In Vivo

4.2.4.2.1. Dynamic Planar Imaging.

DPI showed for [^{123}I]-iodo-HSA no significant blood flow differences in the tumours (all $p < 0.05$) for A549, A2058, C32, Capan2, HT29 and R1M tumour cell lines. Mean RTB for [^{123}I]-iodo-HSA is 1.2 ± 0.1 for all these tumour types. In rat glioma (C6), a slightly elevated $RTB_{[123I]\text{-iodo-HSA}}$ of 1.4 ± 0.2 ($p = 0.03$) is noticed while EF43fgf4 showed a much higher value for $RTB_{[123I]\text{-iodo-HSA}}$ of 3.2 ± 1.1 ($p < 0.001$).

The [^{123}I]-2-iodo-L-phenylalanine and [^{123}I]-2-iodo-D-phenylalanine tumour uptake at steady state (plateau phase at 30 min) were high for all tumours and are summarized in Table 4.2.2. Neither significant differences (ANOVA, $\alpha = 0.05$) in RTB values were observed between both amino acid analogues nor amongst the various tumour types.

TABLE 4.2.2: DPI in vivo [^{123}I]-iodo-L-phenylalanine and [^{123}I]-iodo-D-phenylalanine tumour and contralateral background uptake for the different tumour types at steady state expressed as DUR (t = 30 min p.i.; mean ± st. dev., n = 15). (*) [^{123}I]-iodo-L-phenylalanine or [^{123}I]-iodo-D-phenylalanine. RTB = tumour to contralateral background ratio.

Cell line	L or D*	Tumour DUR	Contralateral Background DUR	RTB	Bladder DUR
A549	L	0.84 ± 0.08	0.49 ± 0.07	1.72 ± 0.23	4.0 ± 0.8
	D	0.88 ± 0.11	0.40 ± 0.03	2.17 ± 0.28	4.8 ± 0.9
A2058	L	0.80 ± 0.09	0.53 ± 0.03	1.50 ± 0.22	3.6 ± 0.9
	D	0.91 ± 0.09	0.49 ± 0.11	1.85 ± 0.21	6.3 ± 1.1
C6	L	1.12 ± 0.07	0.65 ± 0.15	1.73 ± 0.28	2.9 ± 0.4
	D	0.70 ± 0.06	0.30 ± 0.08	2.31 ± 0.21	10.5 ± 0.6
C32	L	0.99 ± 0.09	0.53 ± 0.05	1.88 ± 0.18	2.6 ± 0.5
	D	1.06 ± 0.11	0.55 ± 0.09	1.92 ± 0.22	6.2 ± 0.9
Capan2	L	0.87 ± 0.11	0.48 ± 0.07	1.83 ± 0.25	2.7 ± 0.7
	D	0.89 ± 0.09	0.39 ± 0.05	2.29 ± 0.21	3.3 ± 0.5
EF43fgf4	L	0.92 ± 0.07	0.46 ± 0.09	1.99 ± 0.19	4.5 ± 0.7
	D	1.13 ± 0.16	0.55 ± 0.09	2.04 ± 0.15	7.6 ± 0.9
HT29	L	0.90 ± 0.08	0.42 ± 0.06	2.12 ± 0.26	2.5 ± 0.5
	D	0.80 ± 0.06	0.36 ± 0.08	2.20 ± 0.41	6.8 ± 0.8
R1M	L	1.19 ± 0.09	0.63 ± 0.10	1.89 ± 0.16	3.2 ± 0.7
	D	0.99 ± 0.08	0.59 ± 0.07	1.68 ± 0.18	7.7 ± 0.9

The tracer uptake in the tumour was displaced after IV administration of L-phenylalanine for all tumour types tested (Table 4.2.3). No statistically significant ($\alpha = 0.05$) difference between the L- and D-isomer was observed.

TABLE 4.2.3: DPI displacement study of [^{123}I]-iodo-L-phenylalanine and [^{123}I]-iodo-D-phenylalanine tumour activity by L-phenylalanine (t = 45 min p.i.).
(*) % of all animals in which a significant (α=0.05) displacement of radioactivity was observed (n = 15);
(†) percentage of tracer decrease by administering the displacer L-phenylalanine (mean ± st. dev.).

	[^{123}I]-2-iodo-L-phenylalanine		[^{123}I]-2-iodo-D-phenylalanine	
Cell line	%P*	%D†	%P*	%D†
A549	60	32,6 ± 19,0	87	22,3 ± 17,4
A2058	53	13,2 ± 9,9	53	13,9 ± 9,2
C6	53	10,8 ± 1,8	60	10,7 ± 4,1
C32	47	7,1 ± 2,3	53	8,3 ± 1,9
Capan2	60	21,4 ± 11,3	60	18,1 ± 3,7
EF43fgf4	33	6,0 ± 3,1	40	9,2 ± 2,5
HT29	47	11,3 ± 4,8	47	10,8 ± 3,3
R1M	73	12,3 ± 4,2	53	9,6 ± 2,3

The general kinetic differences between the L- and D-phenylalanine analogues as previously found in the R1M mouse model were confirmed in this study. The blood elimination of both tracers showed a renal clearance to the bladder, with higher amounts accumulated for the D-isomer as compared to its L-analogue (Table 4.2.2, last column). Moreover, two-compartment modelling was applied on the observed DPI blood data, giving

overall results (over all tumour cell lines) similar to previously found results for the R1M cell line alone (Table 4.2.4).

Besides the difference in blood elimination velocity of both tracers, the model showed that [^{123}I]-2-iodo-D-phenylalanine was taken up faster in the peripheral compartment. However, its elimination velocity from the latter compartment was comparable to that of [^{123}I]-2-iodo-L-phenylalnine in all tumour models.

TABLE 4.2.4: Two-compartment blood modelling for [^{123}I]-iodo-L-phenylalanine and [^{123}I]-iodo-D-phenylalanine: overall mean values ± st. dev. (n=8) of both tracers for the primary parameters V_1, $k_{1,0}$, $k_{1,2}$ and $k_{2,1}$.

Kinetic parameters	[^{123}I]-2-iodo-L-phenylalanine	[^{123}I]-2-iodo-D-phenylalanine
V_1 (activity $_{\text{total body}}$/DUR)	9.65±1.31	10.25±2.42
$k_{1,0}$ (1/min)	0.028±0.008	0.056±0.016
$k_{1,2}$ (1/min)	0.59±0.14	0.84±0.46
$k_{2,1}$ (1/min)	0.35±0.09	0.47±0.21

4.2.4.2.2. Biodistribution by Dissection.

The most relevant biodistribution data of [^{125}I]-2-iodo-L-phenylalanine in all tumour bearing athymic mice are shown in Table 4.2.5.

TABLE 4.2.5: Dissection [^{125}I]-iodo-L-phenylalanine blood, tumour and contralateral background uptake in A549, A2058, C6, C32, Capan 2, EF43fgf4, HT29 and R1M inoculated athymic mice expressed as differential absorption ratio (DAR; mean ± st. dev., n=3) and the resulting ratio tumour to contralateral background (RTB).

	A549 (DAR values)					A2058 (DAR values)				
	2	**30**	**60**	**120**	**180**	**2**	**30**	**60**	**120**	**180**
Blood	2.56±0.53	1.60±0.32	1.45±0.19	1.53±0.41	1.62±0.21	2.16±0.35	1.48±0.27	1.25±0.31	1.44±0.22	0.47±0.07
Cnt. Bck	1.01±0.10	0.88±0.23	1.03±0.13	0.90±0.12	1.15±0.13	1.35±0.42	0.46±0.21	0.57±0.08	0.77±0.21	0.33±0.12
Tumour	0.66±0.15	1.86±0.22	2.66±0.25	2.32±0.24	2.81±0.27	0.56±0.26	1.25±0.18	1.51±0.11	1.81±0.18	1.32±0.07
RTB	0.67±0.21	2.31±0.26	2.56±0.36	2.54±0.39	2.49±0.31	0.40±0.31	2.90±0.39	3.82±0.27	3.99±0.33	4.10±0.39
	C6 (DAR values)					**C32 (DAR values)**				
	2	**30**	**60**	**120**	**180**	**2**	**30**	**60**	**120**	**180**
Blood	2.83±0.44	2.49±0.19	1.65±0.11	1.53±0.15	1.14±0.07	1.96±0.42	1.61±0.27	1.69±0.17	1.37±0.14	1.35±0.26
Cnt. Bck	1.60±0.23	1.34±0.10	1.11±0.17	1.13±0.13	1.10±0.11	1.58±0.29	1.13±0.22	1.08±0.09	1.08±0.12	1.06±0.15
Tumour	0.97±0.08	1.45±0.13	2.93±0.23	2.25±0.21	1.86±0.24	0.83±0.18	2.66±0.26	2.75±0.25	2.45±0.19	2.42±0.10
RTB	0.34±0.29	1.40±0.24	2.54±0.37	1.99±0.31	1.25±0.27	0.53±0.31	2.54±0.33	2.57±0.27	2.38±0.35	2.33±0.29
	Capan 2 (DAR values)					**EF43fgf4 (DAR values)**				
	2	**30**	**60**	**120**	**180**	**2**	**30**	**60**	**120**	**180**
Blood	3.52±0.59	2.63±0.29	2.83±0.49	2.25±0.32	2.51±0.38	2.40±0.58	1.94±0.36	1.77±0.37	1.76±0.35	1.89±0.46
Cnt. Bck	1.56±0.36	1.06±0.15	1.41±0.19	0.91±0.25	1.11±0.13	0.78±0.49	1.04±0.25	1.02±0.12	1.04±0.20	1.03±0.22
Tumour	1.60±0.26	3.88±0.29	4.62±0.22	3.93±0.19	4.66±0.44	1.10±0.23	1.32±0.18	1.20±0.23	1.33±0.13	1.19±0.19
RTB	1.04±0.24	3.66±0.54	3.26±0.36	4.33±0.51	4.20±0.43	1.02±0.33	1.30±0.17	1.39±0.27	1.41±0.19	1.30±0.23
	HT29 (DAR values)					**R1M (DAR values)**				
	2	**30**	**60**	**120**	**180**	**2**	**30**	**60**	**120**	**180**
Blood	2.30±0.08	1.68±0.31	1.6±0.06	1.63±0.10	1.74±0.02	1.76±0.94	1.46±0.37	1.06±0.31	1.23±0.25	1.16±0.21
Cnt. Bck	1.69±0.23	1.53±0.22	1.27±0.31	1.23±0.29	1.64±0.15	0.77±0.23	0.43±0.38	0.56±0.24	0.59±0.15	0.47±0.12
Tumour	1.11±0.21	1.52±0.41	2.06±0.33	2.54±0.23	2.29±0.19	1.13±0.11	2.58±0.61	3.76±0.32	4.32±0.16	3.02±0.95
RTB	0.63±0.15	0.96±0.21	1.56±0.26	2.08±0.19	1.48±0.21	1.61±0.72	3.58±0.97	6.71±1.26	7.47±1.63	6.35±1.05

For all tumour cell lines, the net [^{125}I]-2-iodo-L-phenylalanine tumour uptake reached equilibrium at 60 minutes p.i. The equilibrium plateau RTB values at 120 min were compared and a statistically significant difference between the different tumour cell lines was found. Post-hoc analysis (Tukey HSD) and graphical multiple means comparison by box-plots

showed this to be primarily R1M related (RTB ~ 7.47) opposed to all others (RTB range ~ 1.41 to 4.33). However, all tumour cell lines tested showed a RTB higher than 1.

ANOVA testing demonstrated that no significant differences in DAR results were observed between the different tumour cell lines for each other dissected organ (all $p > 0.283$). [^{125}I]-2-Iodo-L-phenylalanine was cleared very fast through the kidneys (no significant difference was noticed for the kidney [^{125}I]-2-iodo-L-phenylalanine uptake values amongst the different tumour types). A significant uptake of radioactivity in the pancreas was consistently observed. No significant accumulation of radioactivity was observed in other abdominal organs such as liver, lungs, small intestine and large intestine, neither in the brain.

The comparative biodistribution data of [^{125}I]-iodo-L-phenylalanine and [^{125}I]-2-iodo-D-phenylalanine in R1M bearing mice obtained by dissection are shown in Table 4.2.6.

TABLE 4.2.6: Comparative biodistribution of [^{125}I]-iodo-L-phenylalanine and [^{125}I]-iodo-D-phenylalanine by dissection in R1M inoculated athymic mice expressed as differential absorption ratio (DAR; mean ± st. dev., n=3) and ratio tumour to contralateral background (RTB).

	R1M (DAR values)							
Tracer	**[^{125}I]-iodo-L-phenylalanine**				**[^{125}I]-iodo-D-phenylalanine**			
Time (min)	**2**	**30**	**60**	**120**	**2**	**30**	**60**	**120**
Blood	1.76±0.94	1.46±0.37	1.06±0.31	1.23±0.25	3.10±0.12	1.25±0.21	1.08±0.12	1.06±0.05
Brain	0.34±0.01	0.49±0.09	0.63±0.16	0.61±0.12	0.33±0.07	0.36±0.06	0.42±0.05	0.38±0.10
Stomach	0.88±0.20	1.98±1.23	3.34±0.24	2.63±0.47	0.68±0.20	1.87±1.13	2.14±1.15	2.83±1.75
Liver	0.88±0.08	0.52±0.17	0.53±0.08	0.43±0.04	2.21±0.23	0.91±0.16	1.02±0.25	1.07±0.33
Kidneys	4.81±2.16	1.73±0.51	1.45±0.10	1.15±0.11	17.65±2.55	6.88±3.27	2.97±0.24	2.05±0.04
Pancreas	5.37±1.03	4.71±1.00	7.87±2.61	10.36±2.61	10.52±3.63	10.68±5.18	6.84±1.07	6.17±0.53
Contr. Bckgr.	0.77±0.23	0.43±0.38	0.56±0.24	0.59±0.15	1.10±0.21	1.06±0.19	0.68±0.12	0.66±0.04
Tumour	1.13±0.11	2.58±0.61	3.76±0.32	4.32±0.16	2.05±0.82	3.89±1.22	2.30±0.39	2.09±0.54
RTB	1.61±0.72	3.58±0.97	6.71±1.26	7.47±1.63	1.86±0.36	3.64±0.48	3.38±0.52	3.13±0.73

These dissection data showed that the net [^{125}I]-2-iodo-D-phenylalanine tumour uptake reached rapidly equilibrium with a mean DAR value at 60 minutes of 2.30 ± 0.39. At the same time point, [^{125}I]-2-iodo-D-phenylalanine activity in the blood and in the contralateral leg tissue reached a DAR of 1.08 ± 0.12 and 0.68 ± 0.12 respectively.

A significant uptake of radioactivity in the pancreas was observed. No significant accumulation of radioactivity was observed in other abdominal organs such as liver, lungs, small intestine and large intestine, neither in the brain.

4.2.5. DISCUSSION

The in vitro characterisation of all cell lines tested, strongly suggested the presence of functional LAT1: the [^{125}I]-2-iodo-L-phenylalanine uptake was Na^+ independent, as no significant difference in $HEPES^+$ and $HEPES^-$ uptake was observed. Moreover, the tracer uptake could be blocked for > 80 % by the LAT specific inhibitor BCH, whereas the A/ASC transport system specific inhibitor MeAIB blocked the tracer uptake only for a small part (< 20 %) (Table 4.2.1). These phenotypic results confirmed the obtained RT-PCR data: all cell lines showed hLAT1 as well as CD98 (4F2hc) expression. The latter is very important since the LAT1 requires CD98 for its functional expression: in absence of this glycoprotein, the

LAT1 proteins remain in the intracellular compartment. The latter hypothesis was also confirmed in vivo by the displacement study: a significant displacement of the radioactivity in the tumour could be detected for all tumour types (all $p < 0.05$; Table 4.2.3). This shows that the transporter system involved is of the "obligatory exchanger" type such as LAT1 and that the tumour uptake is specific.

Concerning the biodistribution measured by DPI and dissection, both amino acid analogues showed the same distribution pattern in the other tumour cell lines as in the R1M rabdomyosarcoma tumour athymic mice model.

[^{123}I]-2-iodo-L-phenylalanine as well as [^{123}I]-2-iodo-D-phenylalanine accumulated quickly to reach high amounts in all tumours at 30 minutes p.i. (Table 4.2.2. and 4.2.5). The EF43fgf4 tumour showed the lowest RTB as compared to the other cell lines (Table 4.2.5.). The EF43fgf4 tumour demonstrated on the one hand reasonable [$^{123/125}$I]-2-iodo-L-phenylalanine and [$^{123/125}$I]-2-iodo-D-phenylalanine tumour uptake (Table 4.2.2), but on the other hand a high RTB for [^{123}I]-HSA (tumour with a high vascularity), resulting in the lowest specific uptake compared to the other tumour cell lines. This could implicate that other tracers should be used to detect this tumour type.

By analogy with [^{123}I]-3-iodo-α-methyltyrosine, 2-compartment modelling was applied in order to evaluate the pharmacokinetics of both tracers in the different tumour bearing athymic mouse models. Both tracers followed almost the same trend in the different tumours as compared to the R1M model, indicating the consistency of the results over the different tumour cell lines. The modelling revealed that in comparison to its L-analogue, [^{123}I]-2-iodo-D-phenylalanine was cleared faster from the blood. These results were confirmed by DPI: the D-isomer reached at the same time point for the same tumour models higher tracer accumulation in the bladder.

These observations together with the fast renal clearance of [^{125}I]-2-iodo-L-phenylalanine and [^{125}I]-2-iodo-D-phenylalanine from the blood and their non significant uptake in the abdominal organs and brain in all tumour models, make both tracers suitable as powerful and general tumour detecting agents.

4.2.6. CONCLUSION

[$^{123/125}$I]-2-iodo-L-phenylalanine as well as its D-isomer are promising tumour diagnostics for dynamic planar imaging. Both showed high uptake in those tumours representative for tumour families with a high prevalence in humans. Moreover, 2-iodo-D-phenylalanine showed better pharmacokinetic tracer characteristics. As a consequence, [^{131}I]-2-iodo-D-phenylalanine might serve as a candidate for systemic radiotherapy.

4.2.7. REFERENCES

1. Hustinx R, Lemaire C, Jerusalem G, et al. Whole-body tumour imaging using PET and 2-18F-Fluoro-L-Tyrosine: preliminary evaluation and comparison with 18F-FDG. *J Nucl Med* 2003; 44:533-539.
2. Jager PL, Vaalburg W, Pruim J, et al. Radiolabelled amino acids: basic aspects and clinical applications in oncology. *J Nucl Med*. 2001;42:432–445

3. Lahoutte T, Mertens J, Caveliers V, et al. Comparative biodistribution of iodinated amino acids in rats: selection of the optimal analog for oncologic imaging outside the brain. *J Nucl Med.* 2003;44:1489–1494.
4. Isselbacher KJ. Sugar and amino acid transport by cells in culture – differences between normal and malignant cells. *Seminars in medicine of the Beth Israel Hospital* 1972; 286:929-933.
5. Jager PL, De Vries EGE, Piers DA, et al. Uptake mechanisms of L-3-[125I]-iodo-alfa-methyl-tyrosine in human small-cell lung cancer cell line: comparison with L-1-[14C]-tyrosine. *Nucl Med Comm* 2001;22:87-96.
6. Tamemasa O, Goto R, Suzuki T. Preferential incorporation of some 11C-labeled D-amino acids into tumour bearing animals. *Gann* 1978;69:517-523
7. Yanagida O, Kanai Y, Chairoungdua A, et al. Human L-Type amino acid transport system 1 (LAT1): characterisation of function and expression in tumour cell lines. *Biochim Biophys Acta.* 2001;1514:291–302
8. Yang H, Zheng G, Peng X et al. D-Amino acids and D-Tyr-tRNA^{Tyr} deacylase: stereospecificity of the translation machine revisited. *FEBS Letters* 2003;552:95-98
9. Kersemans V, Cornelissen B, Kersemans K, et al. In Vivo Characterization of 123/125I-2-iodo-LPhenylalanine in an R1M Rhabdomyosarcoma Athymic Mouse Model as a Potential Tumour Tracer for SPECT. *J Nucl Med* 2005;46:532-539
10. Kersemans V, Kersemans K, Cornelissen B, et al. In vivo evaluation of [I-123]-2-Iodo-D-Phenylalanine in tumour inoculated athymic mice by means of SPECT as a potential diagnostic and radionuclide therapy tool. *Eur J Nucl Med 2004*; 31:S219 (meeting abstract).
11. Shotwell A, Jayme DW, Killberg M, et al. Neutral amino acid transport systems in chinese hamster ovary cells. *J Biol Chem* 1981;256:5422-5427.
12. Mertens JJR, Kersemans V, Lahoutte T, et al. Radioiodo-D-2-I-Phenylalanine a new tumour specific tracer for diagnosis and systemic radionuclide therapy. *Eur J Nucl Med 2004*; 31:S220
13. Kudo Y and Boyd CAR. Heterodimeric amino acid transporters: expression of heavy but not light chains of CD98 correlates with induction of amino acid transport systems in human placental trophoblast. *J Physiol* 200;523:13-18.
14. Waterton JC, Alott CP, Pickfort R, et al; Assessment of mouse tumour xenograft volumes in vivo by ultrasound imaging, MRI and calliper measurement. In: *Proceedings of the 19th LH Gray Conference: Quantitative imaging in oncology.* London: Eds Faulkner K, Carey B, Crellin A, Harisson RM; 1997:146–149.
15. Cornelissen B, Kersemans V, Jans L, et al. Comparison between 1 T MRI and non-MRI based volumetry in inoculated tumours in mice. *Br J Radiology* 2005;78:338-342.
16. Thie JA. Understanding the standarized uptake value, its methods and implications for usage. *J Nucl Med* 2004;45:1431-1434.
17. Langen KJ, Pauleit D, Coenen HH. 3-[^{123}I]iodo-alpha-methyl-L-tyrosine: uptake mechanisms and clinical applications. *Nucl Med Biol*. 2002;29:625–631.
18. Kersemans V, Cornelissen B, Kersemans K, et al. In vivo characterisation of 2-iodo-L-phenylalanine in a R1M rabdomyosarcoma mouse model as a potential tumour tracer for SPECT. *J Nucl Med* 2005;46:532-539.

CHAPTER CONCLUSIONS

At the moment, several amino acids have been developed for SPECT tumour imaging. Of these amino acid analogues, [^{123}I]-2-iodo-L-tyrosine has made the largest progressions towards clinical application. Literature illustrated that the latter tracer showed no kidney accumulation and good tumour specificity characteristics. As a consequence, we compared [^{123}I]-2-iodo-L-phenylalanine to [^{123}I]-2-iodo-L-tyrosine in the R1M athymic mouse model whether the former showed comparable or even better characteristics.

Our results confirmed that both [^{123}I]-2-iodo-L-tyrosine and [^{123}I]-2-iodo-L-phenylalanine were transported by the LAT1 transporter as indicated by the in vitro studies in the R1M cell model. In vivo in the athymic mouse model, both tracers demonstrated comparable biodistribution characteristics: high, fast and specific tumour uptake and a renal clearance. However, [^{123}I]-2-iodo-L-phenylalanine demonstrated somewhat better characteristics for oncologic tumour imaging by means of SPECT. The latter hypothesis was confirmed by the dosimetric calculations as performed in Chapter 3: a higher effective dose was obtained for [^{123}I]-2-iodo-L-tyrosine as compared to [^{123}I]-2-iodo-L-phenylalanine.

Although positive results were obtained using [^{123}I]-2-iodo-L-phenylalanine and [^{123}I]-2-iodo-D-phenylalanine, the question whether those two amino acids analogues could be used as “general tumour detecting agents” was not answered yet. As a consequence, both tumour tracers were evaluated in different tumour cells lines, corresponding with those tumours with high prevalence in human.

Concerning the biodistribution and tumour uptake characteristics, the same results were obtained for both tracers as compared to the R1M tumour bearing athymic mouse model. On the one hand fast, high and specific tumour uptake and on the other no accumulation in the other organs was observed. These observations make both tracers suitable as powerful and general tumour detecting agents. Moreover, the differences between the two stereoisomers were confirmed: the modelling revealed that in comparison to its L-analogue, [^{123}I]-2-iodo-D-phenylalanine was cleared faster from the blood. These results were confirmed by DPI: the D-isomer reached at the same time point for the same tumour models higher tracer accumulation in the bladder. Moreover, as a result of these better pharmacokinetic tracer characteristics, [^{131}I]-2-iodo-D-phenylalanine might serve as a candidate for systemic radiotherapy.

CHAPTER 5:

Applications of [^{123}I]-2-iodo-L-phenylalanine

CHAPTER INTRODUCTION

To stipulate the possible use of [^{123}I]-2-iodo-L-phenylalanine as a tumour detecting agent for dynamic planar imaging, the application of the new tracer was evaluated for the diagnosis of cancer in dogs. Indeed, since many owners are prepared to give their pets the maximal care, including radiation and chemotherapy, it is important to have a highly specific tumour tracer at one's disposal.

A case report study described the use of [^{123}I]-2-iodo-L-phenylalanine as diagnostic tool for the detection of synovial cell sarcoma of the tarsus in two dogs. Two dogs were examined with [^{123}I]-2-iodo-L-phenylalanine using static, dynamic and whole body planar imaging.

During the process of curing cancer, there are a lot of other aspects to deal with. An important one is radiotherapy evaluation: the sooner the clinician could tell whether or not a patient is responding to therapy, the sooner it could be adjusted and valuable time will be spared. It is in this aspect that we evaluated [^{123}I]-2-iodo-L-phenylalanine as a radiotherapy response tool. In vitro, accumulation of [^{123}I]-2-iodo-L-phenylalanine in R1M cells was tested after irradiation with ^{60}Co. In vivo, R1M tumour bearing athymic mice were tumour irradiated, contralateral irradiated or not irradiated. Tracer uptake was investigated after various time intervals post-irradiation by means of static planar imaging in tumour tissue, contralateral tissue and front leg tissue.

5.1 Future Perspectives: Is [$^{123/125}$I]-2-iodo-L-phenylalanine Useful as an Early Radiotherapy Response Tool?

Veerle Kersemans, MSc[1*]; Virginie de Gelder, MSc[2]; Indira Madani, MD, MSc[3]; Bart De Spiegeleer, PhD[1]; Hubert Thierens, PhD[2]; Wilfried De Neve, PhD[3]; John Mertens, PhD[4] and Guido Slegers, PhD[1].

[1] Laboratory for Radiopharmacy, Universiteit Gent, Harelbekestraat 72, B-9000 Gent, Belgium.
[2] Laboratory for Anatomy, Embryology, Histology and Medical Physics, Universiteit Gent, Belgium
[3] Division of Radiotherapy, Ghent University Hospital, Gent, Belgium
[4] Laboratory for Medical Imaging and Physics, Vrije Universiteit Brussel, Belgium

Key words: [^{123}I]-2-Iodo-phenylalanine; radiolabeled amino acids; tumor imaging; radiotherapy response

Submitted for Nuclear Medicine Communications

5.1.1 ABSTRACT

Objectives. Today, differentiation of post therapy radiation necrosis remains a challenging imaging problem which has strong implications for disease management. The ideal tracer for this purpose would reproducibly demonstrate a different accumulation pattern in radiation damaged cells from that of viable tumour tissue. In this aspect, [^{123}I]-2-iodo-L-phenylalanine was evaluated as radio-diagnostic tool since it accumulated with high specificity in tumour lesions. **Methods**. In vitro, uptake of [^{123}I]-2-iodo-L-phenylalanine in R1M cells was tested after irradiation with ^{60}Co. In vivo, R1M tumour bearing athymic mice were divided into 3 groups: tumour irradiated, contralateral irradiated or not irradiated. Tracer uptake in tumour tissue, contralateral tissue and front leg tissue was investigated after various time intervals post-irradiation by means of static planar imaging. **Results**. The in vitro tests demonstrated that in the fewer cells surviving at high radiation dose, the tracer uptake was higher. This was also demonstrated for the control tracer ^{18}F-FDG. In vivo, [^{123}I]-2-iodo-L-phenylalanine showed neither accumulation in the irradiated contralateral tissue nor in the not-irradiated front leg tissue. Tumour uptake decreased as a function of post-irradiation time. At 18 hours post-irradiation, accumulation of the tracer in tumour tissue was significantly lower in the tumour irradiated group as compared to the contralateral irradiated group and the not-irradiated group. **Conclusion**. In vivo evaluation confirmed that [^{123}I]-iodo-L-phenylalanine was able to observe irradiation effects on the tumour cells, even at very short time intervals. Moreover, if the mouse data could be extrapolated to humans, clinicians would be able to discover whether or not the tumour is susceptible to radiotherapy within 24 hours post-irradiation, i.e. if an individual would be a radiotherapy responder or not.

5.1.2 INTRODUCTION

Magnetic Resonance Imaging (MRI) and Computed Tomography (CT) are powerful imaging tools but they still can not reliably separate radiotherapy necrosis from recurrent tumour lesions (1-3). Moreover, attempts with ^{18}F-fluorodeoxyglucose (^{18}F-FDG) were only partially successful (4-7). One problem is the high intrinsic uptake of ^{18}F-FDG in the brain (cerebral cortex) leading to difficult differentiation between normal brain tissue and tumour tissue. Another aspect is the wide range of ^{18}F-FDG uptake in different tumours leading to an overlap with the degree of uptake in radiation necrosis and inflammation. Thus, differentiation between post therapy radiation necrosis and inflammation with remaining viable tumour tissue remains a challenging imaging problem which has strong implications for disease management. The ideal tracer for this purpose would reproducibly demonstrate a different accumulation pattern in radiation damaged cells from that of tumour tissue, for example: no accumulation in the necrosis area and high accumulation in the tumour lesion.

[$^{123/125}$I]-2-iodo-L-phenylalanine was evaluated previously as a new tumour tracer for Single Photon Emission Tomography (SPECT). Earlier reports showed high and specific tumour uptake through the overexpressed L-type amino transporter subtype 1 (LAT1), in vitro as well as in vivo, in a variety of tumours corresponding with the highest prevalence in human (8,9).

Diagnosis of a cancerous lesion and detecting the primary tumour is only the first step in curing the patient from cancer. Once the diagnosis is made, therapy could be started where another important aspect in oncology rises: is the tumour still viable or not after therapy? This paper describes the evaluation of [$^{123/125}$I]-2-iodo-L-phenylalanine, in vitro as well as in vivo, as a radiotherapy response tool. Since this amino acid analogue lacked uptake in inflammatory lesions (8), it could show promising results because necrotic areas and irradiated tissue often show the presence of inflammatory cells.

5.1.3 MATERIALS AND METHODS

All the conventional products mentioned were at least of analytical or clinical grade and obtained from Sigma-Aldrich. The solvents were of HPLC quality (Chemlab, Belgium). Cell culture products were obtained from Cambrex, Belgium.

5.1.3.1. Radiochemistry

Radioiodination with $^{123}I^-$ (555 MBq; 37 µl) or $^{125}I^-$ (37 MBq; 10 µl) (Nordion Europe, Belgium) on 1.0 mg 2-iodo-L-phenylalanine was performed by Cu^{1+} assisted isotopic exchange under acidic and reducing conditions (0.2 mg $CuSO_4$, 2.5 mg citric acid, 0.5 mg $SnSO_4$, 1.3 mg gentisic acid in 565 µl; 60 min at 100 °C) (8). The reaction mixture was rendered isotonic and its pH was adjusted to at least 4 by adding tri-sodium citrate dihydrate (71 mM). To remove the small fraction of free $^{123/125}I^-$ and to sterilize the reaction mixture, a 0.22 µm Ag-filter (Millipore, Belgium) and a sterile 0.22 µm filter (Millipore, Belgium) were applied, respectively. Radiolabeling with $^{123}I^-$ or $^{125}I^-$ resulted in a radiochemical purity of > 99 % and a specific activity of 163 GBq/mmol ([^{123}I]-labeling) and 11 GBq/mmol ([^{125}I]-labeling). Chiral chromatography showed no transformation to the D-isomer.

5.1.3.2. In Vitro Experiments

5.1.3.2.1. Cell model.

R1M rabdomyosarcoma cells were purchased from BEFY-VUB, Brussels, Belgium. The cell culture was maintained and treated according to ATCC recommendations. R1M cells were cultured in complete medium (DMEM), enriched with 10 % of fetal bovine serum (FBS) and supplemented with 1 % penicillin-streptomycin and 1 % L-glutamine. The weekly split ratio was 1:20. The cell line grew in an anchorage-dependent manner in tissue culture flasks (NUNC, Belgium). The amount of cells per falcon after the weekly split was tested during the maintenance and the variability was 6.1 % of the total amount of cells per falcon.

All in vitro experiments were carried out in 37 cm^2 culture flasks. Influx of [^{125}I]-2-iodo-L-phenylalanine radioactivity was studied in a Na^+ containing buffer ("HEPES$^+$": pH 7.4; 100 mM NaCl, 2 mM KCl, 1 mM $MgCl_2$, 1 mM $CaCl_2$, 10 mM Hepes, 5 mM Tris, 1 g/l glucose and 1 g/l Bovine Serum Albumine). The influx was terminated after 15 minutes by physical withdrawal of the buffer and by washing 3 times with ice-cold phosphate-buffered saline. Subsequently, complete growth medium was added and the radioactivity of the samples was counted using a NaI detector.

Cells were incubated for 15 min in 4 ml of HEPES$^+$ containing 370 kBq [^{125}I]-2-iodo-L-phenylalanine. The incubation time was chosen from the previous experiments and it is the time when equilibrium was established (10). In parallel, cells were incubated for 3 hours in 4 ml of HEPES+ containing 370 kBq ^{18}F-FDG, as control tracer. The incubation time was chosen by analogy with previously described in vitro experiments using ^{18}F-FDG (11,12).

The cells were counted immediately after measuring the culture flasks on radioactivity. The complete growth medium was removed and 0.5 ml trypsine was added until the cells were detaching. Subsequently, 0.5 ml of PBS was added. Eighty microlitres of this cell suspension was added to 20 µl trypane blue. Viable cells were counted in a Neubauer counting chamber.

5.1.3.2.2. In vitro irradiation

Culture flasks (sham-irradiated) were exposed to radiation doses ranging from 2 to 50 Gy in ^{60}Co γ-ray beam. During the irradiation the culture flasks were kept at 37 °C in a waterbath. The culture flask which received no external irradiation served as control. Two series of experiments were performed: a first experiment with doses up to 50 Gy was followed by a second experiment for a detailed dose-response determination in a narrower dose range up to 20 Gy. All in vitro tracer cell experiments were carried out 24 hours post irradiation. Immediately after the tracer cell experiment, the cells were counted by the trypan blue method, i.e. 24.5 hours and 27.5 hours post irradiation for [^{125}I]-2-iodo-L-phenylalanine and ^{18}F-FDG, respectively. The results were expressed as survival fraction (SF = % viable $cells_{treatment}$ / %viable $cells_{control}$) or as cell death fraction (1-survival fraction) and as %uptake/10^6 viable cells [Activity in remaining viable cells * 10^6/ Total activity added * n remaining viable cells)].

5.1.3.3. In vivo experiments.

The study protocol was approved by the local ethical committee for animal studies at the University Hospital of Ghent and was conform to the Belgian legislation. Guidelines of the National Institute of Health principles of laboratory animal care were followed.

5.1.3.3.1. Laboratory Animals.

Water and food were freely available during the experimental period.

Studies were performed in SWISS~*nu/nu* mice (n = 30) obtained from Bioservices, The Netherlands. The mice were implanted with a R1M (rabdomyosarcoma) tumour, by subcutaneous injection of 5.10^7 R1M cells (BEFY-VUB, Brussels, Belgium) in the right thigh. All mice grew tumours with a volume of approximately 1 ml after 28 days. The experiments were started when the tumour reached a volume of 0.5 ml. The R1M tumour model has been used previously to study the behaviour of radioiodinated amino acids and to characterize and evaluate [^{123}I]-2-iodo-L-phenylalanine as a tumour tracer for SPECT (8,13).

During the irradiation and imaging experiments, anaesthesia was induced by intraperitoneal injection of pentobarbital (1.5 mg in 75 µl per animal; prepared by dilution (1:3) of 60 mg/ml Nembutal from Ceva Santé Animale, Belgium). [^{123}I]-2-iodo-L-phenylalanine was injected intravenously (IV) in the lateral tail vein.

5.1.3.3.2. In vivo irradiation.

The mice were irradiated using the 5 MV photon beam from a medical linear accelerator (Elekta SL75) at a treatment distance of 100 cm and a dose rate of 350 cGy/minute. All irradiated mice received a single treatment of 10 Gy.

The mouse population was divided into 3 groups: group 1 being the control group which was not irradiated, group 2 which received a 10 Gy irradiation to the tumour site (tumour-irradiated group) and group 3 which received a 10 Gy irradiation to the contralateral site of the tumour (contralateral background irradiated group). The uptake of [^{123}I]-iodo-L-phenylalanine in 3 tissues (tumour, contralateral background and front leg) was followed for each of the 3 groups (tumour irradiated, contralateral irradiated and control group). All 3 groups had a R1M tumour. Group 3 was used to control for the possibility of tracer uptake caused by radiation induced inflammation. The mice were restrained in a specially designed box during irradiation to immobilize the mice and ensure that only the legs were irradiated. The box could hold four mice at a time. To ensure that the tumour or contralateral received the correct dose, 1.5 cm of PMMA was placed on top of the box and the radiation opening on the accelerator was adjusted to 14 cm x 14 cm. The mice were placed at the corners of the beam so that just the legs (tumour or contralateral) of the mice were in the radiation beam and thus irradiated. A schematic presentation of the sites of irradiation in the used populations together with the tracer injection scheme is shown in Figure 5.1.1.

FIGURE 5.1.1: Schematic presentation of the sites of irradiation (indicated in grey) in the mouse populations and overview of the injection and scanning protocol.

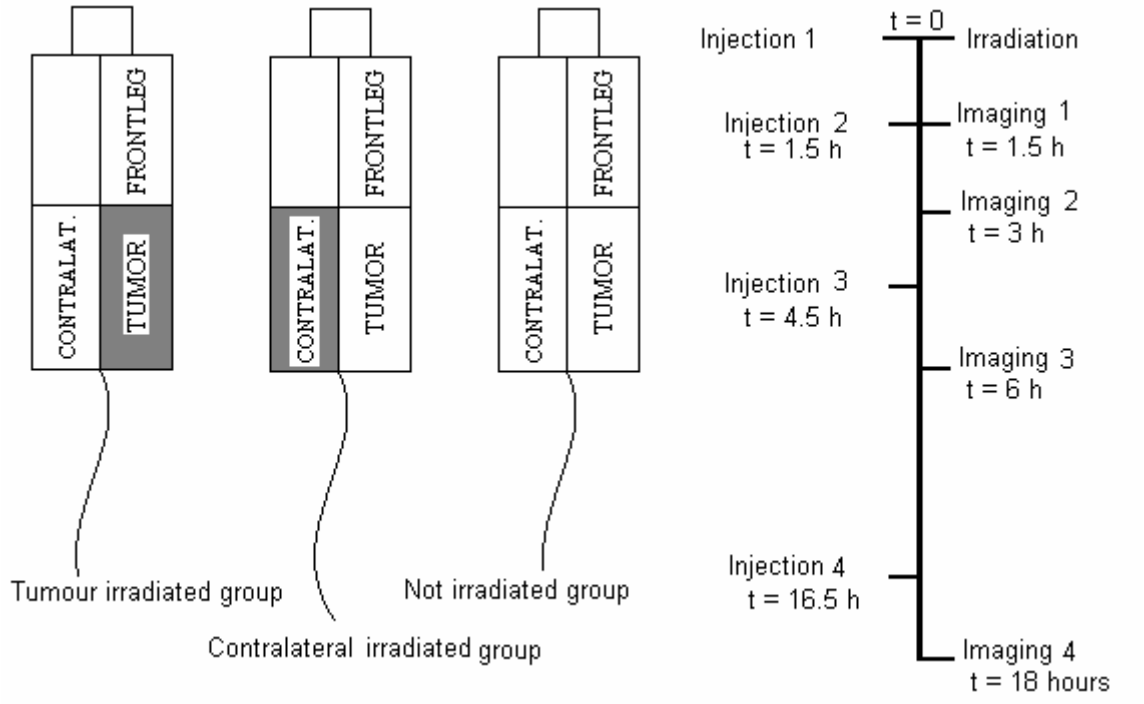

5.1.3.3.3. Static Planar Imaging.

Imaging was performed using a gamma camera (Toshiba GCA-9300A/hg) in planar mode equipped with a high-resolution parallel-hole collimator. Ninety minutes after the IV bolus injection of the [^{123}I]-labeled product in the lateral tail vein, the data were recorded on a 1024 x 1024 matrix (field of view: 23.5 x 12.5 cm) and with a photopeak window set at 15 % around 159 keV. Tracer uptake values in the tumour tissue, contralateral background tissue and front leg tissue were obtained from ROI analysis using a MRI maximum intensity projection as described before (8). The front leg tissue was used as background tissue for both tumour tissue (ratio tumour to background, RTB) and contralateral tissue (ratio contralateral to background, RCB). Moreover, it represents the general body tissue. The tracer uptake was expressed as the differential uptake ratio (DUR): $[(A/P)_{tissue}]/[(A/P)_{total\ body}]$ (A/P = activity per pixel, averaged over the ROI).

Three mice of each population were imaged with 3.7 (for the time intervals 1.5, 3 and 6 h post irradiation) or 9.3 MBq (for the time interval 18 hours post irradiation) [^{123}I]-iodo-L-phenylalanine. The tracer was injected 1.5 hours prior to imaging (Figure 5.1.1).

5.1.3.3.4. Statistical analysis.

Non-linear regression using GraphPad Prism 3.0 was applied to analyse the in vitro results. ANOVA at $\alpha = 0.05$ and boxplot graphical analysis were used for in vivo evaluation of the tracer, using SPSS 12.0. CI's given are the 95 % confidential intervals.

5.1.4 RESULTS

5.1.4.1. In vitro experiments.

The linear-quadratic cell-survival curve fitting ($SF = \exp[-(\alpha * D + \beta * D^2)]$) gave following parameters for our in vitro experiment, determined by non-linear regression using SPSS 12.0: $\alpha = 0.113$ (CI = 0.068 to 0.157) and $\beta = -0.001$ (CI = -0.003 to 0.000) ($R^2 = 0.949$).

Percentage of [^{125}I]-iodo-L-phenylalanine, and the control tracer ^{18}F-FDG, uptake per million remaining viable cells as a function of radiation dose revealed a sigmoidal curve ($R^2 = 0.996$) with higher specific tracer uptake values at higher doses (between 0 and 50 Gy). The uptake as a function of radiation dose for [^{125}I]-iodo-L-phenylalanine is shown in Figure 5.1.2. Statistical analysis resulted in the following data for [^{125}I]-iodo-L-phenylalanine and ^{18}F-FDG respectively: bottom values 0.06 (CI = 0.05 – 0.07) and 0.19 (CI = 0.16 – 0.23) %uptake/10^6 viable cells, top values 0.22 (CI = 0.21 – 0.23) and 0.34 (CI = 0.29 – 0.38) %uptake/10^6 viable cells, D50 values 10.22 (CI = 10.02 – 10.42) and 10.17 (CI = 9.21 – 11.14) Gy.

FIGURE 5.1.2: In vitro specific uptake of [^{125}I]-2-Iodo-L-phenylalanine in gamma irradiated remaining viable R1M rabdomyosarcoma cells as a function of radiation dose, 24 hours post irradiation: an initial first dose-range study up to 50 Gy.

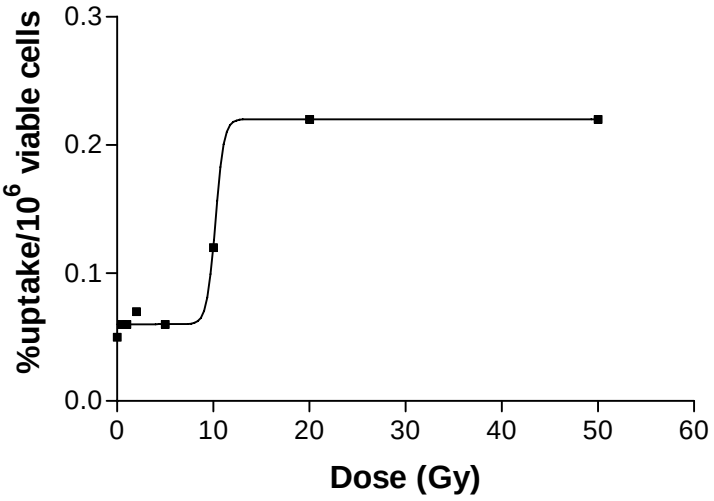

5.1.4.2. In vivo experiments.

The in vivo imaging results are presented in Table 5.1.1.

A 3-factor ANOVA analysis showed that the differential uptake ratio (DUR) was significantly dependent upon organ, experimental group and time interval between irradiation and imaging. The tracer uptake in the tumour tissue differed significantly ($p = 0.003$) from the contralateral tissue and the front leg.

TABLE 5.1.1: In vivo imaging results with [^{123}I]-2-iodo-L-phenylalanine at various time intervals post irradiation. (1) The values of all time-points were taken together. Tissue results are expressed as DUR-values (mean ± st. dev.; n = 3), while RCB and RTB are ratios having no units.

Organ	Tumour irradiated group				Contralateral irradiated group				Control group
	1.5 h	3 h	6 h	18 h	1.5 h	3 h	6 h	18 h	All (1)
Tumour tissue (=T)	1.15 ±0.20	0.96 ±0.15	0.88 ±0.03	0.85 ±0.10	1.27 ±0.15	1.17 ±0.29	1.13 ±0.29	1.06 ±0.13	1.41 ±0.10
Contralateral tissue (=C)	0.61 ±0.06	0.58 ±0.03	0.56 ±0.08	0.59 ±0.07	0.57 ±0.05	0.55 ±0.07	0.64 ±0.05	0.57 ±0.09	0.62 ±0.11
Front leg tissue (=B)	0.64 ±0.14	0.53 ±0.03	0.59 ±0.11	0.70 ±0.09	0.63 ±0.11	0.57 ±0.05	0.69 ±0.12	0.61 ±0.06	0.62 ±0.07
RCB	0.95 ±0.36	1.09 ±0.08	0.95 ±0.22	0.84 ±0.15	0.90 ±0.18	0.96 ±0.14	0.93 ±0.18	0.93 ±0.17	1.00 ±0.21
RTB	2.19 ±0.19	1.83 ±0.35	1.51 ±0.23	1.22 ±0.17	2.04 ±0.18	2.05 ±0.35	2.05 ±0.36	1.73 ±0.09	2.28 ±0.25

For the front leg tissue (= background tissue in this study), no significant effect for the experimental group ($p = 0.268$) or for the time interval ($p = 0.632$) was observed.

Furthermore, no significant differences in uptake were observed for the contralateral tissue between the 3 experimental groups ($p = 0.396$) and the different time points ($p = 0.923$) (Figure 5.1.3). Irradiation of the contralateral tissue did not alter the [^{123}I]-iodo-L-phenylalanine tracer uptake at equilibrium.

Furthermore, no significant (at $\alpha = 0.05$) difference was demonstrated between the contralateral tissue and the front leg tissue, neither between the experimental groups nor between the time intervals post irradiation. This is also indicated by the RCB ratio results.

Graphical representation of this multiple means comparison was performed by clustered box-plots, where the front leg tissue was not included seen its similarity with the contralateral tissue (Figure 5.1.3). The first 3 box-plots of each time-cluster represent the contralateral tissue DUR results for the 3 treatment groups. The last 3 box-plots of each cluster are the tumour DUR values.

FIGURE 5.1.3: Clustered boxplots for the evaluation of the contralateral tissue and the tumour tissue.

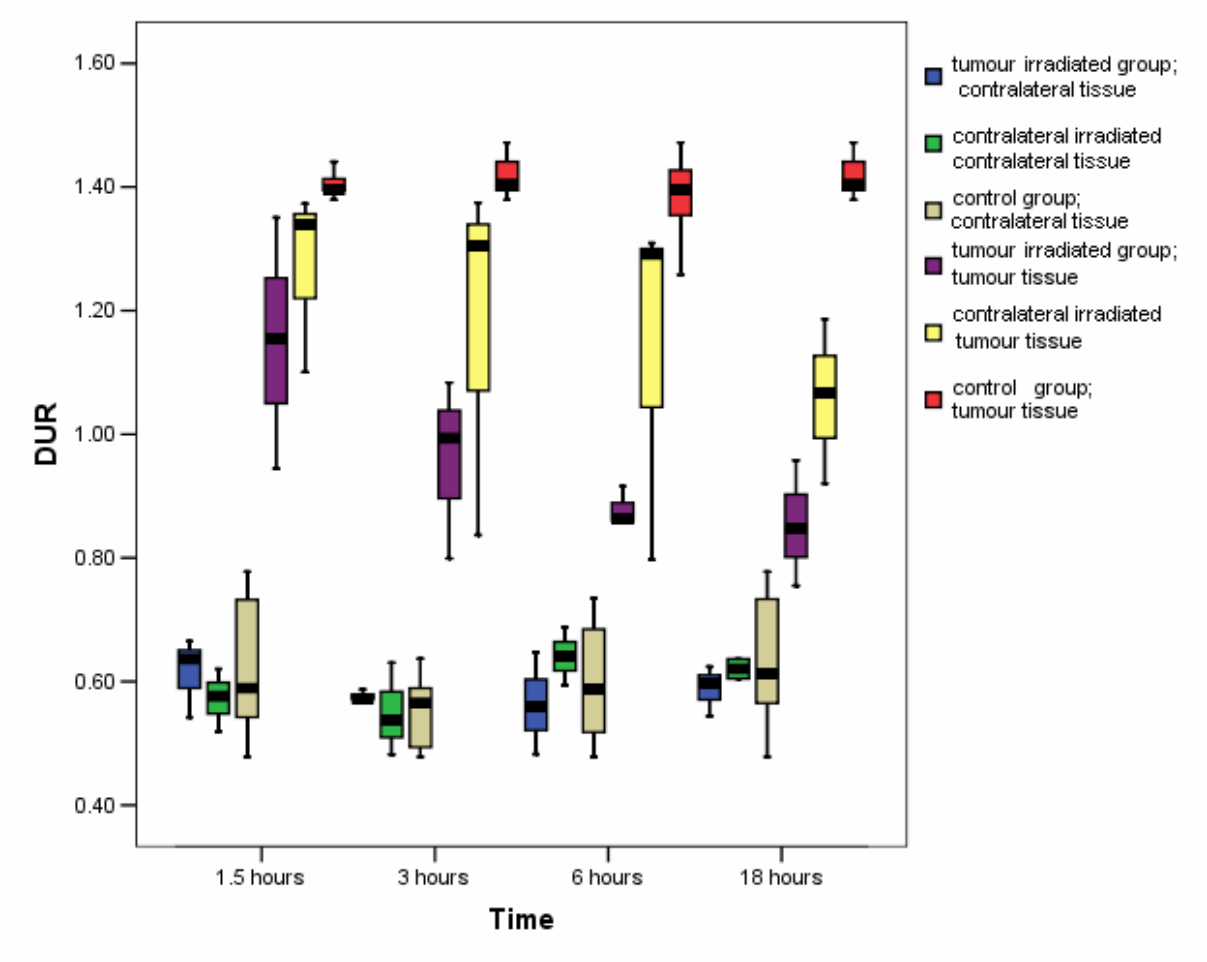

The uptake in the tumour tissue did show highly significant differences between the experimental groups ($p < 0.001$) and the interval times ($p = 0.020$). The tumour tissue of the control group differed significantly ($p < 0.001$) in their uptake from those of the contralateral irradiated group at 18 hours post irradiation - although no significant difference was detected for time intervals up to 6 hours post irradiation (Figure 5.1.3).

Besides the DUR evaluation of the individual organs, the combinations RTB (ratio tumour background) and RCB (ratio contralateral tissue to background) were investigated. The results are graphically represented by clustered box plots in Figure 5.1.4. The first 3 box-plots in each cluster represents the RTB values, while the last 3 box-plots are the RCB results. As expected, the RCB results are situated around a value of 1.0, with no time-trend nor difference between the 3 experimental groups observed. In contrast to the RCB results, RTB demonstrated a significant difference between the experimental groups ($p < 0.001$) and the interval times ($p = 0.001$) and post-hoc analysis (Tukey) revealed that all experimental groups, relative to each other, showed statistically significant differences (all $p < 0.033$).

FIGURE 5.1.4: Statistical analysis by clustered boxplot for the evaluation of RTB and RIB.

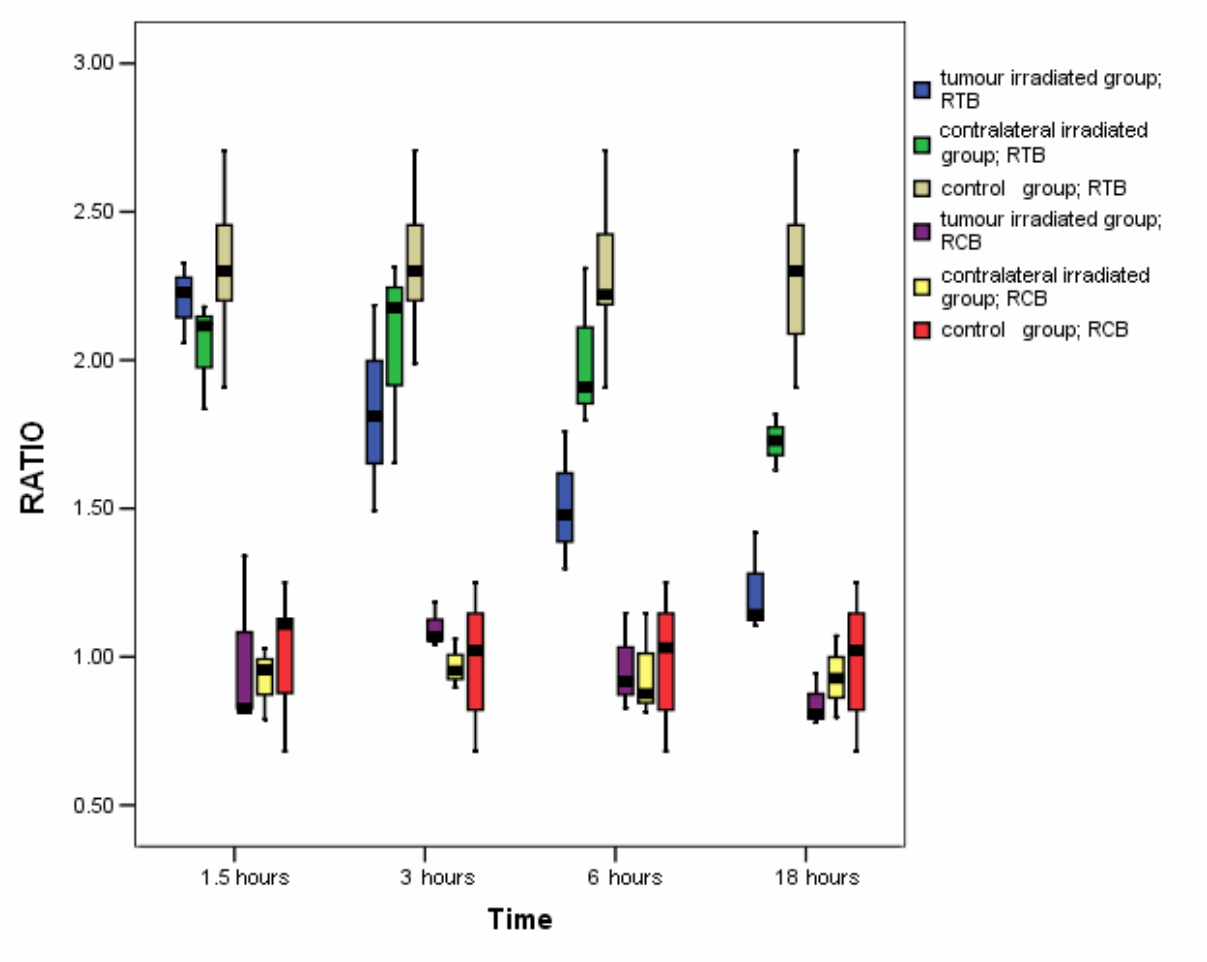

5.1.5. DISCUSSION

Former reports described the promising characteristics of [^{123}I]-2-iodo-L-phenylalanine as tumour detecting agent for SPECT (9,10,14). However, during the process of curing cancer, there are a lot of other aspects to deal with. Important is radiotherapy evaluation: the sooner the clinician could tell whether or not a patient is responding to therapy, the sooner it could be adjusted and valuable time will be spared. It is in this aspect that we evaluated [^{123}I]-2-iodo-L-phenylalanine as a radiotherapy response tool.

The in vitro uptake of both the [^{123}I]-2-iodo-L-phenylalanine tracer and the control tracer [^{18}F]-FDG in remaining viable R1M cells as a function of radiation dose described a sigmoidal curve. These observations could have important implications for in vivo residual tumour imaging: although as expected, fewer cells survive at higher radiation dose, the radiation-surviving remaining viable cells accumulated the tracer in larger amounts. The latter might be due to cell recovering after irradiation which not only requires energy but also building blocks e.g. for protein synthesis. The same D50 was observed for the uptake of both tracers, which could be an indication of the reproducibility of the radiosensitivity of the cell.

The promising in vitro results led us to the in vivo evaluation of this amino acid analogue as a therapy response tool. Evaluation of the DUR data showed that the front leg

tissue could be used as background representing general body tissue where neither tumour nor radiation was induced.

Analysing the contralateral tissue demonstrated that radiation-induced inflammation (because of the high 10 Gy irradiation dose) of the tissue did not alter the [^{123}I]-iodo-L-phenylalanine tracer uptake at equilibrium. This has two alternative explanations: (1) no radiation induced inflammation occurred during the measured time interval, or (2) the uptake of [^{123}I]-iodo-L-phenylalanine was specific for the presence of the tumour. It is very unlikely that the radiation dose (10 Gy) did not induce inflammation.

In contrast to the two former tissues, the tumour tissue did show highly significant effects and at 18 hours post irradiation, the tumour tissue from the control group differed significantly from the tumour tissue of the contralateral irradiated group. The latter could be explained by a general hemodynamic, systemic effect of the radiotherapy under the applied experimental conditions.

Moreover, very important results were derived from the boxplot and the post-hoc ANOVA analyses from RTB and RCB concerning radiotherapy evaluation. Indeed, this evaluation demonstrated individual differences, and not just sample-population differences, between the experimental groups for RTB. The results indicate that there is an optimal time-point for post-irradiation evaluation where a clear cut-off could differentiate between good tumour responders from not-responders: for example, a cut-off for RTB of 1.5 at 18 hours post irradiation (Figure 5.1.4). This will have important implications concerning patient care assuming similar interspecies (mice-human) behaviour and awaiting further clinical evaluation including protocol optimisation: at a relatively short post-irradiation time, the RTB of [^{123}I]-iodo-L-phenylalanine will be able to predict which patients respond or do not respond to radiation therapy, and hence, valuable time can be spared. However, further experiments with various tumour models as well as clinical trials have to be performed in future in order to extrapolate and generalize these results.

5.1.6. CONCLUSIONS

The in vitro as well as the in vivo radiotherapy experiments performed in this study showed promising results concerning therapy evaluation. In vitro testing indicated that although fewer cells survive at high radiation doses, the remaining viable cells accumulated the tracer in higher amounts which could be beneficial for detecting residual tumour lesions. Although the current results should be interpreted with utmost care, in vivo evaluation confirmed that [^{123}I]-iodo-L-phenylalanine was able to detect metabolic changes due to irradiation, even at very short time intervals. The latter observation is very important: within 24 hours post-radiation therapy, clinicians would be able to discover whether or not the tumour in a patient is sensitive to radiotherapy and valuable time could be spared. Another important result was the tumour tissue specific uptake of this phenylalanine analogue since no uptake in the irradiated contralateral background tissue was observed. The obtained results opens perspectives which should be investigated more extensively in the future to establish a time-point post-irradiation where the differences are maximal and to compare this tracer with other tracers like ^{18}F-FDG to find out whether and under what conditions our new tracer is better or not.

5.1.7 REFERENCES

1. Del Sole A, Falini A, Ravasi L, et al. Anatomical and biochemical investigation of primary brain tumours. *Eur J Nucl Med.* 2001;28:1851–1872.
2. Dooms GC, Hecht S, Brant-Zawadzki M, Berthiaume Y, Norman D, Newton TH. Brain radiation lesions: MR imaging. *Radiology.* 1986;158:149 –155.
3. Mikhael MA. Radiation necrosis of the brain: correlation between computed tomography, pathology, and dose distribution. *J Comput Assist Tomogr.* 1978;2:71–80.
4. Chao ST, Suh JH, Raja S, Lee SY, Barnett G. The sensitivity and specificity of FDG PET in distinguishing recurrent brain tumor from radionecrosis in patients treated with stereotactic radiosurgery. *Int J Cancer.* 2001;96:191–197.
5. Kahn D, Follett KA, Bushnell DL, et al. Diagnosis of recurrent brain tumor: value of 201Tl SPECT vs 18F-fluorodeoxyglucose PET. *AJR.* 1994;163:1459 –1465.
6. Ricci PE, Karis JP, Heiserman JE, Fram EK, Bice AN, Drayer BP. Differentiating recurrent tumor from radiation necrosis: time for re-evaluation of positron emission tomography? *AJNR.* 1998;19:407– 413.
7. Thompson TP, Lunsford LD, Kondziolka D. Distinguishing recurrent tumor and radiation necrosis with positron emission tomography versus stereotactic biopsy. *Stereotact Funct Neurosurg.* 1999;73:9 –14.
8. Kersemans V, Cornelissen B, Kersemans K, et al. In vivo characterisation of 2-iodo-L-phenylalanine in a R1M rabdomyosarcoma mouse model as a potential tumor tracer for SPECT. *J Nucl Med* 2005;46:532-539.
9. Kersemans V, Cornelissen B, Kersemans K, et al. Detection of Various Tumour types in Athymic mice using [^{123}I]-2-iodo-L-phenylalanine Planar SPECT. *Eur J Nucl Med Mol Imaging*,2004:31(S2),S380 (meeting abstract).
10. Mertens J, Kersemans V, Bauwens M, et al. Synthesis, radiosynthesis, and *in vitro* characterization of [125I]-2-iodo-L-phenylalanine in a R1M rhabdomyosarcoma cell model as a new potential tumor tracer for SPECT. *Nucl Med Biol* 2004;31:739-746.
11. Deichen JT, Schmidt C, Prante O, et al. Influence of TSH on uptake of [18F]fluorodeoxyglucose in human thyroid cells in vitro. *Eur J Nucl Med Mol Imaging* 2004;31:507–512.
12. Maschauer S, Prante O, Hoffmann M, et al. Characterization of 18F-FDG Uptake in Human Endothelial Cells In Vitro. *J Nucl Med* 2004; 45:455–460.
13. Lahoutte T, Mertens J, Caveliers V, et al. Comparative biodistribution of iodinated amino acids in rats: selection of the optimal analog for oncologic imaging outside the brain. *J Nucl Med.* 2003;44:1489–1494.
14. Kersemans V, Cornelissen B, Kersemans K, et al. In vivo characterisation of 2-iodo-L-phenylalanine in a R1M rabdomyosarcoma mouse model as a potential tumor tracer for SPECT. *J Nucl Med* 2005;46:532-539.

5.2 The use of [^{123}I]-2-iodo-L-phenylalanine in two dogs with synovial cell sarcoma of the tarsus.

Veerle Kersemans, MSc[1*]; Kathelijne Peremans, PhD[2**]; Bart Cornelissen, PhD[1]; Bart De Spiegeleer, PhD[1]; John Mertens, PhD[3] and Guido Slegers, PhD[1].

1 Laboratory for Radiopharmacy, Universiteit Gent, Belgium
2 Department for Medical Imaging of Pets, Universiteit Gent, Belgium
3 Medical Imaging and Physics, Vrije Universiteit Brussel, Belgium

Key words : [^{123}I]-iodo-L-phenylalanine, SPECT, synovial carcinoma, tumour diagnosticum, dogs.

Submitted for Veterinary radiology and ultrasound

5.2.1. ABSTRACT

Objectives. To date, many owners are prepared to give their pets the maximal care, including radiation and chemotherapy. As a consequence, it is important to develop non-invasive and high specific tumour diagnostics for veterinary practice which will help the veterinarian to diagnose the primary lesion. Our research group developed [^{123}I]-iodo-L-phenylalanine which was successfully evaluated in vivo in tumour bearing athymic mice: high and specific tumour accumulation was observed. In this aspect, the latter tracer was used to diagnose synovial cell carcinoma of the tarsus in dogs. **Methods**. [^{123}I]-iodo-L-phenylalanine was quantitatively prepared as a Kit formulation using the Cu^{1+} assisted nucleophilic exchange. Dynamic, static and whole body planar imaging was performed with [^{123}I]-iodo-L-phenylalanine in two dogs bearing a synovial cell carcinoma of the tarsus. The results were expressed as ratio tumour to contralateral background. **Results**. Fast and high [^{123}I]-2-iodo-L-phenylalanine tumour accumulation was observed. Whole body imaging revealed the renal clearance of the tracer. **Conclusions**. [^{123}I]-2-iodo-L-phenylalanine shows good tumor to background contrast in two dogs with synovial cell carcinoma. It is a promising alternative tracer for use in veterinary application to overcome the known limitations of ^{18}F-FDG.

5.2.2. INTRODUCTION

Nuclear oncology is a fast growing discipline within the medical imaging field and many radiopharmaceuticals are developed to diagnose cancerous lesions.

These fast improvements in nuclear oncology are not only important to diagnose tumours in humans but also in pets. Indeed, many owners are prepared to give their pets the maximal care, including radiation and chemotherapy. As a consequence, it is important to develop non-invasive and high specific tumour diagnostics for veterinary practice which will

help the veterinarian to diagnose the primary lesion, to predict therapy outcome and to evaluate therapy response. Moreover, nuclear imaging allows performing whole body acquisitions to locate metastases. Up to today, no "general" tumour diagnosticum with high tumour specificity has been established and clinicians are obliged to use ^{18}F-labelled fluorodeoxyglucose (^{18}F-FDG) despite its well-known limitations: high uptake in normal brain tissue, accumulation in inflamed and other granulomatous tissues and glucose metabolism is not upregulated in all tumours (1). Positron emission tomography (PET) tracers are rarely used in veterinary practice. To present an alternative for PET, several amino acid analogues for Single Photon Emission Tomography (SPECT) are developed, based on the high metabolic requirements of the tumour cells and the overexpression of type A or L amino acid transport systems in tumour cells. Up to today, [^{123}I]-L-3-iodo-α-methyltyrosine (IMT) is the only routinely used amino acid tumour tracer for SPECT. Although it was successful for brain tumours, the abdominal use is limited due to its long-term renal accumulation. [^{123}I]-2-iodo-L-phenylalanine, our new amino acid analogue showed the appropriate properties in vivo in tumour bearing mice and rats of a promising tumour specific SPECT tracer. We decided to evaluate this tracer for the diagnosis of synovial cell carcinoma (SCC) in dogs using dynamic, static and whole body planar imaging.

5.2.3. MATERIALS AND METHODS

All the conventional products mentioned were at least of analytical or clinical grade and obtained from Sigma-Aldrich. The solvents were of HPLC quality (Chemlab, Belgium).
All in vivo studies were carried out in accordance with the Belgian legislation including the approval of the study protocol by the ethical committee for animal studies of the University of Gent. Guidelines of the National Institute of Health principles of laboratory animal care were followed.

5.2.3.1. Radiochemistry

Radioiodination with $^{123}I^-$ (222 MBq; n.c.a., 10 – 20 µl) (Nordion Europe, Belgium) on 1.0 mg 2-I-L-phenylalanine was performed by Cu^{1+}-assisted isotopic exchange under acidic and reducing conditions as described before (2). The reaction mixture was drawn up in a syringe containing the appropriate amount of "make-up solution" (Tri-sodium Citrate dihydrate, 71 mM) to render the solution isotonic and to adjust the pH to at least 4. The reaction mixture was filtered by 0.22 µm Ag-filter (Millipore, Belgium) to remove free $^{123}I^-$ and by a sterile 0.22 µm filter (Millipore, Belgium) for sterilisation into a sterile vacuum vial. Quality control was achieved by RP-HPLC and Sep-pak C18 (Waters, Belgium). Chiral chromatography was used to verify the chiral purity.

5.2.3.2. Animals

Two dogs were included, one Golden Retriever, male, 9 years old and one Flatcoated retriever, neutered female, 9 years old. Both animals had a palpable mass at the level of the left tarsal joint. This mass was identified as a synovial sarcoma by histology.

5.2.3.3. Anesthesia protocol

Imaging was performed under general anaesthesia. Sedation was obtained with 10–30 µg/kg medetomidine hydrochloride intramuscular (Domitor, Pfizer, Belgium). General anaesthesia was induced with 2–3 mg/kg isopropylphenol intravenously (IV) (Rapinovet, Mallinckrodt, Belgium) and maintained with isoflurane (Isoflo, Abbott animal health, UK).

5.2.3.4. Scanning protocol

Imaging was performed using a gamma camera (Single head Toshiba GCA 901) in planar mode equipped with a low energy high-resolution parallel-hole collimator. All static and dynamic planar images were acquired into a 256 x 256 matrix (FOV: 41 x 41 cm) and with a photopeak window set at 15 % around 159 keV. Whole body imaging was performed into a 128 x 512 matrix (FOV: 41 x 164 cm).

Dynamic planar imaging consisting of 21 frames (20 x 6 sec and 1 x 4 min) immediately after tracer injection (4.2 MBq/kg) was used for the first tumour bearing dog to determine the time point for static imaging. Subsequently, a static image of 3 min was recorded, twenty minutes after intravenous injection of [^{123}I]-2-iodo-L-phenylalanine. In the second dog only one static image of 3 min, 20 min p.i., was used to visualize the tumour with [^{123}I]-2-iodo-L-phenylalanine (7.9 MBq/kg) to reduce the duration of sedation. The tracer dose was elevated for the second dog in order to improve imaging. Tracer uptake values in the tumour and the contralateral site to the tumour were obtained from ROI analysis and the ratio tumour to background (RTB) was calculated. Additionally, whole body imaging (image duration = 15 min) was performed immediately after static imaging to observe the general biodistribution of the tracer.

5.2.4. RESULTS

A dorsal view of the two animals is shown in figure 5.2.1.

FIGURE 5.2.1: Uptake of [^{123}I]-2-iodo-L-phenylalanine in two dogs bearing a synovial sarcoma at the tarsus (dorsal view).

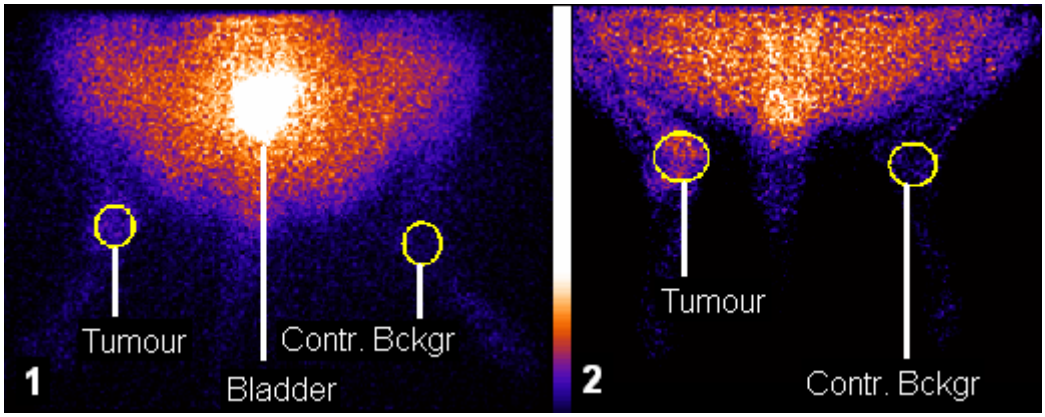

Dynamic planar imaging of the first dog demonstrated fast and high [^{123}I]-2-iodo-L-phenylalanine tumour accumulation since the equilibrium for RTB was reached within the first frame (RTB at equilibrium = 2.11 stdev. 0.43; n = 19) (Figure 5.2.2). Static tumour imaging of the second dog confirmed the high RTB observed in the first dog: a ratio of 1.84 was obtained in the second dog.

FIGURE 5.2.2: RTB values in animal 1 for [^{123}I]-2-iodo-L-phenylalanine

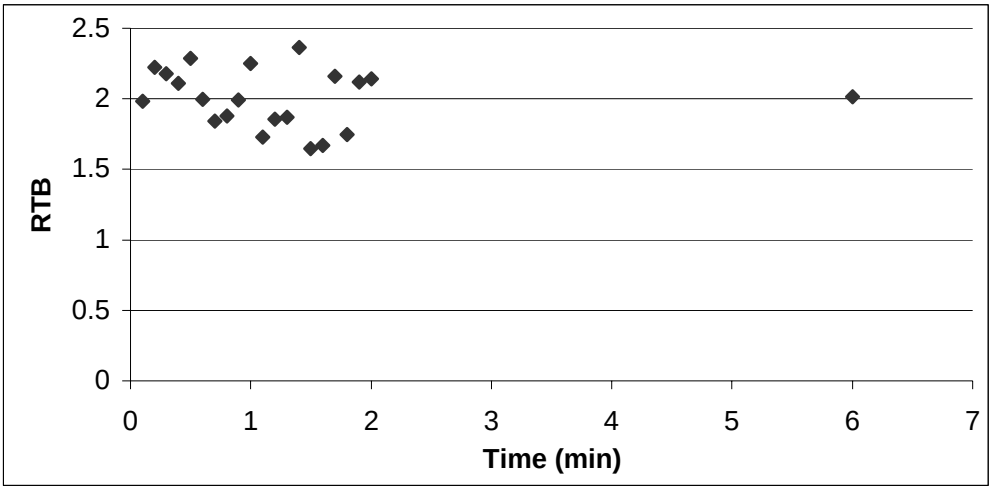

Whole body imaging, as shown in figure 5.2.3, demonstrated a renal clearance of the tracer: bladder accumulation was observed besides kidney accumulation whereas no liver activity was detected. Moreover, the tumour was clearly visible.

FIGURE 5.2.3: Whole body imaging with [^{123}I]-2-iodo-L-phenylalanine (dog was positioned at his left and right lateral side).

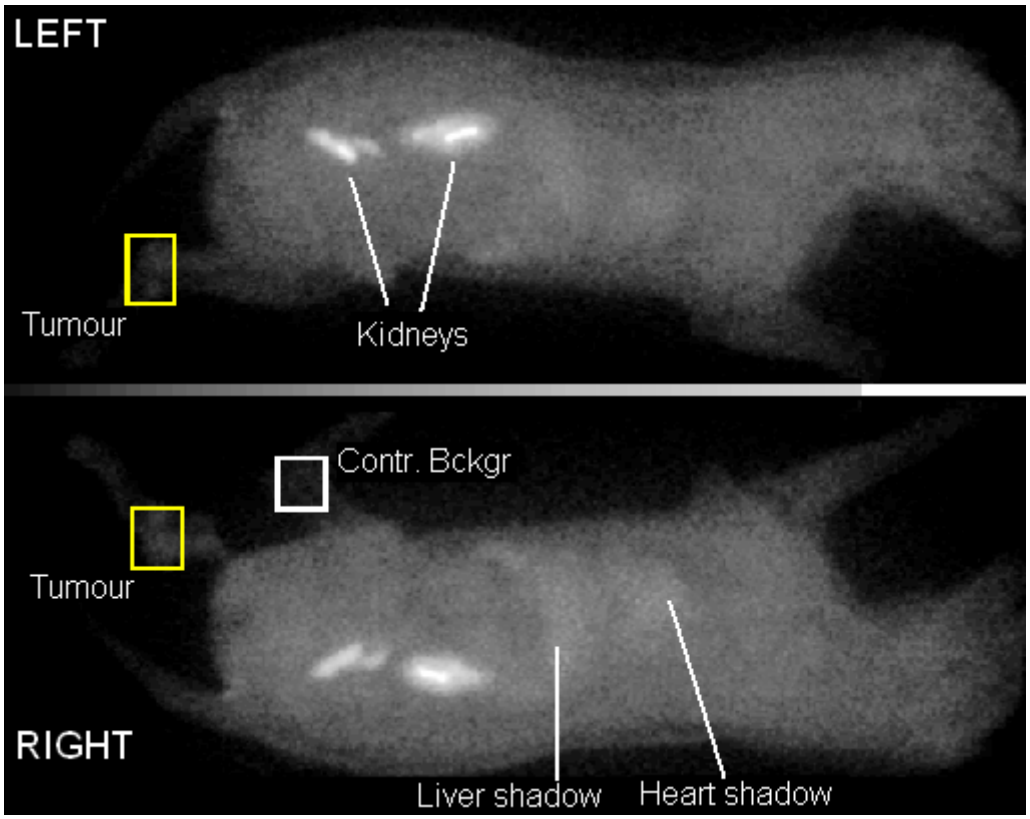

5.2.5. DISCUSSION

[^{123}I]-2-iodo-L-phenylalanine has been shown to exhibit a tumour cell specific uptake in lesions through the LAT amino acid transporter system. This means, it demonstrates no or little build-up in inflammatory regions. Moreover a rapid elimination from the blood compartment to the bladder was noticed (2). For these reasons, we decided to explore the possibilities of this tracer for use in the detection of synovial sarcomas in dogs

Our studies showed that the tumour lesions could be visualised with high contrast. The observed fast uptake in the lesion is in accordance with previously reported results on the fast kinetics of this tracer in mice (2).

The observed fast uptake in the lesion is in concordance with previously reported results on the fast kinetics of this tracer in mice (2,3). Additionally, already after 20 minutes high bladder accumulation was observed indicating that tracer clearance from the blood was very fast. The activity in the kidneys is most probably a transient effect due to the fast elimination of the tracer through the kidneys to the bladder. The latter observation is very important relating to the radiation burden: an accumulation of [^{123}I]-2-iodo-L-phenylalanine in the kidneys will result in high effective radiation doses. The latter was disproved by the dosimetric calculations as a worse case effective dose of 0.0375 mSv/MBq was obtained when extrapolating the mice results to human.

Whole body imaging confirmed the presence of the tumour. Moreover, a heart-shadow and liver-shadow were faintly shown due to the high blood perfusion of these organs. Biodistribution studies in mice demonstrated that the liver and biliary tract was not involved in the clearance of the tracer. Both kidneys showed a flow out to the bladder as illustrated by the kidney-shadow.

Although the use of iodine-123 implies a high cost and thus economical limitations, the application of radioiodinated amino acids possesses many advantages over PET radiopharmaceuticals. For instance: neither specialized infrastructure nor an on site cyclotron is needed and more detailed scanning procedures could be performed due to the longer physical half life of the tracer. Moreover, [^{123}I]-2-iodo-L-phenylalanine can be prepared as a Kit formulation without a cumbersome purification procedure which is a benifit for clinical use.

5.2.6. CONCLUSION

[^{123}I]-2-iodo-L-phenylalanine shows good tumour to background contrast in two dogs with sinovial cell carcinoma. It is a promising alternative tracer for veterinarian tumour detection, to overcome the known limitations of ^{18}F-FDG.

5.2.7. REFERENCES

1. Jager PL, Vaalburg W, Pruim J, et al. Radiolabelled amino acids: basic aspects and clinical applications in oncology. *J Nucl Med*. 2001;42:432–445.
2. Kersemans V, Cornelissen B, Kersemans K, et al. In Vivo Characterization of 123/125I-2-iodo-LPhenylalanine in an R1M Rhabdomyosarcoma Athymic Mouse Model as a Potential Tumour Tracer for SPECT. *J Nucl Med* 2005;46:532-539.
3. Kersemans V, Cornelissen B, Kersemans K, et al. Detection of Various Tumour types in Athymic mice using [^{123}I]-2-iodo-L-phenylalanine Planar SPECT. European Journal for Nuclear Medicine and Molecular Imaging, 2004: 31(S2), S380 (meeting abstract).

CHAPTER CONCLUSIONS

An important factor in curing patients from cancer is radiotherapy evaluation: the sooner the clinician could tell whether or not a patient is responding to therapy, the sooner it could be adjusted and valuable time will be spared. It is in this aspect that we evaluated [^{123}I]-2-iodo-L-phenylalanine as a radiotherapy response tool.

The in vitro as well as the in vivo radiotherapy experiments performed in this report showed promising results concerning therapy evaluation. In vitro testing indicated that although fewer cells survive at high radiation doses, the still viable cells accumulated the tracer in higher amounts which could be beneficial for detecting residual tumour lesions. Although the results should be interpreted with utmost care because of the slight differences in tumour uptake between the tumour and the inflammation group, in vivo evaluation confirmed that [^{123}I]-iodo-L-phenylalanine was able to detect metabolic changes due to irradiation, even at very short time intervals. The latter observation is very important: within 24 hours post therapy, clinicians would be able to discover whether or not to tumor is susceptible to radiotherapy and value time could be spared. However, these results should be investigated more extensively in the future and a comparison with ^{18}F-FDG is necessary to illustrate whether our new tracer is superior.

To stipulate the possible use of [^{123}I]-2-iodo-L-phenylalanine as a tumour detecting agent for dynamic planar imaging, the application of the new tracer was evaluated for the diagnosis of cancer in dogs. A case report study described the use of [^{123}I]-2-iodo-L-phenylalanine as diagnostic tool for the detection of synovial cell sarcoma of the tarsus in two dogs. Both dogs confirmed the results obtained in the mice studies: high and fast tumour accumulation with fast renal clearance of the tracer. This implicates that a fast examination and interpretation of the results is possible, leading to fast decisions and minor inconvenience for the pet owners.

General Conclusions and Future Perspectives.

To conclude this work, we briefly summarize the major results and highlight some future research perspectives.

The goal of chapter 2 was the development and evaluation of [$^{123/125}$I]-2-iodo-L-phenylalanine as a tumour tracer for SPECT. In this respect, we succeeded to develop a highly specific tumour tracer. Not only the straightforward 1-step precursor synthesis which resulted in high yields without the formation of side products, but also the fast and quantitative Kit preparation of [$^{123/125}$I]-2-iodo-L-phenylalanine will result in a great added value for everyday clinical practice. Moreover, in vivo evaluation of the new tracer demonstrated a high metabolic stability, high and specific tumour uptake and a fast blood clearance through the renal system. These characteristics make the tracer suitable for clinical practice. Indeed, not only oncologic brain imaging but also peripheral tumour detection is possible. Moreover, all the tumours could be visualized using dynamic planar imaging and thus no false negative results were observed. However, more research is necessary to form an idea about the overall sensitivity of the tracer. Indeed, in comparison to ^{18}F-FDG a strong decline in false positive results is expected but this was experimentally not investigated. The latter was due to the fact that all imaging experiments were performed using tumour bearing mice.

Chapter 5 highlights a few applications of the newly developed tumour tracer. Besides human applications, [^{123}I]-2-iodo-L-phenylalanine could also be used in veterinary clinical practice. Not only the detection of the primary lesion is possible but also whole body imaging which could be used to detect metastases. Another, very important aspect is radiotherapy evaluation applying [^{123}I]-2-iodo-L-phenylalanine as diagnosticum. Although future experiments are needed to confirm these initial results and to elucidate the observed processes, the new tracer was able to differentiate between radiotherapy responders and non-responders already 18 hours post irradiation. The latter is very important because so far, no single tracer could detect inter-individual differences between patients. It would be an enormous step forward in handling cancer patients. In this respect, it is my sincerest wish that this part of the present work may form the basis for further research.

Besides the evaluation of the L-isomer, [$^{123/125}$I]-2-iodo-D-phenylalanine was also developed because of its unnatural character. Concerning the short time kinetics, very few differences were observed between both isomeric phenylalanine analogues: they both showed high and specific tumour accumulation and a renal clearance. However, the D-analogue demonstrated a faster blood clearance and a faster uptake in the peripheral compartment as compared to [^{123}I]-2-iodo-L-phenylalanine. These results were generalized in different tumour types corresponding to tumour families with a high prevalence in humans. Although dynamic planar imaging showed no difference between the two isomers, dissection revealed much higher RTB for [^{123}I]-2-iodo-L-phenylalanine in the R1M model.

Another aspect is the long term biodistribution of both tracers. Planar imaging revealed a longer retention for the [^{123}I]-2-iodo-L-phenylalanine as compared to [^{123}I]-2-iodo-D-phenylalanine but the latter demonstrated an increase in tumor contrast in contradiction to the former.

The evaluation of both [^{123}I]-2-iodo-L-phenylalanine and [^{123}I]-2-iodo-D-phenylalanine in various tumour types allowed us to choose one amino acid analogue for future clinical application. Taking all the results, from in vitro to in vivo evaluation and from

evaluation in R1M and several other tumour types, I propose the D-amino acid analogue [^{123}I]-2-iodo-D-phenylalanine for further clinical evaluation. Indeed, in vitro testing revealed that the latter amino acid is most probably transported by only the LAT1 transporter system whereas [^{123}I]-2-iodo-L-phenylalanine is also transported by the LAT2 system. This implicates that [^{123}I]-2-iodo-D-phenylalanine uptake is restricted to highly proliferating tissues like the tumour but that [^{123}I]-2-iodo-L-phenylalanine will also be taken up in minor amounts by the normal tissues. Regarding the in vivo results, the arguments for choosing the D-analogue are not abundant due to their similar behaviour. However, taking into account (1) that imaging with amino acids in patients is performed within half an hour to three hours post injection, (2) the better short time kinetics for [^{123}I]-2-iodo-D-phenylalanine, (3) that [^{123}I]-2-iodo-D-phenylalanine demonstrated less dehalogenation 90 min p.i. and (4) the same RTB values for both analogues in various tumour types concerning planar imaging, one can select [^{123}I]-2-iodo-D-phenylalanine for further clinical evaluation.

At last, I will look forward to the application of both phenylalanine analogues as radionuclide therapy tools which could be an interesting field for further research. Our results demonstrate not only the capability of 2-iodo-D-phenylalanine as a tumour detecting agent by SPECT but also that this amino acid analogue opens perspectives as a radiotherapeutic agent. Indeed, meta-iodobenzylguanidine (MIBG), which showed only a tumour uptake of 2 % of the ID, has become an effective anti-neuroblastoma agent, besides its diagnostic tumour imaging application. Apart from its tumour-targeting properties, our new tracer 2-iodo-D-phenylalanine is metabolically stable but shows lower liver uptake and accumulation than MIBG and is rapidly cleared from the circulation via the kidneys, being an ideal starting point for systemic radiotherapy.

Summary.

At present, there is no single test that can accurately diagnose cancer. The complete evaluation of a patient usually requires a detailed history and physical examination along with diagnostic testing. In this aspect, medical imaging has become vital in the early detection and diagnosis of cancer: it can allow treatment of cancer before it spreads to other parts of the body and it can help to minimize the need for massive therapeutic treatment which reduces pain and suffering.

During the last decade, nuclear oncology has improved fast and several imaging strategies were developed to image cancerous lesions. A wide spectrum of molecules has been proposed to target cell types and tumour groups but their use is often limited to a restricted group of tumour types or their clinical role remains unclear.

In the search for a "universal" tracer, able to image the majority of tumour types, ^{18}F-FDG looked suitable, based on the increased metabolic activity of tumour cells. This tracer is widely used for staging of tumours, diagnosing recurrent lesions, evaluating therapy and its response. Although the average ^{18}F-FDG PET sensitivity and specificity across all oncology applications are high (estimated at 84% and 88%, respectively), ^{18}F-FDG imaging is hindered by its high brain uptake and non-specific accumulation in inflammation and granulomatous tissues. Moreover, not all cancers show an elevated glucose metabolism.

Based on another aspect of the increased metabolic activity in tumoural lesions, several radiolabelled amino acid analogues were developed. At the moment, IMT is the only routinely used tracer for SPECT. Despite to its ability to visualize brain and extracranial tumours, this tracer is still inferior to ^{18}F-FDG and its high kidney accumulation hampers the abdominal imaging of tumours. Another SPECT tumour tracer, recently evaluated by Samnick et al, is [^{123}I]-4-iodo-L-phenylalanine. Although this tracer could overcome both the limitations of ^{18}F-FDG and IMT, it showed a high bloodpool activity.

Our research group focussed on the synthesis and evaluation of [^{123}I]-2-iodo-L-phenylalanine. A substitution of the iodine-atom at the 2 position was chosen, allowing the 4 position to be free for enzymatic interaction. Moreover, [^{123}I]-2-iodo-L-phenylalanine was developed as an alternative SPECT tumour tracer to 4-iodo-L-Phenylalanine, 2-iodo-L-tyrosine and IMT to overcome the high bloodpool and inflammation activity, the difficult precursor synthesis or sourcing and the marked long term renal accumulation, respectively.

As described in chapter 2, the precursor 2-iodo-L-phenylalanine was synthesized from its bromo-derivative 2-bromo-L-phenylalanine using the Cu^{1+}-assisted nucleophilic exchange in acidic and reducing conditions. An experimental design allowed us to determine the optimal reaction conditions resulting in a yield of at least 60% without the formation of undesired side products or stereoisomers and with an easy purification procedure. A Kit-formulation based on the same principle allowed fast and quantitative routine radioiodination of 2-iodo-L-phenylalanine without the need for extra purification which is a great added value for everyday clinical practice.

In order to find out whether the new tracer [$^{123/125}$I]-iodo-L-phenylalanine could overcome the limitations expressed by 4-iodo-L-phenylalanine and IMT, the tracer was evaluated in vitro and in vivo in a R1M cell and athymic mouse model, respectively.

The in vitro studies in the R1M cell model illustrated that, although a bulky iodine atom was incorporated at the 2 position of the molecule, 2-iodo-L-phenylalanine is still transported by the L-amino acid transporter subtype 1 (LAT1). Moreover, the new amino acid analogue illustrated almost the same affinity for this transporter system as compared to the

native L-phenylalanine and L-tyrosine (K_m L-phenylalanine = 55 µM, K_m L-tyrosine = 39 µM, K_m 2-iodo-L-phenylalanine = 46 µM). Inhibition experiments and RT-PCR studies showed that 2-iodo-L-phenylalanine is transported for the largest part by LAT1. Indeed, there is no significant difference between the uptake patterns of [^{125}I]-2-iodo-L-phenylalanine in $HEPES^+$ and $HEPES^-$ and stimulated net-efflux in presence of 5 mM L-phenylalanine or 5 mM BCH amounted to about 80% of the initial uptake whereas in absence of amino acids, leaking was limited to approximately 10%. Additionally, 2-iodo-L-phenylalanine is not incorporated into the cell proteins and LAT1 coupled influx of radioactivity is directly related to the requirement of amino acids for protein synthesis or cell metabolism. Thus, even not incorporated, 2-iodo-L-phenylalanine uptake reflected the total "amino acid turn-over" of the tumour cells.

The latter characteristics were promising allowing and requiring in vivo evaluation. At the University of Ghent, a R1M athymic mouse model was chosen while at the Free University of Brussels a R1M rat model was used.

Tumour uptake and biodistribution was studied by Dynamic Planar Imaging and by dissection. Although both research methods differed in resolution and sensitivity, they both demonstrated the same interesting results, namely: fast, high and specific tumour accumulation. Although, Dynamic Planar Imaging resulted in lower tumour to background ratios as compared to the dissection method, the tumour could be clearly identified. The latter fact was an important observation since this technique could offer a fast and non-invasive procedure to examine the patient. In this aspect, visualisation of the tumour pre-dominated the high tumour to background ratios.

As compared to the in vitro studies, the same kinetic approach could be applied: the uptake as a function of time followed a rectangular hyperbolic curve and a pseudo reversible pseudo first order reaction was followed. These observations, together with the displacement [^{123}I]-2-iodo-L-phenylalanine radioactivity in the tumour by L-phenylalanine, strongly indicated that in vivo, [$^{123/1225}$I]-2-iodo-L-phenylalanine is also transported by the LAT1 system, an "obligatory exchanger" transport system.

Regarding the general biodistribution characteristics, 2-iodo-L-phenylalanine was cleared fast from the blood through the kidneys to the bladder. No accumulation was noticed in the kidneys, brain and the abdominal organs with an exception of the pancreas which is typical in rodents. Moreover, the new tracer showed negligible uptake in inflammatory lesions in comparison to ^{18}F-FDG.

Additionally, the effect of sedation and data-acquisition method (dissection or planar imaging) on [^{123}I]-2-iodo-L-phenylalanine distribution in R1M-bearing athymic mice was investigated. Indeed, non-invasive animal imaging experiments require that movements of the animal should be minimized to reduce artefacts. To accomplish the latter setting, the animals were sedated using pentobarbital. However, in order to interpret the results correctly, it is important to identify the influence of sedation on tracer distribution since these preclinical data are used for human extrapolation. Kinetic modelling of the initial biodistribution kinetics revealed that pentobarbital both decreases the elimination velocity ($k_{1,0}$), and thus blood clearance of [^{123}I]-2-iodo-L-phenylalanine, and the biodistribution velocity ($k_{1,2}$) of the compound to the peripheral compartment. Moreover, the method and treatment showed both a highly significant effect on the individual organs: the target tumour organ showed significant lower [^{123}I]-2-iodo-L-phenylalanine uptake values after sedation while the blood and kidney values were elevated. However, the tumour could still be visualized using this non-invasive imaging method in combination with Nembutal despite its worst case scenario.

During the last decades, the development of and the studies with radioactively labelled amino acids for tumour diagnosis were focused on the L-enantiomers as it was supposed that

the amino acid tracers had to be incorporated into the tumour cell proteins. Today, the latter hypothesis is refuted and regarding the unnatural character of D-amino acids, our research group additionally developed [^{123}I]-2-iodo-D-phenylalanine

The precursor 2-iodo-D-phenylalanine was synthesized by analogy with its L-isomer: the optimal reaction conditions for 2-iodo-L-phenylalanine precursor synthesis using the Cu^{1+} assisted nucleophilic exchange in acidic and reducing conditions were applied. Moreover, the same Kit-formulation could be used for the radioiodination of the precursor 2-iodo-D-phenylalanine leading to the same radiochemical yield and purity.

In vitro evaluation of [^{125}I]-2-iodo-D-phenylalanine in the R1M rabdomyosarcoma cell model revealed a difference in uptake kinetics and affinity for influx between [^{125}I]-2-iodo-D-phenylalanine and [^{125}I]-2-iodo-L-phenylalanine which might be due to the fact that the D-form only shows a high affinity for the LAT1 system and much lower affinity for LAT2 while [^{125}I]-2-iodo-L-phenylalanine demonstrates a high affinity for both transporter types. BCH is highly "general L transport" specific but with low affinity so it does not allow to differentiate the LAT types in the current conditions. Concentration depending kinetics illustrated that [^{125}I]-2-iodo-D-phenylalanine was transported into the cells by a single substrate-transport system interaction and that the K_m value (32 µM) for the latter amino acid analogue was comparable to that of L-phenylalanine (32µM) and 2-iodo-L-phenylalanine (46µM).

The positive in vitro results led to the evaluation and the comparison with its L-isomer of 2-iodo-D-phenylalanine in vivo in the R1M tumor bearing athymic mouse model.

[^{123}I]-2-iodo-D-phenylalanine showed in many aspects comparable characteristics to [^{123}I]-2-iodo-L-phenylalanine. Indeed, besides the same general biodistribution characteristics, such as renal clearance of the tracer and the absence of accumulation in the abdominal and brain regions, [^{123}I]-2-iodo-D-phenylalanine tumour accumulation was high and specific and occurred through the same transporter system LAT1. Moreover, in contradiction to ^{18}F-FDG, [^{123}I]-2-iodo-D-phenylalanine uptake in acute inflammation was only slightly increased. Moreover, the two compartment modelling and the excretion as function of time obtained by Dynamic Planar Imaging, both revealed that [^{123}I]-2-iodo-D-phenylalanine was cleared 2 times faster from the blood in comparison with [^{123}I]-2-iodo-L-phenylalanine resulting in better tumour contrast ratios and less radiation burden which was confirmed by the dosimetric calculations.

However, concerning the long time kinetics, both tracers showed some important differences. In vivo planar imaging revealed that although less [^{123}I]-2-iodo-D-phenylalanine remained in the tumour 19 hours p.i. in comparison with its L-analogue, an increase of 352% in tumour was observed whereas the tumour contrast for the L-isomer decreased to 71%.

The in vivo evaluation of [^{123}I]-2-iodo-D-phenylalanine illustrated that this tracer could be used as tumour diagnosticum for SPECT. Moreover, due to its metabolic stability and its fast clearance from the circulation, [^{123}I]-2-iodo-D-phenylalanine might be an interesting tracer for radionuclide therapy applications.

As a valorisation of the tracer characteristics for tumour imaging, the evaluation of and the comparison between both [^{123}I]-2-iodo-L-phenylalanine and [^{123}I]-2-iodo-D-phenylalanine in various tumours, representing those tumour families with highest prevalence in humans, should be performed. Moreover, an additional comparison with the recently developed tumour tracer [^{123}I]-2-iodo-L-phenylalanine would allow us to choose the optimal analogue for clinical practice.

At the moment, several amino acids have been developed for SPECT tumour imaging. Of these amino acid analogues, [^{123}I]-2-iodo-L-tyrosine has made the largest progressions towards clinical application. Literature illustrated that the latter tracer showed no kidney accumulation and good tumour specificity characteristics. As a consequence, we compared

[^{123}I]-2-iodo-L-phenylalanine to [^{123}I]-2-iodo-L-tyrosine in the R1M athymic mouse model whether the former showed comparable or even better characteristics.

Our results confirmed that both amino acids were transported by the LAT1 transporter as indicated by the in vitro studies in the R1M cell model. In vivo in the athymic mouse model, both tracers demonstrated comparable biodistribution characteristics: high, fast and specific tumour uptake and a renal clearance. Although both tracers showed comparable tumour uptake values and tumour to contralateral background ratios, [^{123}I]-2-iodo-L-phenylalanine demonstrated somewhat better characteristics for oncologic tumour imaging by means of SPECT. Indeed, it showed not only a faster blood clearance but the tracer uptake in the tumour reached its equilibrium with the bloodpool activity faster. Moreover, the faster blood clearance of the tracer will result in a lower radiation burden for the animal. The latter hypothesis was confirmed by the dosimetric calculations as performed in Chapter 3: a higher effective dose was obtained for [^{123}I]-2-iodo-L-tyrosine as compared to [^{123}I]-2-iodo-L-phenylalanine.

Although positive results were obtained using [^{123}I]-2-iodo-L-phenylalanine and [^{123}I]-2-iodo-D-phenylalanine, the question whether those two amino acids analogues could be used as “general tumour detecting agents” was not answered yet. As a consequence, both tumour tracers were evaluated in different tumour cells lines, corresponding with those tumours with high prevalence in human.

Concerning the biodistribution and tumour uptake characteristics, the same results were obtained for both tracers as compared to the R1M tumour bearing athymic mouse model. On the one hand fast, high and specific tumour uptake and on the other no accumulation in the other organs was observed. These observations make both tracers suitable as powerful and general tumour detecting agents. Moreover, the differences between the two stereoisomers were confirmed: the modelling revealed that in comparison to its L-analogue, [^{123}I]-2-iodo-D-phenylalanine was cleared faster from the blood. These results were confirmed by DPI: the D-isomer reached at the same time point for the same tumour models higher tracer accumulation in the bladder. Moreover, as a result of these better pharmacokinetic tracer characteristics, [^{131}I]-2-iodo-D-phenylalanine might serve as a candidate for systemic radiotherapy.

To stipulate the possible use of [^{123}I]-2-iodo-L-phenylalanine as a tumour detecting agent for dynamic planar imaging, the application of the new tracer was evaluated for the diagnosis of cancer in dogs. Indeed, since many owners are prepared to give their pets the maximal care, including radiation and chemotherapy, it is important to have a highly specific tumour tracer at one’s disposal. A case report study described the use of [^{123}I]-2-iodo-L-phenylalanine as diagnostic tool for the detection of synovial cell sarcoma of the tarsus in two dogs. Both dogs confirmed the results obtained in the mice studies: high and fast tumour accumulation with fast renal clearance of the tracer. This implicates that a fast examination and interpretation of the results is possible, leading to fast decisions and minor inconvenience for the pet owners.

Chapter 2 and 4 described the promising characteristics of [^{123}I]-2-iodo-L-phenylalanine as tumour detecting agent for SPECT. However, during the process of curing cancer, there are a lot of other aspects to deal with. One important one is radiotherapy evaluation: the sooner the clinician could tell whether or not a patient is responding to therapy, the sooner it could be adjusted and valuable time will be spared. It is in this aspect that we evaluated [^{123}I]-2-iodo-L-phenylalanine as a radiotherapy response tool.

The in vitro as well as the in vivo radiotherapy experiments performed in this report showed promising results concerning therapy evaluation. In vitro testing indicated that although fewer cells survive at high radiation doses, the still viable cells accumulated the

tracer in higher amounts which could be beneficial for detecting residual tumour lesions. Although the results should be interpreted with utmost care because of the slight differences in tumour uptake between the tumour and the inflammation group, in vivo evaluation confirmed that [^{123}I]-iodo-L-phenylalanine was able to detect metabolic changes due to irradiation, even at very short time intervals. The latter observation is very important: within 24 hours post therapy, clinicians would be able to discover whether or not the tumor is susceptible to radiotherapy and value time could be spared. However, these results should be investigated more extensively in the future and a comparison with ^{18}F-FDG is necessary to illustrate whether our new tracer is superior.

SAMENVATTING.

Tot op heden is geen enkele test in staat om op een accurate manier kanker vast te stellen. Meestal is een volledig medisch onderzoek, rekening houdend met zijn voorgeschiedenis, van de patiënt noodzakelijk. Vanuit dit standpunt is medische beeldvorming onmisbaar bij het opsporen van tumoren in een vroeg stadium zodat de patiënt kan genezen vooraleer de tumor zich naar andere delen van het lichaam verspreidt.
Tijdens het laatste decennium heeft de nucleaire oncologie een snelle vooruitgang gekend en verschillende strategieën zijn intussen ontwikkeld om tumoren te detecteren. Vele moleculen werden tot nog toe ontwikkeld en voorgesteld als hét tumor-diagnosticum. Echter, veel van deze producten zijn beperkt tot een welbepaald type kanker en dikwijls is hun klinische relevantie onduidelijk.
Tijdens de zoektocht naar een universele manier om tumoren op te sporen, leek ^{18}F-FDG een geschikte tumor-tracer. Zijn werkingsmechanisme is gebaseerd op de verhoogde metabole activiteit van tumoren. Vandaag wordt deze molecule uitgebreid toegepast voor diagnose, “staging”, opsporen van recurrente lesies, therapie evaluatie en therapie respons. Hoewel de gemiddelde sensitiviteit en de specificiteit van ^{18}F-FDG zeer hoog is (84 % en 88 %, respectievelijk), kent deze molecule toch een aantal belangrijke nadelen. Immers, ^{18}F-FDG beeldvorming wordt gehinderd door zijn niet specifieke hoge opstapeling in de hersenen, in inflammatoir weefsel en in andere granulomateuze aandoeningen. Bovendien vertonen niet alle kankers een verhoogd glucosemetabolisme.
Naast het glucosemetabolisme is eveneens het aminozuur metabolisme verhoogd in tumoren en bijgevolg zijn er een aantal radioactief gemerkte aminozuren ontwikkeld. Tot op heden is IMT de enige SPECT tracer die routinematig wordt toegepast in de kliniek. Hoewel deze tracer in staat is om zowel hersentumoren als perifere tumoren op te sporen, is het gebruik ervan nog steeds inferieur aan ^{18}F-FDG. Een ander belangrijk aspect is zijn hoge opstapeling in de nieren wat beeldvorming van het abdomen quasi onmogelijk maakt. De onderzoeksgroep van Samnick et al. ontwikkelde en evalueerde onlangs het phenylalanine analoog 4-iodo-L-phenylalanine maar de hoge bloedpoel activiteit beperkt het gebruik van deze tumor-tracer.

Onze onderzoeksgroep heeft zich toegelegd op de ontwikkeling en evaluatie van [^{123}I]-2-iodo-L-phenylalanine. Opdat enzymatische interactie met het molecule nog mogelijk zou zijn werd geopteerd voor een substitutie van het jood-atoom op de 2-positie. Bovendien werd deze molecule ontwikkeld als alternatief voor 4-iodo-L-Phenylalanine, 2-iodo-L-tyrosine and IMT.

Zoals werd beschreven in hoofdstuk 2, werd de precursor 2-iodo-L-phenylalanine gesynthetiseerd vanuit het broom-derivaat 2-bromo-L-phenylalanine via een Cu^{1+}-geassisteerde nucleofiele substitutie onder reducerende condities in een zuur milieu. De optimale reactiecondities werden bepaald met een experimenteel design. Onder deze omstandigheden werden geen bijproducten of stereo-isomeren gevormd en werd een rendement van minstens 60% bereikt. Een kit-formulatie gebaseerd op dezelfde reactie-omstandigheden liet snelle en kwantitatieve routinematige radio-jodering van 2-iodo-L-phenylalanine toe. Hierbij was geen extra zuivering nodig, wat een grote toegevoegde waarde betekent voor routinematige productie in een klinische omgeving.

Summary

Om te onderzoeken of de nieuwe tracer [$^{123/125}$I]-iodo-L-phenylalanine niet de limitaties van 4-iodo-L-phenylalanine en IMT vertoonde, werd de tracer geëvalueerd in de R1M cellijn, zowel in vitro als in vivo in een athymisch muismodel.

De in vitro studies in de R1M cellijn illustreerden dat ondanks het zeer grote joodatoom, dat toegevoegd was op de 2-positie van de molecule, 2-iodo-L-phenylalanine nog steeds wordt opgenomen in de cel via het L-aminozuur transportsysteem subtype 1 (LAT1). Ook toonde het nieuwe aminozuuranaloog een zeer vergelijkbare affiniteit voor dit transportsysteem, in vergelijking met de natuurlijke aminozuren L-phenylalanine and L-tyrosine (K_m L-phenylalanine = 55 µM, K_m L-tyrosine = 39 µM, K_m 2-iodo-L-phenylalanine = 46 µM). Inhibitie-experimenten en RT-PCR experimenten demonstreerden dan 2-iodo-L-phenylalanine voor het grootste deel door het LAT1 systeem wordt getransporteerd. Er is geen significant verschil tussen de opnamepatronen van [^{125}I]-2-iodo-L-phenylalanine in $HEPES^+$ en $HEPES^-$. Daarenboven, gestimuleerde netto-efflux in aanwezigheid van 5mM L-phenylalanine of 5 mM BCH bedraagt bijna 80% van de initiële opnamewaarden, terwijl het "lekken" van de tracer beperkt bleef tot minder dan 10%. Daarenboven wordt 2-iodo-L-phenylalanine niet geïncorporeerd in de proteïnen van de cel en is de LAT1-gekoppelde influx van radioactiviteit direct gecorreleerd met de nood aan aminozuren voor de verhoogde proteïnesynthese en het metabolisme van de cel. Daarom reflecteert de verhoogde opname van 2-iodo-L-phenylalanine de verhoogde aminozuur-"turnover", ondanks het feit dat er geen incorporatie is.

Deze laatste eigenschappen waren erg veelbelovend, en een vivo evaluatie was dus veroorloofd. Op de Universiteit Gent werd een muismodel geëvalueerd, terwijl op de Vrije Universiteit Brussel een ratmodel werd geprefereerd.

Tumoropname en biodistributie werden bestudeerd door middel van Dynamische Planaire Beeldvorming en dissectie. Hoewel deze beide methoden verschillen in resolutie en sensitiviteit, toonden ze beiden dezelfde interessante resultaten: Snelle, hoge en specifieke accumulatie in de tumor. Dynamische Planaire Beeldvorming resulteerde wel in lagere tumor-versus-achtergrond waarden, maar de tumor kon toch zeer duidelijk worden gevisualiseerd. Dit laatste feit is erg belangrijk omdat deze techniek een snelle en niet-invasieve procedure voor patiëntonderzoek kan bieden. Hierom was de goede visualisatie belangrijker dan de hoge tumor-versus-achtergrond waarde.

In vergelijking met de in vitro studies kon dezelfde kinetische benadering worden gebruikt: De opname vertoonde een hyperbolische curve in functie van de tijd, en een pseudo-reversibele eerste orde reactie werd gevolgd. Deze observaties, tezamen met de verplaatsing van [^{123}I]-2-iodo-L-phenylalanine radioactiviteit uit de tumor door L-phenylalanine, gaven een sterke indicatie dat ook in vivo het LAT1 transportsysteem verantwoordelijk is voor de opname van [$^{123/1225}$I]-2-iodo-L-phenylalanine.

Wat de algemene biodistributiekarakteristieken van 2-iodo-L-phenylalanine betreft, vertoond de tracer een snelle eliminatie uit het bloed via de nieren naar de blaas. Noch in de nieren, noch in de hersenen of de abdominale organen werd een accumulatie vastgesteld, met uitzondering van de pancreas. Dit laatste is echter typisch voor knaagdieren. Daarenboven toonde de nieuwe tracer nauwelijks opname in inflammatoire laesies, in tegenstelling tot ^{18}F-FDG.

Hiernaast werd ook het effect van sedatie en data-acquisitie (dissectie of planaire beeldvorming) op de resultaten van de distributie van [^{123}I]-2-iodo-L-phenylalanine in R1M-dragende athymische muizen onderzocht. Niet-invasieve beeldvorming van kleine proefdieren vereist namelijk dat de dieren niet bewegen, om artefacten te voorkomen. Hiertoe wordt in onze onderzoeksgroep pentobarbital gebruikt om de dieren te verdoven. Om de resultaten correct te kunnen interpreteren, is het belangrijk om het effect van die verdoving te kennen, aangezien de resultaten uit het muismodel zullen gebruikt worden om de situatie in de humane situatie te extrapoleren. Kinetische modellering van de originele biodistributie-resultaten toonde dat pentobarbital zowel de eliminatiesnelheid ($k_{1,0}$), en daarom ook de bloedklaring van [^{123}I]-2-iodo-L-phenylalanine, en de biodistributiesnelheid ($k_{1,2}$) van de tracer naar het perifere compartiment beïnvloed. Daarenboven vertonen zowel de methode als de verdoving een grote invloed op de individuele organen: de tumor vertoonde een significant lagere traceropname na sedatie terwijl het bloed en de nieren waren verhoogd. Toch kon de tumor nog steeds worden gevisualiseerd met deze niet-invasieve beeldvormingstechniek in combinatie met pentobarbital, hoewel deze combinatie de slechtst denkbare is.

Tijdens de laatste jaren werd de studie van radioactieve gemerkte aminozuren voor tumor diagnose vooral toegespitst op de L-enatiomeren, omdat verondersteld werd dat aminozuurtracers moesten worden geïncorporeerd in de proteïnes van de tumorcel. Tegenwoordig is deze hypothese onwaar gebleken, en in dit licht heeft onze onderzoeksgroep het onnatuurlijke aminozuur [^{123}I]-2-iodo-D-phenylalanine ontwikkeld.

De precursorsyntese gebeurt analoog aan deze van het L-analoog: de optimale condities voor 2-iodo-L-phenylalanine precursor synthese via de Cu^{1+}-methode werden gebruikt. Dezelfde kitformulatie kon worden gebruikt. Ook deze resulteerde in een hoge zuiverheid en een hoog rendement.

In vitro evaluatie van [^{125}I]-2-iodo-D-phenylalanine in het R1M rabdomyosarcoma celmodel toonde een verschil in opnamekinetiek en affiniteit voor influx in vergelijking met [^{125}I]-2-iodo-L-phenylalanine. Dit kan bijvoorbeeld worden veroorzaakt door het feit dat de D-vorm enkel een hoge affiniteit vertoond voor het LAT1 systeem, en niet voor LAT2, terwijl [^{125}I]-2-iodo-L-phenylalanine een hoge affiniteit heeft voor beide transporters. BCH is specifiek voor de LAT-transportsystemen, mar kan geen onderscheid maken tussen beide types onder de gebruikte omstandigheden. Concentratie-afhankelijke kinetiek illustreerde de dat de influx van [^{125}I]-2-iodo-D-phenylalanine veroorzaakt werd door interactie met één enkel substraat-transportsysteem en dat de K_m-waarde (32 µM) voor het [^{125}I]-2-iodo-D-phenylalanine vergelijkbaar was met L-phenylalanine (32 µM) en met 2-iodo-L-phenylalanine (46µM).

De positieve in vitro resultaten leidden tot vergelijking met zijn L-isomeer en tot in vivo evaluatie van 2-iodo-D-phenylalanine in het R1M tumor dragende athymische muismodel. [^{123}I]-2-iodo-D-phenylalanine demonstreerde op vele vlakken vergelijkbare eigenschappen als [^{123}I]-2-iodo-L-phenylalanine. Naast dezelfde algemene biodistributie, zoals renale klaring van de tracer en de afwezigheid van accumulatie in de abdominale organen en in de hersenen, was de tumoropname van [^{123}I]-2-iodo-D-phenylalanine hoog en specifiek en werd gemedieerd door hetzelfde LAT1 transportersysteem. Ook was ook de opname in acute inflammaties erg laar in vergelijking tot ^{18}F-FDG. Daarenboven toonden twee-compartiment modellering en de excretie in functie van de tijd beide dat [^{123}I]-2-iodo-D-phenylalanine tweemaal sneller uit het bloed werd geklaard in vergelijking met [^{123}I]-2-iodo-L-phenylalanine. Dit resulteerde in betere tumor contrastwaarden en in lagere stralingsbelasting, wat bevestigd werd door dosimetrie-berekeningen.

Als echter de lange-termijn kinetiek in beschouwing wordt genomen, vertoonden beide tracers enkele belangrijke verschillen. In vivo planaire beeldvorming toonde dat alhoewel minder [^{123}I]-2-iodo-D-phenylalanine in de tumor aanwezig bleef op 19 uur na injectie in vergelijking met het L-analoog, er en toename was van 353% van het tumorcontrast. Dit in vergelijking met een afname tot 71% voor het L-isomeer.

De in vivo evaluatie van [^{123}I]-2-iodo-D-phenylalanine illustreerde dat deze tracer gebruikt zou kunnen worden als een tumor diagnosticum voor SPECT. Daarenboven zou het ook een interessante tracer kunnen zijn voor radionuclide therapie, omwille van zijn metabole stabiliteit en snelle klaring.

Als validatie voor de tracereigenschappen voor beeldvorming van tumoren, moet de evaluatie van en de vergelijking tussen [^{123}I]-2-iodo-L-phenylalanine en [^{123}I]-2-iodo-D-phenylalanine herhaald worden in een aantal andere tumormodellen, die de meest voorkomende soorten kanker representeren. Ook zou een vergelijking met de recent ontwikkelde tracer [^{123}I]-2-iodo-L-tyrosine ons toelaten om een optimaal product te selecteren voor klinische toepassing.

Tot op heden werden verschillende aminozuur analogen ontwikkeld voor SPECT tumor beeldvorming. Van deze aminozuren is 2-iodo-L-tyrosine de meeste vooruitgang gemaakt naar klinische toepassingen toe. De literatuur illustreert dat deze laatste tracer geen nieraccumulatie en goede specificiteit voor tumoren vertoond. Hierom hebben we [^{123}I]-2-iodo-L-phenylalanine met [^{123}I]-2-iodo-L-tyrosine vergeleken in het R1M muismodel, om te onderzoeken of het eerste vergelijkbare of nog betere eigenschappen vertoond.

Onze in vitro resultaten in R1M cellen bevestigen dat beide aminozuren via het LAT1 transporter systeem geïnternaliseerd worden. In vivo vertoonde beide tracers een vergelijkbare biodistributie: hoge, snelle en specifieke tumoropname en een renale klaring. Hoewel bede tracers vergelijkbare tumor-versus-achtergrond ratio’s vertonen, had 2-iodo-L-phenylalanine licht betere karakteristieken voor oncologische beeldvorming via SPECT: Niet enkel vertoonde het een snellere bloedklaring, maar ook bereikte het sneller het evenwicht tussen de tumor en het bloed. Deze snellere bloedklaring zal resulteren in een lagere stralingsdosis voor het dier. Deze hypothese werd bevestigd door de dosimetrie berekeningen zoals berekend in Hoofdstuk 3: een hogere effectieve dosis werd berekend voor [^{123}I]-2-iodo-L-tyrosine in vergelijking met [^{123}I]-2-iodo-L-phenylalanine.

Hoewel positieve resultaten werden bekomen met [^{123}I]-2-iodo-L-phenylalanine en [^{123}I]-2-iodo-D-phenylalanine, resteert de vraag of deze twee aminozuur analogen kunnen worden gebruikt als “algemene” tumordetectie tracers. Hiertoe werden beide tracers geëvalueerd in verschillende tumordragende muismodellen, die de meest in mensen voorkomende tumorsoorten representeren.

Wat biodistributie n tumoropname betreft, werden voor beide tracers dezelfde resultaten bekomen als voor het R1M model: Snelle, hoge en specifieke tumoropname en geen accumulatie in andere organen werd bekomen. Deze eigenschappen maken beide tracers geschikt als potente algemene tumor diagnosticae. Daarenboven werden de verschillen tussen beide stereo-isomeren bevestigd: kinetische modellering toonde dat [^{123}I]-2-iodo-D-phenylalanine sneller uit het bloed werd geklaard in vergelijking met zijn L-analoog. Deze resultaten werden ook bevestigd door Dynamische Planaire Beeldvorming: het D-isomeer

bereikte voor dezelfde tijdspunten en dezelfde tumormodellen hogere opnames in de blaas. Omwille van deze betere farmacokinetische eigenschappen zou [^{131}I]-2-iodo-D-phenylalanine misschien kunnen gebruikt worden voor systemische radiotherapie.

Om de mogelijkheden van [^{123}I]-2-iodo-L-phenylalanine als tumor diagnosticum nog verder te verkennen, werd de mogelijk onderzocht om de tracer te gebruiken als diagnosticum voor kanker in honden. Omdat vele eigenaars bereid zijn hun huisdier de best denkbare verzorging te geven, inclusief chemo- en radiotherapie, is het belangrijk om een zeer specifieke tracer ter beschikking te hebben. Twee gevallen waarbij [^{123}I]-2-iodo-L-phenylalanine wordt gebruikt voor de detectie van synoviaal cel sarcoma in het tarsus van een hond, worden beschreven. Beide dieren bevestigden het resultaat van de muisstudies: hoge en snelle opname in de tumor met snelle renale klaring van de tracer. Dit impliceert dat een snel onderzoek en interpretatie van de data mogelijk is, wat kan leiden tot snelle beslissingen en minimale tijdsbelasting voor de eigenaars.

Hoofdstuk 2 en 4 beschreven de veelbelovende eigenschappen van [^{123}I]-2-iodo-L-phenylalanine als tumor diagnosticum voor SPECT. Er zijn echter meer aspecten tijdens het proces van het genezen van kanker waar deze tracer zijn nut zou kunnen hebben. Eén van deze is radiotherapie-evaluatie: hoe sneller de arts kan beslissen of een patiënt al dan niet positief reageert op de therapie, hoe sneller de therapie kan worden aangepast, waardoor waardevolle tijd kan worden gewonnen. Het is in dit licht dat we [^{123}I]-2-iodo-L-phenylalanine verder onderzochten als een tracer voor radiotherapie respons evaluatie.

De in vitro zowel als de in vivo radiotherapie experimenten die werden beschreven in dit werk zijn erg veelbelovend. De in vitro tests gaven een indicatie dat hoewel minder cellen overleven bij hogere stralingsdosissen, de overlevende cellen de tracer in hogere mate opnamen. Dit zou waardevol kunnen zijn om residueel tumorweefsel te kunnen detecteren. Hoewel de resultaten met grote voorzichtigheid moeten worden geïnterpreteerd, omwille van de kleine verschillen in tumoropname tussen de tumor- en de inflammatiegroep, bevestigde de in vivo evaluatie dat [^{123}I]-2-iodo-L-phenylalanine metabole veranderingen kon detecteren in de tumor ten gevolge van de bestraling, zelfs na erg korte tijdsintervallen. Deze laatste observatie is erg belangrijk: binnen de 24 na radiotherapie zouden de artsen reeds in staat kunnen zijn om te ontdekken of de tumor beantwoord aan de radiotherapie, waardoor waardevolle tijd kan worden bespaard. Natuurlijk moeten deze resultaten in de toekomst in meer detail worden onderzocht. Verder is ook een vergelijking met ^{18}F-FDG nodig, omdat deze laatste nog steeds geld als de gouden standaard, en om te evalueren of onze nieuwe tracer superieur is.

ERRATA

The improvements are printed in **bold**.

Page 3, last sentence:

The characteristics of both imaging devices are compared in table 1.1 **which** presents the advantages and disadvantages of each technique (3-5).

Page 5, last paragraph:

Several hypoxia imaging tracers **have** been developed, either for SPECT or PET.

Page 6, paragraph cell death imaging:

Normally, this molecule is restricted to the intracellular **leaflet** of the plasma membrane. As cells undergo apoptosis, this phosphatidyl serine will be exposed at the extracellular **leaflet** of the membrane due to the activity of floppase.

Page 7, cell surface receptor imaging – first sentence:

Cell surface receptors **can** be divided into three families: (1) G-protein coupled receptors, (2) tyrosine kinase receptors and (3) the non-tyrosine kinase receptors.

Page 37, Figure 2.1.1.:

The figure should be replaced by the following figure, containing error bars.

FIGURE 2.1.1: Influence of the pH on the reaction yield of the precursor 2-iodo-L-phenylalanine (n = 3).

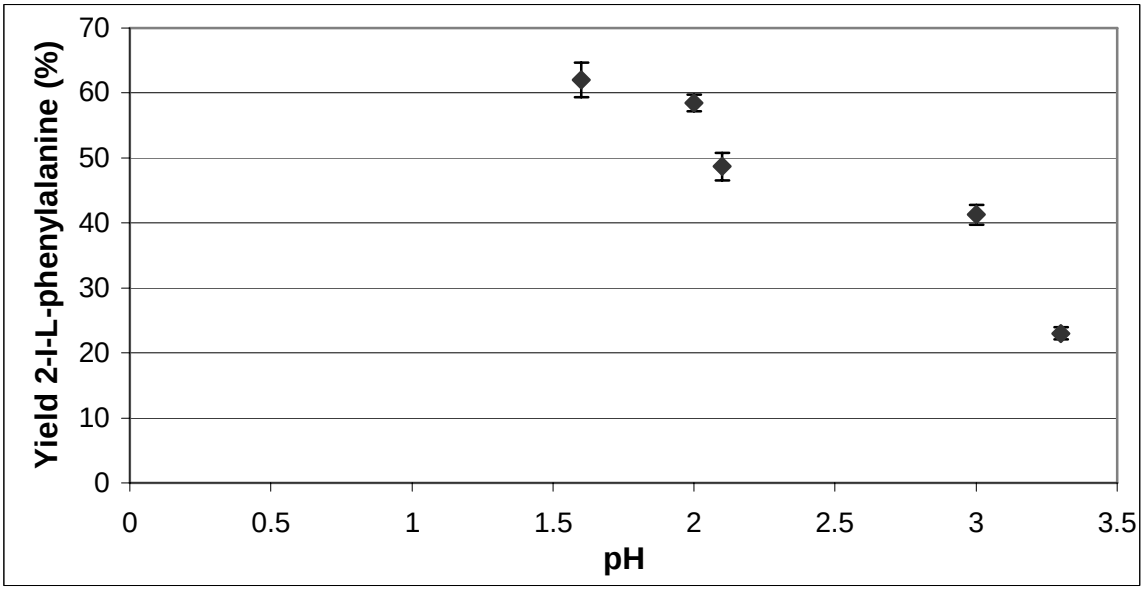

Page 39, Figure 2.1.3:

The caption of figure 2.1.3 is replaced by following text, containing more detailed information.

FIGURE 2.1.3: Main effects plot, resulting from the screening design. Temp: temperature; Phe: 2-bromo-L-phenylalanine; CA: citric acid and GA: gentisic acid. The impact of the tested parameter on the reaction yield (2-iodo-L-phenylalanine) is represented by the slope of the straight lines: steeper slopes correspond with a higher impact.

Page 117, title:

Comparative biodistribution between [^{123}I]-2-iodo-L-phenylalanine, [^{123}I]-2-iodo-L-tyrosine and **[^{123}I]-2-iodo-D-phenylalanine**.

Page 118, last sentence:

Dynamic planar imaging and dissection were performed to study on the one hand the general tracer characteristics **and on the other hand the individual differences in tracer kinetics and tumour accumulation.**

Page 119/129, last sentence:

Both tracers could overcome the limitations of both ^{18}F-FDG and IMT: a higher tumor specificity and no kidney accumulation was observed, respectively.

Page 132, second paragraph:

For these reasons, amino acid transport tracers are **proven** to be valuable to reflect the malignancy of tumour.

Curriculum vitae

Kersemans Veerle
Rozenlaan 42
2275 Lille
België

Telefoon: ++ 32 495 670984
E-Mail: Veerle.Kersemans@UGent.be

Geboren te Turnhout op 10 april 1979
Burgelijke stand: ongehuwd

Opleiding:

Lagere school: Rijksbasisschool Beerse
Karel van Nijenlaan 12
2340 Beerse

1985 – 1986 tot 1990 – 1991

Middelbare School: Koninklijk Atheneum Turnhout
Boomgaardstraat 56
2300 Turnhout

1st graad: 1991 – 1992: Latijn
1992 – 1993: Latijn – Grieks
2de graad: 1993 – 1994 en 1994 – 1995: Latijn – Wiskunde
3de graad: 1995 – 1996 en 1996 – 1997: Latijn – Wiskunde (8u)

Universiteit: Licentiaat in de Biomedische Wetenschappen
Vrije Universiteit Brussel (VUB)
Medische Campus Jette
Laarbeeklaan 103
1090 Jette

1997 – 1998: Biomedische Wetenschappen, 1st kandidatuur, onderscheiding
1998 – 1999: Biomedische Wetenschappen, 2de kandidatuur, onderscheiding
1999 – 2000: Biomedische Wetenschappen, 1st licentie, onderscheiding
2000 – 2001: Biomedische Wetenschappen, 2de licentie, grote onderscheiding
Thesis : Celbiologische effect van cytoskeletaire modificaties in de ziekte van Alzheimer
Te: Janssen Pharmaceutica, Beerse, België
Thesis-promotor: Prof. Dr. Hugo Geerts

Universiteit: Universiteit Gent
Doctoraatsbursaal (augustus 2001 t/m juli 2005)
Laboratorium voor Radiofarmacie
Faculteit Farmaceutische Wetenschappen
Universiteit Gent
Harelbekestraat 72
B-9000 Gent

Extra opleidingen:

Hoger reddersbrevet (BLOSO): 26/01/1997
Meest recente bijscholing: 30/04/2005
Ervaring: 4 jaar vakantiewerk als redster in open water
Initiator/ Jeugdsportbegeleider Judo (BLOSO): 09/02/2001 met 2 jaar ervaring als trainer.
Judo 3de Dan (VJF): 25/04/2004

Talenkennis:

Nederlands	Moedertaal	(lezen, schrijven, begrijpen, spreken)
Engels	Zeer goed	(lezen, schrijven, begrijpen, spreken)
Frans	Goed	(lezen, begrijpen, spreken)

Begeleiding thesisstudenten:

- Kristof Vandenkerckhove; Tweede Proef Apotheker Universiteit Gent. Optimalisatie van de synthese en evaluatie in vivo van L-2-^{123}I-Phenylalanine als SPECT-tracer.
- Lien Van Hauwermeiren; Tweede Proef Apotheker Universiteit Gent. Een overzicht van de radioactief gemerkte aminozuren en hun toepassingen in de oncologie.
- Joeri Vermeiren; 3de jaar graduaat in de laboratorium- en voedingstechnologie, optie farmaceutische en biologische technieken Vesalius Hogeschool Gent. In vitro en in vivo evaluatie van L-2-*I-Phenylalanine als een nieuwe tracer voor SPECT.
- Acke Sylvie; Tweede Proef Apotheker Universiteit Gent. In vitro en in vivo evaluatie van radio-isotoop gemerkt 2-iodo-L-fenylalanine.

Deelname aan congressen en symposia:

- BGNG, Belgisch Genootschap voor Nucleaire Geneeskunde; Knokke, België(juni 2003)
- EANM, European Association of Nuclear Medicine; Amsterdam, Nederland (september 2003)
- Post-EANM meeting; Gent, België (september 2003)
- Molecular imaging symposium; Brussel, België (maart 2003)
- SNM, Society of Nuclear Medicine; Philadelphia, VSA (juni 2004)
- EANM, European Association of Nuclear Medicine; Helsinki, Finland (september 2004)
- ICRRC, International Congress of Radiopharmacy and Radiopharmaceutical Chemistry Istanbul, Turkije (september 2004)
- SNM, Society of Nuclear Medicine, Toronto, Canada (juni 2005).

Publicaties:

Abstracts:

1. **V. KERSEMANS**, J. MERTENS, T. LAHOUTTE, C. JOOS, G. SLEGERS, A. BOSSUYT. Kit preparation and in vitro evaluation of radioiodinated L-2-I-Phenylalanine. Belgisch Tijdschrift voor Nucleaire Geneeskunde, **2003** (in press).

2. **V. KERSEMANS**, T. LAHOUTTE, M. BAUWENS, B. CORNELISSEN, C. JOOS, A. BOSSUYT, G. SLEGERS AND J. MERTENS. In vivo evaluation of L-2-123I-PHENYLALANINE in tumour inoculated athymic mice and Wag/Rij rats. European Journal of Nuclear Medicine and Molecular Imaging, **2003**: 30(S2), S175.

3. **V. KERSEMANS**, K. KERSEMANS, B. CORNELISSEN, E. ACHTEN, R. DIERCKX, J. MERTENS AND G. SLEGERS. In Vivo Evaluation of [123I]-2-Iodo-D-Phenylalanine in Tumour Inoculated Thymic Mice by means of SPECT as a Potential Diagnostic and Radionuclide Therapy Tool. European Journal for Nuclear Medicine and Molecular Imaging, **2004**: 31(S2), S219

4. **V. KERSEMANS**, B. CORNELISSEN, K. KERSEMANS, M. BAUWENS, C. JOOS, E. ACHTEN, R. DIERCKX, J. MERTENS AND G. SLEGERS. In Vivo Characterization of [123I]-2-Iodo-L-Phenylalanine in growing R1M Rabdomyosarcoma bearing Athymic Mice as a potential Tumour Tracer for SPECT. European Journal for Nuclear Medicine and Molecular Imaging, **2004**: 31(S2), S380

5. **V. KERSEMANS**, B. CORNELISSEN, K. KERSEMANS, E. ACHTEN, R. DIERCKX, J. MERTENS AND G. SLEGERS. Detection of Various Tumour types in Athymic mice using [^{123}I]-2-Iodo-L-Phenylalanine Planar SPECT. European Journal for Nuclear Medicine and Molecular Imaging, **2004**: 31(S2), S380

6. **V KERSEMANS**, B CORNELISSEN, M BAUWENS, K KERSEMANS, C JOOS, E ACHTEN, R DIERCKX, G SLEGERS AND J MERTENS. In vitro and in vivo characterization of 123I-2-Iodo-L-Phenylalanine in R1M rabdomyosarcoma cells and an athymic mice model as a potential tumor tracer for SPECT. Journal of Nuclear Medicine, 2004:45(S5) P1404

7. **VEERLE KERSEMANS**, KEN KERSEMANS, BART CORNELISSEN, JOHN MERTENS AND GUIDO SLEGERS. [^{123}I]-2-Iodo-L-Phenylalanine, a new spect tumour tracer: Optimisation of precursorsynthesis, radiolabeling and in vivo evaluation. World Journal of Nuclear Medicine, 2004: 3(p240).

8. **V KERSEMANS**, K KERSEMANS, C CORNELISSEN, E ACHTEN, R DIERCK, J MERTENS AND G SLEGERS. Comparison of the new tumor tracer 2-Iodo-L-phenylalanine with 2-Iodo-L-tyrosine. **Accepted** for poster presentation at **SNM 2005**.

9. J.R. MERTENS, **V. KERSEMANS**, C. JOOS, G. SLEGERS. Quantitative yield kit-preparation of radioiodinated aromatic amino acids. European Journal of Nuclear Medicine, **2002**, supplement 1

10. B. CORNELISSEN, T. THONISSEN, **V. KERSEMANS**, C. VANDEWIELE, O. BOERMAN, W. OYEN, G. SLEGERS. Comparative study of the biodistribution pattern of 123I-hEGF and Tc-99m-HYNIC-hEGF in wild type NMRI mice and in tumour inoculated athymic mice. European Journal of Nuclear Medicine, **2002**, supplement 1, S378.

11. M. BAUWENS, **V. KERSEMANS**, C. JOOS, B. CORNELISSEN, A. BOSSUYT, G. SLEGERS, J. MERTENS. In Vitro and in vivo evaluation of 123I-3,5-diiodo-L-Tyrosine in R1M rhabdomyosarcoma cells. Belgisch Tijdschrift voor Nucleaire Geneeskunde **2003** (in press)

12. T. LAHOUTTE, J. MERTENS, **V. KERSEMANS**, C. JOOS, G. SLEGERS, A. BOSSUYT. In vivo (rat) evaluation of radioiodinated L-2-I-Phenylalanine and L-2-I-Tyrosine as potential tumor tracers for SPECT. Belgisch Tijdschrift voor Nucleaire Geneeskunde, **2003** (in press).

13. B. CORNELISSEN, **V. KERSEMANS**, C. VAN DE WIELE, R.A DIERCKX, G. SLEGERS. A rapid in vivo diagnostical assay to assess the effect of a farnesyl transferase inhibitor on LoVo cells using 123I-hEGF. Belgisch Tijdschrift voor Nucleaire Geneeskunde, **2003** (in press).

14. B. CORNELISSEN, A. JANSSENS, **V. KERSEMANS**, R. OLTENFREITER, R. DIERCKX, G. SLEGERS. Biodistribution of 123/125I-VEGF165 in wild type NMRI and A2058 tumor inoculated athymic mice Belgisch Tijdschrift voor Nucleaire Geneeskunde, **2003** (in press).

15. B CORNELISSEN, A JANSSENS, **V KERSEMANS**, R OLTENFREITER, RA DIERCKX, G SLEGERS. Biodistribution og 123/125I-VEGF in Wild Type NMRI and A2058 Tumor Inoculated Athymic Mice. European Journal for Nuclear Medicine and Molecular Imaging, **2003**: 30(S2), S323

16. L STAELENS, R OLTENFREITER, F DUMONT, **V KERSEMANS**, B CORNELISSEN, G SLEGERS. Synthesis and in Vivo Evaluation in Mice and Rabbits of [123I]-3-(4-iodobenzyl)-8-methoxy-1,2,3,4-tetrahydrochromeno[3,4-c]pyridin-5-one as Possible Agent for Imaging of the Dopamine D4-Receptor. European Journal for Nuclear Medicine and Molecular Imaging, **2003**: 30(S2), S315

17. B CORNELISSEN, **V KERSEMANS**, C VANDEWIELE, RA DIERCKX, G SLEGERS. A Rapid In Vivo Diagnostical Assay to assess the Effect of a Farnesyl Transferase Inhibitor on LoVo Cells Using 123I-hEGF. Cancer Biotherapy & Radiopharmaceuticals, **2003**: 18(2) 283

18. J. MERTENS, **V. KERSEMANS**, T LAHOUTTE, M. BAUWENS, C. JOOS, G. SLEGERS. Radioiodo-D-2-I-Phenylalanine a New Tumour Specific Tracer for Diagnosis and Systemic Radionuclide Therapy. European Journal for Nuclear Medicine and Molecular Imaging, **2004**: 31(S2), S220

19. K. KERSEMANS, C. JOOS, M BAUWENS, **V. KERSEMANS,** J.R.R. MERTENS. Synthesis of [18F]-fluoro-2-methylphenylalanine, a new potential tracer for tumor specific diagnosis in humans with PET. European Journal for Nuclear Medicine and Molecular Imaging, **2004**: 31(S2), S219

20. B CORNELISSEN, **V KERSEMANS**, C VAN DE WIELE, RA DIERCKX, E BONNANO, A SIGNORE, G SLEGERS. ^{123}I-EGF uptake in tumour cells predicts long-term farnesyltransferase therapy outcome in athymic mice. European Journal for Nuclear Medicine and Molecular Imaging, **2004**: 31(S2), S393

21. B CORNELISSEN, K REMAUT, **V KERSEMANS**, R OLTENFREITER, I BURVENICH, G SLEGERS. ^{123}I-EGF internalisation in tumour cells *in vitro* is inhibited by farnesyltransferase inhibitor therapy: possible target for early therapy response prediction. European Journal for Nuclear Medicine and Molecular Imaging, **2004**: 31(S2), S391

22. INGRID BURVENICH, BART CORNELISSEN, **VEERLE KERSEMANS**, PETER BLANCKAERT, STEVE SCHOONOOGHE, ELISABETH COENE, CLAUDE CUVELIER, NICO MERTENS AND GUIDO SLEGERS. Biodistribution study and planar imaging with radiolabelled monoclonal antibody 14C5 in A549 tumour-bearing mice. **In press** Cancer Biotherapy & Radiopharmaceuticals, **2004**

23. B CORNELISSEN, **V KERSEMANS**, I BURVENICH, O BOERMAN, C VANDEWIELE, G SLEGERS. ^{99m}Tc-HYNIC-hEGF is a Candidate for Early Farnesyltransferase Inhibitor Therapy Response Monitoring. **In press** Cancer Biotherapy and Radiopharmaceuticals, **2004**.

24. B CORNELISSEN, K REMAUT, **V KERSEMANS**, G SLEGERS. Blocking of internalization of EGF by farnesyltransferase inhibitors is correlated with disruption of microtubular networks. Proceedings of the 18th meeting of the European association for cancer research, July 2004 (p192)

25. B CORNELISSEN, C LAHORTE, E BONNANO, **V KERSMANS**, C VAN DE WIELE, A SIGNORE, G SLEGERS. In vivo visualization of farnesyltransferase inhibitor induced apoptosis in tumour bearing mice using radiolabeled Annexin V. Proceedings of the 12th European Symposium on Radiopharmacy and radiopharmaceuticals, September **2004** (p20)

26. LUDOVICUS STAELENS, RUTH OLTENFREITER, **VEERLE KERSEMANS**, RIKKI N. WATERHOUSE, CHRISTOPHE VAN DE WIELE AND GUIDO SLEGERS. Preliminary evaluation in tumour inoculated mice of [^{123}I]-4-iodo-N-(4-(4-(2-methoxyphenyl)piperazin-1-yl)butyl)benzamide as a

radioligand for *in vivo* detection of tumours by binding to sigma receptors. **Accepted** for poster presentation at **SNM 2005**.

27. RUTH OLTENFREITER, LUDOVICUS STAELENS, **VEERLE KERSEMANS**, LIESBET VERVOORT, FRANCIS FRANKENNE, JEAN-MICHEL FOIDART, C. VAN DE WIELE, GUIDO SLEGERS. Tumour imaging using ^{123}I labeled matrix metalloproteinase inhibitors. **Accepted** for poster presentation at **SNM 2005**

28. MATTHIAS BAUWENS, TONY LAHOUTTE, **VEERLE KERSEMANS**, KEN KERSEMANS, CONNY JOOS, AXEL BOSSUYT, JOHN MERTENS. Long term retention of [^{123}I]-2-iodo-D-phenylalanine and [^{123}I]-2-iodo-L-phenylalanine in R1M rabdomyosarcoma in rats: potential radiopharmaceuticals for diagnosis and radionuclide therapy. **Accepted** for oral presentation at **SNM 2005**

29. BAUWENS M., LAHOUTTE T, JOOS C., KERSEMANS K., **KERSEMANS V**, MERTENS J. [123I]-2-iodo-D-phenylalanine A Potential Tumour Tracer For SPECT And Radionuclide Therapy. In Vivo Characterization In A R1M Rhabdomyosarcoma Model. **Accepted** for oral presentation at Belgian Society for Nuclear Medicine **(2005).**

30. R. OLTENFREITER, L. STAELENS, **V. KERSEMANS**, L. VERVOORT, M. VAN STEENKISTE, F. FRANKENNE, A. NOËL, C. VAN DE WIELE, G. SLEGERS. In Vivo Evaluation of Small Organic Metalloproteinase Inhibitors as Potential Tumour Imaging Agents European Journal for Nuclear Medicine and Molecular Imaging. Accepted EANM **2005**

Artikels:

1. **VEERLE KERSEMANS**, BART CORNELISSEN, KEN KERSEMANS, ERIK ACHTEN, RUDI A. DIERCKX, JOHN MERTENS AND GUIDO SLEGERS. In vivo characterization of [123/125I]-2-Iodo-L-Phenylalanine in a R1M rabdomyosarcoma athymic mice model as a potential tumor tracer for SPECT. *J Nucl Med* 2005;46:532-539.

2. **VEERLE KERSEMANS**, BART DE SPIEGELEER, JOHN MERTENS AND GUIDO SLEGERS. Influence of sedation and data-acquisition-method on tracer uptake in animal models: [^{123}I]-2-iodo-L-phenylalanine in pentobarbital sedated tumour bearing athymic mice. **Accepted for Nucl Med Biol**

3. **VEERLE KERSEMANS**, BART CORNELISSEN, MATTHIAS BAUWENS, KEN KERSEMANS, RUDI A. DIERCKX, BART DE SPIEGELEER, JOHN MERTENS, AND GUIDO SLEGERS. [123/125I] Labeled 2-iodo-L-phenylalanine and 2-iodo-D-phenylalanine: Comparative Uptake in Various Tumor Types and Biodistribution in Mice. **Submitted** for European Journal of Nuclear medicine and Molecular imaging.

4. **VEERLE KERSEMANS**; KEN KERSEMANS; BART CORNELISSEN; LUDOVICUS STAELENS; BART DE SPIEGELEER; JOHN MERTENS AND GUIDO SLEGERS. Optimization by experimental design of precursor synthesis of 2-iodo-L-phenylalanine, a novel amino acid for tumor imaging. **Submitted** for Journal of Labelled Compounds and Radiopharmaceuticals.

5. **VEERLE KERSEMANS**, BART CORNELISSEN, KLAUS BACHER, KEN KERSEMANS, HUBERT THIERENS, RUDI A. DIERCKX, BART DE SPIEGELEER, GUIDO SLEGERS, AND JOHN MERTENS. [123I]-2-iodo-D-phenylalanine: a new potential tumor specific tracer for SPECT. In Vivo Evaluation and dosimetry in a R1M Rabdomyosarcoma Athymic Mice Model. **Accepted** for Journal of Nuclear Medicine.

6. **VEERLE KERSEMANS**, BART CORNELISSEN, KEN KERSEMANS, MATTHIAS BAUWENS, Conny Joos, Erik Achten, Rudi A. Dierckx,; John Mertens, and Guido Slegers. Comparative Biodistribution study Of The New Tumor Tracer [123I]-2-Iodo-L-phenylalanine With [123I]-2-Iodo-L-tyrosine. **Accepted** for Nuclear Medicine and Biology.

7. **VEERLE KERSEMANS**, VIRGINIE DE GELDER, INDIRA MADANI, BART DE SPIEGELEER, HUBERT THIERENS, WILFRIED DE NEVE,; JOHN MERTENS, AND GUIDO SLEGERS. Future Perspectives: Is 2-iodo-L-phenylalanine Useful as an Early Radiotherapy Response Tool? **Submitted** for Nuclear Medicine Communications

8. **VEERLE KERSEMANS**, KATHELIJNE PEREMANS, BART CORNELISSEN, BART DE SPIEGELEER, JOHN MERTENS, AND GUIDO SLEGERS. SPECT diagnosis of with synovial cell sarcoma of the tarsus with [123I]-2-iodo-L-phenylalanine in two dogs. **Submitted** for Veterinary Radiology and Ultrasound.

9. BART CORNELISSEN, CHRISTOPHE LAHORTE, **VEERLE KERSEMANS**, GABRIELA CAPRIOTTI, ELENA BONNANO, ALBERTO SIGNORE, CHRISTOPHE VAN DE WIELE, RUDI A DIERCKX, GUIDO SLEGERS. *In vivo* apoptosis detection with radiolabeled Annexin V in LoVo tumour bearing mice following Tipifarnib (Zarnestra, R115777) farnesyltransferase inhibitor therapy. Nuclear Medicine and Biology **2005**, 32(3): 233-239.

10. LUDOVICUS STAELENS, RUTH OLTENFREITER, PETER BLANCKAERT, **VEERLE KERSEMANS**, KATIA VANDENBULCKE, CHRISTOPHE VAN DE WIELE AND GUIDO SLEGERS. In vivo evaluation of [I-123]-3-(4-iodobenzyl)-1,2,3,4-tetrahydro-8-hydroxychromeno [3,4-c]pyridin-5-one: a presumed dopamine D-4 receptor ligand for SPECT studies. Nuclear Medicine and Biology **2005**;32:293-299.

11. BART CORNELISSEN, **VEERLE KERSEMANS**, LENNART JANS, LUDOVICUS STAELENS, RUTH OLTENFREITER, THOMAS THONISSEN, ERIC ACHTEN, GUIDO SLEGERS. Comparison between 1 T MRI and non-MRI based volumetry in inoculated tumours in mice. British Journal of Radiology **2005**; 78:338-342.

12. BART CORNELISSEN, **VEERLE KERSEMANS,** INGRID BURVENICH, RUTH OLTENFREITER, VANDERHEYDEN JL, BOERMAN O, VANDEWIELE C, SLEGERS G. Synthesis, biodistribution and effects of farnesyltransferase inhibitor therapy on tumour uptake in mice of Tc-99m labelled epidermal growth factor. Nuclear Medicine Communications 2005;26:147-153.

13. H. DEMAEGDT, P. VANDERHEYDEN, JP DE BACKER, S. MOSSELMANS, H. LAEREMANS, M. TAM LE, **V. KERSEMANS**, Y. MICHOTTE AND G. VAUQUELIN Endogenous cystinyl aminopeptidase in Chinese hamster ovary cells: characterisation by [125I]-Ang IV binding and catalytic activity. Biochemical Pharmacology, **2004**; 68(5): 885-892

14. HEIDI DEMAEGDT, HILDE LAEREMANS, JEAN-PAUL DE BACKER, SABRINA MOSSELMANS, MINH TAM LE, **VEERLE KERSEMANS**, YVETTE MICHOTTE, GEORGES VAUQUELIN AND PATRICK M.L. VANDERHEYDEN Synergistic modulation of cystinyl aminopeptidase by divalent cation chelators. Biochemical Pharmacology, **2004**; 68(5): 892-900.

15. CORNELISSEN B, THONISSEN T, **KERSEMANS V**, VANDEWIELE C, LAHORTE C, DIERCKX R, SLEGERS G. Influence of farnesyl transferase inhibitor treatment on epidermal growth factor receptor status. Nuclear Medicine and Biology 2004; 31:679-689.

16. J. MERTENS, **V. KERSEMANS**, M. BAUWENS, C. JOOS, T. LAHOUTTE, A. BOSSUYT, G. SLEGERS Synthesis, Radiosynthesis and In vitro characterisation of [125I]-2-Iodo-L-phenylalanine in a R1M rhabdomyosarcoma cell model as a new potential tumour tracer for SPECT. Nuclear Medicine and Biology **2004**, 31(6): 739-746.

17. TAM LE, P. M.L. VANDERHEYDEN, M SZASZAK, L HYNYADY, **V KERSEMANS**, G VAUGUELIN. Peptide and nonpeptide antagonist interaction with constitutively active human AT1 receptors M. Biochemical Pharmacology, **2003**: 65(8), 1329-1338.

18. BART CORNELISSEN, RUTH OLTENFREITER, **VEERLE KERSEMANS**, LUDOVICUS STAELENS, RUDI A DIERCKX, FRANCIS FRANKENNE, GUIDO SLEGERS. In vitro and in vivo evaluation of [123I] I-$VEGF_{165}$ as a potential tumor marker. Nuclear Medicine and Biology, **in press**

19. HILDE LAEREMANS, HEIDI DEMAEGDT, JEAN-PAUL DE BACKER, MINH TAM LE, **VEERLE KERSEMANS**, YVETTE MICHOTTE, GEORGES VAUQUELIN AND PATRICK M VANDERHEYDEN. Biochemical Journal; **in press**

20. RUTH OLTENFREITER, LUDOVICUS STAELENS, SORAYA LABIED, LIESBET VERVOORT, **VEERLE KERSEMANS**, FRANCIS FRANKENNE, AGNES NOËL, C. VAN DE WIELE, GUIDO SLEGERS. In vivo evaluation of metalloproteinase inhibitors as potential tumour diagnostic agents. Cancer Biotherapy and Radiopharmaceuticals, Accepted.

21. LUDOVICUS STAELENS, RUTH OLTENFREITER, PETER BLANCKAERT, **VEERLE KERSEMANS**, KATIA VANDENBULCKE, CHRISTOPHE VAN DE WIELE AND GUIDO SLEGERS. Preliminary evaluation in tumour inoculated mice of [123I]-4-iodo-N-(4-(4-(2-methoxyphenyl)piperazin-1-yl)butyl)benzamide as a radioligand for in vivo detection of cancer by binding to sigma receptors. Journal of Labelled Compounds and Radiopharmaceuticals **Submitted**

22. RUTH OLTENFREITER, LUDOVICUS STAELENS, **VEERLE KERSEMANS**, BART CORNELISSEN, LIESBET VERVOORT, FRANCIS FRANKENNE, JEAN-MICHEL FOIDART, C. VAN DE WIELE, GUIDO SLEGERS. Tumour imaging using ^{123}I labeled matrix metalloproteinase inhibitors, a comparative study. European Journal for Nuclear Medicine and Molecular Imaging. **Submitted**.

Referenties:

Prof. dr. sc. Apr. Guido Slegers (promotor doctoraatswerk)
Laboratorium voor Radiofarmacie
Universiteit Gent
Harlbekestraat72
9000 Gent
++32 (0) 9 264 8063
guido.slegers@ugent.be

Prof. dr. John Mertens (co-promotor doctoraatswerk)
Dienst BEFY
Vrije Universiteit Brussel
Laarbeeklaan 103
1090 Jette
++32 (0)2 477 4856
jmerten@vub.ac.be